RICE UNIVERSITY

Characterization of Atmospheric Aerosols in Kathmandu, New Hampshire, and Texas: Carbonaceous, Isotopic, and Water-soluble Organic Composition

by

Kabindra Man Shakya

A THESIS SUBMITTED
IN PARTIAL FULFILLMENT OF THE
REQUIREMENTS FOR THE DEGREE

Doctor of Philosophy

APPROVED, THESIS COMMITTEE:

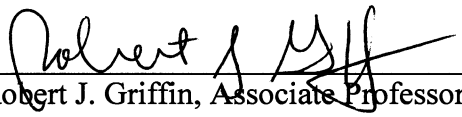

Robert J. Griffin, Associate Professor, Chair
Civil and Environmental Engineering

Philip B. Bedient, Herman Brown Professor
of Engineering, Civil and Environmental Engineering

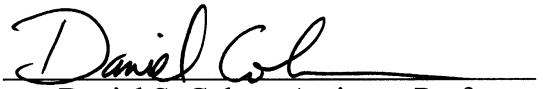

Daniel S. Cohan, Assistant Professor
Civil and Environmental Engineering

Caroline A. Masiello, Assistant Professor
Earth Science

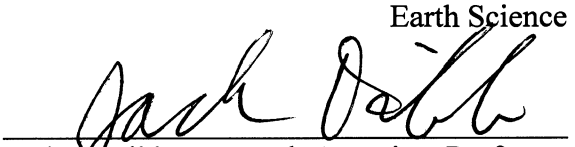

Jack E. Dibb, Research Associate Professor
Earth Sciences and EOS, University of New Hampshire

HOUSTON, TEXAS
MAY 2011

Abstract

Comprehensive characterization of atmospheric aerosols: Carbonaceous, isotopic, and water-soluble organic composition

by

Kabindra Man Shakya

To improve the understanding of aerosol composition, sources, and spatial and temporal variations, atmospheric aerosols were characterized in three locations. Ambient aerosols were characterized using 24-hour samples collected from Kathmandu, Nepal (urban), New Hampshire (semi-rural) and Houston (urban). Results are reported in the main chapters. Chamber studies of secondary organic aerosols (SOA) formation from polycyclic aromatic hydrocarbons (PAHs) and the effects of *in-situ* SOA formation on atmospheric mercury oxidation are described in the appendices.

Carbonaceous, ionic, and isotopic species in aerosols from Kathmandu identified local primary emissions, most likely vehicular exhaust as the most important aerosol sources. Carbonaceous aerosols collected in Kathmandu (24.5 μg C m^{-3}) were much larger than those in New Hampshire (3.74 μg C m^{-3}) during winter. Stable carbon isotope in aerosols of Kathmandu and New Hampshire were similar ($\Delta\delta^{13}C < 0.5‰$) while stable nitrogen isotope were much lower in aerosols of Kathmandu ($\Delta\delta^{15}N = 8.3‰$).

Aerosols in New Hampshire exhibited a large seasonal variation for carbonaceous aerosols, stable nitrogen isotope, and the aromatic fraction of water-soluble organic carbon (WSOC). Pure aliphatics (H-C) were the dominant functional group in WSOC. Results illustrate the importance of secondary aerosol sources throughout the year, with

enhanced importance of primary sources during winter. Stable carbon isotope values suggest a consistent isotopic signature of carbonaceous aerosol sources, while the nitrogen isotope values indicate the variable nitrogenous sources and the strong influence of meteorological parameters (temperature and relative humidity) on nitrogen isotope fractionation.

Characteristics of methoxyphenols (lignin macropolymers) in the ambient aerosols are reported for the first time using CuO oxidation method. The study illustrates the use of lignin oxidation products (LOPs) in aerosols as potential tracers of primary biological aerosol particles (PBAP). The methoxyphenols identified soil organic matter and altered woody angiosperms, with minor influence from soft tissues and gymnosperms as the important PBAP sources in mainly coarse particles in Houston atmosphere. Solvent-extracted methoxyphenols (lignin monomers) and anhydrosugars (levoglucosan, mannosan, and galactosan) in aerosols were either absent or very small, suggesting very limited biomass burning influence with any trace-level presence originating from long-range transport.

Dedicated to my great grandmother Lani Maya Sthapit

Acknowledgements

First of all, I am very grateful to my advisor, Dr. Rob Griffin, for his support, guidance, encouragement, and help throughout my graduate studies. I would also like to thank the committee members Dr. Phil Bedient, Dr. Dan Cohan, and Dr. Carrie Masiello for their valuable advice and feedbacks, and especially Dr. Jack Dibb for his suggestions and guidance.

I would also like to thank Dr. Luke Ziemba, Dr. Xuyi Cai, and Phil Place from Rob's research group for their help and guidance in my research. Kevan Carpenter, Pieter Beckman, Dr. Barkley Sive, and Dr. Yong Zhou are also appreciated for their support and guidance on the laboratory instrumentation. Andy Ouimette is also aprpeciated for his help in isotope analyses.

I also appreciate the guidance and help from Dr. Andrew Rutter and Dr. Patrick Louchouarn in the collaborative research work of mercury and lignin oxidation products. The funding agencies of several research grants obtained by Dr. Rob Griffin, including American Chemical Society Petroleum Research Fund (ACS PRF), United States Environmental Protection Agency, and Rice University Shell Center for Sustainability, are also acknowledged for funding of my studies and research.

Finally, my wife Utpala, who entered my life during my Ph.D., has been instrumental in shaping me with her love, patience, and encouragement. I love you. My parents, my sister Kabina and my nephew Shashank have also been a source of inspiration to me.

Table of Contents

List of Tables

walls. The ratio between filter-based and real time measurements, and the SOA mass lost to the walls provide insight into the loss mechanisms for RM and the performance of the RM measurement method. The fraction of RM which was collected on the rear filter is shown as a fraction of the filter-based measurement column, which is a sum of both the front and rear filter measurements.

A3.3 Regression parameters for the relationships between the deficit between measured and modeled GEM, and various species in the SOA model. The units of the slopes are ppb of species in the left column per ng m^{-3} of difference in GEM between the model and measurements. This could also be expressed ppb per pg m^{-3} of deficit between expected and measured reactive mercury formation. The uncertainty in the slope is the standard error (sde) from the regression package in MS Excel.

A3.4 Pearson correlation coefficients for the relationships between the deficit between measured and modeled GEM, and various species in the SOA model

List of Figures

A2.3 Second order model fits of the $Hg^0_{(g)}$ measurements made in the $Hg^0_{(g)}$ + ozone experiments.

A2.4 Oxidative losses of $Hg^0_{(g)}$ with ozone at low mercury concentrations. Numerical model fits are shown using previously published rate coefficients.

A2.5 Size resolved measurements of particle concentration with a TSI SMPS in the $Hg^0_{(g)}$ + ozone + propene experiment, revealing nucleation and then particle growth by gas to particle conversion.

A2.6 Oxidation of GEM by ozone and OH in a SOA forming reaction system consisting of propene, α-pinene, isoprene, and toluene, initiated with ozone (a); size resolved surface area from a TSI SMPS (b and c). The measurements of GEM were compared to a numerical model which included losses by ozone and OH oxidation. Uncertainties in GEM measurements were estimated from averages of the residuals from fits of the wall loss data presented in the supplemental materials.

A3.1 Replicate measurements of $Hg^0_{(g)}$ oxidative loss in the dark with OH scavenger case during the first hour and a half, with a first order fit and 1 standard error uncertainties to provide a measure of the precision of the experimental set up.

A3.2 Measurements of $Hg^0_{(g)}$ in the four secondary organic aerosol systems each generated by ozone initiation of α-pinene, isoprene, and toluene: (a) dark; (b) UV light; (c) dark with 2-butanol OH scavenger; and, (d) UV light with 2-butanol OH scavenger. The measurements are compared with a numerical model which included ozone and OH oxidation.

CHAPTER 1

Introduction

1.1 Background

In addition to impacting atmospheric chemistry and physics, aerosols play an important role in climate (direct and indirect effects), and public health (Pöschl, 2005). Aerosols affect the Earth's radiative balance by absorption and scattering of aerosols, known as the direct effect (Charlson et al., 1992). Aerosols can act as cloud condensation nuclei (CCN); increased aerosol concentrations lead to enhanced CCN concentrations which increase cloud droplet, number concentrations and decrease cloud droplet size (Twomey, 1974). The results are increased cloud albedo and less frequent precipitation, known as first and second indirect effects, respectively (Twomey, 1974; Albrecht, 1989). Exposure to aerosols, particularly in fine size fraction (diameter<2.5 μm), has been associated with mortality, morbidity, and several cardiovascular, respiratory, and allergic diseases (Folinsbee, 1992; Pöschl, 2005).

Parameters such as size, morphology, concentration, and composition dictate these various effects (Pöschl, 2005). Aerosols are composed of mainly carbonaceous species (elemental and organic carbon), inorganic ions (sulfate, ammonium, and nitrate being dominant), and heavy metals. The contribution of these species to aerosol mass varies spatially and temporally.

Carbonaceous aerosols

The distinction and quantification of elemental (EC) and organic (OC) carbon is based on thermal-optical methods of analysis (Birch and Cary, 1996). Elemental carbon

is only emitted directly while particulate OC is both emitted by primary sources and formed via secondary processes. EC (because of its black carbon fraction) absorbs light efficiently and has a direct effect on climate. Elemental carbon also provides a surface for heterogenous reactions (Andreae and Crutzen, 1997; Grassian, 2001). Particulate organic carbon, composed of primary (POC) and secondary (SOC) fractions, is generated as a result of both anthropogenic and natural sources (Jacobson et al., 2000). Some specific OC constituents, such as polycyclic aromatic hydrocarbons (PAHs), have known adverse health effects (Kameda et al., 2005). Organic aerosols contribute to indirect climate forcing, facilitate or inhibit water condensation, and play a role in visibility degradation through scattering (Jacobson et al., 2000; Raymond and Pandis, 2002; Twohy et al., 2005). Primary (POA) or secondary organic aerosol (SOA) has been reported to be dominant depending on the location as well as the clean versus polluted days (Donahue et al., 2009 and references therein). The classification POA and SOA is particularly helpful in designing air pollution controls. Though traditionally thought as non-volatile and non-reactive, POA has recently been reported to undergo further oxidation as well as volatilization (Robinson et al., 2007).

Secondary organic aerosols

Secondary organic aerosols (SOA) are formed from the homogenous nucleation or the condensation of non- or semi-volatile oxidation product of volatile organic compounds (VOCs). These products are formed from the oxidation of VOCs (emitted from biogenic and anthropogenic sources) by hydroxyl (OH) and nitrate (NO_3) radicals, ozone (O_3), and halogens (Griffin et al. 1999a; Presto et al. 2005a, 2005b; Ng et al.

2007a, 2007b; Cai and Griffin, 2006). The atmospheric SOA burden from biogenic precursors alone has been estimated to be 18.5 Tg y^{-1} (Griffin et al., 1999b). However, the range of SOA formation in the atmosphere is quite large (12 to 70 Tg y^{-1}, Kanakidou et al., 2005), and models actually tend to underestimate SOA formation in the atmosphere (Volkamer et al., 2006). This is because many VOCs with the potential to form SOA are either unidentified (Goldstein and Galbally, 2007) or yet to be incorporated in the aerosol models (Heald et al., 2005). For example, the polycyclic aromatic hydrocarbons are one of the compound classes explored only recently with respect to SOA formation (Chan et al., 2009; Shakya and Griffin, 2010). In addition, most recently reported SOA in ambient air from semi-volatile (SVOC) or intermediate volatility (IVOC) organic compounds also are the missing SOA precursors in the atmosphere (de Gouw et al., 2011).

Water-soluble organic carbon (WSOC)

The solubility of aerosols is an important parameter that indicates the capability of aerosols to act as CCN. These water-soluble organic aerosols can act as CCN either alone or mixed with inorganic species (Twohy et al., 2005) and have important implications on climate. Water-solubility of aerosols affects their wet and dry deposition processes and determines their lifetime (Kanakidou et al., 2005). Saxena and Hildemann (1996) listed dicarboxylic acids, dicarbonyls, ketoacids, polyols, hydroxyamines, amino acids, nitrophenol, and multifunctional compounds such as malic acid, citric acid, and glyceraldehydes as the most important species in WSOC.

Organic material remains the least characterized component of aerosol (Kanakidou et al., 2005; Fuzzi et al., 2006). Proton nuclear magnetic resonance (H^+-

NMR) spectroscopy is a technique used recently to characterize the aerosol WSOC and has the advantage of accounting for a large fraction (>90%) of the carbon compared to traditional gas chromatograph - mass spectrometry (<20%) (Decesari et al., 2000; 2001).

Stable carbon and nitrogen isotope

Stable carbon and nitrogen isotopes of aerosols are another important property that can provide insight into aerosol sources and processing and atmospheric input into the biogeochemical cycles (Jacobson et al., 2000; Cachier et al., 1986; Cachier, 1989). Two stable carbon isotopes, ^{13}C and ^{12}C in carbon dioxide (CO_2) have an abundance of 1.1 and 98.9%, respectively (O'Leary, 1988), while two stable nitrogen isotopes, ^{15}N and ^{14}N in nitrogen (N_2) have an abundance of 0.366 and 99.643%, respectively (IUPAC, 1991). Carbon isotope fractionation occurs for plants depending on habitat and photosynthetic pathways, with land plants having the lower carbon isotope ratio of ^{13}C to ^{12}C by about 20‰ and marine plants by 10‰ and C_3 plants having $\delta^{13}C$ of about -28‰ and C_4 plants having about -14‰ (Smith and Epstein, 1971).

The basis for the carbon isotope fractionation in C_3 and C_4 plants lies within different mechanisms of carbon dioxide (CO_2) uptake and the distinct pathways (Calvin-Benson cycle for C_3 plants and Hatch-Slack cycle for C_4 plants) used for CO_2 fixation in these plants (O'Leary, 1988). Variation in $\delta^{13}C$ also occurs depending on the processing of SOA precursors (Irei et al., 2006) and marine or continental influence (Cachier, 1989). Thus, the variability of stable carbon isotopes can be used as a tool to study the aerosol characteristics originating from different sources using the distinct isotopic signatures in different emission sources (Cachier, 1989). However, the processing of aerosols and

precursor gases might also affect the stable isotope values. Stable carbon isotopes of aerosols emitted from biomass burning also can distinguish C_3- from C_4-plants because aerosols originating from burning of C_3-plants are 0.5‰ larger and those from C_4-plants are 3.5‰ smaller in $\delta^{13}C$ (Turekian et al., 1998).

The nitrogen isotope composition of aerosols also helps to identify sources, which has implications in air pollution management and the understanding of atmospheric deposition of nitrogen to terrestrial and marine ecosystems. Cornell et al. (1995) observed lower $\delta^{15}N$ in nitrogenous material in rain from remote compared to developed locations and in inorganic nitrogen (NO^{3-} and NH_4^+) compared to organic nitrogen compounds. In a study of atmospheric nitrate deposition in the Midwestern and Northeastern United States, Elliott et al. (2007) observed the strong correlation of $\delta^{15}N$ with nitrogen oxide (NO_x) emissions from the surrounding stationary sources, suggesting the stationary sources to be the most important source of atmospheric total reactive nitrogen species (NO_y) deposition inputs to the landscape of the Eastern United States, rather than vehicular emissions as suggested by the monitoring data alone.

Lignins

Lignins are the collective phenylpropanoid macromolecules that form the major structure of vascular plants (Hatfield and Vermerris, 2001). Chemically, lignins are made up of the polymers from three aromatic alcohols (*p*-coumaryl, coniferyl, and sinapyl alcohols), and also the phenolics (Hatfield and Vermerris, 2001). After cellulose, lignins are the most abundant naturally occurring polymers. Besides providing a defense mechanism to plants by supporting the plant cell walls, lignins facilitate water transport

and impede the degradation of wall polysaccharides. Lignins are relatively resistant to biodegradation compared to other plant materials such as cellulose and hemicellulose and are the best preserved component of vascular plants in environmental samples (Louchouarn et al., 2010).

Biological materials in carbonaceous aerosols remain poorly studied, and the contribution of lignins to ambient aerosols is yet to be investigated. Analysis of lignin oxidation products (LOPs) using a CuO oxidation method can provide important information on both natural background aerosol concentrations and plant-combustion derived aerosols. Free lignin-derived phenols have long been used as tracers of biomass burning in aerosols (Simoneit, 2002). Furthermore, LOPs in aerosols can reflect various characteristics of the source plants (gymnosperms or angiosperms, herbaceous or woody species, fresh or altered materials, etc.) (Hedges and Mann, 1979; Opsahl and Benner, 1995).

1.2 Research objectives and approach

The main objective of this thesis is to characterize ambient aerosols using different analytical methods with a focus on organic aerosols. Analytical instruments include a Sunset EC and OC analyzer, a total carbon analyzer, an ion chromatograph, an isotope ratio mass spectrometer, a proton nuclear magnetic resonance spectroscopy, and a gas chromatography-mass spectrometry. Sampling site in Kathmandu, Nepal is chosen as a representative of urban location. Sampling locations in Durham, New Hampshire and Houston, Texas are the representatives of a semi-rural and an urban location,

respectively, and also have the advantage of having several other air quality and meteorology parameters available.

Chapter 2 describes the characterization of aerosols in an urban location in Kathmandu, Nepal, to provide the base information on composition, concentration, and sources of aerosols. The comprehensive characterization of aerosols had not been performed previously in Kathmandu. Carbonaceous species, water-soluble organic carbon, inorganic ions, and stable carbon and nitrogen isotopes species were analyzed on aerosols collected during winter, and a principal component analysis and regression analysis was performed to identify the possible aerosol sources in Kathmandu. Hypotheses were that the ambient aerosols at this location are most likely to be influenced by primary sources, there would a good correlation of EC and OC, and most of OC would be contributed by POC. Less influence from biomass burning and some influence from the dust transport are assumed to be present at this site.

The objectives of chapter 3 and 4 are to study the seasonal variation in aerosol characteristics and to identify potential aerosol sources at a semi-rural location in New Hampshire. Chapter 3 focuses on examining the functional group composition of water-soluble organic aerosol by using H^+-NMR spectroscopy, and chapter 4 focuses on examining stable carbon and nitrogen isotopes to identify potential sources. Influences of environmental conditions such as air mass origin and meteorology also were investigated. Hypotheses included the dominance of secondary aerosol sources, and a strong seasonal variation in carbonaceous, water-soluble organic, and stable carbon ($\delta^{13}C$) and nitrogen ($\delta^{15}N$) isotopic composition of aerosols at this semi-rural site. The ambient aerosols are expected to be processed and aged, with the influence from air mass transport. It is also

hypothesized that the functional group composition of WSOC, and $\delta^{13}C$ and $\delta^{15}N$ in aerosols would be helpful in assigning the sources and understanding the aerosol formation processes.

The objective of Chapter 5 is to study primary biological aerosol material in an urban location in Houston. Lignin-derived phenols were quantified using a CuO oxidation method, and the taxonomic class of parent lignin macropolymers was identified using relative ratios of lignin oxidation products. Additionally, solvent-extracted free phenols and isomers of sugars were analyzed. Stable carbon and nitrogen isotope ratios and total carbon and nitrogen content in aerosols were also analyzed. Hypotheses include the dominance of lignin macropolymers in the coarse particles, and the less influence from biomass burning sources at this urban site.

Chapter 6 summarizes the main findings from the characterization studies at three different locations. It also includes suggestions for future work. The appendices include the chamber studies performed to quantify secondary organic aerosol from polycyclic aromatic hydrocarbons, and to investigate the influence of *in situ* SOA formation on the oxidation of gaseous elemental mercury by ozone, performed during the graduate research.

1.3 References

Albrecht, B.A. Aerosols, cloud microphysics, and fractional cloudiness. Science 245, 1227-1230, 1989.

Andreae, M.O. and Crutzen, P.J. Atmospheric Aerosols: Biogeochemical sources and role in atmospheric chemistry. Science 276, 1052-1058, 1997.

Birch, M.E., and Cary, R.A. Elemental carbon-based method for monitoring occupational exposures to particulate diesel exhaust. Aerosol Sci. Technol. 25, 221-241, 1996.

Cachier, H., Buat-Menard, P., Fontugne, M., and Chesselet, R. Long-range transport of continentally-derived particulate carbon in the marine atmosphere: evidence from stable carbon studies. Tellus 38B, 161-177, 1986.

Cachier, H. Isotopic characterization of carbonaceous aerosols. Aerosol Sci.Technol. 10,379-385, 1989.

Cai, X. and Griffin, R.J. Secondary aerosol formation from the oxidation of biogenic hydrcocarbons by chlorine atoms. J. Geophys. Res. 111, D14206, doi:1029/2005JD006857, 2006.

Chan, A.W.H.; Kautzman, K.E.; Chhabra, P.S.; Surratt, J.D.; Chan, M.N.; Crounse, J.D.; Kurten, A.; Wennberg, P.O.; Flagan, R.C.; Seinfeld, J.H. Secondary organic aerosol formation from photooxidation of naphthalene and alkylnaphthalenes: implications for oxidation of intermediate volatility organic compounds (IVOCs). Atmos. Chem. Phys. 9, 3049-3060, 2009.

Charlson, R.J., Schwartz, S.E., Hales, J.M., Cess, R.D., Coakley Jr., J.A., Hansen, J.E., and Hofmann, D.J. Climate forcing by anthropogenic aerosols, Science 255, 423-450, 1992.

Cornell, S., Rendell, A., and Jickells, T. Atmospheric inputs of dissolved organic nitrogen to the oceans. Nature 376, 243-246, 1995.

Decesari, S., Facchini, M.C., Fuzzi, S., Tagliavini, E. Characterization of water-soluble organic compounds in atmospheric aerosol: A new approach, J. Geophys. Res. 105, 1481-1489, 2000.

Decesari, S., Facchini, M.C., Matta, E., Lettini, F., Mircea, M., Fuzzi, S., Tagliavini, E., and Putaud, J.-P. Chemical features and seasonal variation of fine aerosol water-soluble organic compounds in the Po Valley, Italy. Atmos. Environ. 35, 3691-3699, 2001.

de Gouw, J.A. et al. Organic aerosol formation downwind from the deepwater horizon oil spill. Science, 331, 1295-1297, 2011.

Donahue, N.M., Robinson, A.L, and Pandis, S.N. Atmospheric organic particulate matter: From smoke to secondary organic aerosol. Atmos. Environ. 43, 94-106, 2009.

Elliott, E.M., Kendall, C., Wankel, S.D., Burns, D.A., Boyer, E.W., Harlin, K., Bain, D.J., and Butler, T.J. Nitrogen isotopes as indicators of NO_x source contributions to atmosphere nitrate deposition across the Midwestern and Northeastern United States. Environ. Sci. Technol. 41, 7661-7667, 2007.

Fuzzi, S., Andreae, M.O., Huebert, B.J., Kulmala, M., Bond, T.C., Boy, M., Doherty, S.J., Guenther, A., Kanakidou, M., Kawamura, K., Kerminen, V.-M., Lohmann, U., Russell, L.M., and Pöschl, U. Critical assessment of the current state of scientific knowledge, terminology, and research needs concerning the role of organic aerosols in the atmosphere, climate, and global change. Atmos. Chem. Phys. 6, 2017-2038, 2006.

Folinsbee, L.J. Human health effects of air pollution. Env. Health Persp., 100, 45-56, 1992.

Goldstein, A.H.; Galbally, I.E. Known and unexplored organic constituents in the earth's atmosphere. Environ. Sci. Technol. 41, 1514-1521, 2007.

Grassian, V.H. Heterogenous uptake and reaction of nitrogen oxides and volatile organic compounds on the surface of atmospheric particles including oxides, carbonates, soot and mineral dust: implications for the chemical balance of the atmosphere. Int. Reviews Phys.Chem. 20, 467-548, 2001.

Griffin, R.J., Cocker III, D.R., Flagan, R.C., and Seinfeld, J.H. Organic aerosol formation from the oxidation of biogenic hydrocarbons. J. Geophys. Res. 104, D3, 3555-3567, 1999a.

Griffin, R.J., Cocker III, D.R., Seinfeld, J.H., and Dabdub, D. Estimate of global atmospheric organic aerosol from oxidation of biogenic hydrocarbons. Geophys. Res. Lett. 26, 2721-2724, 1999b.

Hatfield, R. and Vermerris, W. Lignin formation in plants. The dilemma of linkage specificity. Plant Physiol. 126, 1351-1357, 2001.

Hedges, J.I. and Mann, D.C. The characterization of plant tissues by their lignin oxidation products. Geochim. Cosmochim. Acta 43, 1803-1807, 1979.

Heald, C.L., Jacob, D.J., Park, R.J., Russell, L.M., Huebert, B.J., Seinfeld, J.H., Liao, H., and Weber, R.J. A large organic aerosol source in the free troposphere missing from current models. Geophys. Res. Lett. 32, L18809, doi: 10.1029/2005GL023831, 2005.

Irei, S., Huang, L., Collin, F., Zhang, W., Hastie, D., and Rudolph, J. Flow reactor studies of the stable carbon isotope composition of secondary particulate organic matter generated by OH-radical-induced reactions of toluene. Atmos. Environ. 40, 5858-5867, 2006.

IUPAC. Isotopic compositions of the elements 1989. Pure Appl. Chem. 63, 991-1002, 1991.

Jacobson, M.C., Hansson, H.C., Noone, K.J., and Charlson, R.J. Organic atmospheric aerosols: Review and state of the science. Rev. Geophy. 38, 2: 267-294, 2000.

Kameda, Y., Shirai, J., Komai, T., Nakanishi, J., and Masunaga, S. Atmospheric polycyclic aromatic hydrocarbons: size distribution, estimation of their risk and their depositions to the human respiratory tract. Sci. Tot. Environ. 340, 71-80, 2005.

Kanakidou, M., Seinfeld, J.H., Pandis, S.N., Barnes, I., Dentener, F.J., Facchini, M.C., Van Dingenen, R., Ervens, B., Nenes, A., Nielsen, C.J., Swietlicki, E., Putaud, J.P., Balkanski, Y., Fuzzi, S., Horth, J., Moortgat, G.K., Winterhalter, R., Myhre, C.E.L., Tsigaridis, K., Vignati, E., Stephanou, E.G., and Wilson, J. Organic aerosol and global climate modeling: A review. Atmos. Chem. Phys. 5, 1053-1123, 2005.

Louchouarn, P., Amon, R.M.W., Duan, S., Pondell, C., Seward, S.M., White, N. Analysis of lignin-derived phenols in standard reference materials and ocean dissolved organic matter by gas chromatography/tandem mass spectrometry. Mar. Chem.118, 85-97, 2010.

Ng, N.L., Chaabra, P.S., Chan, A.W.H., Surratt, J.D., Kroll, J.H., Kwan, A.J., McCabe, D.C., Wennberg, P.O., Sorooshian, A., Murphy, S.M., Dalleska, N.F., Flagan, R.C., and Seinfeld, J.H. Effect of NO_x level on secondary organic aerosol (SOA) formation from the photooxidation of terpenes. Atmos. Chem. Phys. 7, 5159-5174, 2007a.

Ng, N.L., Kroll, J.H., Chan, A.W.H., Chhabra, P.S., Flagan, R.C., and Seinfeld, J.H. Secondary organic aerosol formation from m-xylene, toluene, and benzene. Atmos. Chem. Phys. 7, 3909-3922, 2007b.

O'Leary, M.H. Carbon isotopes in photosynthesis. BioSci. 38, 328-336, 1988.

Opsahl, S. and Benner, R. Early diagenesis of vascular plant tissues: Lignin and cutin decomposition and biogeochemical implications. Geochmi. Cosmochim. Acta, 59, 4889-4904, 1995.

Pöschl, U. Atmospheric aerosols: Composition, transformation, climate and health effects. Angew. Chem. Int. Ed. 44, 7520-7540, 2005

Presto, A.A., Huff Hartz, K.E., and Donahue, N.M. Secondary organic aerosol production from terpene ozonolysis. 1. Effect of UV radiation. Environ. Sci. Technol. 39, 7036-7045, 2005a.

Presto, A.A., Huff Hartz, K.E., Donahue, N.M. Secondary organic aerosol production from terpene ozonolysis. 2. Effect of NO concentration. Environ. Sci. Technol. 39, 7046-7054, 2005b.

Raymond, T.M. and Pandis, S.N.: Cloud activation of single-component organic aerosol particles, J. Geophys. Res. 107, D24, 4787, doi: 10.1029/2002JD002159, 2002.

Robinson, A.L., Donahue, N.M., Shrivastava, M.K., Weitkamp, E.A., Sage, A.M., Grieshop, A.P., Lane, T.E., Pierce, J.R., and Pandis, S.N. Rethinking organic aerosols: Semivolatile emissions and photochemical aging. Science 315, 1259, doi: 10.1126/science.1133061, 2007.

Saxena, P. and Hildemann, L.M. Water-soluble organics in atmospheric particles: a critical review of the literature and application of thermodynamics to identify candidate compounds. J. Atmos. Chem. 24, 57-109, 1996.

Shakya, K.M. and Griffin, R.J. Secondary organic aerosol from photooxidation of polycyclic aromatic hydrocarbons. Environ. Sci. Technol. 44, 8134-8139, 2010.

Simoneit, B.R.T. Review. Biomass burning – a review of organic tracers for smoke from incomplete combustion. Appl. Geochem. 17, 129-162, 2002.

Smith, B.N. and Epstein, S. Two categories of $^{13}C/^{12}C$ ratios for higher plants. Plant Physiol. 47, 380-384, 1971.

Turekian, V.C., Macko, S., Ballentine, D., Swap, R.J., and Garstang, M. Causes of bulk carbon and nitrogen isotopic fractionations in the products of vegetation burns: laboratory studies. Chem. Geol. 152, 181-192, 1998.

Twohy, C.H., Anderson, J.R., and Crozier, P.A. Nitrogenated organic aerosols as cloud condensation nuclei, Geophys. Res. Lett., 32, L19805, doi:10.1029/2005GL023605, 2005.

Twomey, S. Pollution and the planetary albedo. Atmos. Environ. 8, 1251-1256, 1974.

Volkamer, R., Jimenez, J.L., Martini, F.S., Dzepina, K., Zhang, Q., Salcedo, D., Molina, L.T., Worsnop, D.R. and Molina, M.J. Secondary organic aerosol formation from anthropogenic air pollution: Rapid and higher than expected. Geophys. Res. Lett. 33, L17811, doi:10.1029/2006GL026899, 2006.

CHAPTER 2

Characteristics and sources of carbonaceous, ionic, and isotopic species of wintertime atmospheric aerosols in Kathmandu Valley, Nepal

Reference: Shakya, K.M., Ziemba, L.D., and Griffin, R.J. *Aer. Air Qual. Res.* 10, 219-230, 2010.

Abstract

To investigate the air pollution from aerosols in Kathmandu during winter, bulk aerosol samples were collected during winter 2007-2008 to characterize carbonaceous and ionic species and carbon and nitrogen isotopes. This study illustrates the applications of carbon and nitrogen isotope data for characterizing aerosols and their implications for identifying sources that were inconsistent with the results for the carbonaceous and ionic aerosols. Mean concentrations of organic carbon (OC), elemental carbon (EC), and water soluble organic carbon (WSOC) in Kathmandu during the period were 20.02 ± 6.59 (1σ), 4.48 ± 1.17, and 10.09 ± 3.64 μgC m^{-3}, respectively. Elemental carbon and OC were correlated (R^2 = 0.56), likely indicating common sources for both species, as well as for the precursors that led to the formation of secondary organic carbon (SOC). The mean estimated SOC contribution to OC was 31%, suggesting that local emission is more important than transport and processing during winter in Kathmandu. On average, 50% of the OC was water soluble, and the correlation of SOC with WSOC (R^2 = 0.66) suggests that the majority of SOC and some primary organic carbon (POC) were water soluble in Kathmandu. The mean $\delta^{13}C$ of –25.74 ± 0.19‰ observed in aerosols of Kathmandu

confirms consistent anthropogenic sources such as fossil fuel combustion. Heavier carbon also was observed to be associated with the water-soluble fraction of OC in aerosols. The mean $\delta^{15}N$ of 9.45 ± 0.87‰ suggests the limited influence of biomass burning and its strong correlation with crustal cations Ca^{2+} (R^2 = 0.74, $p<0.05$) and Mg^{2+} (R^2 = 0.71, $p<0.05$) indicates distant sources. Principal component analysis revealed four major sources/pathways for particles: local and vehicular emissions, secondary gas-to-particle conversion, aqueous processing, and dust transport, each explaining ~ 39, 23, 11, and 9% of the variance.

2.1 Introduction

Respiratory ailments, including cough and bronchitis (Folinsbee 1992), have been associated with particulate matter (PM), which also affects climate directly and indirectly and reduces visibility. Visibility reduction and the direct effect are related to absorption and scattering of radiation by aerosols (Charlson 1969; Charlson et al. 1992). The indirect effect is related to alteration of cloud albedo (Twomey 1974) and lifetime through particles acting as cloud condensation nuclei and ice nuclei.

Carbonaceous aerosol species include elemental carbon (EC) and organic carbon (OC), where this distinction typically is based on thermal analysis (Birch and Cary 1996). However, it should be stressed that EC is not equivalent to black carbon (BC), which is defined and measured based on optical properties and absorbs light more strongly than EC. Elemental carbon is a primary pollutant emitted directly from combustion sources that absorbs light efficiently (because a significant fraction is BC) and has a direct effect on the radiative balance of the Earth surface. Organic carbon aerosol is emitted directly

(known as primary OC or POC) and formed secondarily (known as secondary OC or SOC) from the partitioning to the condensed phase of semi- or non-volatile products of the oxidation of volatile organic compounds or by aqueous-phase processing. POC and SOC are generated from both anthropogenic and biogenic sources (Jacobson et al. 2000).

In addition to carbonaceous material, aerosols also include inorganic species, often as cations and anions in an aqueous phase. For example, oxidation of sulfur dioxide and nitrogen oxides leads to the formation of sulfate (SO_4^{2-}) and nitrate (NO_3^-) in aerosols via sulfuric and nitric acids, respectively. Ammonium (NH_4^+) ions buffer these acidic species, which typically exist in ambient aerosol as partially or fully neutralized salts. Inorganic species may also be emitted directly to the atmosphere in the particulate phase.

Stable carbon isotope ratios of ^{13}C to ^{12}C ($\delta^{13}C$) reveal the chemical fractionation associated with processes involved in PM formation such as photosynthesis, atmospheric oxidation (Jacobson et al. 2000), and phase changes. This ratio also reveals the relative contributions of C_3 (Calvin-Benson cycle) or C_4 (Hatch-Slack cycle) plants (Cachier 1989). Similarly, nitrogen isotope ratios can be used to characterize atmospheric aerosol (Turekian et al. 1998).

Kathmandu, the capital of Nepal, has a land area of 395 km^2, a rapidly increasing population of 1.08 million, and a vehicle usage rate that is growing by approximately 10 percent per year (CBS 2005; Faiz et al. 2006). The city is located inside a valley with restricted free wind movement, resulting in poor air quality, especially with regard to PM. For example, Aryal et al. (2009) observed concentrations of PM with diameters smaller than 2.5 micron ($PM_{2.5}$) of 90 ± 24 (1σ) μg m^{-3} during the 2006-2007 winter in Kathmandu. The main objective of this study is to characterize the winter ambient

aerosols of Kathmandu in terms of OC, EC, water-soluble organic carbon (WSOC), inorganic ions, and isotopes of carbon and nitrogen.

2.2 Materials and Methods

2.2.1 Sampling

Sampling was performed on the roof of a five-story building in urban Kathmandu where air quality likely is influenced mainly by vehicular emissions, as the vehicular traffic in the nearby roads remains heavy throughout the day. The sampling site is located in Sorhakhutte, Thamel, a main tourist area in Kathmandu. The volume of traffic on the roads of Kathmandu is estimated to be 100 to 500 vehicles per hour (CBS 2009).

Bulk aerosols were collected on quartz fiber filters (Whatman, QM-A) using a pump with a flow rate of 50 liters per minute. To reduce background contamination, all filters were pre-baked at 600°C for 24 hours and Teflon®-sealed in polyethylene dishes prior to sampling. The samples were collected for periods ranging from 18 to 24 hours depending on scheduled power outrages and rain events. Collected samples were also stored inside dishes that were Teflon®-sealed. Twenty-five samples and eight field blanks were collected from 26 December 2007 through 30 January 2008. The field blanks were collected after every two subsequent sample collections, and all data described subsequently are corrected by subtracting average values of field blanks. The storage, transportation, and analysis of field blanks were identical to those of samples. All the samples were stored in a freezer prior to shipment to the University of New Hampshire for analysis.

2.2.2 Analyses

EC and OC

Elemental and organic carbon were analyzed by a thermal/optical method using a 1.5-cm^2 filter punch in a Sunset EC/OC analyzer, as described by Birch and Cary (1996). Instrumental calibration was performed using succinic and phthalic acid standards. The associated uncertainties, calculated as two times the standard deviation of the eight field blanks using the average volume of air drawn for the sampling, were 0.24 and 0.12 μgC m^{-3} for OC and EC, respectively.

Secondary Organic Carbon (SOC)

Because EC can be used as an indicator of primary combustion emissions, the smallest observed ratio of OC to EC, $(OC/EC)_{minimum}$, provides an estimate of a typical ratio of POC to EC assuming no or very low contribution from non-combustion POC and residual SOC (Castro et al. 1999). This POC/EC ratio is assumed to be constant for a specific location for a specific period of time (Turpin and Huntzicker 1991). The secondary organic carbon (SOC) is then defined as:

$$SOC = OC - EC * (OC/EC)_{minimum} \quad (1)$$

where POC is the product of the observed EC and $(OC/EC)_{minimum}$. The contribution of SOC in the sample with minimum OC/EC is assumed to be negligible; the main source for EC and POC in this sampling site is assumed to be the emissions from fossil fuel combustion. Non-combustion related POC is assumed to be negligible (Castro et al. 1999).

Water Soluble OC (WSOC)

Three punches, each 1.5 cm^2, were cut from each filter and extracted with 15 ml of milli-Q water. The extract was shaken manually, allowed to sit passively for 10 minutes, and centrifuged for 10 minutes to separate the filter and aqueous solution. The aqueous solution was divided into aliquots, each of 5 ml. One aliquot was used to analyze WSOC using a total organic carbon analyzer (Model 800 TOC, Sievers). The related uncertainty, calculated as two times the standard deviation of the eight field blanks, using the average volume of air drawn for the sampling was 0.65 $\mu gC\ m^{-3}$.

Water-Soluble Ions

Sulfate, NO_3^-, nitrite (NO_2^-), chloride (Cl^-), and oxalate ($C_2O_4^{2-}$)) anions and ammonium (NH_4^+), potassium (K^+), magnesium (Mg^{2+}), and calcium (Ca^{2+}) cations were analyzed from one of the aliquots. Analysis was performed by ion chromatography (Dionex 500, Dionex Corp, Sunnyvale, California). Anions were analyzed with an AS22, 4X250-mm column equipped with ASRS 300, a 4-mm suppressor, and a 4.5-mM sodium carbonate/1.5-mM sodium bicarbonate eluent. Cations were analyzed with a CS12A, 4X250-mm column equipped with CSRS 300, a 4-mm suppressor, and an 18-mM methanesulfonic acid eluent. A conductivity detector was used for both anion and cation analysis. Sodium (Na^+) data were discarded due to probable contamination. Calibration was performed using mixed standards. The associated uncertainty values, calculated as two times the standard deviation of the field blanks using the average volume of air for sampling, were 0.01, 0.01, 0.06, and 0.03 $\mu g\ m^{-3}$ for Cl^-, NO_2^-, NO_3^-, and SO_4^{2-},

respectively, and 0.08, 0.16, 0.05, and 0.15 μg m^{-3} for NH_4^+, K^+, Mg^{2+}, and Ca^{2+}, respectively.

Molar hydrogen ion (H^+) concentration was calculated from an ion balance assuming that SO_4^{2-}, NO_3^-, and NH_4^+, and H^+ are the dominant ions that control the charge balance, particularly in fine particles (Schwab et al. 2004; Ziemba et al. 2007):

$$[H^+] = 2[SO_4^{2-}] + [NO_3^-] - [NH_4^+] \quad (2)$$

where the brackets represent molar concentrations. Assuming $[NH_4^+]$ is the only buffer counteracting the acidity in the aerosol, a neutralization ratio also was calculated by (Stevens et al. 1980; Ziemba et al. 2007):

$$f = \frac{[NH_4^+]}{2[SO_4^{2-}] + [NO_3^-]} \quad (3)$$

Carbon and Nitrogen Isotopes

For isotopic analyses, two punches cut from each filter were analyzed using a Costech Elemental Analyzer coupled to a Delta Plus XP Mass Spectrometer. The isotopic analysis was performed for the following eight samples in order to characterize a wide range of aerosol conditions (Total carbon (TC) is the sum of OC and EC.): maximum EC (12/27/07), minimum EC/TC and maximum OC and WSOC (01/05/08), maximum WSOC/OC (01/08/08), minimum WSOC/OC (01/19/08), maximum EC/TC (01/20/08), minimum EC, OC, and WSOC (01/30/08), and two randomly chosen (01/04/08 and 01/26/08). Carbon and nitrogen isotope ratios are calculated in per mil (‰) as follows (Turekian et al. 1998):

$$\delta Y = \left[\frac{R_{sample}}{R_{std}} - 1 \right] * 1000 \quad (4)$$

where Y = ^{13}C and $R = \frac{^{13}C}{^{12}C}$ for carbon and Y = ^{15}N and $R = \frac{^{15}N}{^{14}N}$ for nitrogen. The standard material was NIST 1515.

Statistical Analyses

The statistical software package JMP version 7.0.2 was used for statistical analyses. These analyses included linear regression and a principal component analysis (PCA) including factor rotation.

2.2.3 Meteorological Data

Meteorological data (maximum and minimum temperature and relative humidity (RH)) were taken from the archived report of the meteorological forecasting division of the Nepalese government (MFD 2008). These parameters are included in the PCA. Temperature data are included in Figure 2.1.

2.3 Results

2.3.1 OC and EC

The daily concentrations of EC and constituents of OC during the sampling campaign are shown in Figure 2.1 and summarized in Table 2.1. Mean concentrations of OC and EC (with its standard deviation) were 20.02 ± 6.59 and 4.48 ± 1.17 μgC m^{-3}, respectively. On average, OC accounted for approximately 81% of the carbonaceous aerosol. Overall, there was a decreasing trend for both EC and OC during the sampling period. Despite a stronger decreasing overall trend (Figure 2.1) in OC, OC and EC

showed a correlation with R^2 of 0.56 (Figure 2.2), suggesting a common source for EC and OC. The OC/EC ratio ranged between 3.01 and 6.59, with an average of 4.47 ± 0.93.

2.3.2 SOC

Using the observed $(OC/EC)_{minimum}$ of 3.01, which occurred on the day following the one significant rain event during the sampling period, Equation (1) yields SOC concentrations in the range of 0 to 18.45 μgC m^{-3}, with an average of 6.81 ± 4.48 μgC m^{-3}. Daily POC and SOC concentrations are also shown in Figure 2.1 and Table 2.1. On average, SOC constituted 31% of OC, with POC accounting for the remaining 69%. Overall SOC also has a decreasing trend during the sampling campaign. Total organic aerosol mass concentrations were calculated by summing the POC and SOC after multiplying each by 1.2 and 2.0, respectively (Turpin and Lim, 2001). The mean organic aerosol mass concentration was 29.26 ± 11.24 μgC m^{-3}.

2.3.3 WSOC

The mean concentration of WSOC was 10.09 ± 3.64 μgC m^{-3} (Figure 2.3 and Table 2.1). Throughout the study period, WSOC accounted for a large portion of OC, with WSOC/OC ranging from 0.39 to 0.60, with an average of 0.50 ± 0.06. A scatter plot of WSOC versus SOC shows significant correlation ($R^2 = 0.66$, $p<0.0001$) (Figure 2.4).

2.3.4 Water Soluble Ions

The dominant anions were SO_4^{2-}, NO_3^-, Cl^-, and $C_2O_4^{2-}$ with average concentrations of 3.16 ± 1.04, 1.80 ± 0.63, 1.70 ± 0.38, and 0.12 ± 0.08 μg m^{-3},

respectively (Figure 2.5 and Table 2.1). Nitrite contributed negligibly overall, with an average concentration of 0.02 ± 0.01 μg m^{-3}. The dominant cations were Ca^{2+} and NH_4^+, with average concentrations of 1.16 ± 0.58 and 0.81 ± 0.46 μg m^{-3}, respectively (Figure 2.5 and Table 2.1). Potassium and Mg^{2+} were found to have smaller concentrations, with averages of 0.32 ± 0.47 and 0.07 ± 0.04 μg m^{-3}, respectively. Note again that Na^+ was not considered in this discussion.

The average ionic concentration was 9.06 ± 2.49 μg m^{-3}, and the mass of NH_4^+, SO_4^{2-}, and NO_3^- accounted for 64% of the total observed ionic mass concentration. Ammonium was correlated to both SO_4^{2-} (R^2 = 0.48, $p<0.005$) and NO_3^- (R^2 = 0.39, $p<0.001$). There was very little difference between median and mean. On average, ions accounted for 23% of the total observed aerosol concentration (ions and OM). On average, the aerosol $[H^+]$ (Figure 2.6) was calculated to be 49.99 ± 18.66 nmol m^{-3} and exhibited a large range of 9.14 to 84.32 nmol m^{-3}.

2.3.5 Carbon and Nitrogen Isotopes

The average $\delta^{13}C$ in the samples was –25.74 ± 0.19‰, and ranged from –26.05 to –25.51‰. The average $\delta^{15}N$ was 9.45 ± 0.87‰, and it varied from 8.13 to 10.56‰ (Table 2.1 and Figure 2.7). Isotopic content is compared to that measured elsewhere in Table 2.2.

2.4 Discussion

2.4.1 OC and EC

During the study period, OC exhibited greater temporal variability than EC, where Figure 2.1 indicates an overall decreasing trend in OC. A small decreasing trend in EC suggests, in general, consistent local primary emissions sources of aerosols and boundary layer dynamics. Because the majority of OC is POC, total OC follows trends similar to those for POC and EC. The strong correlation between EC and OC ($R^2 = 0.56$, $p<0.0001$) at the sampling site likely indicates a common source for EC and OC including the precursors that lead to SOC.

The average EC and OC of 4.49 and 20.02 μgC m^{-3}, respectively, in Kathmandu are comparable to those measured during winter in other urban Asian cities. Average EC and OC during winter of 2005 in Guangzhou, China, were 4.2 and 23.9 μgC m^{-3} and in Hong Kong were 2.5 and 12.4 μgC m^{-3}, respectively (Duan et al. 2007), and during winter of 2006 in Xi'an, China were 23.7 and 4.6 μg m^{-3}, respectively (Shen et al., 2009). Carrico et al. (2003) observed EC of 1.0 ± 0.7 μgC m^{-3} during October 1999 to January 2000 in Nagarkot, a site inside Kathmandu valley that is approximately 20 kilometers from the site of the current study.

In general, OC to EC ratios depend on emission sources and secondary organic aerosol formation. Hildemann et al. (1991) found OC/EC in fine particles of 2.2 for light-duty gasoline vehicles and 0.8 for heavy-duty gasoline vehicles. The OC/EC values in Kathmandu were larger than these ratios on all days. Cao et al. (2005) found an average OC/EC ratio of 4.1 for vehicle exhaust, a value close to that observed in Kathmandu. Thus, the common source is most likely vehicular emissions. The variation of OC/EC

during the sampling period and the values larger than 3.01 indicate the importance of SOC, assuming no fluctuations in emission ratios.

Emission from vehicles appears to be one of the most important sources of aerosols. Kondo et al. (2005) also concluded that the transport-related emissions are the main sources of air pollution in Kathmandu valley, which is further corroborated by the observations of Panday and Prinn (2009) that showed peaks in concentrations of PM_{10} during the mornings from 2004 to 2005. Further, they observed more concentrated air pollution during winter compared to summer. In Kathmandu, numerous poorly maintained and old vehicles and low-grade and adulterated fuel are often the norms (Faiz et al. 2006). Poor road conditions also contribute to emissions related to vehicle use. The total length of road in Kathmandu is 1279.09 km, of which only about 40% is paved (CBS 2009). In 2005, PM_{10} emission from vehicular activities and suspension of road dust in Kathmandu valley is estimated to be 7890 tons/year (62% of total PM_{10}). The contribution from industrial sources was estimated to be approximately 17% (ICIMOD 2007). In comparison, Cao et al. (2005) attributed approximately 73% and 23% of TC in Xi'an, Shaanxi Province, China during fall 2003 to gasoline and diesel engine exhaust, respectively, while only 44% and 3% of TC during winter 2003-2004 to gasoline and diesel engine exhaust, respectively.

Open waste burning practices are also an important source contributing to the aerosol loadings in Kathmandu. Refuse burning was estimated to emit approximately 172 tons of PM_{10} in 2005 in Kathmandu valley (ICIMOD 2007). In addition, protests called by various groups often include the burning of vehicle tires on the streets, emitting CO,

SO_2, and NO_2 (Shakya et al. 2008); uncontrolled tire fires may also be significant aerosol sources in Kathmandu.

2.4.2 SOC

The average observed percent contribution of secondary OC to carbonaceous aerosol in Kathmandu (31%) is smaller than but comparable to values observed in other urban Asian cities, though it should be noted here that the values presented in this study likely represent a lower bound because some SOC could have been present during the period associated with the minimum OC/EC ratio. Lin and Tai (2001) reported that the SOC contribution to OC was larger in $PM_{2.5}$ (40%) compared to PM_{10} (32.4%) during November 1998 to April 1999 in Kaohsiung City, Taiwan. In Guangzhou, China, the average SOC concentration during winter 2005 was 11.5 $\mu gC\ m^{-3}$ (Duan et al. 2007), which is larger than that observed in Kathmandu. During winter 2006-2007 in Tianjin, China, Li et al. (2009) observed SOC contribution to OC of 37.3-50.3% compared to mean of ~34% observed in Kathmandu. The majority of OC was primary in nature in Kathmandu, comparable to the measurements made in the San Joaquin Valley of California, where secondary contributions to OC were smaller in winter due to decreased mixing heights and photochemistry (Strader et al. 1999). The smaller percentage of SOC relative to OC suggests that motor vehicles and other local emissions (as opposed to transport and processing) are the major factors controlling concentrations of carbonaceous aerosols. However, the strong relationship between OC and EC ($R^2 = 0.56$) indicates that any SOC likely was derived from volatile organic compounds co-emitted with POC and EC.

2.4.3 WSOC

The correlation of WSOC with SOC (R^2 = 0.66 and slope of approximately unity, Figure 2.4) indicates the likelihood that a large fraction, if not all, of the SOC is WSOC. Like OC, there was an overall decreasing trend in WSOC during the sampling; no such trend was observed for WSOC/OC. WSOC/OC was observed to be the smallest (0.39) during the rain event (4.9 mm) on 19 January 2008, likely indicating favorable wet deposition of WSOC and decreased photochemical processing. WSOC did not show any significant correlation with SO_4^{2-} and only a weak correlation with NO_3^- (R^2 = 0.31, $p<0.005$). The lack of significant correlation of WSOC with SO_4^{2-} and NO_3^- indicates that WSOC likely is formed primarily via pathways that are different than those for SO_4^{2-} and NO_3^-. This is in stark contrast to the strong correlation between WSOC and SO_4^{2-} and NO_3^- observed in urban and suburban sites in Nanjing, China (Yang et al. 2005).

The non-zero intercept (i.e. –3.57) in Figure 2.4 underscores that some fraction of the POC in Kathmandu is likely water-soluble. If it is assumed that all SOC is WSOC, the fraction of POC that is WSOC can be found by (WSOC-SOC)/POC. This value, on average, is 0.26, likely a lower bound because not all SOC will definitively be WSOC. In Houston, Anderson et al. (2008) also noted an increase in particulate WSOC associated with rush hour, suggesting a primary source for WSOC. A large WSOC fraction is usually assumed to be indicative of processed aerosol or SOA (Sullivan et al. 2004; Weber et al. 2007). The average ratio of WSOC to OC (~0.18) in Lahore, Pakistan during spring 2006 with very large average PM_{10} concentrations (459 $\mu g\ m^{-3}$) mainly as a result of vehicular activities (Zhang et al., 2008) was smaller than the observed ratio of ~0.50 in the present study.

2.4.4 Water Soluble Inorganic Ions

Because K^+, a tracer of biomass burning, was found in small concentrations, biomass burning seems to have a small influence on aerosol mass loadings in Kathmandu in winter. However, K^+ increased significantly after 25 January 2008, possibly because of the influence of biomass burning after this day. The average K^+/EC before 01/25/08 was very small (0.03). A K^+/EC ratio of 0.03 was also observed in a location influenced by vehicular emissions in Auckland, New Zealand (Wang et al. 2005). The average ratio of K^+ to total ionic aerosols was less than 0.14%, compared to 7.3% observed during winter 2006-2007 in Tianjin, China (Li et al., 2009). However, the ratio increased unusually to ~24% on 28 January 2008. Fires made by street vendors for heat during winter and open refuse burning may have played a role in increased K^+ concentrations at the end of the campaign.

The strong correlation of Ca^{2+} with Mg^{2+} ($R^2 = 0.59$, $p<0.0001$) suggests crustal sources of aerosols in Kathmandu. Carrico et al. (2003) also reported the influence of dust transport inside Kathmandu valley from a Saharan region. The influence of dust transport was highly variable, with Ca^{2+} and Mg^{2+} contribution to total ionic aerosols ranging from 6 to 22%.

Sulfate was significantly correlated with NH_4^+ ($R^2 = 0.48$, $p<0.005$). The average winter SO_4^{2-} concentration in Kathmandu (3.16 $\mu g\ m^{-3}$) was smaller than the annual mean SO_4^{2-} observed in Seoul (8.70 $\mu g\ m^{-3}$) (Lee et al. 1999) and larger than in Nagarkot, Kathmandu valley (2.5 $\mu g\ m^{-3}$) (Carrico et al. 2003). The neutralization ratio ranged from 0.15 to 0.92 during the campaign and had a mean of 0.45 ± 0.19. Clearly, NH_4^+ was not

sufficient to neutralize the aerosols, which were most likely acidic unless they were neutralized by compounds other than NH_4^+.

Daily aerosol acidity ranged from 9.14 to 84.32 nmol m^{-3} in Kathmandu during winter. This is larger than the mean H^+ concentration observed in Seoul during fall (5.19 nmol m^{-3}) (Lee et al. 1999). Peak [H^+] concentration coincided with those of SO_4^{2-} and NO_3^-. The molar ratio of H^+ to SO_4^{2-} was found to range from 0.31 to 2.35. Lee et al. (1999) observed a range for the H^+ to SO_4^{2-} ratio of 0.013 to 0.184 during fall in Seoul with the presence of $(NH_4)_2SO_4$ and $(NH_4)_3H(SO_4)_2$.

Organic mass (OM) to SO_4^{2-} ratios are compared to H^+ and EC concentrations in Figure 2.6. The maximum OM/SO_4^{2-} (19.31) occurred on 5 January 2008, which also had the smallest [H^+] (9.15 nmol m^{-3}) and the largest OC, SOC, WSOC, OC/EC, and OM. The minimum OM/SO_4^{2-} ratio (4.53) was observed on 30 January 2008, associated with [H^+] of 67.53 nmol m^{-3}. The largest H^+ (nmol m^{-3}) was observed on 17 January 2008 with the smallest OC, SOC, WSOC, and OM. During the day (20 January 2008) with one of the smallest OM to SO_4^{2-} ratios (4.74), one of the highest $\delta^{13}C$ (-25.6‰) also was observed. In a rural location with biogenic influence, Ziemba et al. (2007) reported larger OM/SO_4^{2-} (6.4) and smaller H^+ (1.7 nmol m^{-3}), attributed to stronger biogenic influence and less photochemical aging, and a smaller OM/SO_4^{2-} (0.4 and 0.6) and larger H^+ (69 and 56 nmol m^{-3}), attributed to anthropogenic influence and photochemical aging.

2.4.5 Carbon and Nitrogen Isotopes

The aerosol data indicate that Kathmandu is polluted and that the dominant source most likely is fossil fuel combustion. In such an area, smaller $\delta^{13}C$ values are expected

(Cachier 1989). Furthermore, Cachier (1989) found mean $\delta^{13}C$ values of –25.5 and –26.5‰ for industrial and vegetation combustion, respectively, compared to –22.5‰ for vegetative emission. The mean $\delta^{13}C$ of -25.74‰ in the samples is consistent with a dominant fossil fuel combustion source, and is comparable to the values observed in aerosols collected from urban areas (Table 2.2). The minimum $\delta^{13}C$ (-26.05‰) was observed on 8 January 2008, with the maximum WSOC/OC, while the maximum $\delta^{13}C$ (-25.51‰) was observed on 19 January 2008, with the minimum WSOC/OC. Though $\delta^{13}C$ was not correlated to WSOC, it had a strong correlation with WSOC/OC ($R^2 = 0.79$; $p<0.01$) indicating its association with water-soluble fraction of OC and that the variation in $\delta^{13}C$ may be linked to processing. The little variation in these samples, however, indicates the consistent source of carbonaceous material. The mean $\delta^{13}C$ observed in Kathmandu is comparable to the observations made in other urban and anthropogenically influenced locations around the world (Table 2.2).

The mean $\delta^{15}N$ (9.45 ± 0.87‰) observed in this study is comparable to the aerosol samples collected from Paris during winter (10.00 ± 3.4‰) (Widory 2007). The maximum $\delta^{15}N$ (10.31‰) was observed on 5 January 2008, associated with maximum OC and WSOC and minimum EC/TC. The minimum $\delta^{15}N$ (8.13‰) was observed on 30 January 2008 with minimum EC, OC, and WSOC. There was a strong correlation of $\delta^{15}N$ with NH_4^+/NO_3^- ($R^2 = 0.84$, $p<0.005$) (Figure 2.8). Yeatman et al. (2001) observed the larger $\delta^{15}N$ (-1 to 7‰) in aerosol NO_3^- (10 to 12‰) compared to that in aerosol NH_4^+ from the samples collected next to vehicle sources in London. The correlation of $\delta^{15}N$ with crustal cations such as Ca^{2+} ($R^2 = 0.74$, $p<0.05$) and Mg^{2+} ($R^2 = 0.71$, $p<0.05$) indicates that heavier nitrogen isotopes and some associated nitrates may have originated

from distant sources related to dust. Because larger $\delta^{15}N$ values in aerosols indicate residual material from the combustion of vegetation (Turekian et al. 1998), the smaller $\delta^{15}N$ values observed in this study indicate the lack of an influence of biomass burning. Further, the aerosol sources from fuel oil and coal ($\delta^{15}N < 0‰$) are less likely because the aerosols in this study were enriched in ^{15}N (Widory 2007).

2.4.6 Principal Component Analysis (PCA)

The PCA found four factors with Eigenvalues greater than unity that explained a combined 82.2% of the variance in the data (Table 2.3). Factor 1 explained the most of the variance, 38.7%, and had strong loadings of EC, POC, SOC, WSOC, Cl^-, and maximum temperature. Factor 1 is attributed to the primary local sources, mainly from vehicular emissions. Interestingly, it had a high negative loading of K^+, suggesting the role of biomass burning when local vehicular emission sources decrease. During the end of the sampling campaign, the smallest values for carbonaceous aerosol concentrations were observed, and K^+ values peaked. Factor 2, with strong loadings from NH_4^+ and NO_3^- explained an additional 23.0% of the variance. This factor appears to be associated with secondary aerosol formation via gas-to-particle partitioning. Factor 3, with strong loadings from SO_4^{2-}, RH, and minimum temperature likely represents aqueous processing and accounts for 11.4% of the variance. Interestingly, minimum temperature and RH fall in this category, possibly suggesting the sensitivity of aqueous phase oxidation of SO_2 to RH levels and the relationship between minimum temperature and RH. Moreover, the dominance of SO_4^{2-} together with RH in factor 3 may mean that the major pathway for SO_4^{2-} formation in this locality is mainly through heterogenous reactions (Kai et al.

2007). The strong loadings of mineral aerosols (Ca^{2+} and Mg^{2+}) indicate that Factor 4 is associated with transport of dust. This factor explained an additional 9.1% of the variance. However, the loading of NH_4^+ in this factor is minor, and thus, the transport of NH_4^+ with dust also appears to be minor. In summary, the PCA performed on this data shows that primary local emissions from vehicular activity had the strongest influence on particle concentrations at this site during winter, followed by secondary processing and long-distance dust transport.

2.5 Conclusions

Kathmandu, the capital of Nepal, experiences very large levels of air pollution due to urbanization and being located inside a valley. In winter, the capacity of aerosols to accumulate in ambient air increases in the absence of major deposition processes such as precipitation. Thus, this study was carried out to gain information regarding the composition, concentration, and sources of aerosols in Kathmandu winter. The daily OC/EC ratio varied between 3.01 and 6.59. Correlation of EC and OC ($R^2 = 0.56$), large POC contribution to carbonaceous aerosol, and smaller $\delta^{13}C$ (–25.74 ± 0.19‰) all imply that local vehicular emission is the single most important source in Kathmandu. Principal component analysis revealed that other important sources/pathways include dust transport and secondary processing. The strong correlation of Ca^{2+} and Mg^{2+} ($R^2 = 0.59$) supports some crustal aerosol sources for the transported dust. Biomass burning did not play a significant role in aerosol formation/emissions, except at the end of the sampling period.

Most (69%) of the observed OC was estimated to be primary. About half of the OC observed in Kathmandu was water-soluble, with contributions from both SOC and

POC. Ionic concentrations are approximately a factor of two smaller than those of organic carbon and are dominated by SO_4^{2-}, NO_3^-, and NH_4^+. The neutralization ratio indicated that the aerosols in Kathmandu are acidic in nature, as NH_4^+ was not sufficient to neutralize the acidity in fine particles. Sulfates were the dominant ion, confirming the anthropogenic source of aerosols. Analysis of carbon isotopes indicates fossil fuel combustion sources, while nitrogen isotopes indicate transport from distant sources and minimal influence from biomass burning.

2.6 References

Anderson, C., Dibb, J.E., Griffin, R.J., and Bergin, M.H. Simultaneous measurements of particulate and gas-phase water-soluble organic carbon concentrations at remote and urban-influenced locations. Geophys. Res. Lett. 35, L13706, doi:10.1029/2008GL033966, 2008.

Aryal, R.K., Lee, B.K., Karki, R., Gurung, A., Baral, B., and Byeon, S.H. Dynamics of $PM_{2.5}$ concentrations in Kathmandu Valley, Nepal. J. Hazard. Mater., doi:10.1016/j.hazmat.2009.02.086, 2009.

Birch, M.E., and Cary, R.A. Elemental carbon-based method for monitoring occupational exposures to particulate diesel exhaust. Aer. Sci. Technol. 25, 221-241, 1996.

Cachier, H. Isotopic characterization of carbonaceous aerosols. Aer. Sci. Technol. 10, 379-385, 1989.

Cao, J.J., Wu, F., Chow, J.C., Lee, S.C., Li, Y., Chen, S.W., An, Z.S., Fung, K.K., Watson, G., Zhu, C.S., and Liu, S.X. Characterization and source apportionment

of atmospheric organic and elemental carbon during fall and winter of 2003 in Xi'an, China. Atmos. Chem. Phys. 5, 3127-3137, 2005.

Carrico, C.M., Bergin, M.H., Shrestha, A.B., Dibb, J.E., Gomes, L., and Harris, J.M. The importance of carbon and mineral dust to seasonal aerosol properties in the Nepal Himalaya. Atmos. Environ. 37, 2811-2824, 2003.

Castro, L.M., Pio, C.A., Harrison, R.M. and Smith, D.J.T. Carbonaceous aerosol in urban and rural European atmospheres: estimation of secondary organic carbon concentrations. Atmos. Environ. 33, 2771-2781, 1999.

CBS. Statistical Year Book of Nepal. Central Bureau of Statistics (CBS), National Planning Commission Secretariat, Government of Nepal, 2005.

CBS. District Profile, Kathmandu (2062). Central Bureau of Statistics (CBS), National Planning Commission Secretariat, Government of Nepal, 2009.

Charlson, R.J. Atmospheric visibility related to aerosol mass concentration: review. Environ. Sci. Technol. 3, 913-918, 1969.

Charlson, R.J., Schwartz, S.E., Hales, J.M., Cess, R.D., Coakley Jr., J.A., Hansen, J.E., and Hofmann, D.J. Climate forcing by anthropogenic aerosols. Science 255, 423-450, 1992.

Duan, J., Tan, J., Cheng, D., Bi, X., Deng, W., Sheng, G., Fu, J., and Wong, M.H. Sources and characteristics of carbonaceous aerosol in two largest cities in Pearl River Delta Region, China. Atmos. Environ. 41, 2895-2903, 2007.

Faiz, A., Ale, B.B., and Nagarkoti, R.K. The role of inspection and maintenance in controlling vehicular emissions in Kathmandu valley, Nepal. Atmos. Environ. 40, 5967-5975, 2006.

Folinsbee, L.J. Human Health Effects of Air Pollution. Environ. Heal. Persp. 100, 45-56, 1992.

Hildemann, L.M., Markowski, G.R., Cass, G.R. Chemical composition of emissions from urban sources of fine organic aerosol. Environ. Sci. Technol. 25, 744–759, 1991.

Ho, K.F., Lee, S.C., Cao, J.J., Li, Y.S., Chow, J.C., Watson, J.G., and Fung, K. Variability of organic and elemental carbon, water soluble carbon, and isotopes in Hong Kong. Atmos. Chem. Phys. 6, 4569-4576, 2006.

Huang, L., Brook, J.R., Zhang, W., Li, S.M., Graham, L., Ernst, D., Chivulescu, A., and Lu, G. Stable isotope measurements of carbon fractions (OC/EC) in airborne particulate: A new dimension for source characterization and apportionment. Atmos. Environ. 40, 2690-2705, 2006.

ICIMOD. Kathmandu Valley Environment Outlook. International Centre for Integrated Mountain Development, Kathmandu, Nepal, 2007.

Jacobson, M.C., Hansson, H.C., Noone, K.J., and Charlson, R.J. Organic atmospheric aerosols: Review and state of the science. Rev. Geophy. 38, 267-294, 2000.

Kai, Z., Yuesi, W., Tianxue, W., Yousef, M., and Frank, M. Properties of nitrate, sulfate and ammonium in typical polluted atmospheric aerosols (PM_{10}) in Beijing. Atmos. Res. 84, 67-77, 2007.

Kaplan, I.R. and Gordon, R.J. Non-Fossil-Fuel Fine-Particle Organic Carbon Aerosols in Southern California Determined During the Los Angeles Aerosol Characterization and Source Apportionment Study. Aer. Sci. Technol. 21, 343-359, 1994.

Kondo, A., Kaga, A., Imamura, K., Inoue, Y., Sugisawa, M., Shrestha, M.L., and Sapkota, B. Investigation of air pollution concentration in Kathmandu valley during winter season. J. Environ. Sci. 17, 1008-1013, 2005.

Lee, H.S., Kang, C.M., Kang, B.W., and Kim, H.K. Seasonal variations of acidic air pollutants in Seoul, South Korea. Atmos. Environ. 33, 3143-3152, 1999.

Lin, J.J. and Tai, H.S. Concentrations and distributions of carbonaceous species in ambient particles in Kaohsiung City, Taiwan. Atmos. Environ. 35, 2627-2636, 2001.

Li, W., Bai, Z., Liu, A., Chen, J., and Chen, L. Characteristics of Major $PM_{2.5}$ components during winter in Tianjin, China. Aer. Air. Qual. Res. 9, 105-119, 2009.

Martinelli, L.A., Camargo, P.B., Lara, L.B.L.S., Victoria, R.L., and Artaxo, P. Stable carbon and nitrogen isotopic composition of bulk aerosol particles in a C4 plant landscape of southeast Brazil. Atmos. Environ. 36, 2427-2432, 2002.

MFD. Government of Nepal, Meteorological Forecasting Division (MFD), Archive Report, 2008.

Panday, A.K. and Prinn, R.G. Diurnal cycle of air pollution in the Kathmandu Valley, Nepal: Observations. J. Geophys. Res. 114, D09305, doi:10.1029/2008JD009777, 2009.

Schwab, J.J., Felton, H.D., and Demerjian, K.L. Aerosol chemical composition in New York state from integrated filter samples: Urban/rural and seasonal contrasts. J. Geophys. Res. 109, D16S05, doi:10.1029/2003JD004078, 2004.

Shakya, P.R., Shrestha, P., Tamrakar, C.S., and Bhattarai, P.K. Studies on potential emission of hazardous gases due to uncontrolled open-air burning of waste vehicle tyres and their possible impacts on the environment. Atmos. Environ. 42, 6555-6559, 2008.

Shen, Z., Cao, J., Tong, Z., Liu, S., Reddy, L.S.S., Han, Y., Zhang, T., and Zhou, J. Chemical characteristics of submicron particles in winter in Xi'an. Aer. Air. Qual. Res. 9, 80-93, 2009.

Stevens, R.K., Dzubay, TG., Shaw, W., McClenny, W.A., Lewis, C.W., and Wilson, W.E. Chacterization of the aerosol in the Great Smoky Mountains. Environ. Sci. Technol. 14, 1491-1498, 1980.

Strader, R., Lurmann, F., and Pandis, S.N. Evaluation of secondary organic aerosol formation in winter. Atmos. Environ. 33, 4849-4863, 1999.

Sullivan, A.P., Weber, R.J., Clements, A.L., Turner, J.R., Bae, M.S., and Schauer, J.J. A method for on-line measurement of water-soluble organic carbon in ambient aerosol particles: results from an urban site. Geophy. Res. Lett. 31, L13105, doi:10.1029/2004GL019681, 2004.

Tanner, R.L. and Miguel, A.H. Carbonaceous aerosol sources in Rio de Janeiro. Aer. Sci. Technol. 10, 213-223, 1989.

Turekian, V.C., Macko, S., Ballentine, D., Swap, R.J., and Garstang, M. Causes of bulk carbon and nitrogen isotopic fractionations in the products of vegetation burns: laboratory studies. Chem. Geo. 152, 181-192, 1998.

Turpin, B.J., and J.J. Huntzicker. Secondary formation of atmospheric aerosol in the Los Angeles Basin, A descriptive analysis of organic and elemental carbon concentrations. Atmos. Environ. 25, 207-215, 1991.

Turpin, B.J. and Lim, H.J. Species Contributions to $PM_{2.5}$ Mass Concentrations: Revisiting Common Assumptions for Estimating Organic Mass. Aer. Sci. Technol. 35, 602–610, 2001.

Twomey, S. Pollution and the planetary albedo. Atmos. Environ. 8, 1251-1256, 1974.

Wang, H., Kawamura, K., and Shooter, D. Carbonaceous and ionic components in wintertime atmospheric aerosols from two New Zealand cities: Implications for solid fuel combustion. Atmos. Environ. 39, 5865-5875, 2005.

Weber, R.J., Sullivan, A.P, Peltier, R.E., Russell, A., Yan, B., Zheng, M., de Gouw, J.A., Warneke, C., Brock, C., Holloway, J.S., Atlas, E.L., and Edgerton, E. A study of secondary organic aerosol formation in the anthropogenic-influenced southeastern United States. J. Geophys. Res. 112, D13302, doi:13310.11029/12007JD008408, 2007.

Widory, D. Nitrogen isotopes: Tracers of origin and processes affecting PM_{10} in the atmosphere of Paris. Atmos. Environ. 41, 2382-2390, 2007.

Yang, H., Yu, J.Z., Ho, S.S.H., Xu, J., Wu, W., Wan, C.H., Wang, X., Wang, X., and Wang, L. The chemical composition of inorganic and carbonaceous materials in $PM_{2.5}$ in Nanjing, China. Atmos. Environ. 39, 3735-3749, 2005.

Yeatman, S.G., Spokes, L.J., Dennis, P.F., and Jickells, T.D. Comparisons of aerosol nitrogen isotopic composition at two polluted coastal sites. Atmos. Environ. 35, 1307-1320, 2001.

Zencak, Z., Elmquist, M., and Gustafsson, O. Quantification and radiocarbon source apportionment of black carbon in atmospheric aerosols using the CTO-375 method. Atmos. Environ. 41, 7895-7906, 2007.

Zhang, Y., Quraishi, T., and Schauer, J.J. Daily variations in sources of carbonaceous aerosol in Lahore, Pakistan during a High pollution spring episode. Aer. Air. Qual. Res. 8, 130-146, 2008.

Ziemba, L.D, Fischer, E., Griffin, R.J., and Talbot, R.W. Aerosol acidity in rural New England: Temporal trends and source region analysis. J. Geophys. Res. 112, D10S22, doi:10.1029/2006JD007605, 2007.

Table 2.1. Statistics for aerosol concentrations of carbonaceous species, inorganic ions, and carbon and nitrogen isotopes and for derived parameters in Kathmandu during winter.

Parameter	Mean	Median	1σ	5th percentile	95th percentile	n*
OC ($\mu gC\ m^{-3}$)	20.02	19.79	6.59	11.39	29.38	25
OM ($\mu g\ m^{-3}$)	29.26	27.77	11.24	13.78	44.24	25
EC ($\mu gC\ m^{-3}$)	4.48	4.40	1.17	3.12	6.41	25
TC ($\mu gC\ m^{-3}$)	24.51	24.14	7.51	15.15	35.77	25
OC/EC	4.47	4.36	0.93	3.08	6.03	25
SOC ($\mu gC\ m^{-3}$)	6.81	5.84	4.48	0.77	13.54	25
POC ($\mu gC\ m^{-3}$)	13.48	13.23	3.52	9.37	19.26	25
SOC/OC	0.31	0.31	0.14	0.06	0.50	25
WSOC ($\mu gC\ m^{-3}$)	10.09	10.49	3.64	5.01	14.71	25
WSOC/OC	0.50	0.51	0.06	0.39	0.57	25
WSOC/TC	0.41	0.41	0.05	0.32	0.47	25
Cl^- ($\mu g\ m^{-3}$)	1.70	1.78	0.38	1.06	2.29	24
NO_2^- ($\mu g\ m^{-3}$)	0.02	0.02	0.01	0.01	0.03	8
NO_3^- ($\mu g\ m^{-3}$)	1.80	1.69	0.63	1.07	3.06	24
SO_4^{2-} ($\mu g\ m^{-3}$)	3.16	2.85	1.04	1.88	4.95	24
$C_2O_4^{2-}$ ($\mu g\ m^{-3}$)	0.12	0.12	0.08	0.01	0.25	16
NH_4^+ ($\mu g\ m^{-3}$)	0.81	0.64	0.46	0.29	1.69	24
K^+ ($\mu g\ m^{-3}$)	0.32	0.12	0.47	0.01	0.85	21
Mg^{2+} ($\mu g\ m^{-3}$)	0.07	0.07	0.04	0.02	0.12	23
Ca^{2+} ($\mu g\ m^{-3}$)	1.16	1.08	0.58	0.41	2.39	24
H^+ ($nmol\ m^{-3}$)	49.99	49.53	18.66	20.71	72.31	24
f	0.45	0.43	0.19	0.23	0.75	24
Total speciated aerosol ($\mu g\ m^{-3}$)	39.08	35.42	11.91	23.69	54.89	24
$\delta^{15}N$ (‰)	9.45	9.53	0.87	8.18	10.47	8
$\delta^{13}C$ (‰)	- 25.74	- 25.70	0.19	-26.01	-.25.53	7

*Number of samples. For those less than 25, see Table 2.S1 to see if samples were below detection limit or if analyses were not performed. For statistics, only those samples for which measured values were above detection limits are included.

Table 2.2. Carbon and nitrogen isotope ratios in aerosol collected in different locations.

Location	**Type**	**Date**	**$\delta^{13}C$ (‰)**	**$\delta^{15}N$ (‰)**	**Reference**
Kathmandu, Nepal	Urban	Dec. 2007 – Jan. 2008	-25.74 ± 0.19 (TC)	9.45 ± 0.87	This work
Downtown LA, USA	Urban	Fall 1987	-23.41 (TC)		Kaplan and Gordon, 1994
Stockholm, Sweden	Urban	Oct. – Nov. 2005	-27.3 ± 0.1 (TOC)		Zencak et al., 2007
Hong Kong, China	Urban	Nov. 2000 – Feb. 2001	-26.9 ± 0.6 (OC) -25.6 ± 0.1 (EC)		Ho et al., 2006
Cassier Tunnel, Canada	Anthropogenic	Aug. 2001	-27.13 (OC) -26.97 (EC)		Huang et al., 2006
Rio de Janeiro, Brazil	Urban	Jun.-Jul. 1985	-24.1 to –25.6 (OC) -23.3 to –26.4 (EC)		Tanner and Miguel, 1989
Pracicaba, Brazil	C_4 plantations	Aug. 1999 – Sep. 2000	-20.9 ± 0.8 (TC)	10.6 ± 2.8	Martinelli et al., 2002
Paris, France	Urban	Feb. – Apr. 2003 Jun. – Aug. 2003		3.9 – 5.4 (diesel - vehicles) 2.9 – 15.4 (natural gas – heating source) -19.4 – 2.9 (fuel oil – heating source) -5.3 (coal – heating source) 5.5 – 8 (waste incinerators)	Widory, 2007

Table 2.3. Principal component analysis of carbonaceous components, water-soluble organic, water-soluble inorganic ions, and meteorological data. Only factors with eigenvalues exceeding unity were included. The largest absolute factor loading for each variable is shown in bold (if the original loading was positive).

Variable	Factor 1	Factor 2	Factor 3	Factor 4	Communality
EC	**0.87**	0.13	0.19	0.22	0.87
POC	**0.87**	0.13	0.19	0.22	0.87
SOC	**0.63**	0.55	-0.39	-0.24	0.91
WSOC	**0.87**	0.37	-0.27	0.01	0.96
Cl^-	**0.74**	0.28	-0.13	0.23	0.69
NO_3^-	0.34	**0.86**	0.15	0.03	0.88
SO_4^{2-}	-0.16	0.42	**0.70**	0.43	0.88
NH_4^+	-0.07	**0.88**	0.11	0.26	0.86
K^+	-0.77	0.05	0.09	0.24	0.66
Mg^{2+}	0.09	0.06	0.08	**0.89**	0.82
Ca^{2+}	0.16	0.56	-0.04	**0.72**	0.86
MaxT	**0.72**	-0.17	-0.27	-0.08	0.63
MinT	-0.33	-0.09	**0.85**	0.18	0.87
RH	0.24	0.13	**0.74**	-0.36	0.75
Eigenvalue	5.42	3.22	1.60	1.27	
Cumulative% variance	38.74	23.00	11.43	9.05	
Estimated Source	Local/ Vehicles	Secondary Gas-to-Particle	Aqueous Processing	Dust transport	

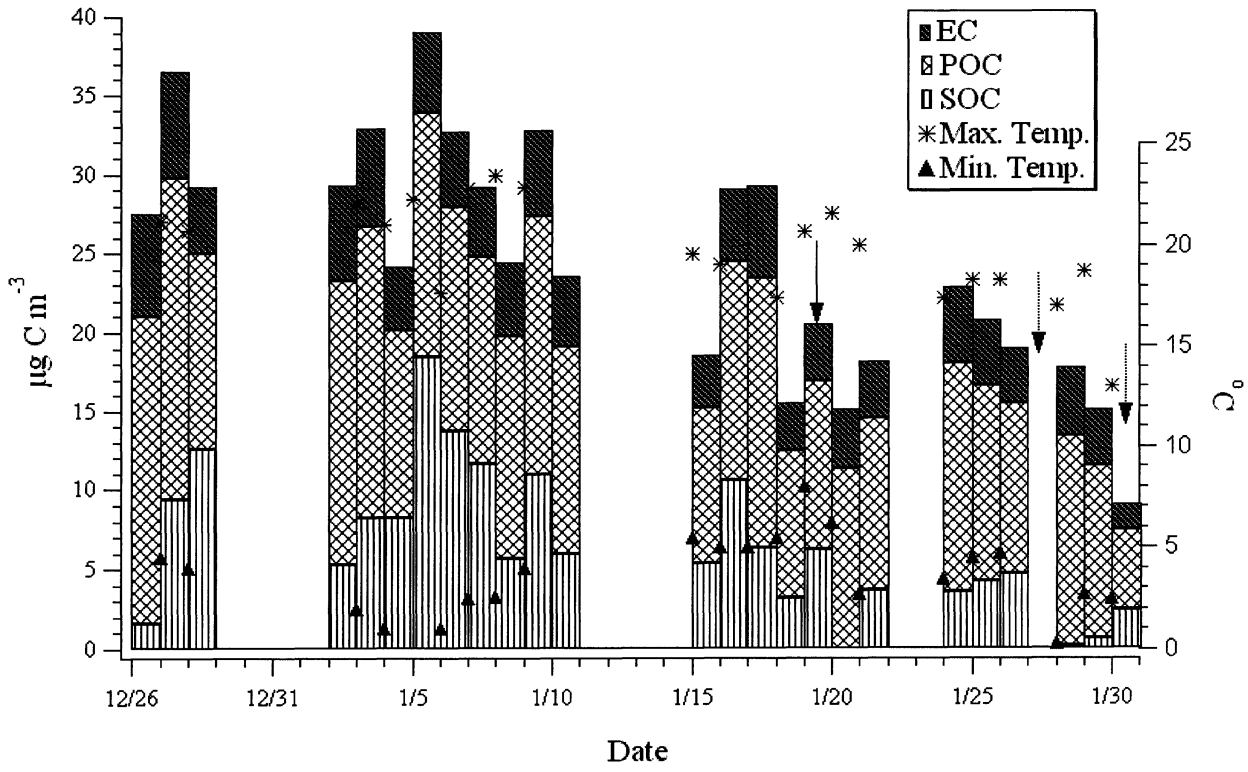

Figure 2.1. Time series of EC, POC, SOC, and minimum and maximum temperature. Arrows indicate rainfall (4.9 mm on 1/19, trace amounts on other days).

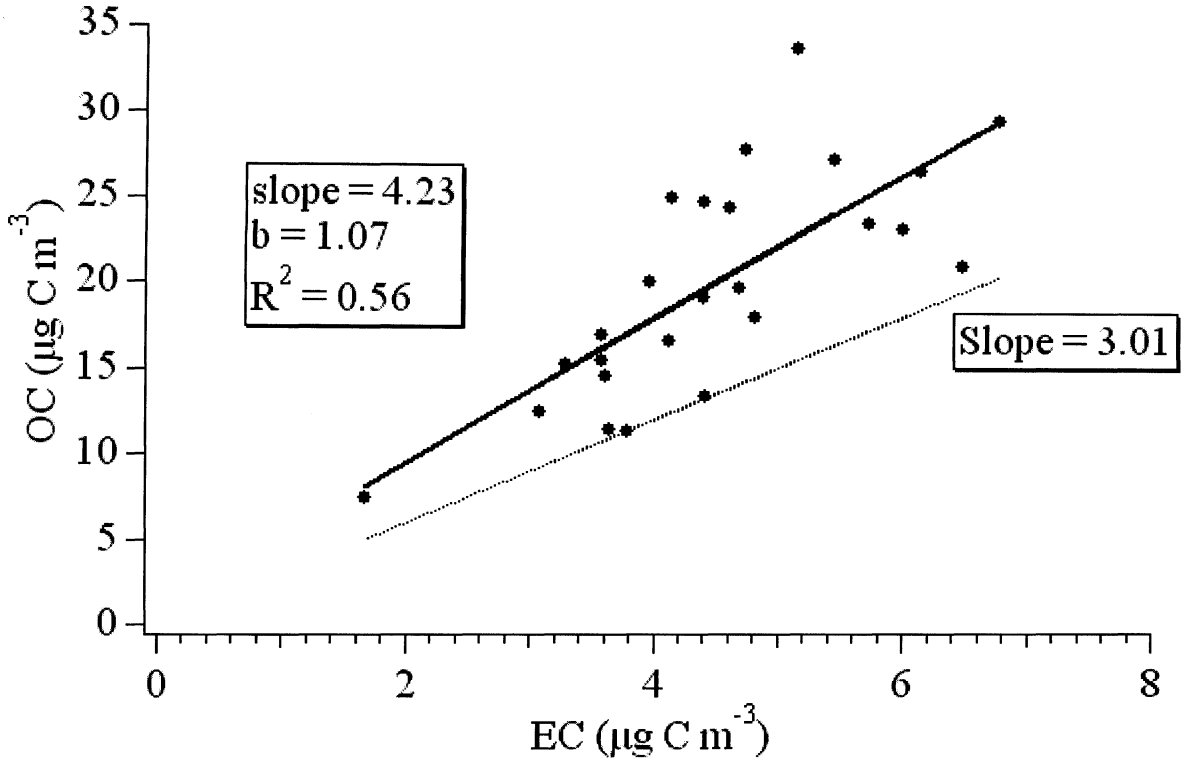

Figure 2.2. Regression of EC versus OC during the sampling period. The darker line indicates the regression through the observed values, while the lighter line indicates the minimum ratio of OC/EC used for estimating SOC.

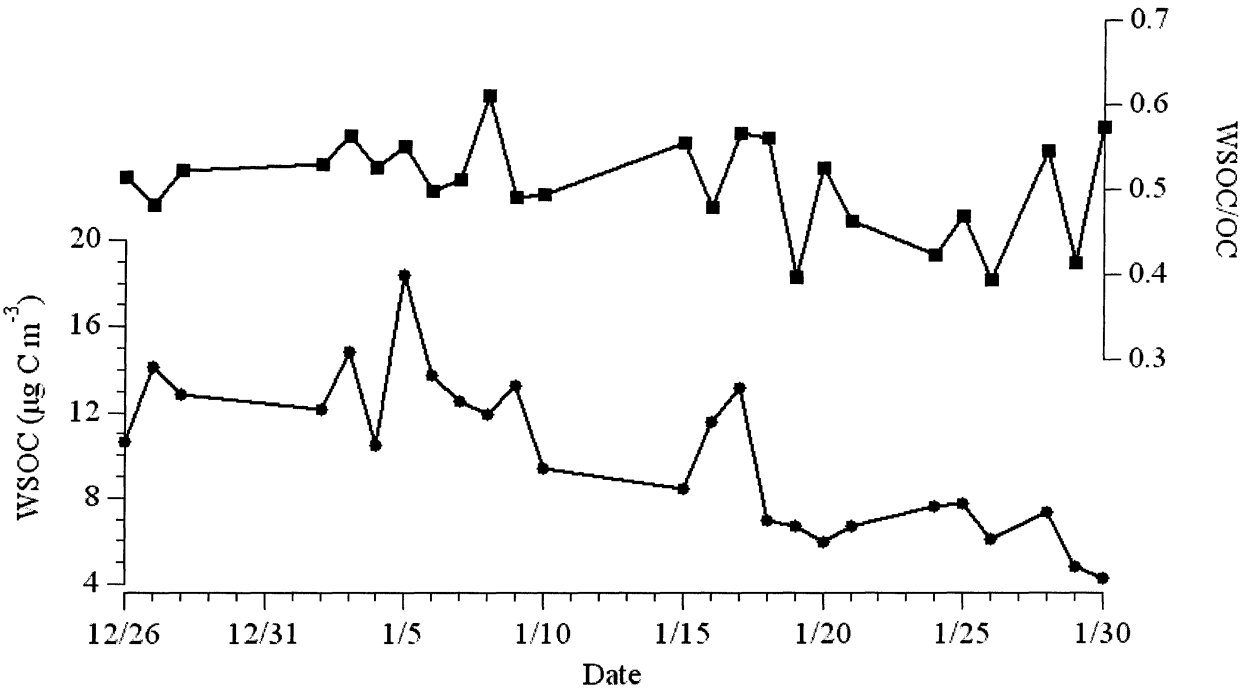

Figure 2.3. Time series of WSOC concentrations and WSOC/OC in Kathmandu during the sampling period.

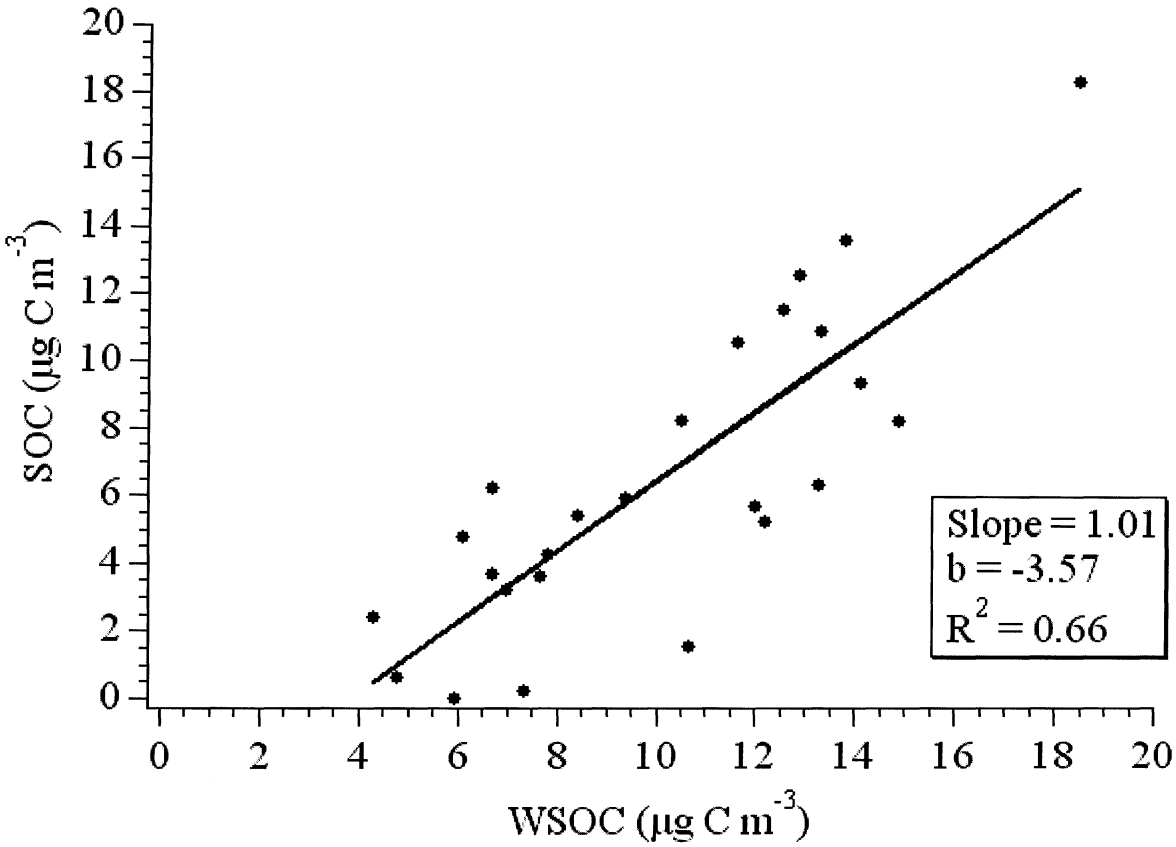

Figure 2.4. Regression of WSOC versus SOC during the sampling period.

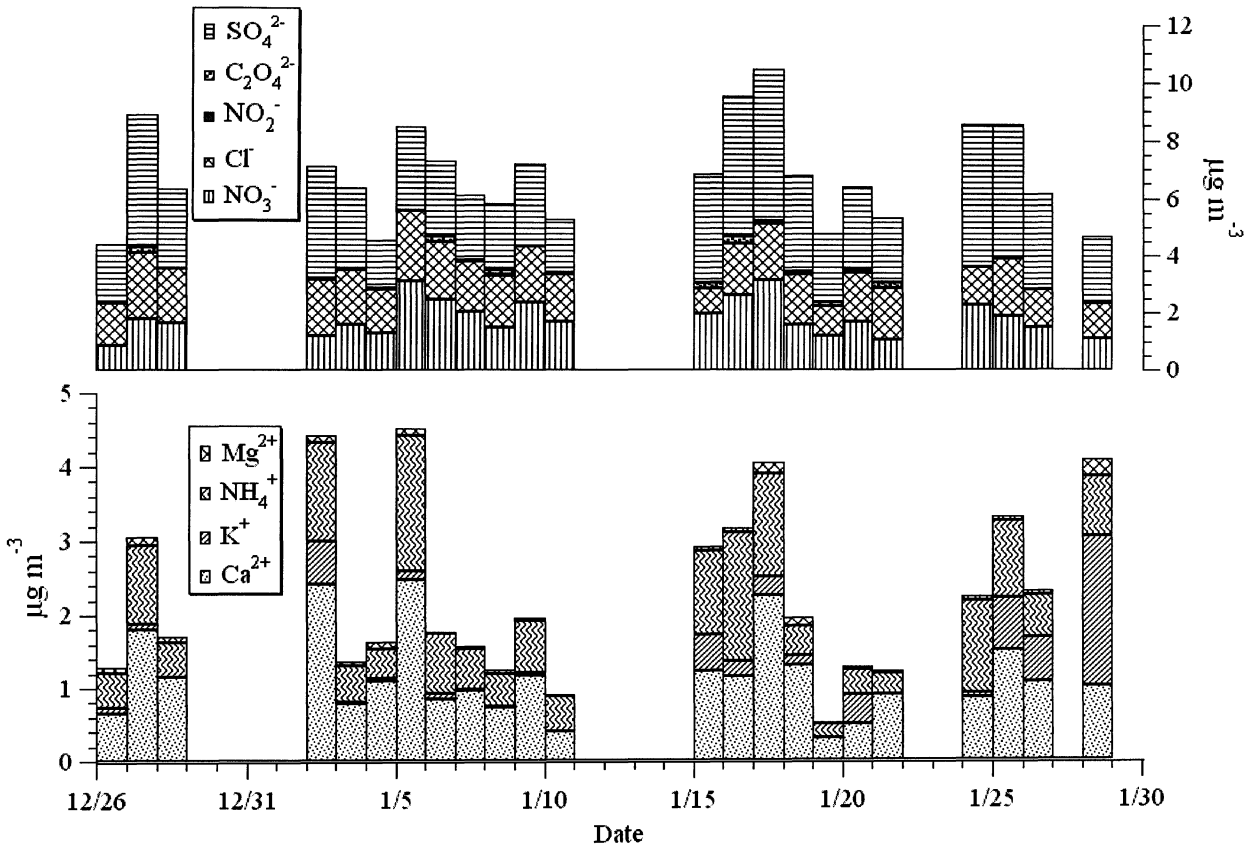

Figure 2.5. Anion (top) and cation (bottom) concentrations observed in aerosols of Kathmandu during the sampling period.

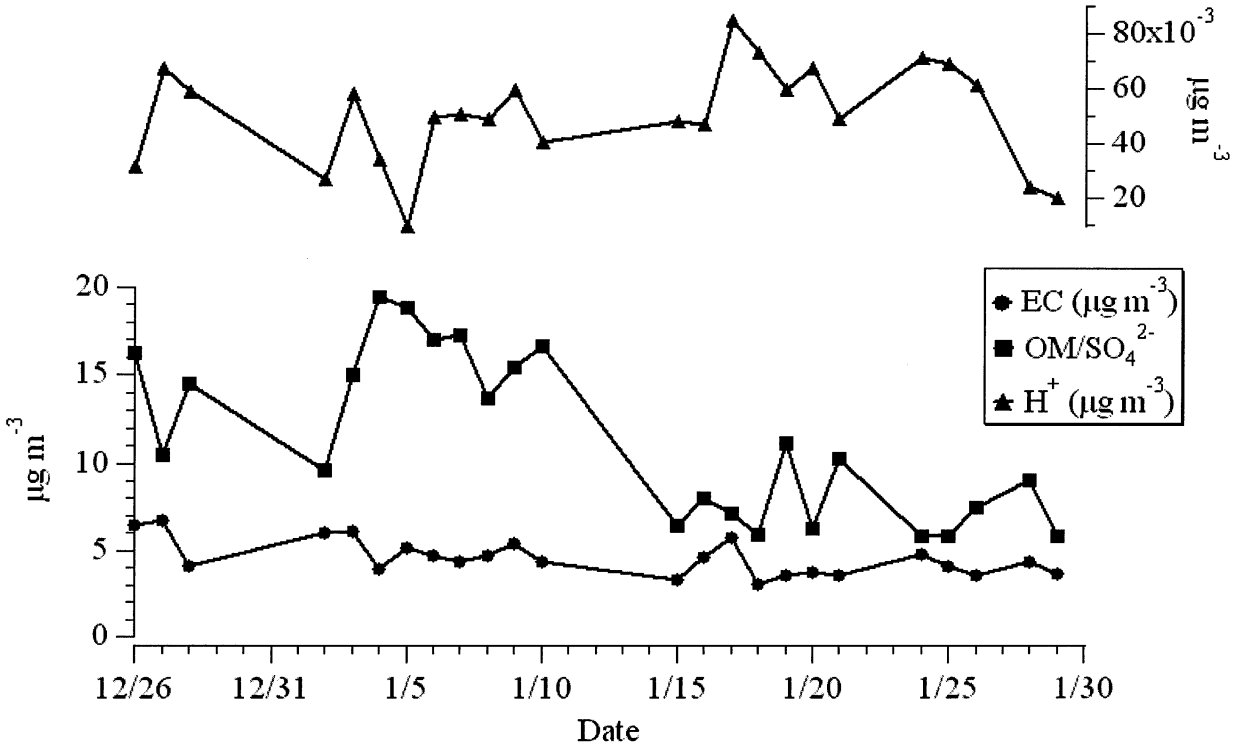

Figure 2.6. Time series of EC, [H^+], and the ratio of OM to SO_4^{2-} during the sampling period.

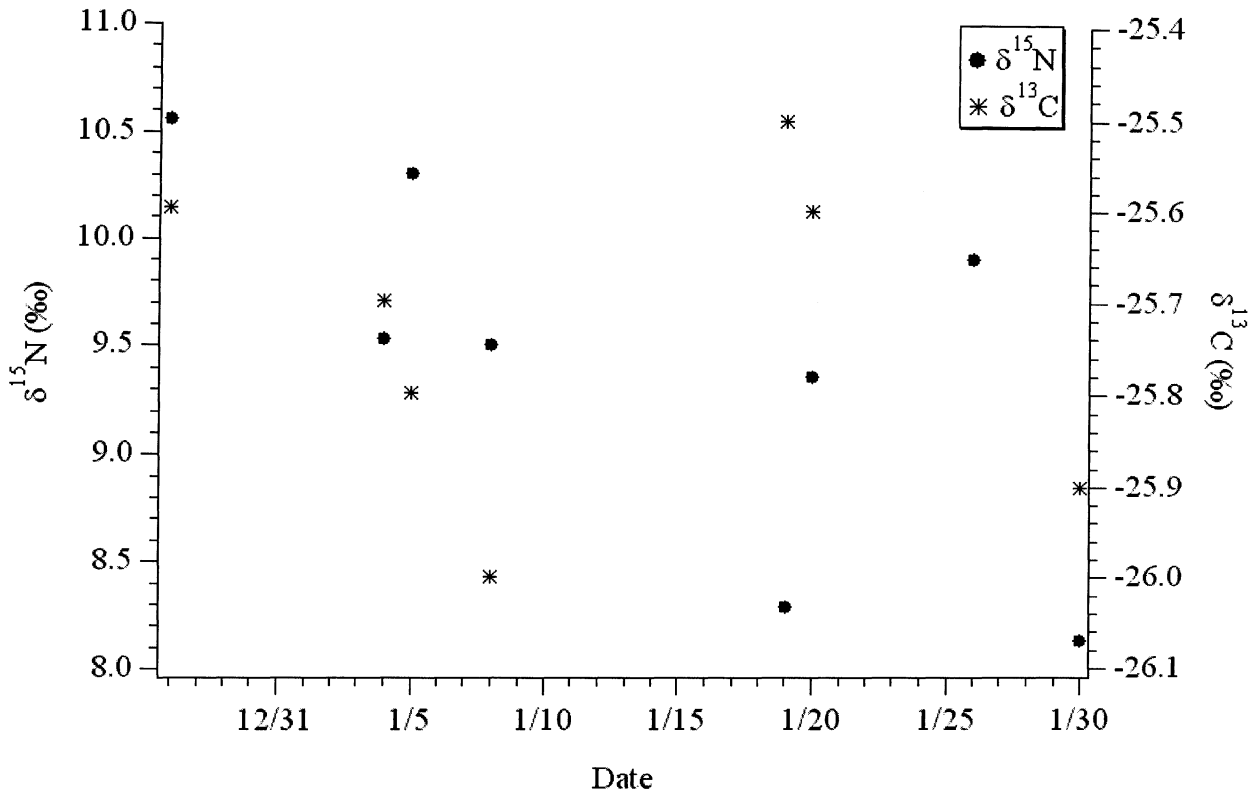

Figure 2.7. Carbon and nitrogen isotope ratios in aerosols in Kathmandu during the sampling period.

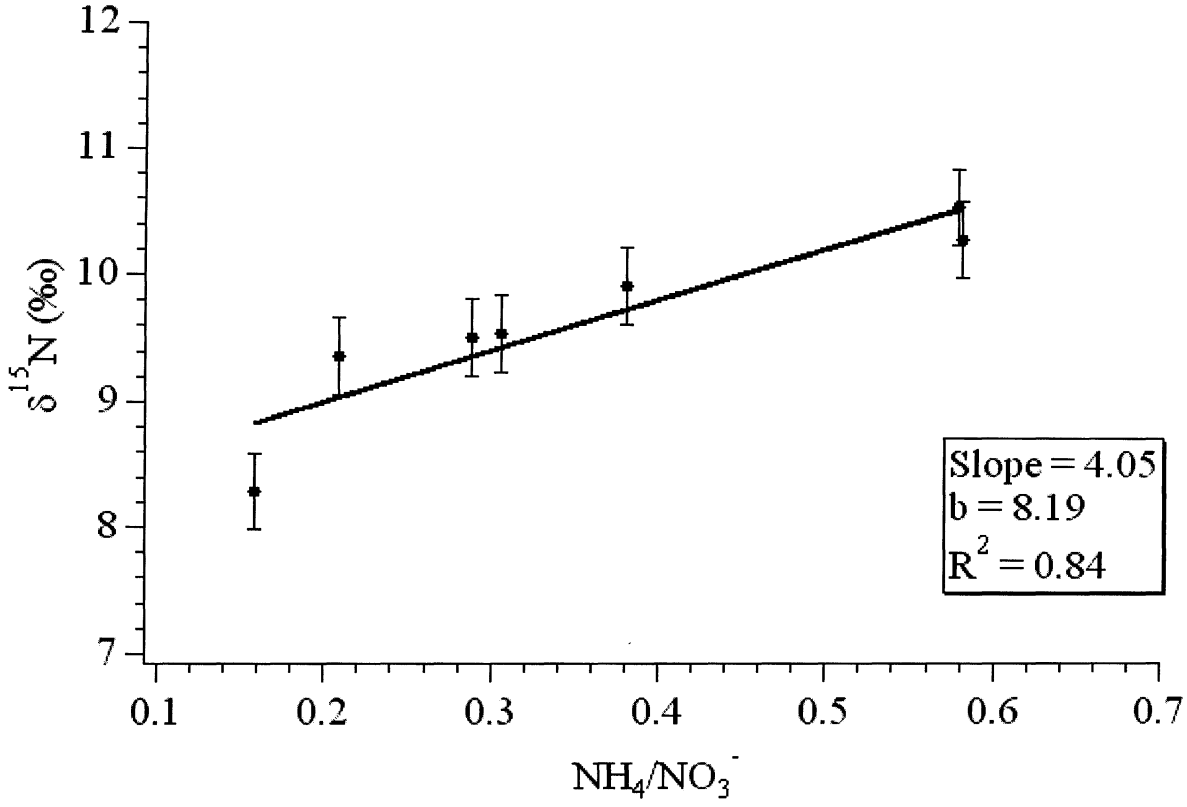

Figure 2.8. Regression of NH_4^+/NO_3^- versus $\delta^{15}N$ during the sampling period.

Chapter 3

Seasonal variation in particle characteristics at a semi-rural New England location – Part 1: Carbonaceous aerosol and organic functionality

Abstract

Ambient aerosol samples (n = 287) collected at a semi-rural location, Thompson Farm (TF) in Durham, New Hampshire, from August 2007 to 2008 exhibited seasonal variation, characterized by the largest total carbon (TC) concentrations during winter (3.7 ± 2.6 μg C m^{-3}) and the smallest during summer (1.2 ± 1.2 μg C m^{-3}). On average, 92% of TC was organic (OC), of which 69% on average was observed to be water-soluble (WSOC). This study focuses on characterizing the WSOC functional groups using Proton Nuclear Magnetic Resonance (H^+-NMR) spectroscopy on a subset of the samples (n = 108). Three aliphatic groups (H-C, H-C-C=, and H-C-O) accounted for 78.9% of the characterized WSOC carbon mass. Pure aliphatic groups (H-C) were the dominant functional group with an average of 30.6% of WSOC carbon mass followed by oxygenated aliphatic (25.4%, H-C-O) and unsaturated aliphatic (22.9%, H-C-C=) groups. The arylic group (H-Ar) contributed an average of 20.7% of WSOC carbon mass but exhibited large seasonal variation compared to the aliphatic groups. Vinylic/acetalic groups (=C-H and O-CH-O) were present only in select samples and contributed less than 1% of WSOC carbon mass. Precipitation affected mainly the WSOC and the H-C-C= functional group, which showed consistent decreases following rainfall events. Strong

correlation between elemental carbon (EC) and OC and the dominance of air masses from the continental Midwest during winter shows that primary emissions (from local heating or industrial emissions) were the main sources during winter. In contrast to winter, enhanced secondary formation and processed aerosols were dominant during other seasons. Air masses originating from the continental midwest were associated with higher levels of EC, primary OC, and H-C-O at TF.

3.1 Introduction

Aerosols are an important part of the atmosphere and affect the health of humans and biota, atmospheric chemistry and physics, hydrology, and climate (Pöschl, 2005). Organic material, on average, contributes a large fraction of aerosol mass (20 to 70%) (Saxena and Hildemann, 1996; Zhang et al., 2007). Specifically, organic components in aerosols can cause as much as 60% of visibility degradation through scattering (Jacobson et al., 2000), impact the ability of particles to act as cloud condensation nuclei (CCN), and facilitate or inhibit water condensation (Saxena et al., 1995; Shulman et al., 1996; Raymond and Pandis, 2002; Twohy et al., 2005; VanReken et al., 2005). In addition, the water-solubility of organic material affects haze formation (Facchini et al., 2000; Watson, 2002) and both wet and dry deposition processes that determine the lifetime of carbonaceous aerosols (Kanakidou et al., 2005).

Carbonaceous aerosols are often characterized according to elemental (EC) or organic carbon (OC) fraction and water-solubility. Proton nuclear magnetic resonance (H^+-NMR) spectroscopy is a powerful tool for the characterization of functional groups within particulate water-soluble OC (WSOC) (Decesari et al., 2000). Functional group

distribution measured by H^+-NMR provides information on the overall chemical composition, oxidation state, and reactivity of organic particulate mass, but not the actual identification of the particular compound (Pöschl, 2005). For H^+-NMR, no additional sampling requirements are needed; an aqueous extract such as that used for determining WSOC is used for the H^+-NMR analysis, making the sample preparation easy. Further, there is no interference of inorganics during analysis (Decesari et al., 2007). Other spectroscopic techniques such as fast Fourier transform infrared (FTIR) spectroscopy also have been applied to study functional group composition of OC (Gilardoni et al., 2007; Russell et al., 2009). The main advantages of using H^+-NMR spectroscopy is its insusceptibility towards inorganic ions, small sample volume (<1 ml) requirement, and the identification of chemical structure of low molecular weight organic compounds without requiring a separation procedure (Suzuki et al., 2001). Disadvantages include the requirement of standards for specific single compounds to identify the structure in the spectra and the low sensitivity towards highly unsaturated functional groups (Suzuki et al., 2001; Graham et al., 2002).

The characterized functional groups accounted for approximately 90% of WSOC aerosols in previous sampling campaigns (Decesari et al., 2000; 2001), in contrast to the traditionally characterized 10-20% of WSOC from gas chromatography-mass spectrometry (GC-MS) techniques. The H^+-NMR technique has been used to characterize aerosols from different parts of the world (Graham et al., 2002; Cavalli et al., 2004, 2006; Decesari et al., 2006; Tagliavini et al., 2006; Moretti et al. 2008). Furthermore, H^+-NMR fingerprints for three major types of WSOC aerosols (biomass

burning, secondary organic aerosol (SOA), and marine) have been proposed (Decesari et al., 2007).

Part 1 of this manuscript focuses on the carbonaceous species (OC and EC), the WSOC fraction, and the functional group composition of WSOC. In part 2, stable carbon and nitrogen isotope compositions of aerosols are investigated.

3.2 Experimental

3.2.1 Sampling

Twenty-four hour bulk atmospheric aerosol samples were collected at Thompson Farm (TF) in Durham, NH, at the University of New Hampshire (UNH) AIRMAP Atmospheric Observatory. The TF area is surrounded by mixed forests, alfalfa farms, and open fields. From August 22, 2007, to June 24, 2008, aerosol samples were collected from the TF site located at 43.1092°N, 70.9484°W (24 m above sea level); from July 3, 2008 to August 13, 2008, aerosol samples were collected at a second location at TF (43.1078° N, 70.9517° W; 39.9 m elevation) that is 0.31 kilometers away from the first sampling site. The sampling site is located approximately 15-20 km away from the Atlantic Ocean. Throughout this paper, both sites will be referred to as TF because both locations generally are influenced by the same air masses based on total aerosol number (R^2 = 0.72; slope = 1.13) and ozone (R^2 = 0.96; slope = 0.96) concentration measured simulatenously at the two sites (treating the first site as the independent variable) from July 3 to August 13, 2008.

Aerosols at this sampling site are reported to be slightly acidic due to the importance of sulfate, while OC in summer is aged and secondary with mixed biogenic

and anthropogenic origins (Ziemba et al., 2007; Cottrell et al., 2008). Bulk aerosols were collected using quartz fiber filters (90-mm diameter) at the top of a 12-m (first location) or 24-m (second location) tower. Blank samples were collected regularly, usually for 24 hours. All the sample and blank substrates were stored at -20°C inside Petri dishes until analysis. Prior to sampling, all the filter substrates were pre-baked at 600°C for 24 hours. Data collected during the one-year sampling campaign were classified into four seasons: Winter (December to February), Spring (March to May), Summer (June to August), and Fall (September to November).

3.2.2 Analysis

3.2.2.1 Organic and Elemental Carbon

A thermal-optical method (Sunset analyzer) was used to determine EC and OC concentrations (Birch and Cary, 1996). A 1.5-cm^2 punch from the filter substrate was used for the analysis of EC and OC. Standards of succinic acid were used for calibration. A total of 22 field blanks were collected during the sampling campaign. Uncertainties calculated using the average sampling volume from the sampling campaign and two times the standard deviations of field blanks for OC and EC are 0.35 and 0.06 μg C m^{-3}, respectively. A few outliers that exhibited concentrations exceeding 12 times the standard deviation of all other field blanks were removed due to the probable contamination of the blanks. All data for OC and EC were blank corrected, and any negative values were removed. The precision of the measurement calculated as the relative standard deviation from 13 sample replicates for OC and 12 sample replicates for EC was 14 and 10%, respectively.

Primary OC (POC) and secondary OC (SOC) were estimated by

$$POC = EC \times \left(\frac{OC}{EC}\right)_{min} \quad (1)$$

$$SOC = TOC - POC \quad (2)$$

where $\left(\frac{OC}{EC}\right)_{min}$ is the minimum OC to EC ratio (OC/EC) obtained for each season, and TOC is the total OC obtained from the Sunset measurement. The assumptions and limitations of this method are described elsewhere (Turpin and Huntzicker, 1991; Castro et al. 1999; Strader et al., 1999).

3.2.2.2 Analysis of WSOC

Extracts from the aerosol samples were prepared by passively soaking four 1.5-cm^2 filter punches in 10 mL of Milli-Q water for 10 minutes, followed by 10 minutes of mechanical mixing in a centrifuge. A 5-ml aliquot of the extract was analyzed for WSOC using a total carbon analyzer (Sievers 800). The WSOC data were blank corrected. Uncertainty estimated as two-times the standard deviation of WSOC blanks is 0.19 μg C m^{-3}.

3.2.2.3 H^+-NMR

For functional group analysis, a 5-ml aliquot of the extract was analyzed by H^+-NMR (Varian Unity INOVA 500 MHz) with an inverse probe utilizing a D_2O solvent. Before analysis, the extract was freeze dried in a vacuum for ~8 hours and then mixed in D_2O. This solution was then transferred to a 5-mm H^+-NMR tube for analysis. A PRESAT pulse sequence was used to suppress the D_2O solvent, and 1024 scans were

acquired for each spectrum. A 5th-order polynomial was used to correct the baseline of the raw spectra, and a line broadening of 0.5 was applied.

The signals obtained from H^+-NMR spectra were integrated in five ranges of chemical shifts to classify five functional groups (Moretti et al., 2008): 0.6-1.80 ppm, aliphatic hydrogens or purely aliphatic groups (H-C, FG1); 1.8-3.2 ppm, hydrogens in the α position to unsaturated carbons or unsaturated aliphatics (H-C-C=, FG2); 3.2-4.4 ppm, hydrogens bound to alcoholic, ethereal, or estereal carbons or oxygenates (H-C-O, FG3); 5.0-5.5 ppm, acetalic and vinylic hydrogens (O-CH-O and =C-H, FG4); and 6.5-8.2 ppm, arylic hydrogens or aromatic groups (H-Ar, FG5). A carbonylic/carboxylic aliphatic group (H-C-C=O, FG6) was estimated by subtracting the estimated aromatic contribution (based on FG5) from FG2 (Decesari et al., 2007). The signals obtained for the protons of the respective functional groups from H^+-NMR spectra were converted into corresponding carbon content using a H/C ratio of 2.0 for FG1 and FG2, 1.1 for FG3, 1.0 for FG4, 0.4 for FG5, and 1.0 for FG6 (Fuzzi et al., 2001; Decesari et al., 2007). All the functional group data are presented in terms of carbon.

3.2.3 Meteorological and Supplemental Data

Meteorological data (outdoor temperature, relative humidity, precipitation, wind direction, and wind speed), trace gas data (carbon monoxide (CO), nitric oxide (NO), and ozone (O_3)), and aerosol number concentration data during the sampling campaign were acquired from AIRMAP. A summary of meteorological parameters during the four seasons of the sampling campaign is presented in Table 3.1.

3.2.4 Backward Trajectories

Five-day backward trajectories were analyzed to track air mass origin and understand the sources during pollution episodes using the Hybrid Single-Particle Lagrangian Integrated Trajectory model (Draxler and Rolph, 2010). Modeled five-day backward trajectories arrived at 500 m above ground level assuming air transport along an isentropic surface and using the Global Data Assimilation System. A few trajectories were run with an arrival height of 750 m to avoid the trajectories intercepting the ground. Three trajectories were run within each 24-hour sampling period to represent the source region for each sample. The air mass origin for each sample was classified into one of seven source regions: 1. Marine Canada (MC1); 2. Continental Canada (CC1); 3. Marine (Mar); 4. Continental Midwest (CM); 5. Continental Coastal (CC2); 6. Marine Coastal (MC2); and 7. Marine Influenced (MI). Details on the first six categories are presented in Figure 3.1 and described in Ziemba et al. (2007). Samples were classified as marine influenced if trajectories traveled over the ocean via different regions. Twenty-four hour periods without two trajectories belonging to a single source region were not included in one of the above classifications.

3.3 Results

A total of 287 samples, including 22 field blanks and 13 replicates, were collected and analyzed for carbonaceous content. A subgroup (n = 108) of selected samples was analyzed for WSOC and functional groups. Mean concentrations of carbonaceous aerosol material (EC, OC, POC, and SOC) and WSOC and the mean OC/EC and WSOC to OC ratio (WSOC/OC) in four seasons are summarized in Table 3.2 after application of

the blank correction. Seasonal variation in functionality of WSOC identified from H^+-NMR spectra also is presented in Table 3.2.

3.3.1 Carbonaceous aerosols

Carbonaceous aerosol showed a seasonal trend with both OC and EC exhibiting the largest values in winter and the smallest values in summer (Table 3.2 and Figure 3.2). Overall, the aerosol total carbon (TC) was comprised of 92% OC and 8% EC during the sampling campaign. There was a strong correlation of OC with EC during winter (R^2=0.83; p<0.0001, slope = 11.34) compared to spring (R^2=0.73; p<0.0001; slope = 9.78) and fall (R^2=0.42; p<0.001; slope = 7.22); there was no correlation during summer (Figure 3.3).

In equation (1), the $(OC/EC)_{min}$ from each season was used separately for estimating POC and SOC; they were 8.31, 3.34, 1.18, and 2.56 for winter, spring, summer, and fall, respectively. Though no seasonal variation of mean OC/EC was observed, a large variation in minimum OC/EC was observed for four seasons. Estimation of POC and SOC were made only for the values greater than the uncertainty of EC (0.06) and OC (0.35). Uncertainties in the estimation of SOC arises from the selection of a representative primary OC/EC ratio that is affected by the influence of meteorological factors, temporal emission fluctuations, local sources, transport, and varying OC/EC ratios by emission source (Na et al., 2004).

POC and SOC each showed a seasonal trend, with the largest POC in winter (2.39 ± 1.55 μg C m^{-3}) and SOC highest in fall (2.80 ± 1.34 μg C m^{-3}) (Table 3.2 and Figure 3.2). The total organic mass (OM) concentration was obtained by multiplying POC by a

factor of 1.2 and SOC by a factor of 2.0 to account for the contribution of other atoms contained in organic molecules (H, O, N, S, etc.) (Turpin and Lim, 2001). Organic mass concentrations were largest in the fall (6.39 ± 2.90 μg m^{-3}) and the smallest in summer (3.26 ± 2.96 μg m^{-3}).

3.3.2 WSOC

The concentrations of WSOC did not vary considerably between the four seasons, with an annual average concentration of 2.10 ± 0.86 μg C m^{-3} (Table 3.2). The value of WSOC/OC also did not exhibit a seasonal dependence, with an annual mean of 0.69 ± 0.13 and an annual range of 0.67 to 0.73, despite the strong increase in the relative contribution of POC to OC in winter. This indicates some solubility of POC compounds and/or aging of POC, even in winter. There was a strong correlation of WSOC with OC during all four seasons (R^2>0.80; p<0.001) (Figure 3.4). During summer, WSOC was negatively correlated with RH (R^2=0.66; p<0.01; slope = -0.101).

3.3.3 Functional groups

Functional group analysis showed that aliphatic groups (FG1) were the most important chemical structure, contributing 30.6 ± 5.3% of WSOC carbon mass (Table 3.2 and Figure 3.5). Overall, unsaturated groups (FG2), oxygenates (FG3), and arylic hydrogens (FG5) accounted for 22.9 ± 6.1%, 25.4 ± 7.0%, and 20.7 ± 13.4%, respectively. Vinylic/ acetalic hydrogens (FG4) contributed less than 1% of WSOC. The three groups (FG1, FG2, and FG3) that contribute the largest fraction of WSOC (79%) did not exhibit a strong seasonal variability, while FG4 and FG5 showed strong seasonal

variability. Arylic groups were the largest during winter (25.9%) and the smallest during summer (13.2%). Similar to FG5, vinylic/acetalic groups were also the largest (0.5%) during winter. This change in functional group contribution is linked to a change in either emissions speciation (e.g. increased aromatic content in POC in winter) or processing (e.g., increased consumption of aromatic rings due to stronger photochemistry in summer). The last two groups were not present in all samples. Spectra obtained from H^+-NMR analysis for the blank and examples of spectra from the four seasons are shown in Figure 3.6. The distinct peak seen around 5.25 ppm was stronger in winter compared to spring; this peak was absent in most of the samples collected during summer and fall. Also, stronger signals in peaks around 7-8 ppm were observed in aerosol samples collected during winter compared to other seasons.

Correlation analysis performed for all the seasons showed that four functional groups (FG1, FG2, FG3, and FG4) were correlated strongly ($R^2>0.88$; $p<0.0001$) to one another; FG5 did not have strong correlation with any other functional group. WSOC had a stronger correlation with FG1, FG2, and FG3 ($R^2>0.61$, $p<0.001$) in spring compared to that with FG1 ($R^2>0.41$, $p<0.0001$) and FG2 ($R^2>0.51$, $p<0.0001$) in fall. WSOC was not correlated with any functional groups during winter, and there were an insufficient number of samples with both WSOC and FG data in summer to show a correlation within confidence intervals.

3.3.4 Seasonal variation in air mass transport

In all, 156 samples were classified into different source regions (Figure 3.7). Backward trajectories showed more than half of the air masses (58%) originated from

continental Canada. Other frequent air masses origins were continental midwest (33%), marine Canada (30%), and continental coastal (12%). Winter samples were dominated by the transport from the continental midwest (55%) and continental Canada (30%), spring samples from continental Canada (42%) and marine Canada (23%), summer samples from continental Canada (41%), and fall samples from marine Canada (36%) and continental Canada (36%).

3.4 Discussion

3.4.1 Carbonaceous aerosols

The seasonal variation of TC and organic fractions observed in bulk aerosols at TF are similar to the values reported for fine aerosols in Po Valley, Italy (Simpson et al., 2006). On the other hand, seasonal average OC concentrations of 1.12 to 3.46 μg C m^{-3} at TF are smaller than those for other domestic sites (Na et al., 2004 and references therein). The summer mean TC concentration of 1.21 μg C m^{-3} is larger than the annual fine TC (<1 μg C m^{-3}) for the rural western United States, while the mean TC concentrations of 2.13 to 3.74 μg m^{-3} for other seasons are comparable to the rural Northwest and Southeast (3 μg m^{-3}) and urban sites (4 μg m^{-3}) in the United States (Schichtel et al., 2008). Hence, TF is not representative of a truly rural site as the larger concentrations are be due to the influence of transported pollutants from upwind industrial and urban locations. The smallest TC observed in summer results from the smaller influence of primary sources and from increased vertical mixing. In contrast to other seasons, summer did not exhibit a significant correlation between OC and EC, suggesting multiple/secondary sources. Compared to the other seasons, summer also had

the largest frequency of air mass transport from the continental coastal regions (Figure 3.7).

The overall dominance of OC with respect to TC (92%) and SOC contributing the most to OC indicate that secondary aerosols are the main type of aerosols at TF, which corroborates the summer measurements of Cottrell et al. (2008). However, primary aerosols were relatively important during winter compared to all other seasons, as indicated by the larger concentrations of EC and POC, a strong correlation between them, the largest POC/OC (66%), and the dominant air mass transport from the continental midwest region. The larger CO and NO mixing ratios in winter underscore the increased importance of primary combustion sources. The large POC/OC is similar to that (69%) observed in a polluted urban Asian city with a large anthropogenic influence (Shakya et al., 2010).

The largest seasonal mean OC/EC ratio (14.93 ± 7.04), the largest seasonal SOC concentration, and the comparatively weaker OC-EC correlation suggest the relative importance of secondary sources of OC during fall at TF. Similar phenomena were observed in Mira Loma, California (Na et al., 2004), indicating large impacts from upwind pollutant transport and significant SOC formation.

The annual mean OC/EC was 13.25 ± 5.88, and little variation was observed in the mean OC/EC by seasons. The observed OC/EC in this study can be compared to those from different emission sources such as paved road dust (13.1), natural gas home appliances (12.7), and forest fires (pinion and juniper; 14.51) (Watson et al., 2001; Na et al., 2004 and references therein). The mean OC/EC at TF is larger than the values reported for cities in the United States (Na et al., 2004 and references therein) and is

drived by small EC concentrations, similar to carbonaceous aerosols studied in Milan, Italy (Lonati et al., 2007). Because this sampling site is hypothesized to be affected mainly by oxidized/processed/aged aerosols, EC concentrations likely were diluted during transport, while SOC concentrations likely increased due to processing (Salma et al., 2001). The OC/EC did not correlate with OC in any season; the OC/EC was close to the mean values in the samples with the largest OC concentrations (Figure 3.8).

3.4.2 Pollution episodes

There were two carbonaceous pollution episodes, defined as days with abnormally large peaks of TC concentrations, during the sampling campaign, as illustrated in Figure 3.9. The first occurred on January 6 and 7, 2008, with TC of 12.66 and 11.63 μg C m^{-3}, respectively. The second occurred on April 20, 2008, with TC of 13.56 μg C m^{-3}. The first episode corresponded very well with a large CO peak. During the first episode, the air mass traveled from the southern US, passing through Pennsylvania and New York (Figure 3.10). This is in agreement with the inference made by Chen et al. (2007) for pollution events in southern New England to be associated with long distance transport. During the TC event in spring, CO did not increase. In contrast to the first event, the air mass came from eastern Canada and over the ocean during the second episode (Figure 3.10), suggesting that marine sources might have affected the TC concentration. The O_3 mixing ratio on this day (44.8 ppb) was close to the 95^{th} percentile of the campaign and SOC contribution (62%) to TC was greater than the previous episode, likely indicating the role of processing. Furthermore, POC was almost two-

times larger than SOC during the first event and less than half of SOC during the second event.

3.4.3 WSOC

Relatively little seasonal variation was observed for WSOC concentration and WSOC/OC, confirming the importance of processed/secondary aerosol. The large WSOC/OC observed in this study indicates aged aerosol and the predominance of polar and oxidized organic compounds, which are formed mainly from the oxidation of volatile organic compounds or primary organic aerosol (Saxena and Hildemann, 1996). The likely presence of aged and oxidized OC at TF also is supported by the strong correlation of WSOC with OC during all seasons. The strongest correlation of WSOC with SOC during summer ($R^2 = 0.97$, $p<0.001$) and the weakest ($R^2 = 0.41$, $p<0.001$) during winter shows the seasonal differences in the WSOC composition. Negative correlation of WSOC with RH for bulk aerosols at TF is in contrast to the studies conducted on WSOC in fine aerosols in Atlanta during summer (Hennigan et al., 2008). The discrepancy in the results might be due to the smaller number of samples in the current study ($n = 8$), the smearing of the relationship over a longer time scale (24 hours) for bulk aerosols (a greater number of size fractions), or some sort of salting out effect with biogenic SOC (Cocker et al., 2001).

A box plot diagram of WSOC (Figure 3.11a) classified by precipitation data shows a consistent decrease in WSOC concentrations with increased precipitation. Aerosol number concentrations measured by a condensation nuclei counter (CNC) were also larger during dry periods (5634 ± 2151 cm^{-3}) compared to wet periods (4929 ± 1944

cm^{-3}), similar to observations made in the Amazon Basin (Mircea et al., 2005). The effect of precipitation on WSOC and CNC confirms the effects of water solubility on aerosol deposition processes and consequently lifetime (Kanakidou et al., 2005). A decrease of approximately 19% was observed for TC concentrations during dry (2.90 ± 2.42 μg C m^{-3}) versus wet periods (2.34 ± 1.74 μg C m^{-3}).

3.4.4 Functional groups

Signals from aliphatic groups (FG1, FG2, FG3) were the dominant peaks in H^+-NMR spectra (Figure 3.6). These three aliphatic groups were the most important components, contributing ~79% of identified WSOC (Figure 3.5). These groups showed relatively little seasonal dependence with respect to relative composition. Aromatic groups showed a seasonal variation, with a distinct minimum (13.2%) in the summer, almost half of the winter maximum (25.9%). In comparison to a previous study at this location (Ziemba et al., 2011), the relative contributions in this study of FG1 and FG5 are very similar, that of FG3 is larger (~Δ9%), and those of FG2 (~Δ11%) and FG4 (<Δ2%) are smaller. It should be stressed that the previous study focused on variation of functional groups with particle size for a limited number of samples during fall.

Aromatic groups observed in humic-like substances of aerosols collected in suburban location in Switzerland showed a four-fold increase in winter compared to summer, which was attributed to the increase in wood combustion for residential heating during winter (Samburova et al., 2007). Fine aerosols emitted from wood combustion contain many aromatic groups (e.g., syringols, guaiacols) (Fine et al., 2001), and the larger fraction of aromatic compounds observed in aerosols at TF during winter may thus

be related to wood combustion in fireplaces. The smaller aromatic contributions in summer may also be related to increased photochemical strength and oxidation capacity during this season relative to others, particularly winter.

The correlation of the functional groups, mainly FG1, FG2, and FG3, suggests similar sources or chemical processes associated with these groups. These FGs exhibited a consistent presence in WSOC and did not vary seasonally. No correlation of FG5 with the previous FGs and its seasonality suggest a different source, most likely from local home heating sources as described previously. This is also in supported by the lack of correlation of any of these FGs with WSOC during winter compared to spring and fall.

To determine if the functional group distribution could indicate WSOC sources (Decesari et al., 2007), the ratio of oxygenates (FG3, H-C-O) to total aliphatics was plotted against the ratio of carbonylic and carboxylic groups (FG6, H-C-C=O) to total aliphatics (Figures 3.12 and 3.13). Based on the source signature plots, WSOC aerosols at TF appear spectroscopically similar to SOA and biomass burning aerosols measured at other locations. Anthropogenic and aged aerosols with some influence from biogenic emissions and biomass burning have been reported previously at TF during summer (Ziemba et al., 2007; Cottrell et al., 2008), and some wood burning might have been used for home heating during winter. However, the majority of data points falling into the biomass burning source signature plot during summer is inconsistent with SOA being the main component of organic aerosols during this season (Figure 3.13). Thus, the boundaries of the signature boxes, especially for SOA and biomass burning, might be different at TF than outlined in Decesari et al. (2007). Furthermore, aged organic aerosol from combustion-related vehicular emissions, which are one of the major sources at TF

from upwind, are not included specifically in this plot. The aromatic fraction also appeared to have no influence on this analysis at TF.

When Figure 3.12 is replotted based on air mass origins (Figure 3.14), none of the samples with marine air source origins were indicated to consist of marine aerosol, which is consistent with less influence of marine organic matter to aerosols at TF as shown by stable carbon isotopic analyses (Part 2). This suggest that marine organic matter emitted along the New England coast falls out prior to arrival at TF or that its signal is swamped in this analysis by the signal from other types of organic material.

Individual peaks in H^+-NMR spectra (Figure 3.6) were compared to previously-identified specific peaks (Suzuki et al., 2001; Cavalli et al., 2004). Several peaks appeared in the pure aliphatic region; one of them is at 1.13 ppm (2-methylerythritol) indicating the influence of biogenic volatile organic compounds at TF because this compound is a photooxidation product of isoprene and OH radicals in low-nitrogen-oxide environments (Claeys et al., 2004; Surratt et al., 2010. Within unsaturated aliphatics, peaks for dimethyl sulfoxide (DMSO) (2.72 ppm) were observed during all seasons. The presence of DMSO indicates that marine organics contributed to WSOC at TF (Decesari et al., 2001) despite the fact that the overall signal did not indicate large influence of marine aerosol on WSOC at TF. Mannitol (3.8-4.0 ppm), a sugar alcohol often known as a tracer of airborne fungal spores (Lewis and Smith, 1967; Claeys et al., 2010), was observed to be one the main compounds contributing to oxygenates of aerosol at TF. The absence of peak at 5.4 ppm (levoglucosan) indicates that biomass burning is not an important source of aerosols during this study (Graham et al., 2002; Cavalli et al., 2004) unless it has been decayed by heterogeneous oxidation mechanisms (Hennigan et al.,

2010; Hoffmann et al., 2010). Aldehydes at chemical shifts 9-10 ppm were not observed in aerosol samples, similar to aerosols from Bologna, Italy (Moretti et al., 2008) and marine aerosols in Ireland (Cavalli et al., 2004).

A comparison of H^+-NMR spectra for aerosols collected on clean and polluted days based on CO data is shown in Figure 3.15. There was almost a ten-fold increase in OC (10.80 μg C m^{-3}) and a four-fold increase in WSOC (4.26 μg C m^{-3}) on the polluted day (01/07/08) compared to the unpolluted day (10/28/07). The H^+-NMR spectra differed primarily in the intensity of peaks in the chemical shifts of 1.3 to 1.7 and 3 to 4 ppm between these two days. Intensities of methyl peaks between 1.3 and 1.7 ppm and within FG2 between 2.5 and 3.2 ppm show relatively stronger signals on the polluted day. Larger contributions of FG2 (by ~7%) and FG3 (by ~16%) indicate the dominance of oxidized structures during the polluted day (Table 3.3) despite the organic aerosols being mainly of primary origin compared to the unpolluted day. FG5 (by ~21%) also decreased on the polluted day compared to the cleaner day, indicating the potential oxidation of aromatics on the polluted day.

Mean aliphatic (FG1) and aromatic group (FG5) contributions to WSOC decrease by ~2% and 10%, respectively, during polluted periods (>300 ppb CO) compared to the less polluted periods (<150 ppb CO), while the mean unsaturated (FG2) and oxygenated group (FG3) contributions increase by 5% and 6%, respectively, during the same periods (Table 3.3). Due to almost the two-fold increase in WSOC concentrations in polluted periods compared to less polluted ones, all functional group concentrations increase, similar to observations made at a boreal forest site in Hyytiälä, Finland during spring (Cavalli et al., 2006). No significant difference was observed between WSOC

concentrations and functional group composition between two extreme photochemical periods represented by ozone levels (Table 3.3). These results confirm the complexities involved in interpreting the studies from functional group analyses from different locations and aerosol samples.

Precipitation events mainly affected FG2 and FG5 contributions, in addition to WSOC concentrations (Table 3; Figures 3.11a, 3.11b, and 3.11c). There was a decrease in FG2 and an increase in FG5 during wet periods compared to dry periods. There was a consistent decrease in FG2 with the increase in precipitation intensities, implying FG2 contributed the most to the decrease in WSOC concentrations following the precipitation events (Figure 3.11b).

3.4.5 Influence of air mass transport

Backward trajectories reveal that air mass transport from continental Canada was frequent during all seasons at TF (Figure 3.7). The continental midwest sources dominate mainly during winter and seem to be associated with the largest concentrations of TC, especially POC, observed during winter (Figure 3.2). Dominance of midwest transport during winter suggests that transport of polluted air masses (in addition to local sources) might be responsible for the large EC and POC concentrations. The upwind anthropogenic pollution sources and regional transport are always important in this sampling area because the continental air masses originating from industrial areas in midwestern United States and traffic-related urban sources often pass through this location (Chen et al., 2007; Ziemba et al., 2007; Jordan et al., 2009; White et al., 2009). When the air mass originated from the continental midwest, EC and POC concentrations

increased compared to the other source regions (Figure 3.11d, 3.11e, and 3.11f). The comparative increase in gas-phase pollutants such as CO, NO, and sulfur dioxide (SO_2) were observed with air mass transport from the continental midwest. The observations indicate that upwind industrial and urban emissions are related to plumes received at TF. Among the functional groups, FG3 peaked with air mass transport from the continental midwest.

3.5 Conclusions

Carbonaceous aerosols demonstrated seasonal variation at TF, with the largest OC and EC during winter and the smallest during summer. On average, TC was almost three times larger, with POC being eight times larger, in winter compared to summer, indicating the dominance of primary sources in winter compared to other seasons. The larger TC and POC concentrations during winter also were related to the dominance of air mass transport from the continental midwest, possibly from industrial emissions that also affected the contribution of FG3 to WSOC. WSOC aerosols and the FG2 composition were lower during precipitation events. Overall, small EC concentrations and consequently large OC/EC indicate minimal influence from primary sources compared to secondary sources on carbonaceous aerosols at TF on a yearly basis. Aliphatic groups (pure aliphatics, unsaturated structures, and alcohols and esters) accounted for most of the characterized WSOC functional groups (79%) throughout the sampling campaign and did not exhibit much seasonal variation. The remaining aromatic and vinylic and acetalic groups exhibited a stronger seasonal variation. The largest aromatic content was observed during winter (26%) and the smallest during summer

(13%). The strong correlation among only four functional groups (FG1 to FG4) suggests a similar source or behavior with respect to processing for these four groups. Oxidized functional groups (H-C-O) are observed to be more dominant during polluted events than unpolluted events. Based on H^+-NMR source signatures, WSOC aerosol at Thompson Farm appears spectroscopically similar to SOA and biomass burning aerosol observed elsewhere. However, the H^+-NMR source signatures failed to classify possible marine aerosol influence and indicated strong input from biomass burning, though it did not appear to be a major source at this location. Thus, while H^+-NMR analyses are useful in other ways, the source attributions appear to have limited utility in an environment in which transport and different mixed sources are influential during a given 24-hour period.

3.6 References

Birch, M.E. and Cary, R.A. Elemental carbon-based method for monitoring occupational exposures to particulate diesel exhaust. Aer. Sci. Technol. 25, 221-241, 1996.

Castro, L.M., Pio, C.A., Harrison, R.M., and Smith, D.J.T. Carbonaceous aerosol in urban and rural European atmospheres: Estimation of secondary organic carbon concentrations. Atmos. Environ. 33, 2721-2781, 1999.

Cavalli, F., Facchini, M.C., Decesari, S., Emblico, L., Mircea, M., Jensen, N.R., and Fuzzi, S. Size-segregated aerosol chemical composition at a boreal site in southern Finland, during the QUEST project. Atmos. Chem. Phys. 6, 993-1002, 2006.

Cavalli, F., Facchini, M.C., Decesari, S., Mircea, M., Emblico, L., Fuzzi, S., Ceburnis, D., Yoon, Y.J., O'Dowd, C.D., Putaud, J.P., and Dell'Acqua, A. Advances in

characterization of size-resolved organic matter in marine aerosol over the North Atlantic. J. Geophy. Res. 109, D24215, doi: 10.1029/2004JD005137, 2004.

Chen, M.R., Talbot, R., Mao, H., Sive, B., Chen, J., and Griffin, R.J. Air mass classification in coastal New England and its relationship to meteorological conditions. J. Geophy. Res. 112, D10S05, doi: 10.1029/2006JD007687, 2007.

Claeys, M., Graham, B., Vas, G., Wang, W., Vermeylen, R., Pashynska, V., Cafmeyer, J., Guyon, P., Andreae, M.O., Artaxo, P., and Maenhaut, W. Formation of secondary organic aerosols through photooxidation of isoprene. Science 303, 1173-1176, 2004.

Claeys, M., Kourtchev, I., Paschynska, V., Vas, G., Vermeylen, R., Wang, W., Cafmeyer, J., Chi, X., Artaxo, P., Andreae, M.O., and Maenhaut, W. Polar organic marker compounds in atmospheric aerosols during the LBA-SMOCC 2002 biomass burning experiment in Rondonia, Brazil: sources and source processes, time series, diel variations and size distributions. Atmos. Chem. Phys. 10, 9319-9331, 2010.

Cocker III, D.R., Clegg, S.L., Flagan, R.C., and Seinfeld, J.H. The effect of water on gas-particle partitioning of secondary organic aerosol. Part I: alpha-pinene/ozone system, Atmos. Environ., 35, 6049-6072, 2001.

Cottrell, L., Griffin, R.J., Jimenez, J.L., Zhang, Q., Ulbrich, I., Ziemba, L.D., Beckman, P.J., Sive, B.C., and Talbot, R.W. Submicron particles at Thompson Farm during ICARTT measured using aerosol mass spectrometry. J. Geophy. Res. 113, D08212, doi:10.1029/2007JD009192, 2008.

Decesari, S., Facchini, M.C., Fuzzi, S., Tagliavini, E. Characterization of water-soluble organic compounds in atmospheric aerosol: A new approach. J. Geophys. Res. 105, 1481-1489, 2000.

Decesari, S., Facchini, M.C., Matta, E., Lettini, F., Mircea, M., Fuzzi, S., Tagliavini, E., and Putaud, J.-P. Chemical features and seasonal variation of fine aerosol water-soluble organic compounds in the Po Valley, Italy. Atmos. Environ. 35, 3691-3699, 2001.

Decesari, S., Mircea, M., Cavalli, F., Fuzzi, S., Moretti, F., Tagliavini, E., and Facchini, M.C. Source attribution of water-soluble organic aerosol by nuclear magnetic resonance spectroscopy. Environ. Sci. Technol. 41, 2479-2484, 2007.

Draxler, R.R. and Rolph, G.D. HYSPLIT (Hybrid Single-Particle Lagrangian Integrated Trajectory) Model access via NOAA ARL READY Website (http://ready.arl.noaa.gov/HYSPLIT.php). NOAA Air Resources Laboratory, Silver Spring, MD, 2010.

Facchini, M.C., Decesari, S., Mircea, M., Fuzzi, S., and Loglio, G. Surface tension of atmospheric wet aerosol and cloud/fog droplets in relation to their organic carbon content and chemical composition. Atmos. Environ. 34, 4853-4857, 2000.

Fine, P., Cass, G., and Simoneit, B. Chemical characterization of fine particle emissions from fireplace combustion of woods grown in the northeastern United States, Environ. Sci. Technol. 35, 2665-2675, 2001.

Fuzzi, S., Decesari, S., Facchini, M.C., Matta, E., and Mircea, M. A simplified model of the water-soluble organic component of atmospheric aerosols. Geophys. Res. Lett. 20, 4079-4082, 2001.

Gilardoni, S., Russell, L.M., Sorooshian, A., Flagan, R.C., Seinfeld, J.H., Bates, T.S., Quinn, P.K., Allan, J.D., Williams, B., Goldstein, A.H., Onasch, T.B. and Worsnop, D.R. Regional variation of organic functional groups in aerosol particles on four U.S. east coast platforms during the International Consortium for Atmospheric Research on Transport and Transformation 2004 campaign. J. Geophys. Res. 112, D10S27, doi: 10.1029/2006JD007737, 2007.

Graham, B., Bracero, O.L.M., Guyon, P., Roberts, G.C., Decesari, S., Facchini, M.C., Artaxo, P., Maenhaut, W., Koll, P., and Andreae, M.O. Water-soluble organic compounds in biomass burning aerosols over Amazonia. 1. Characterization by NMR and GC-MS. J.Geophys. Res. 107(D20), 8047, doi:10.1029/2001JD000336, 2002.

Hennigan, C.J., Sullivan, A.P., Collett, J.L., and Robinson, A.L. Levoglucosan stability in biomass burning particles exposed to hydroxyl radicals. Geophys. Res. Lett. 37, L09806, doi:10.1029/2010GL043088, 2010.

Hoffmann, D., Tilgner, A., Iinuma, Y., and Herrmann, H. Atmospheric stability of levoglucosan: A detailed laboratory and modeling study. Environ. Sci. Technol. 44, 694-699, 2010.

Jacobson, M.C., Hansson, H.C., Noone, K.J., and Charlson, R.J. Organic atmospheric aerosols: Review and state of the science. Rev. Geophy. 38, 267-294, 2000.

Jordan, C., Fitz, E., Hagan, T., Sive, B., Frinak, E., Haase, K., Cottrell, L., Buckley, S., and Talbot, R. Long-term study of VOCs measured with PTR-MS at a rural site in New Hampshire with urban influences. Atmos. Chem. Phys. 9, 4677-4697, 2009.

Kanakidou, M., Seinfeld, J.H., Pandis, S.N., Barnes, I., Dentener, F.J., Facchini, M.C., Dingener, R.V., Ervens, B., Nenes, A., Nielsen, C.J., Swietlicki, E., Putaud, J.P., Balkanski, Y., Fuzzi, S., Horth, J., Moortgat, G.K., Winterhalter, R., Myhre, C.E.L., Tsigaridis, K., Vignati, E., Stephanou, E.G., and Wilson, J. Organic aerosol and global climate modeling: a review. Atmos. Chem. Phys. 5, 1053-1123, 2005.

Lewis, D.H. and Smith, D.C. Sugar alcohols (polyols) in fungi and green plants: 1. Distribution, physiology and metabolism. New Phytol. 66, 143-184, 1967.

Lonati, G., Ozgen, S., and Giugliano, M. Primary and secondary carbonaceous species in PM2.5 samples in Milan (Italy). Atmos. Environ. 41, 4599-4610, 2007.

Mircea, M., Facchini, M.C., Decesari, S., Cavalli, F., Emblico, L., Fuzzi, S., Vestin, A., Rissler, J., Swietlicki, E., Frank, G., Andreae, M.O., Maenhaut, Rudich, Y., and Artaxo, P. Importance of the organic aerosol fraction for modeling aerosol hygroscopic growth and activation: a case study in the Amazon Basin. Atmos. Chem. Phys. 5, 3111-3126, 2005.

Moretti, F., Tagliavini, E., Decesari, S., Facchini, M.C., Rinaldi, M., and Fuzzi, S. NMR determination of total carbonyls and carboxyls: A tool for tracing the evolution of atmospheric oxidized organic aerosols. Environ. Sci. Technol. 42, 4844-4849, 2008.

Na, K., Sawant, A.A., Song, C., and Cocker III, D.R. Primary and secondary carbonaceous species in the atmosphere of Western Riverside County, California. Atmos. Environ. 38, 1345-1355, 2004.

Pöschl, U. Atmospheric Aerosols: Composition, Transformation, Climate and Health Effects. Angew. Chem. Int. Ed. 44, 7520-7540, 2005.

Raymond, T.M. and Pandis, S.N. Cloud activation of single-component organic aerosol particles. J. Geophys. Res. 107, D24, 4787, doi: 10.1029/2002JD002159, 2002.

Russell, L.M., Bahadur, R., Hawkins, L.N., Allan, J., Baumgardner, D., Quinn, P.K., and Bates, T.S. Organic aerosol characterization by complementary measurements of chemical bonds and molecular fragments. Atmos. Environ. 43, 6100-6105, 2009.

Salma, I., Maenhaut, W., Zemplen-Papp, E., and Zaray, G. Comprehensive characterization of atmospheric aerosols in Budapest Hungary: physicochemical properties of inorganic species. Atmos. Environ. 35, 4367-4378, 2001.

Samburova, V., Didenko, T., Kunenkov, E., Emmenegger, C., Zenobi, R., and Kalberer, M. Functional group analysis of high-molecular weight compounds in the water-soluble fraction of organic aerosols. Atmos. Environ. 41, 4703-4710, 2007.

Saxena, P. and Hildemann, L.M. Water-soluble organics in atmospheric particles: a critical review of the literature and application of thermodynamics to identify candidate compounds. J. Atm. Chem. 24, 57-109, 1996.

Saxena, P., Hildemann, L.M., McMurry, P.H., and Seinfeld, J.H. Organics alter hygroscopic behavior of atmospheric particles. J. Geophy. Res. 100, 18755-18770, 1995.

Schichtel, B.A., Malm, W.C., Bench, G., Fallon, S., McDade, C.E., Chow, J.C., and Watson, J.G. Fossil and contemporary fine particulate carbon fractions at 12 rural and urban sites in the United States. J. Geophy. Res. 113, D02311, doi:10.1029/2007JD008605, 2008.

Shakya, K.M., Ziemba, L.D., and Griffin, R.J. Characteristics and sources of carbonaceous, ionic, and isotopic species of wintertime atmospheric aerosols in Kathmandu Valley, Nepal. Aer. Air Qual. Res. 10, 219-230, 2010.

Shulman, M.L., Jacobson, M.C., Carlson, R.J., Synovec, R.E., and Young, T.E. Dissolution behavior and surface tension effects of organic compounds in nucleating cloud droplets, Geophy. Res. Lett. 23, 277–280, 1996.

Simpson, A.J., Lam, B., Diamond, M.J., Donaldson, D.J., Lefevre, B.A., Moser, A.Q., Williams, A.J., Larin, N.I., Kvasha, M.P. Assessing the organic composition of urban surface films using nuclear magnetic resonance spectroscopy. Chemosphere 63, 142-152, 2006.

Strader, R., Lurmann, F., Pandis, S.N. Evaluation of Secondary organic aerosol formation in winter. Atmos. Environ. 33, 4849-4863, 1999.

Surratt, J.D., Chan, A.W.H., Eddingsaas, N.C., Chan, M.N., Loza, C.L., Kwan, A.J., Hersey, S.P., Flagan, R.C., Wennberg, P.O., and Seinfeld, J.H. Reactive intermediates revealed in secondary organic aerosol formation from isoprene. Proc. Natl. Acad. Sci. USA 107, 6640-6645, 2010.

Suzuki, Y., Kawakami, M., and Akasaka, K. ^{1}H NMR application for characterizing water-soluble organic compounds in urban atmospheric particles. Environ. Sci. Technol. 35, 2656-2664, 2001.

Tagliavini, E., Moretti, F., Decesari, S., Facchini, M.C., Fuzzi, S., and Maenhaut, W. Functional group analysis by H NMR/chemical derivatization for the characterization of organic aerosol from the SMOCC field campaign. Atmos. Chem. Phys. 6, 1003-1019, 2006.

Turpin, B.J. and Huntzicker, J.J. Secondary formation of organic aerosol in the Los Angeles basin: A descriptive analysis of organic and elemental carbon concentrations. Atmos. Environ. 25A, 207-215, 1991.

Turpin, B.J. and Lim, H.J. Species contributions to $PM_{2.5}$ mass concentrations: Revisiting common assumptions for estimating organic mass. Aer. Sci. Technol. 35, 602-610, 2001.

Twohy, C.H., Anderson, J.R., and Crozier, P.A. Nitrogenated organic aerosols as cloud condensation nuclei. Geophys. Res. Lett. 32, L19805, doi:10.1029/2005GL023605, 2005.

VanReken, T.M., Ng, N.L., Flagan, R.C., and Seinfeld, J.H. Cloud condensation nucleus activation properties of biogenic secondary organic aerosol. J. Geophys. Res. 110, D07206, doi: 10.1029/2004JD005465, 2005.

Watson, J.G. Visibility: science and regulation. J. Air. Waste Manage. Assoc. 52, 628-713, 2002.

Watson, J.G., Chow, J.C., and Houck, J.E. $PM_{2.5}$ chemical source profiles for vehicle exhaust, vegetative burning, geological material, and coal burning in Northwestern Colorado during 1995. Chemosphere 43, 1141-1151, 2001.

White, M.L., Russo, R.S., Zhou, Y., Ambrose, J.L., Haase, K., Frinak, E., Varner, R.K., Wingenter, O.W., Mao, H., Talbot, R., and Sive, B.C. Are biogenic emissions a significant source of summertime atmospheric toluene in rural Northeastern United States? Atmos. Chem. Phys. 9, 81-92, 2009.

Zhang et al. Ubiquity and dominance of oxygenated species in organic aerosols in anthropogenically-influenced Northern Hemisphere midlatitudes, Geophys. Res. Lett. 2007, 34, L13801, doi:10.1029/2007GL029979, 2007.

Ziemba, L.D., Fischer, E., Griffin, R.J., and Talbot, R.W. Aerosol acidity in rural New England: Temporal trends and source region analysis. J. Geophy. Res. 112, D10S22, doi:10.1029/2006JD007605, 2007.

Ziemba, L.D., Griffin, R.J., Whitlow, S., and Talbot, R.W. Characterization of water-soluble organic aerosol in coastal New England: Implications of variations in size distribution. Submitted, 2011.

Table 3.1. Meteorological parameters in four seasons during the sampling campaign. Mean parameters are presented except for precipitation, for which total accumulation is presented.

Season	Temperature (^{0}C)	Precipitation (inches)	RH (%)	Wind direction[5] (Degrees)	Wind speed (m/s)
Winter	-2.30	11.88[1]	69.89	225.70	1.38
Spring	6.95	9.64[2]	62.91	212.37	1.67
Summer	20.28	10.80[3]	80.99	195.88	1.01
Fall	10.70	8.97[4]	74.73	215.19	1.20

RH: Relative humidity

[1]From 27 days of rainfall; [2]From 26 days of rainfall; [3]From 19 days of rainfall; [4]From 25 days of rainfall. [5]Zero degrees is due north.

Table 3.2. Mean concentrations of carbonaceous aerosols and contributions of functional groups (based on %C) during four seasons and the entire sampling campaign. Values inside parentheses refer to the standard deviation, and *n* refers to the number of samples.

	EC $\mu gC/m^3$	OC $\mu gC/m^3$	OC/EC	POC $\mu gC/m^3$	SOC $\mu gC/m^3$	WSOC $\mu gC/m^3$	WSOC/OC	H-C %	H-C-C= %	H-C-O %	O-CH-O/ =C-H (%)	Ar-H %
Winter	0.28	3.46	13.15	2.39	1.22	2.21	0.70	27.34	20.30	25.97	0.51	25.88
	(0.19)	(2.37)	(3.35)	(1.55)	(1.14)	(0.83)	(0.14)	(4.86)	(4.68)	(7.81)	(0.89)	(12.25)
Spring	0.19	1.96	12.49	0.70	1.76	1.79	0.73	31.04	23.66	22.95	0.23	22.12
	(0.17)	(1.87)	(4.55)	(0.58)	(1.41)	(0.79)	(0.11)	(4.63)	(6.09)	(6.72)	(0.63)	(13.37)
Summer	0.17	1.12	10.53	0.28	1.65	1.83	0.66	33.92	24.09	28.44	0.35	13.20
	(0.14)	(1.16)	(10.03)	(0.15)	(1.46)	(1.16)	(0.19)	(5.28)	(6.85)	(6.40)	(0.74)	(11.82)
Fall	0.24	3.15	14.93	0.67	2.80	2.18	0.67	30.30	23.54	25.20	0.37	20.59
	(0.15)	(1.67)	(7.04)	(0.35)	(1.34)	(0.85)	(0.12)	(4.92)	(6.21)	(6.55)	(0.63)	(13.62)
Annual	0.23	2.49	13.25			2.10	0.69	30.59	22.99	25.35	0.35	20.72
	(0.17)	(2.06)	(5.88)			(0.86)	(0.13)	(5.28)	(6.10)	(7.02)	(0.71)	(13.42)
n	208*	234	179	177	177	146	146	108	108	108	108*	108*

*Many samples were below detection limit; only those above detection limit are included.

Many EC values were below detection limit during summer, and thus the number of samples for which SOC was calculated was smaller than the number of samples for OC. Thus, mean SOC value is greater than mean OC. Values for summer include 11 days from August 2007, when OC typically was larger than August 2008.

Table 3.3: Functional group distribution (% of C) obtained from H^+-NMR spectra from various samples.

Sample	Distinction	FG1 (%)	FG2 (%)	FG3 (%)	FG4 (%)	FG5 (%)	WSOC ($\mu gC/m^3$)
Clean day (10/28/2007)	CO: 92 ppb	30.54	16.86	19.00	0.00	33.59	0.88
Polluted day (01/07/2008)	CO: 530 ppb	25.90	23.77	34.50	2.82	13.01	4.14
Low CO periods	<150 ppb	31.29	20.97	24.95	0.07	22.72	1.63
(n = 26 for FGs & 39 for WSOC)		(6.07)	(6.24)	(5.79)	(0.18)	(14.21)	(0.73)
High CO periods	>300 ppb	29.66	25.81	30.58	1.57	12.39	3.22
(n = 3 for FGs & 6 for WSOC)		(3.79)	(2.36)	(3.77)	(1.11)	(1.42)	(0.64)
Low O_3 periods	<15 ppb	30.62	23.67	27.51	0.82	17.38	2.40
(n = 9)		(5.33)	(5.46)	(8.00)	(1.04)	(13.30)	(1.04)
High O_3 periods	35-60 ppb	30.14	23.19	24.28	0.31	22.08	2.11
(n = 41)		(5.11)	(5.44)	(7.76)	(0.71)	(12.89)	(1.05)
Dry periods	0 inches rainfall	31.39	24.30	24.83	0.38	19.09	2.27
(n = 60)		(5.53)	(6.04)	(6.57)	(0.73)	(13.21)	(0.84)
Very wet periods	>1 inch rain event	30.61	18.06	25.57	0.39	25.36	1.58
(n = 5)		(6.23)	(3.48)	(5.84)	(0.87)	(9.33)	(0.29)

Standard deviations are given inside parentheses. 92 ppb and 530 ppb of CO were the minimum and maximum during the sampling campaign.

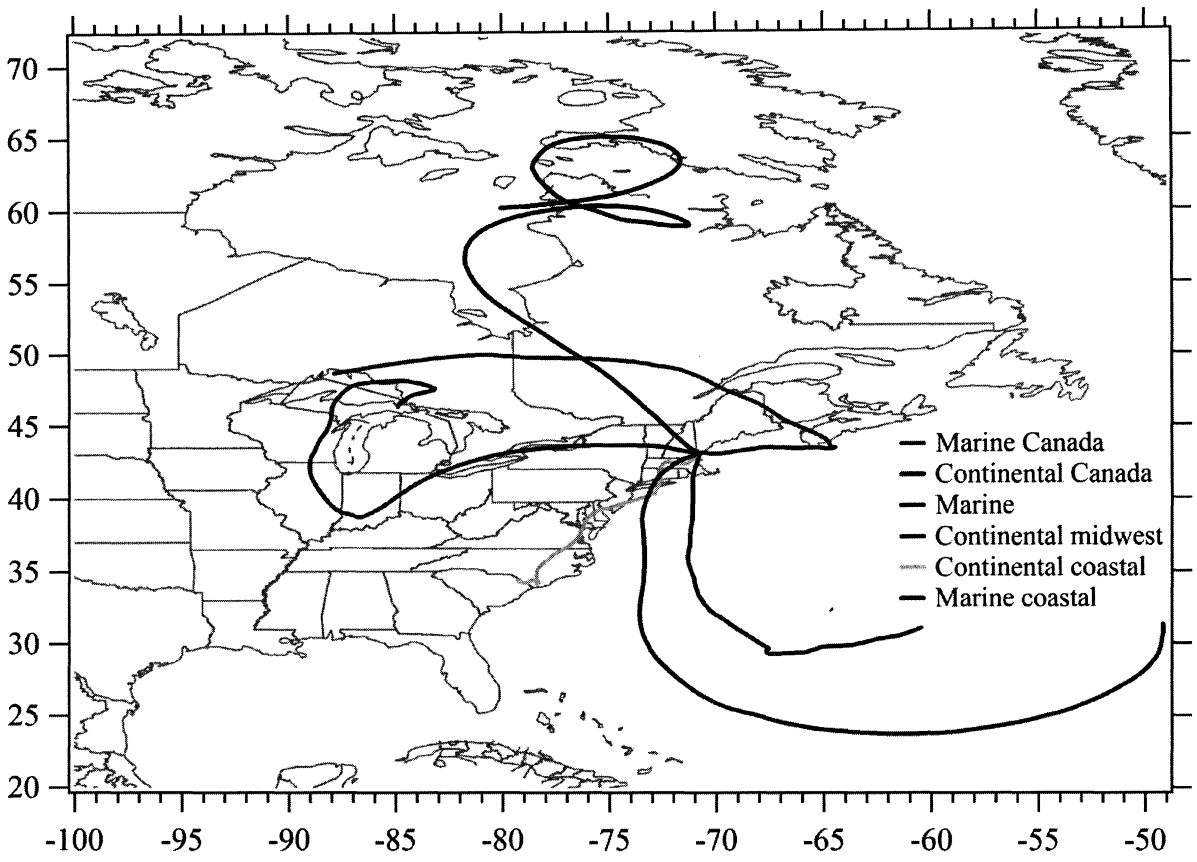

Figure 3.1. Six backward trajectories illustrating the classification of different air mass origins.

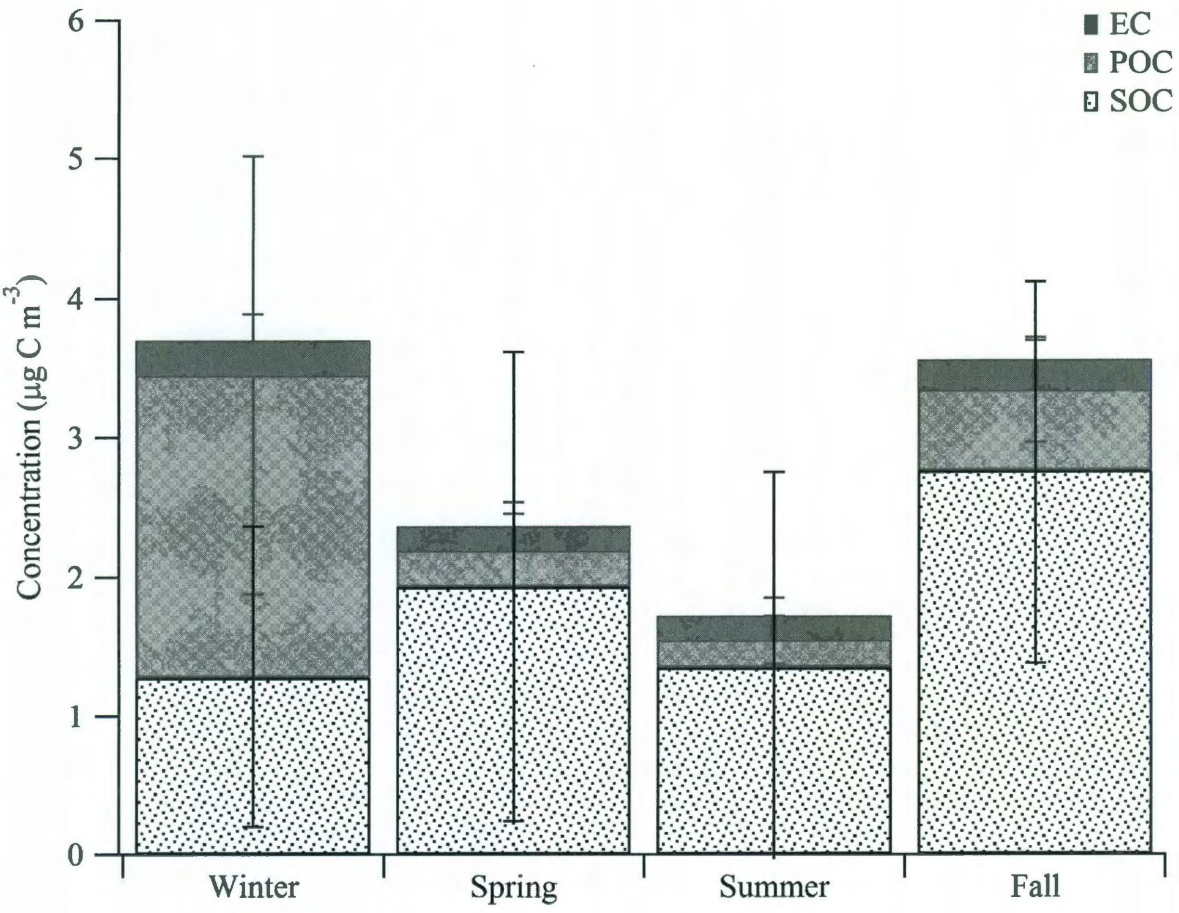

Figure 3.2. Seasonal concentrations of EC, POC, and SOC during four seasons of the sampling campaign.

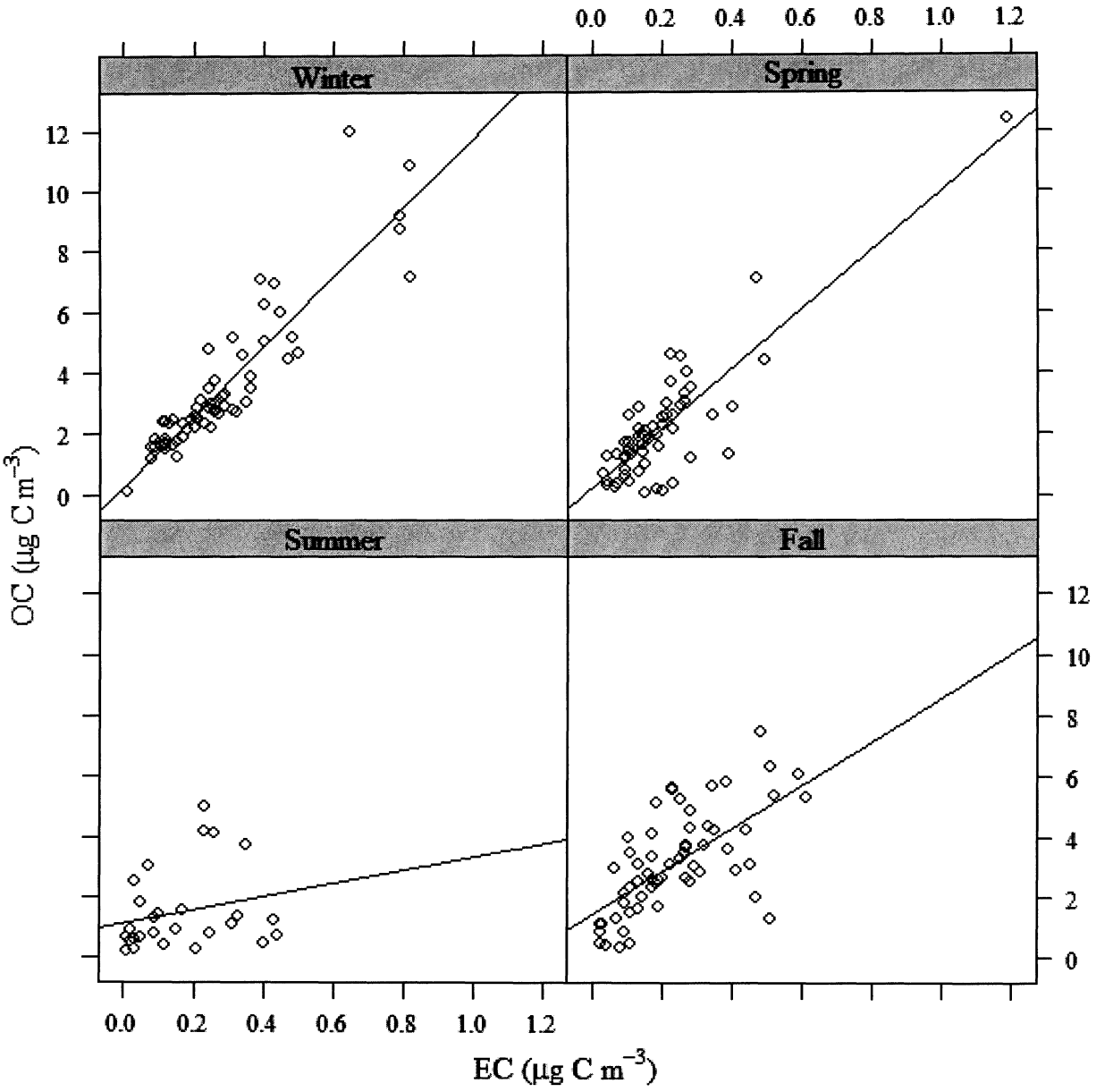

Figure 3.3. Correlation of OC and EC in winter (R^2=0.83; p<0.0001; slope = 11.34), spring (R^2=0.73; p<0.0001; slope = 9.78), and fall (R^2=0.42; p<0.001; slope = 7.22). No correlation was observed in summer.

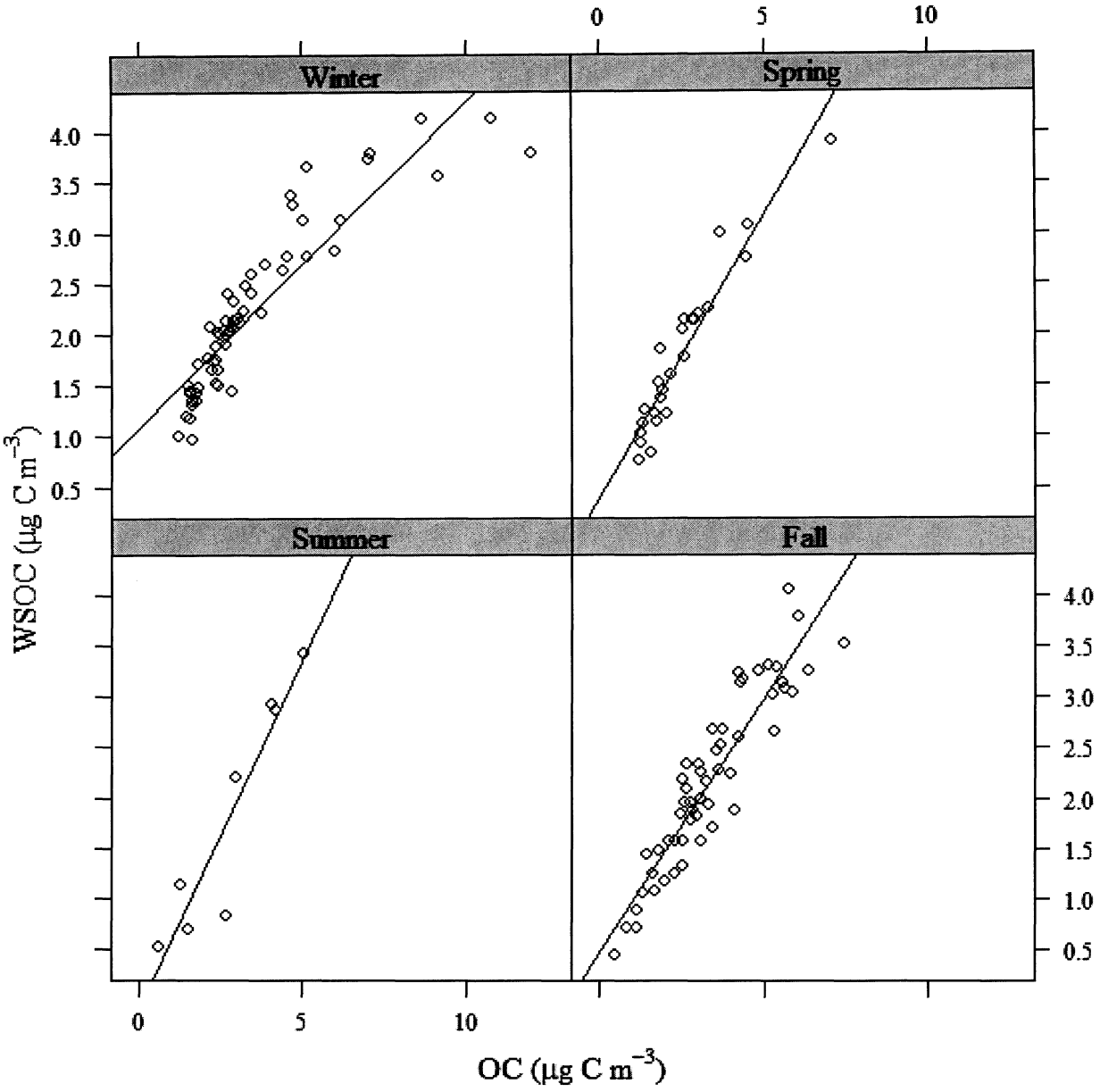

Figure 3.4. Correlation of WSOC and OC in winter (R^2=0.80; p<0.0001; slope = 0.32), spring (R^2=0.90; p<0.0001; slope = 0.56), summer (R^2=0.87; p<0.001; slope = 0.69), and fall (R^2=0.85; p<0.0001; slope = 0.50).

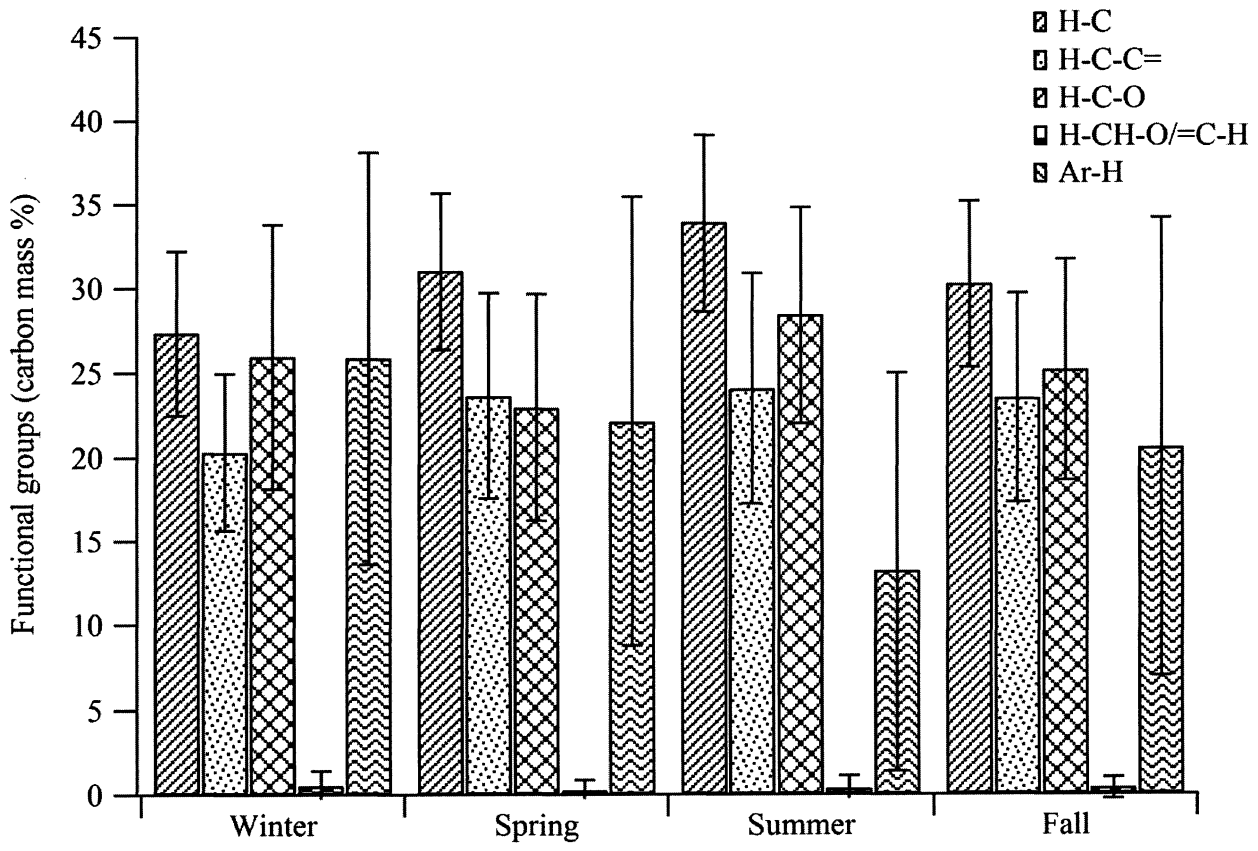

Figure 3.5. Seasonal trends of functional group composition of WSOC. Error bars indicate standard deviations.

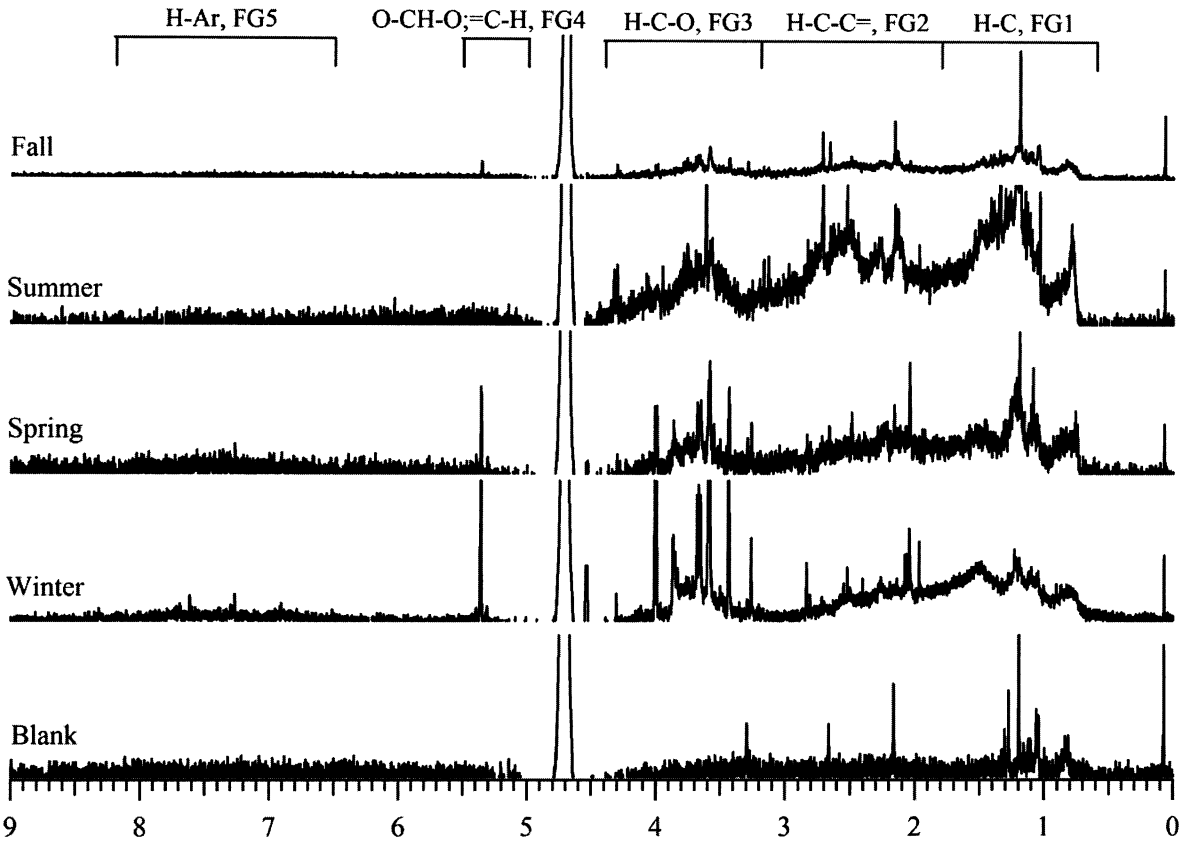

Figure 3.6. H^+- NMR spectra of aerosol samples; blank; winter (12/06/2007); spring (03/02/08); summer (07/12/08); fall (09/18/07).

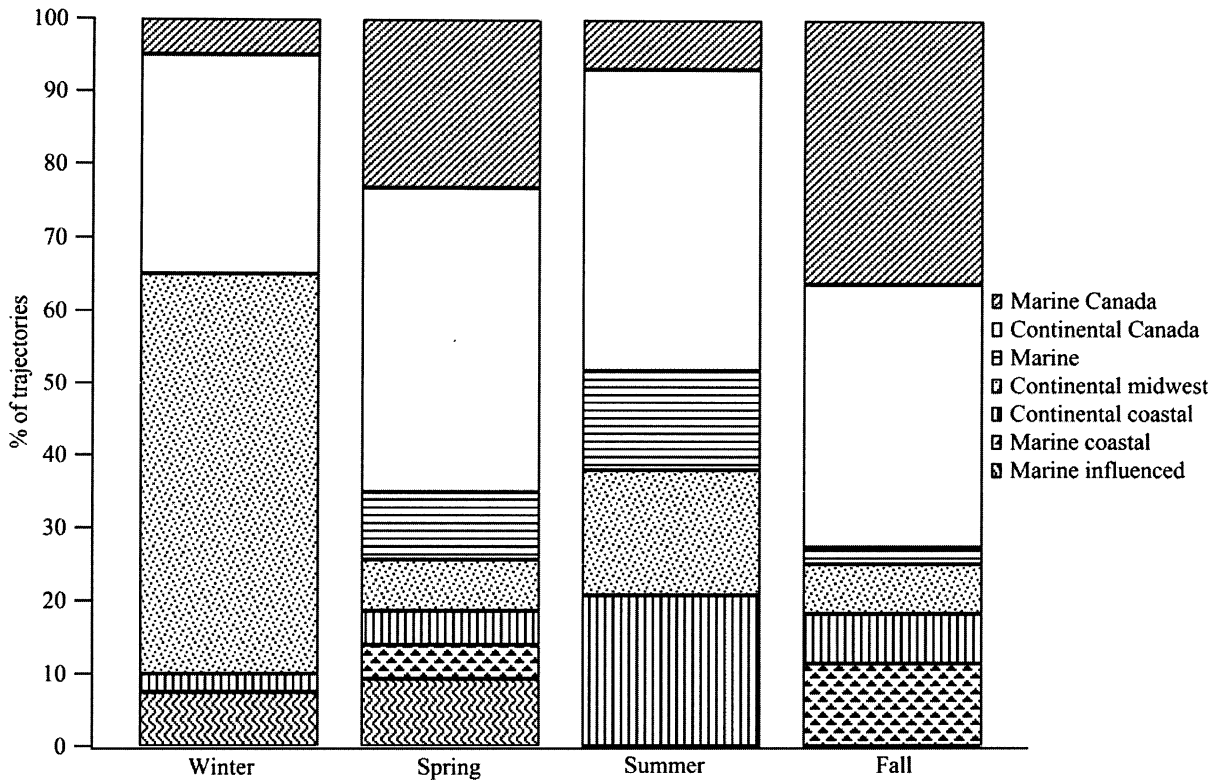

Figure 3.7. Classification of air masses arriving at TF based on backward trajectory analysis. Twenty-four hour periods without two associated backward trajectories showing the same region are not included. This does not represent the typical air mass influence for these seasons as the data are shown only for sampling days and the days with mixed air mass origin are not included.

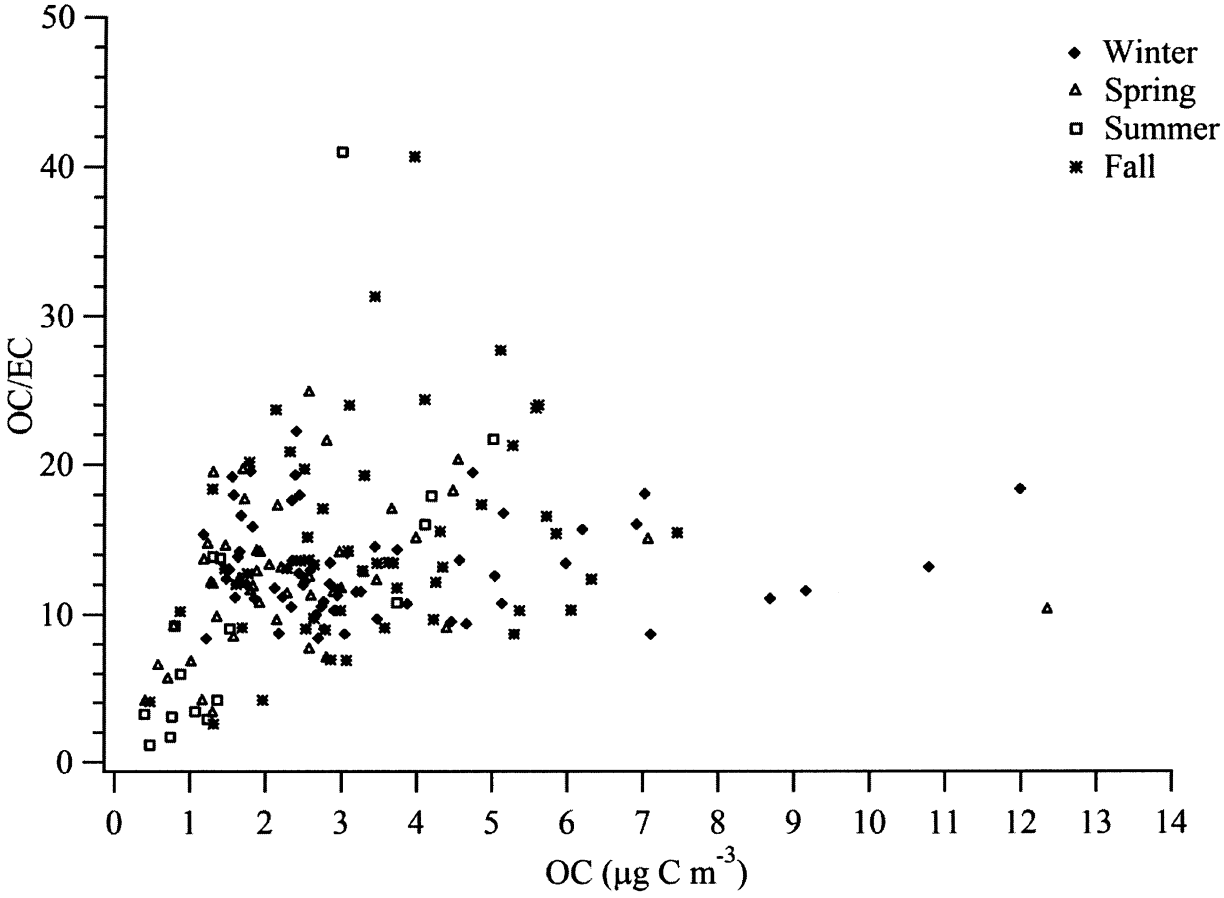

Figure 3.8. Seasonal relationship between OC/EC and OC concentrations.

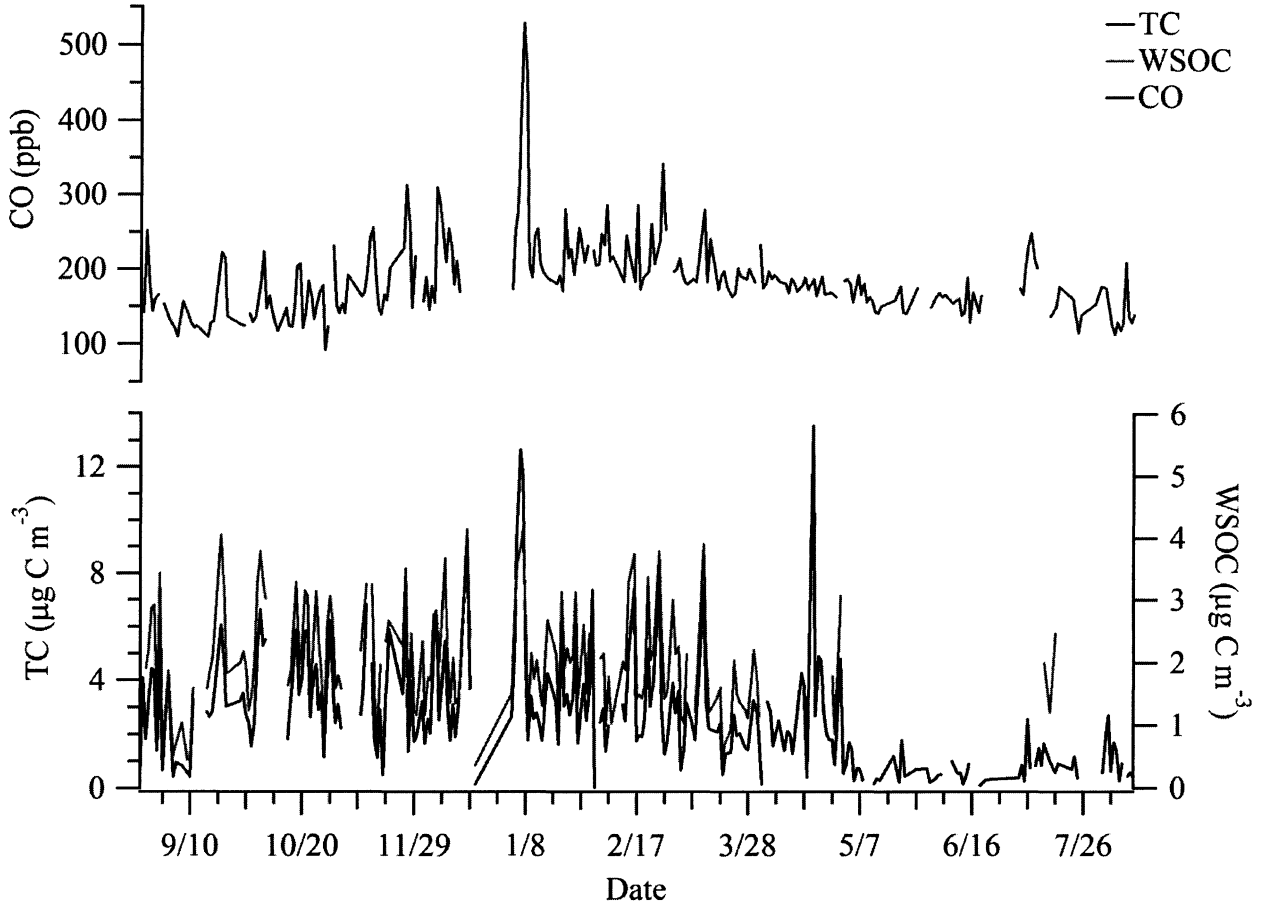

Figure 3.9. Time series of CO, TC and WSOC concentrations during the sampling campaign.

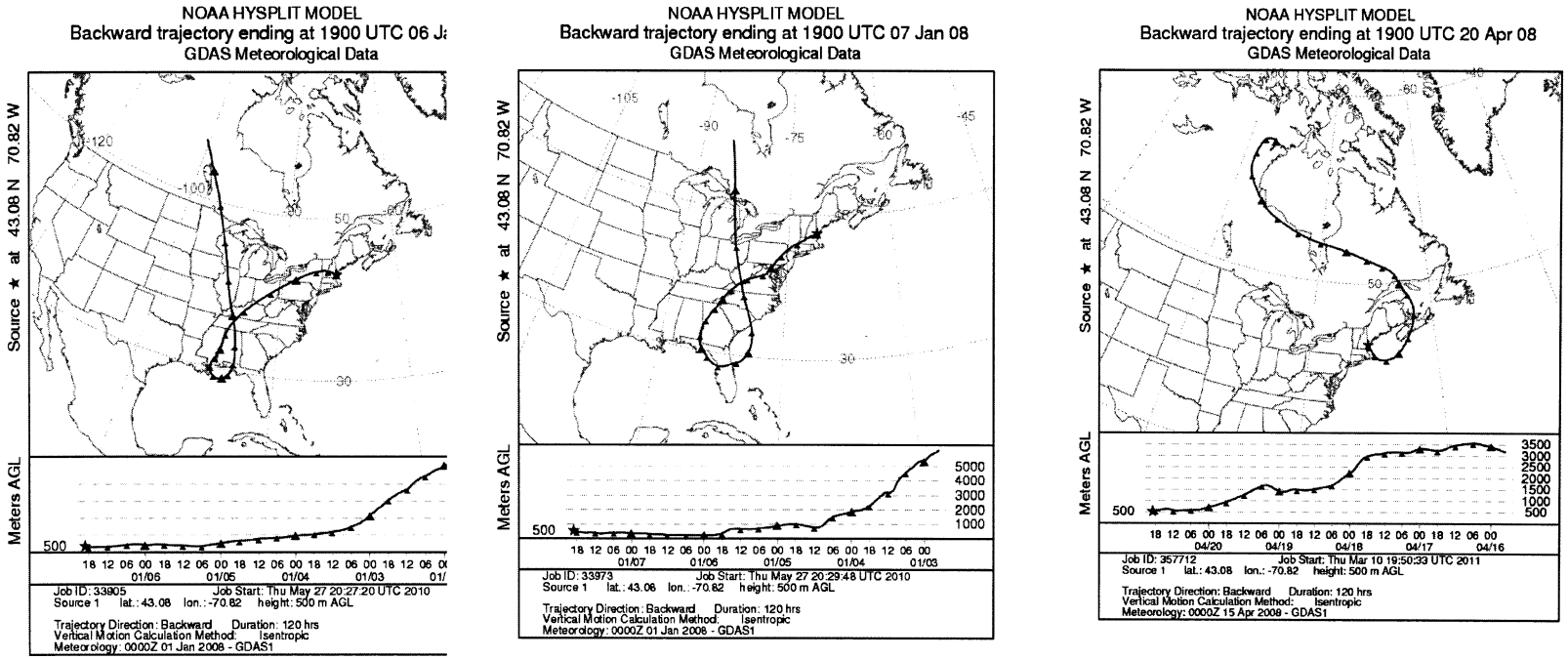

Figure 3.10. Air mass backward trajectories arriving at TF during two pollution episodes (January 6-7 and April 20, 2008).

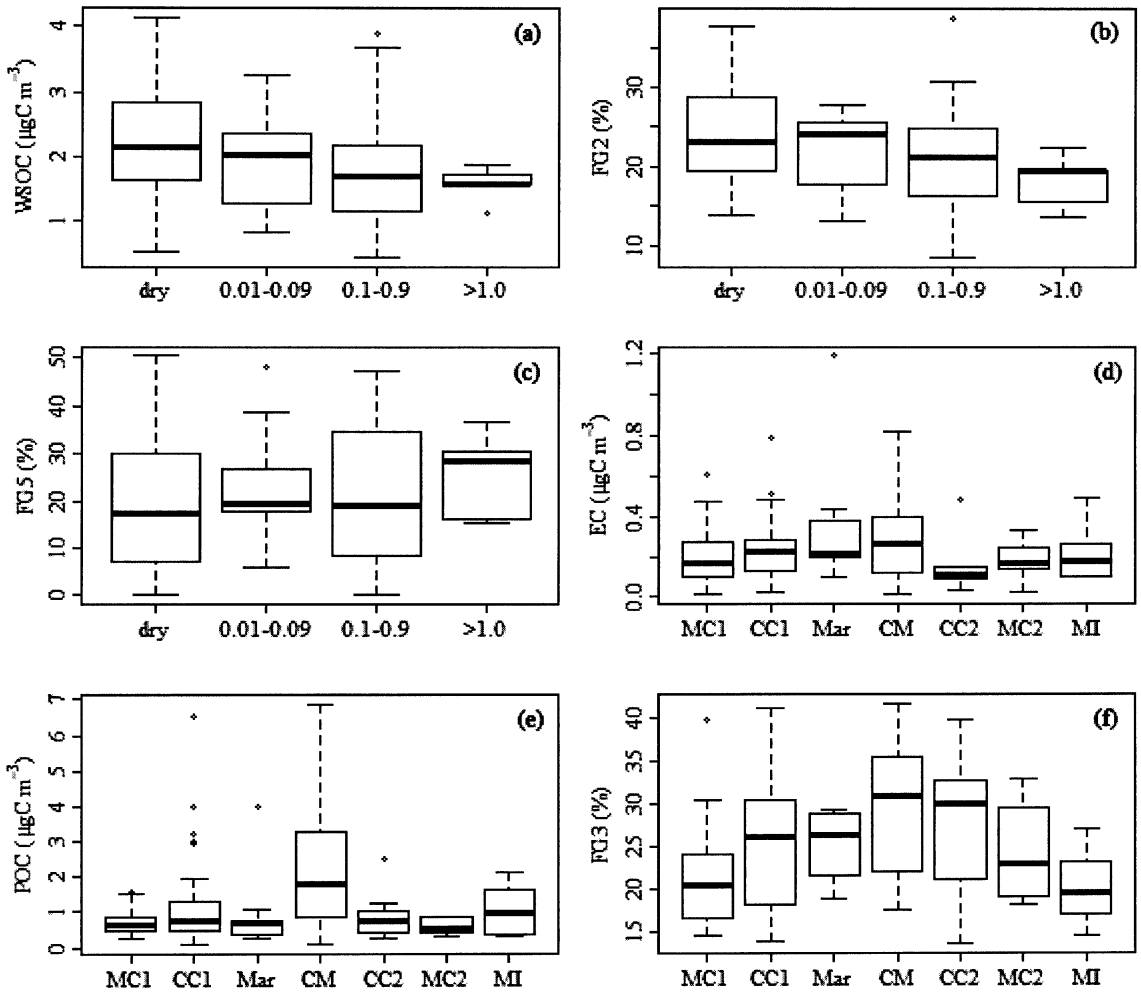

Figure 3.11. a-c.) The effect of precipitation on WSOC concentrations and functional group contributions (FG2 and FG5); x-axis represents four periods: dry, 0.01 to 0.09, 0.1 to 0.9, and >0.1 inches of precipitation. d-f.) The influence of air mass origin on aerosol composition (EC, POC, and FG3); x-axis represents the air mass transport regions: MC1: marine Canada; CC1: continental Canada; Mar: marine; CM: continental Midwest; CC2: continental coastal; MC2: marine coastal; MI: marine influenced.

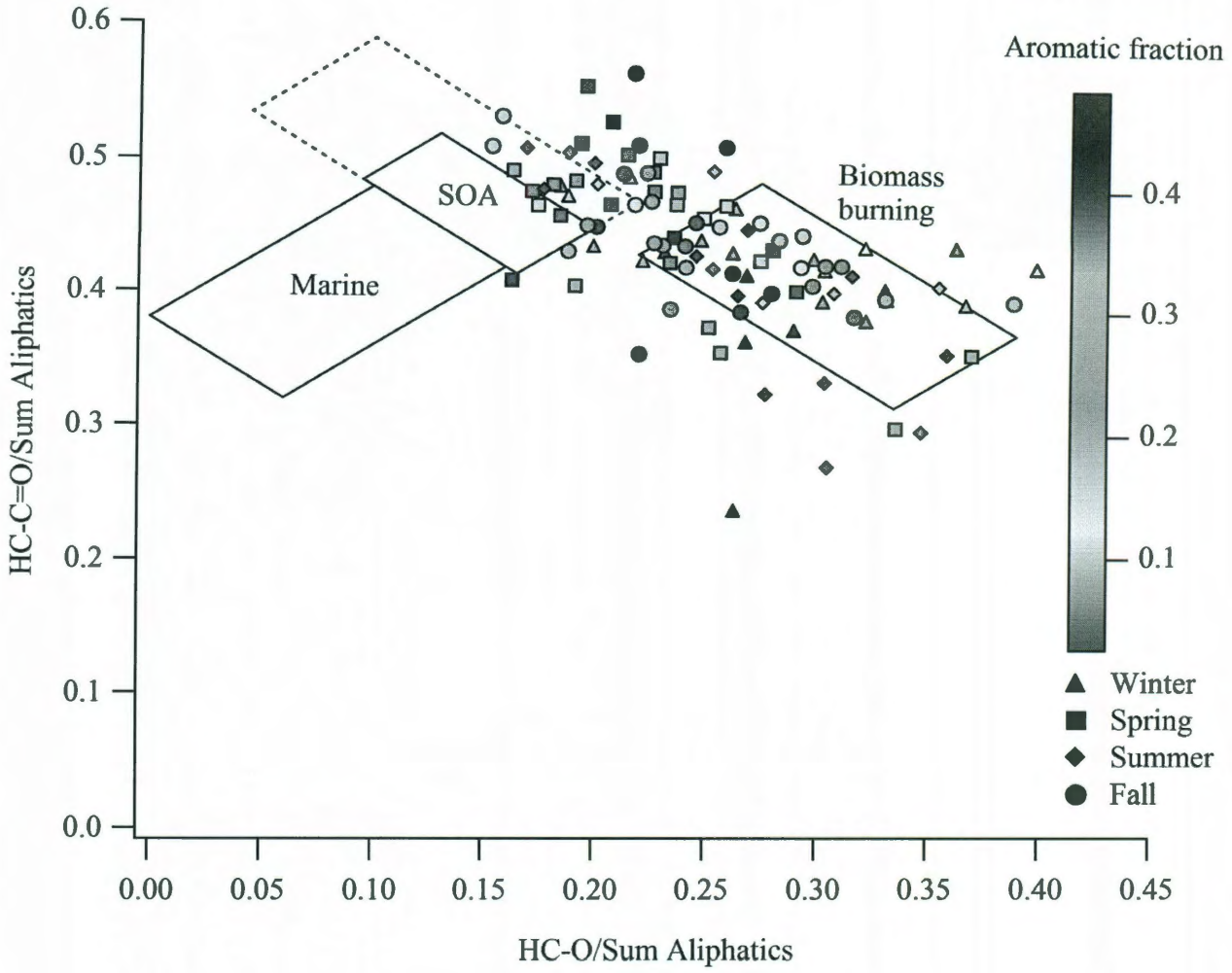

Figure 3.12. Composition of WSOC illustrated by the ratio of FG6 to total aliphatics and FG3 to total aliphatics. Boxes representing specific fingerprint sources of marine, SOA, and biomass burning aerosols were recreated based on Decesari et al. (2007). Color bars illustrate the corresponding aromatic fraction in the observed aerosols, and different symbols represent aerosols from different seasons.

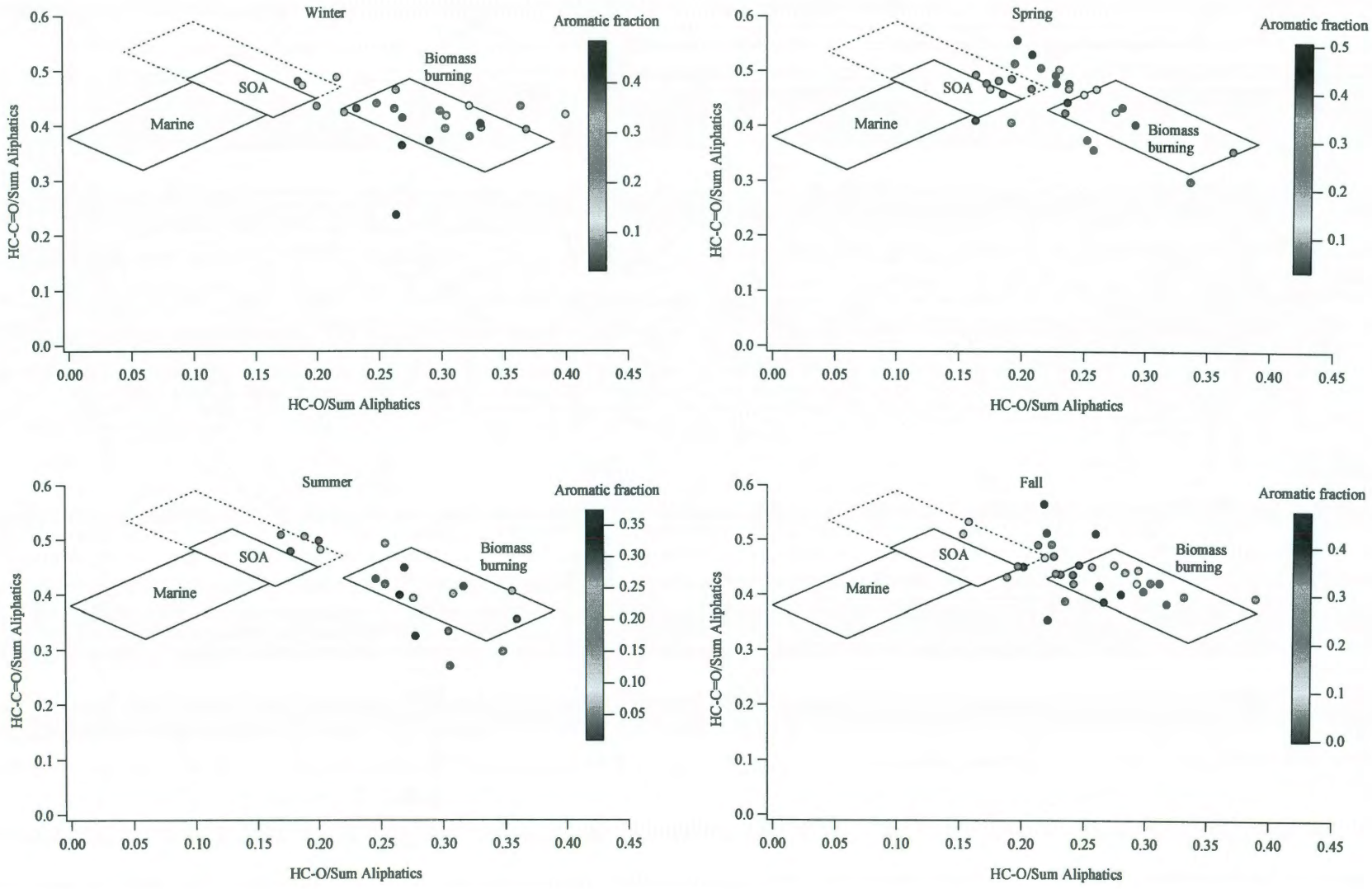

Figure 3.13. A comparison of FG6 to total aliphatics versus FG3 to total aliphatics among four seasons. Boxes represent the aerosol sources signatures of marine, SOA, and biomass burning given by Decesari et al. (2007). The color bar indicates the aromatic fraction in WSOC.

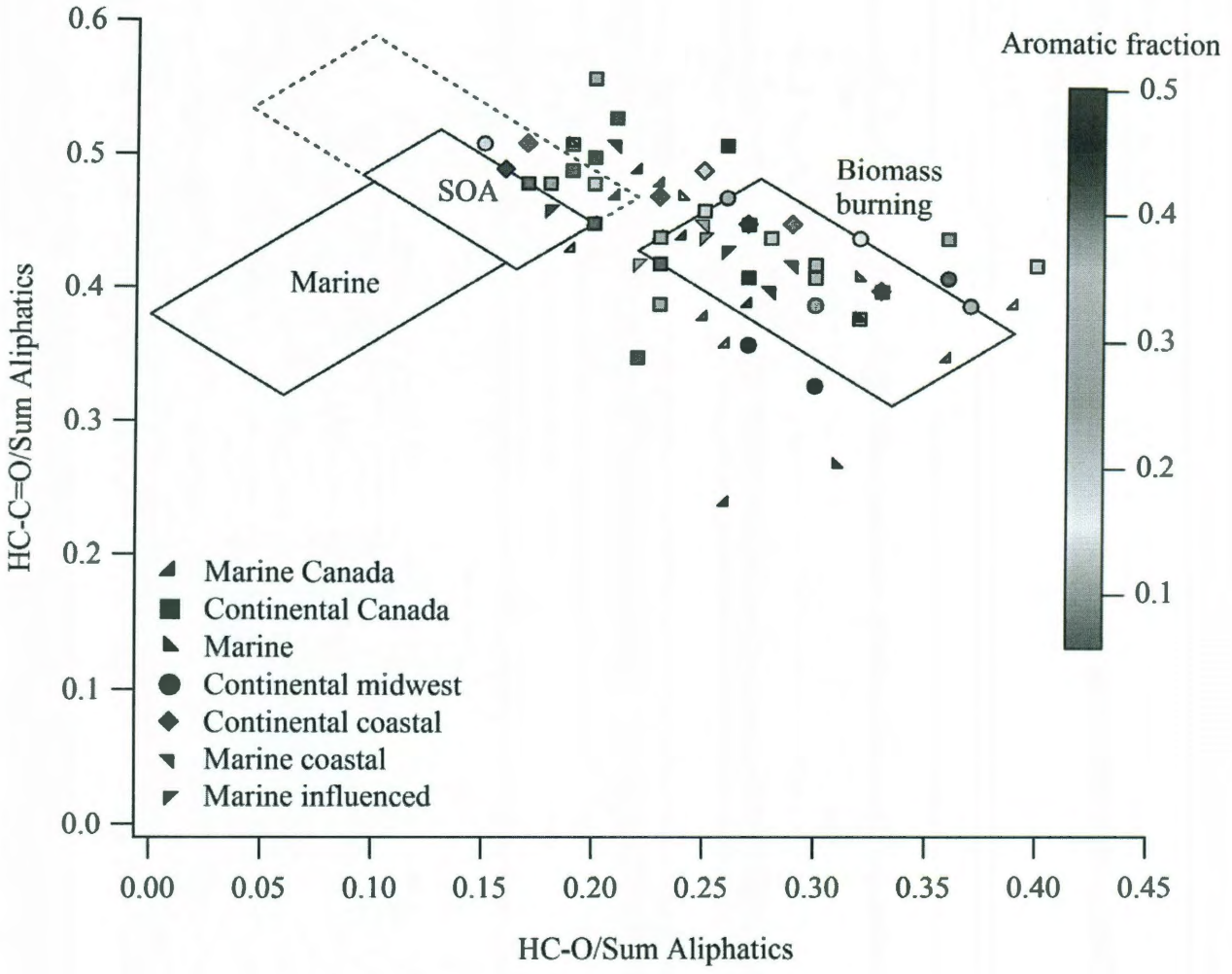

Figure 3.14. Ratio of HC-O to total aliphatics versus ratio of HC-C=O to total aliphatics classified by seven air mass origins. Figure 7 is replotted based on air mass instead of seasons.

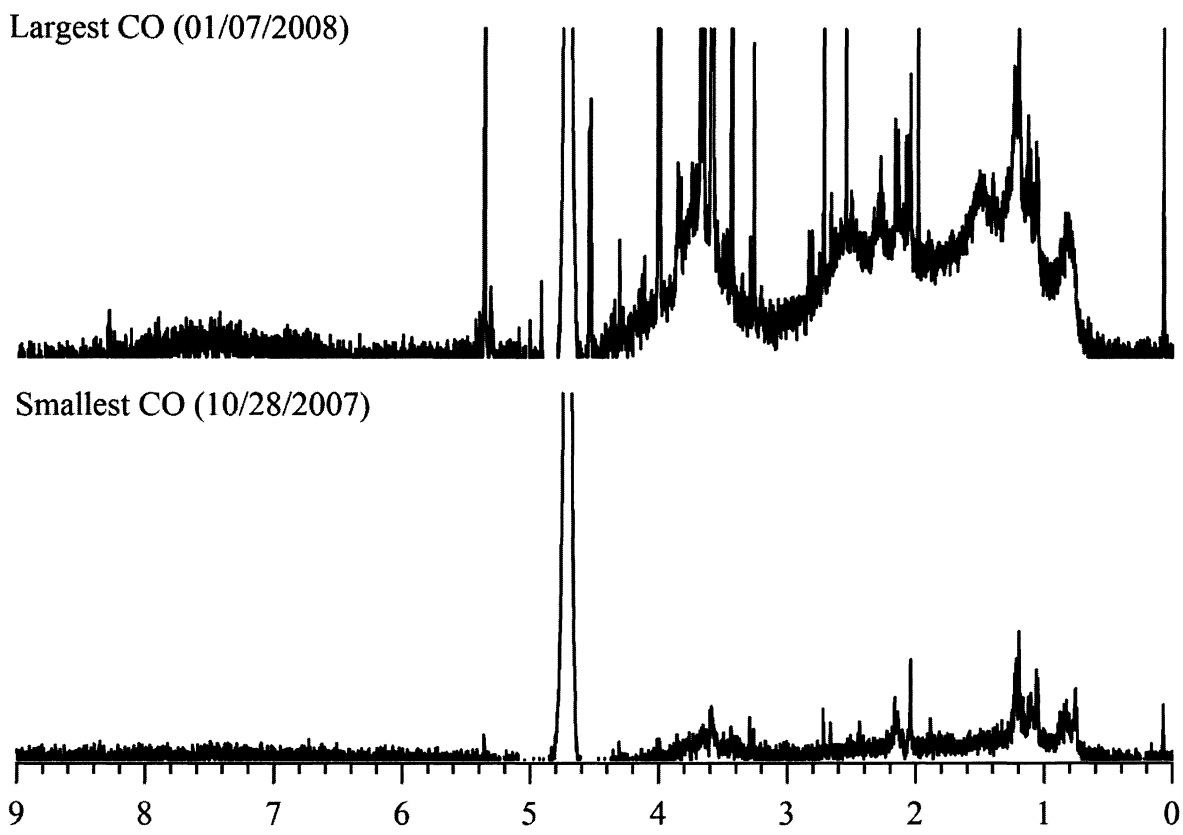

Figure 3.15. H^+-NMR spectra of aerosol samples during the least polluted day (10/28/2007: 92 ppb CO) and the most polluted day (01/07/2008: 530 ppb CO).

Chapter 4

Seasonal variation in particle characteristics at a semi-rural New England location – Part 2: Stable carbon and nitrogen isotope composition

Abstract

The stable carbon and nitrogen isotope composition of aerosols collected from a semi-rural site in New England from August 23, 2007, until August 12, 2008, were used to study the characteristics and temporal dynamics of aerosol sources. The narrow range (mean: -26.0 ± 1.4‰, 1σ) of stable carbon isotope composition ($\delta^{13}C$) of aerosols suggests a consistent isotopic signature of sources of carbonaceous aerosol, with any biogenic sources most likely being from C_3 plants. The wider range (mean: 4.4 ± 5.8‰) of stable nitrogen isotopes ($\delta^{15}N$) of the aerosols most likely reflects the variable nitrogenous aerosol sources. Summer aerosols were enriched ($\delta^{15}N$ = 7.7 ± 4.9‰), and winter aerosols were depleted ($\delta^{15}N$ = 1.2 ± 6.4‰) in ^{15}N, while $\delta^{13}C$ did not vary seasonally. Variation of $\delta^{15}N$ is associated strongly with temperature and relative humidity, suggesting that meteorology may play an important role in nitrogen isotope fractionation. Stable carbon and nitrogen isotope source signatures at this site suggest seasonal influences of motor vehicle traffic, fuel combustion, industrial emissions, and natural gas combustion.

4.1 Introduction

Stable carbon isotope ($\delta^{13}C$) variability in aerosols has been used to characterize the variety of sources and mechanisms from which aerosols originate (Cachier, 1989). Continental aerosols (diameter ≤ 0.5 μm) in the northern hemisphere have a lower $\delta^{13}C$ (-25.5‰ ± 2) compared to that for the marine aerosols in the southern hemisphere (-23.5‰ ± 0.5), suggesting the influence of anthropogenic versus natural emission sources in the respective hemispheres (Cachier et al., 1986). Carbon isotopic composition of aerosols also can indicate the influence of marine or continental sources (Cachier, 1989) and in tracing biomass burning events. C_3- and C_4-plants have $\delta^{13}C$ of approximately -28‰ and -14‰, respectively (Smith and Epstein, 1971). The $\delta^{13}C$ in C_3- and C_4-plants are different enough (about 14‰) to be useful, although burning and the resulting particle creation diminishes the separation to about 10‰ (Turekian et al., 1998). Particle $\delta^{13}C$ also varies as a result of the processing of secondary organic aerosol precursors (Irei et al., 2006).

Oxidation of nitrogen oxides (NO_x) potentially leads to nitrate (NO_3^-) and organic nitrogen, both of which also can be emitted directly, in aerosols. An additional important form of nitrogen in aerosol is ammonium (NH_4^+). Knowledge of nitrogen isotope composition of aerosols aids in determining the sources of these nitrogen-containing materials because aerosols from specific geographic regions or sources often have distinct isotopic signatures. Marine particulate organic matter, marine dissolved organic nitrogen (DON), soil organic matter, and terrestrial plants are enriched (mostly positive $\delta^{15}N$) while inorganic nitrogen and dissolved organic nitrogen in rainwater are depleted in ^{15}N (mostly negative $\delta^{15}N$) (Cornell et al., 1995). The $\delta^{15}N$ in the DON in rain

samples from remote sites were lower compared to urban and rural sites (Cornell et al., 1995). Nitrogen oxides and ammonia (NH_3) in unpolluted air were lower in $\delta^{15}N$ compared to the NO_x from automobile exhaust and NH_3 in barnyard samples (Moore, 1977). Atmospheric nitrates in Polar regions contain very low $\delta^{15}N$ (Morin et al., 2009).

Knowledge of isotopic composition also aids in the quantification of atmospheric deposition of nitrogen to terrestrial and marine ecosystems (Cornell et al., 1995; Kawamura et al., 2004; Elliott et al., 2007; Miyazaki et al., 2010). For example, stationary sources were found to determine the atmospheric total reactive nitrogen (NO_y) deposition rate in the eastern United States based on a strong correlation between $\delta^{15}N$ and NO_x emissions from surrounding stationary sources (Elliott et al., 2007).

An extensive data set (n = 156) on carbon and nitrogen isotope composition of bulk aerosols collected for a year at a semi-rural location with an urban influence (Thompson Farm, New Hampshire) is presented here. Seasonal variations in isotopes, the association of isotope values with other aerosol components (carbonaceous, ionic, and organic), and the influence of environmental parameters (temperature, photochemical activity) and trace gases (nitric oxide (NO), NO_y, and carbon monoxide (CO)) are examined.

Ziemba et al. (2007) observed weakly acidic ionic aerosols dominated by sulfate and ammonium at this sampling site from 2000 to 2004. Cottrell et al. (2008) identified the dominance of organic matter and sulfate compared to ammonium and nitrate in submicron, non-refractory aerosols at this site during the ICARTT campaign in summer 2004. Based on these studies, this site appears to be influenced more by transport and processed pollutants rather than local point sources. This paper is the first to investigate

the isotopic composition of aerosols in this region, adds to the knowledge on their sources, and complements part 1 of this paper in which functional groups in water-soluble organic aerosols are characterized.

4.2 Methodology

4.2.1 Sampling

Bulk aerosol samples were collected on 90-mm quartz-fiber filters (QFF) at the University of New Hampshire (UNH) Atmospheric Observing Station located at Thompson Farm, Durham, New Hampshire. Aerosols were collected from Thompson Farm at two sampling sites that are 0.31 kilometers apart: site 1 (43.1092° N, 70.9484° W; 24 m elevation above sea level) from August 22, 2007, to July 2, 2008, and site 2 (43.1078° N, 70.9517° W; 39.9 m elevation above sea level) from July 3, 2008, to August 13, 2008. As in Part 1, it is assumed that the change in sample collection location did not affect the data. The Thompson Farm location is one of the sites within the larger AIRMAP monitoring network. Contemporaneous data describing meteorology, aerosol optical properties, several gases such as NO, CO, NO_y, and ozone (O_3), and inorganic aerosol species were available from AIRMAP and averaged over the 24-hour period of the sampling. The usual time-span of each sample was 24 hours. The sampling was performed from atop a 12-m (site 1) or 24-m (site 2) tower that extended above the forest canopy. The filters were analyzed for carbonaceous material (elemental and organic), water-soluble organic carbon (WSOC), and functional groups using proton nuclear magnetic resonance (H^+-NMR) spectroscopy. These results are mentioned briefly here but reported fully in Part 1 of this paper. Isotopic analysis is described here.

4.2.2 Analysis

Two punches, each of 1.5 cm^2, were cut from each QFF and put inside an aluminum-foil cup using tweezers. Total carbon (TC), total nitrogen (TN), and stable carbon and nitrogen isotope ratios were analyzed using a Costech elemental analyzer coupled to a Delta Plus XP Isotope Ratio Mass Spectrometer (IR-MS).

Carbon and nitrogen isotope ratios are expressed as $\delta^{13}C$ or $\delta^{15}N$ in per mil (‰), where

$$\delta^{13}C \text{ or } \delta^{15}N = \left[\frac{R_{sample}}{R_{std}} - 1\right] * 1000 \quad (1)$$

where $R = \frac{^{13}C}{^{12}C}$ for $\delta^{13}C$ and $R = \frac{^{15}N}{^{14}N}$ for $\delta^{15}N$ in the respective samples and standards (std). The standard for the stable carbon isotope content is that of Vienna Pee Dee Belemnite, while the standard for the nitrogen isotope content is that of atmospheric nitrogen.

4.2.3 Air mass origins

Hybrid Single-Particle Lagrangian Integrated Trajectory (HYSPLIT) model (Draxler and Rolph, 2010) backward trajectories were run for five days using Global Data Assimilation System meteorological data and isentropic vertical motion assuming a boundary layer height of 500 meters above ground level. Air masses were classified into seven classes, based on geographical origin: marine Canada, continental Canada, marine, continental Midwest, continental coastal, marine coastal, and marine influenced as described in Part 1 and in Ziemba et al. (2007). Three trajectories at different time

periods for each 24-hour sample were run; air masses with mixed origins were not included in this classification.

4.3 Results and discussion

A total of 156 bulk aerosol samples were analyzed for stable carbon and nitrogen isotope content. Due to the low N and C contents on the filters, multiple blank filters (two punches each) were analyzed and used to blank correct all N and C data. Isotope values are segregated by season: winter (December to February), spring (March to May), summer (June to August), and fall (September to November).

4.3.1 Stable carbon isotope

4.3.1.1 Seasonal variation

Overall little variation was observed for $\delta^{13}C$ in aerosols during the sampling campaign (Table 4.1 and Figure 4.1). Mean and median values were very similar in all seasons, and monthly variation also was small for $\delta^{13}C$ values. The largest shift in $\delta^{13}C$ occurred during late summer. Mean $\delta^{13}C$ increased by 1.8‰ from July 2008 to August 2008 and decreased by 0.7‰ from August 2007 to September 2007. The highest and the lowest monthly means of $\delta^{13}C$ were observed during August 2008 (-24.9 ± 3.54‰) and March 2008 (-27.4 ± 3.5‰), respectively.

The slightly lower $\delta^{13}C$ values observed in winter (-26.2‰) and spring (-26.3‰) coincided with larger elemental carbon (EC) values and a stronger correlation between EC and aerosol organic carbon (OC), possibly indicating the importance of fossil fuel combustion sources (Part 1). Carbon isotopes in OC are expected to vary more than in

EC because EC is generally much less amenable to processing compared to OC (Huang et al., 2006). The $\delta^{13}C$ variation was not related to changes in OC concentrations.

4.3.1.2 Relationship of $\delta^{13}C$ to water-soluble OC (WSOC), organic functional groups, and air mass origins

The $\delta^{13}C$ was correlated positively with WSOC (R^2= 0.41, $p<0.05$; n = 11) during spring (Figure 4.2), indicating enriched ^{13}C with aerosol aging because WSOC is assumed to increase with increased oxidation/processing (Saxena and Hildemann, 1996). A similar trend was observed in inland China where an increase in $\delta^{13}C$ was correlated to increased concentration ratios of oxalic acid to OC (Wang et al., 2010). Fisseha et al. (2009) also reported the increase of $\delta^{13}C$ in TC in Zurich when WSOC constituted a predominant fraction of TC. It is possible that aerosol photochemical aging caused isotope fractionation, leading to oxidation products with the lighter ^{12}C to favor the gas phase and a condensed phase enriched in ^{13}C (Wang et al., 2010). There were an insufficient number of samples with both $\delta^{13}C$ and WSOC values available in summer, and no such correlation was observed during winter and fall.

During summer, $\delta^{13}C$ was correlated negatively with pure aliphatic carbon (FG1) (R^2= 0.62, $p<0.005$; n = 12), unsaturated aliphatic carbon (FG2) (R^2= 0.36, $p<0.05$; n = 12), and oxygenates (FG3) (R^2= 0.57, $p<0.005$; n = 12), as identified by H^+-NMR (Part 1). No correlation was observed for aromatic groups. The $\delta^{13}C$ values did not correlate with any of the five functional groups obtained from H^+-NMR spectroscopy during winter, spring, and fall. Higher $\delta^{13}C$ with the decrease in FG1, FG2, and FG3 suggests favored revolatilization or heterogeneous reactions of these functional groups during

summer conditions (higher temperatures and stronger photochemistry); isotope fractionation during these processes may leave the remaining aerosol enriched with ^{13}C. Data on carbonaceous aerosols suggest secondary sources rather than primary sources are dominant during summer at Thompson Farm (Cottrell et al., 2008; Part 1).

The functional group composition of aerosols differed for the samples with the extreme observed values of depleted- and enriched-^{13}C (Table 4.2). The contributions of functional groups such as pure aliphatics and oxygenates were larger in ^{13}C-depleted aerosols compared to the enriched ones. In contrast to this, the aromatic group contribution was smaller in ^{13}C-depleted aerosol compared to enriched samples. No major change was observed in the contribution of unsaturated functional groups between the depleted and enriched samples. Aliphatics from plant waxes are depleted in ^{13}C relative to other plant components (leaves, roots or total plant carbon) (Conte et al., 2003; Hobbie and Werner, 2004), which could indicate influence of primary biological particles during this event. Enriched oxygenate functional groups (hydroxyl) also may be related to carbohydrates/sugars from primary biological aerosol particles (Graham et al., 2003 and references there in; Yttri et al., 2007).

The contributions of marine (m) and continental (c) sources to total carbon in the bulk aerosols were estimated assuming influence from only these two sources using (Chesselet et al., 1981):

$$\delta^{13}C_{TC} \times TC = \delta^{13}C_m \times C_m + \delta^{13}C_c \times C_c \quad (2)$$

$$TC = C_m + C_c \quad (3)$$

where $d^{13}C_{TC}$ and TC are measured values from the samples, C_m and C_c are the carbon from marine and continental sources, respectively, and the values of -21‰ and -26‰ are their respective $d^{13}C$ values. Days with $\delta^{13}C$ values below -26‰ (n = 82) were not included in this exercise as it is assumed that such samples have negligible marine influence.

Marine organic carbon is estimated to contribute only ~10% of total carbonaceous aerosol mass at Thompson Farm for those samples for which this calculation was performed. The largest and the smallest marine contribution occurs during summer (~19%) and winter (~6%), respectively. The relatively small contribution of marine organic matter to aerosols at Thompson Farm using this analysis corroborates the lack of a distinct marine source signature in the functional group analysis of WSOC (Part 1).

Backward trajectories revealed that aerosols associated with air masses of marine origins (Marine Canada, marine, and marine coastal) were slightly enriched in ^{13}C (by ~ 0.5‰) compared to those of continental origins (Continental Canada, continental Midwest, and continental coastal) (Figure 4.3), which is in agreement with Cachier et al. (1986) and Smith and Epstein (1971). However, the differences were not very large, and $\delta^{13}C$ (~-25‰) in aerosols from this subset of the current samples were lower than those previously reported for marine origin (-21‰) (Chesselet et al., 1981; Cachier et al., 1986). The inconsistency may be due to a lack of biological materials in the current samples because less biologically influenced marine aerosols (~-25‰) had lower $\delta^{13}C$ than highly biologically influenced aerosols (~-23 ‰) collected during summer 2008 over the North Pacific (Miyazaki et al., 2010). The observed small difference also agrees with the finding of small marine influence on carbonaceous aerosols at Thompson Farm.

4.3.1.3 Comparison with other sites

The campaign mean $\delta^{13}C$ (-26.0 ± 1.4‰) at Thompson Farm is comparable to the values reported at other locations such as Mexico City (-25 to -26‰; Marley et al., 2009), Vancouver, Canada (~-27.3‰; Huang et al., 2006), a C_3-plant-dominated site in Brazil (-26.9 to -24.9‰; Martinelli et al., 2002), a traffic-dominated site at an urban location in Kathmandu, Nepal (-26.1 to -25.5‰; Shakya et al., 2010), urban sites in Hong Kong (-25.4 to -27.7‰; Ho et al., 2006), and vehicle tunnels in Rio de Janeiro, Brazil (-25.6 to -25.3‰; Tanner and Miguel, 1989) (Figure 4.4). These comparisons suggest the dominance of anthropogenic and C_3-plant related sources. Most $\delta^{13}C$ values were below -24.0‰ (95th percentile: -24.64‰), indicating the negligible influence of C_4 plants in aerosols at Thompson Farm and values for $\delta^{13}C$ close to those reported for urban aerosols. Turekian et al. (1998) found that the $\delta^{13}C$ of aerosols emitted from the combustion of C_3 plants was 0.5‰ enriched compared to source plants, while Widory et al. (2004) reported $\delta^{13}C$ of -22.6 to -27.2‰ for the aerosols emitted from the combustion of regular-, unleaded-, and diesel- fuel, making it difficult to distinguish natural C_3-plant-based organic material from anthropogenically derived carbon.

4.3.1.4 Comparison with emission sources

Aerosol isotopic fingerprints for various emission sources help to identify the potential aerosol sources when isotopic fractionation is minimal in the emitted aerosols. Carbonaceous aerosols at Thompson Farm seem to have been less influenced by biomass burning, as the $\delta^{13}C$ values in the aerosols were smaller than -24‰, which is the value for the aerosols from the air influenced by biomass burning (Figure 4.4a). The $\delta^{13}C$ values

also vary depending on the various evolutionary stages of biomass burning (Cachier et al., 1985). The aerosols may originate from ^{13}C-depleted plant-related sources such as waxes, lignins, lipids, and fatty acids (Nadelhoffer and Fry, 1988; Ballentine et al., 1998; Poole et al., 2002, Conte et al., 2003; Hobbie and Werner, 2004). Most of the aerosol samples (150 out of 156 samples collected) in this study have $\delta^{13}C$ between -24.1 and -27.8‰, suggesting mixed isotopic source signatures from traffic-related, fuel-combustion, and industrial emissions as well as C_3-plants (Figure 4.4a). The secondary aerosol precursor values match those for aromatic volatile compounds and for rural biogenic isoprene (Figure 4.4a).

4.3.2 Nitrogen isotope

4.3.2.1 Seasonal variation and comparison with other sites and emission sources

The monthly and seasonal variations of $\delta^{15}N$ are presented in Figure 4.5. In contrast to $\delta^{13}C$, $\delta^{15}N$ varied greatly among different months and seasons (Table 4.1 and Figure 4.5), with the highest mean $\delta^{15}N$ during summer (7.7‰) and the lowest mean during winter (1.2‰). The relative difference between the mean and median values was the largest during winter, when the mean (1.2‰) was approximately two times larger than the median (0.5‰). The $\delta^{15}N$ value increased from February to June, reached peak values during June and July, and decreased to the lowest $\delta^{15}N$ value during February.

Seasonal variations of $\delta^{15}N$ values at Thompson Farm are in contrast to the isotopic measurements from other locations. Particulate nitrate had higher $\delta^{15}N$ during winter than summer in a moderately polluted area in Jülich, Germany (Freyer, 1991) and in Jeju Island, South Korea (Kawamura et al., 2004). The differences in seasonal

variation might be due to the differences in emission sources or the composition of collected nitrogen.

In contrast to Thompson Farm, the study site at Jülich (Freyer, 1991; Freyer et al., 1993) is in close proximity (within 30-km radius) to five coal-fired power plants, and Jeju Island was influenced significantly by coal combustion and/or soil organic nitrogen during winter (Kawamura et al., 2004).

Most (122 out of 156) $\delta^{15}N$ values were enhanced relative to atmospheric N_2. However, most of the negative $\delta^{15}N$ values occurred during winter (20 samples) and spring (8 samples); negative $\delta^{15}N$ values have been reported in NO_x emitted from vehicles and chemical industries as a result of isotopic fractionation during fuel combustion (Heaton, 1990). Specifically, vehicle exhaust from reduced-load vehicles exhibits lower $\delta^{15}N$ (-13‰) in NO_x compared to heavy-load vehicles (-2‰). In addition, the $\delta^{15}N$ of NH_3 ranges from -10‰ to -40‰ depending on the sources (Garcia et al., 2009). Therefore, in a period of enhanced importance of primary emissions, more negative values of $d^{15}N$ would be expected. This is the case in winter at Thompson Farm, as indicated by the large CO (237.76 ± 80.14 ppb) and NO (1.35 ± 2.70 ppb) mixing ratios (See Part 1, Table 3). In contrast to this, summer, with the highest $\delta^{15}N$, had the smallest CO (163.36 ± 30.06 ppb) and NO (0.14 ± 0.13 ppb) mixing ratios. This again supports that the seasonality of $\delta^{15}N$ at Thompson Farm is most likely to be affected by emission sources. However, it must be noted that differences in boundary layer heights, auto-exhaust mechanisms, and atmospheric oxidation rates during winter and summer may also have played a role in variation in CO and NO.

With respect to composition, the ammonium to nitrate ratios (NH_4^+/NO_3^-) were much larger at this study site (Ziemba et al., 2007) compared to those from previously published studies. Thus, the different $\delta^{15}N$ behavior in this study may be due to the differences in relative contribution of isotopic source signatures for NH_4^+ and NO_3^-, as well as the differences in temperature-dependent isotope fractionation mechanisms outlined for NH_4^+ and NO_3^- previously (Freyer, 1991; Yeatman et al., 2001).

Most of the seasonal $\delta^{15}N$ values fall in the range of more than one source signature (Figure 4.4b), suggesting nitrogenous aerosol at Thompson Farm to be related to mixed sources, most likely vehicular emissions and multiple types of combustion. Furthermore, $\delta^{15}N$ values in the precursor gases of aerosol nitrogen seem to indicate the major emission sources to be from vehicle exhaust. The bulk aerosol $\delta^{15}N$ will be affected by the respective contributions of NH_4^+ and NO_3^- species and the isotope fractionations during the formation of these species from NH_3 and NO_x. Furthermore, the combination of both carbon and nitrogen isotope results reduces the ambiguity in identifying the sources. The $\delta^{13}C$ and $\delta^{15}N$ source signatures in primarily emitted aerosols, its precursors and the values from different locations (Figure 4.4a and 4.4b) points to the strong influence from combustion-related and urban sources.

4.3.2.2 Inorganic ions

In contrast to the strong correlation of $\delta^{15}N$ with NH_4^+/NO_3^- in aerosols collected during winter in Kathmandu (Shakya et al., 2010), aerosols collected at Thompson Farm (08/25/2007 to 11/05/2007) did not exhibit such a correlation. In Kathmandu, values of NH_4^+/NO_3^- ratio were less than unity while at Thompson Farm, NH_4^+/NO_3^- ratios were

generally much greater than one. When NH_4^+ is present at much larger concentrations (by a factor of 30) than NO_3^-, aerosols were relatively ^{15}N-depleted. When the NH_4^+/NO_3^- value decreased after a rain event, $\delta^{15}N$ values also decreased, indicating more efficient wet scavenging of NH_4^+ compared to NO_3^- and further corroborating the findings that isotopic fractionation favors the incorporation of $^{15}NH_4^+$ in rain over $^{14}NH_4^+$ (Heaton, 1987).

4.3.2.3 Total nitrogen

Concentrations of TN were the largest during winter (1.24 ± 1.59 μg N m^{-3}) relative to the other seasons (spring: 0.91 ± 0.78 μg N m^{-3}; fall: 0.90 ± 0.85 μg N m^{-3}; summer: 0.89 ± 0.63 μg N m^{-3}). Particles emitted from diesel and fuel oil combustion have larger nitrogen content than coal or natural gas combustion and waste incinerators (Widory, 2007). The largest TN and the lowest $\delta^{15}N$ during winter suggest the dominance of combustion-related primary emission sources. Total nitrogen and $\delta^{15}N$ did not show any significant correlation. Total nitrogen was positively correlated with FG1, FG2, and FG3 of water-soluble aerosols during winter with R^2 of 0.49, 0.44, and 0.36 ($p<0.05$), respectively, and during spring with R^2 of 0.43, 0.48, and 0.46 ($p<0.005$), respectively. The association of TN with FGs of water-soluble aerosols might indicate the presence of organic nitrogen in association with these functional groups (e.g. amino acids, aliphatic amines) during winter and spring. Sorption of nitrogen compounds on carbonaceous aerosols and any similarity in emission sources might also have influenced these correlations. In general, organic nitrogen content in aerosol might be larger during winter and spring compared to other seasons. In Davis, California, relative water-soluble

organic nitrogen concentrations were larger during winter and early spring compared to the annual mean (Zhang et al., 2002).

4.3.2.4 Correlation with different parameters

The similar pattern of temperature and $\delta^{15}N$ (Figure 4.6) suggests that temperature dependent nitrogen isotope fractionation processes or emission behaviors (such as home heating) are responsible for the seasonal variation of $\delta^{15}N$ during the sampling campaign. It is hypothesized that increased gas- to particle- partitioning of ^{15}N- depleted products during winter lead to the aerosol depleted in ^{15}N. The opposite may be the case during summer.

The effects of relative humidity (RH) on $\delta^{15}N$ appeared to differ in summer (Figure 4.7) compared to other seasons. The $\delta^{15}N$ was correlated negatively with RH in summer ($R^2 = 0.45$, $p<0.001$) but not in other seasons. This might be due to the enhanced evaporation (with lower RH) of increased volatility nitrogenous products during summer. If evaporation was the cause, the evaporation processes discriminated ^{15}N over ^{14}N, and the increased evaporation left the substrate enriched in ^{15}N.

4.3.2.5 Interpretation of seasonal variation

The seasonal temperature-$\delta^{15}N$ relationship suggests that temperature-dependent isotope fractionation processes (including those driven photochemically) are important with respect to the equilibrium and kinetic processes of formation and dissociation for important nitrogen aerosol species such as NH_4NO_3 (Heaton, 1987; Freyer, 1991). For example, lower $\delta^{15}N$ in aerosols in inland China during spring and winter was attributed

to adsorption and condensation of gas-phase NH_3 and HNO_3 (Wang et al., 2010 and references therein). Thus, the lowest $\delta^{15}N$ during winter and spring at Thompson Farm similarly might be a result of adsorption and condensation processes for aerosol formation, in addition to combustion-related sources (diesel, fuel oil; Figure 4.4b).

4.3.2.6 Extreme $\delta^{15}N$ values during the campaign

The aerosol sample collected on 05/12/2008 had the lowest $\delta^{15}N$ of -14.1‰, and that on 01/07/2008 had the highest $\delta^{15}N$ of 17.8‰. HYSPLIT backward trajectories showed that air masses originated from areas near Greenland and northern Canada on 05/12/2008, suggesting the lowest $\delta^{15}N$ observed on that day is related to less polluted sources. In contrast to this, the origin of air masses arriving at Thompson Farm on 01/07/2008 was from the southeastern United States; this day was the most polluted in terms of CO and NO mixing ratios, with the largest CO (530 ppb) and the second largest NO (11.44 ppb) of the entire sampling campaign; the WSOC/OC ratio was also small (0.38) compared to average data (Part 1), indicating the influence of primary emissions and the lack of photochemical processing. Aerosols collected from snow-covered and Polar regions have very low and negative $\delta^{15}N$ values while those associated with pollution plume have high and positive $\delta^{15}N$ values (Morin et al., 2009). Thus, the highest $\delta^{15}N$ is most likely to be associated with anthropogenic sources.

4.3.3 Coupling of carbon and nitrogen isotopic and mass compositions

The relationship between $\delta^{13}C$ and $\delta^{15}N$ for different seasons and a comparison to different sampling sites are shown in Figure 4.8, which illustrates that most of the values

for Thompson Farm for $\delta^{15}N$ fall within the range of previously reported values from different locations, except from the inland sites in China. The corresponding carbon isotope values at Thompson Farm are lower than the other sites, except for an urban site in Kathmandu, Nepal. The sites in China had larger TC concentrations (31-87 μg C m^{-3}) than Thompson Farm (~3 μg C m^{-3}) and were influenced by dust and coal emissions (Wang et al., 2010). The site at Jeju Island also was influenced by dust (Kawamura et al., 2004) and had a very wide range of values for $\delta^{13}C$ and $\delta^{15}N$. Despite the overlap of $\delta^{13}C$ for the emission sources (Figure 4.4a) and the smaller variability at Thompson Farm, $\delta^{13}C$ helped to distinguish the differences in aerosol source signatures such as coal or dust at other sites from mainly combustion-derived aerosols at Thompson Farm.

In Figure 4.9, carbon to nitrogen ratios (C/N) are plotted versus corresponding $\delta^{15}N$ values. Though there was no significant correlation between $\delta^{15}N$ and C/N ratio, the general trend was an increase in $\delta^{15}N$ with a decrease in TN. As TC and TN were correlated in the aerosol samples at Thompson Farm, the loss of TN from the aerosols might have left remaining TN enriched in ^{15}N (though not very significantly). The C/N ratios varied widely, ranging from 0.99 to 16.51, with an average of 4.80 ± 2.86. Previously reported values of C/N ratios are similar (1.3 to 17.4 with an average of 4 ± 3 in marine aerosols collected from a cruise in the western Pacific and Southern Ocean from November 1994 to February 1995 (Bendle et al., 2007); 0.81 to 8.3 in aerosols collected at Jeju Island in East Asia during April 2001 to March 2002 (Kawamura et al., 2004)). The aerosols at Thompson Farm also might be influenced by soil organic matter. The C/N ratios varied seasonally, with the largest value during summer (6.66 ± 3.83) and the smallest during winter (3.88 ± 1.84). The mean C/N ratio in fall (5.18 ± 3.15) was

larger than in spring (4.10 ± 1.95). The seasonal variation in C/N ratio follows the same trend of variability with the seasonal mean temperature (winter: -2.30 °C; spring: 6.95 °C; fall: 10.70 °C; summer: 20.28 °C). The variability in C/N ratio was driven more by TC than TN. This stronger increase in carbon content relative to nitrogen content in summer likely indicates the importance of secondary organic aerosol formation.

Total carbon and TN measurements correlated in all seasons, with the strongest correlation during winter (R^2 = 0.91, $p<0.0001$) followed by spring (R^2 = 0.57, $p<0.0001$), summer (R^2 = 0.45, $p<0.001$), and fall (R^2 = 0.43, $p<0.01$). These correlations suggest that sources for both nitrogenous and carbonaceous aerosols are similar, especially during winter. Isotopic values at Thompson Farm during winter closely resembled $\delta^{13}C$ and $\delta^{15}N$ signatures in primary aerosols emitted from diesel and unleaded fuel (Figure 4.4a and 4.4b). Total carbon and TN had the highest variability during winter compared to other seasons. Decreases in the strength of correlations with the seasons matched the trend of seasonal means in CO (Table 4.3). Because CO, an indicator of primary emission sources, and NO, generally an indicator of anthropogenic sources, were larger in winter than in other seasons (Table 4.3), primary sources of carbon and nitrogen likely dominate during winter and secondary sources are predominant during summer.

4.4 Conclusions

Stable carbon isotopes analyzed in aerosol samples (n = 156) collected over one year at Thompson Farm did not vary greatly (annual mean of $\delta^{13}C$ -26.0 ± 1.4, 1σ), indicating a consistent continental isotopic source signature with an anthropogenic

influence from heating fuel, internal combustion engines, and industry. Some contribution from C_3 plant-related sources was probable as well. Variations may have been caused by occasional marine influence (leading to the increase in $\delta^{13}C$) due to the proximity of the sampling location to the Atlantic Ocean. The negative correlation of $\delta^{13}C$ with three organic functional groups in aerosols (pure aliphatics, unsaturated aliphatics, and oxygenates) during summer also suggests the occurrence of isotopic fractionation during secondary processes. In contrast to $\delta^{13}C$, $\delta^{15}N$ varied widely during the sampling campaign, reflecting different nitrogenous sources of aerosols and different isotope fractionation during different seasons. Seasonal variations of $\delta^{15}N$, with lower values during winter and higher values during summer, paralleled the similar peaks in CO and NO, suggesting winter aerosols are influenced by primary emissions, potentially from home heating. This likely was true for both carbonaceous and nitrogenous aerosols, as indicated by the strong correlation between TC and TN during winter. Seasonal variation of $\delta^{15}N$ is likely due to the variation in emission sources (with some sources being related to temperature such as increased home heating with colder temperatures), differences in NH_4^+/NO_3^-, and the influence from the respective isotopic source signatures of NH_4^+ and NO_3^-. Additionally, the variations might be caused by different chemical mechanisms (such as kinetic or equilibrium reactions), especially during the warmer summer months. Negative correlation of $\delta^{15}N$ with RH during summer indicates that the evaporation of nitrogenous products might have contributed to the higher $\delta^{15}N$ during lower RH conditions.

4.5 References

Ballentine, D.C., Macko, S.A., and Turekian, V.C. Variability of stable carbon isotopic compositions in individual fatty acids from combustion of C_4 and C_3 plants: implications for biomass burning. Chem. Geol. 152, 151-161, 1998.

Bendle, J., Kawamura, K., Yamazaki, K., and Niwai, T. Latitudinal distribution of terrestrial lipid biomarkers and *n*-alkane compound-specific stable carbon isotope ratios in the atmosphere over the western Pacific and Southern Ocean. Geochim. et Cosmochim. Acta 71, 5934-5955, 2007.

Cachier, H. Isotopic characterization of carbonaceous aerosols. Aerosol Sci. Technol. 10, 379-385, 1989.

Cachier, H., Buat-Menard, P. Fontugne, M. and Chesselet, R. Long-range transport of continentally-derived particulate carbon in the marine atmosphere: evidence from stable carbon isotope studies. Tellus 38B, 161-177, 1986.

Cachier, H., Buat-Menard, P., Foutugne, M., Rancher, J. Source terms and source strengths of the carbonaceous aerosol in the tropics. J. Atmos. Chem. 3, 469-489, 1985.

Chesselet, R., Fontugne, M., Buat-Ménard, P., Ezat, U. and Lambert, C.E. The origin of particulate organic carbon in the marine atmosphere as indicated by its stable carbon isotopic composition. Geophys. Res. Lett. 8, 345-348, 1981.

Conte, M.H., Weber, J.C., Carlson, P.J. Molecular and carbon isotopic composition of leaf wax in vegetation and aerosols in a northern prairie ecosystem. Oecologia 135, 67-77, 2003.

Cornell, S., Rendell, A., Jickells, T. Atmospheric inputs of dissolved organic nitrogen to the oceans. Nature 376, 243-246, 1995.

Cottrell, L.D., Griffin, R.J., Jimenez, J.L., Zhang, Q., Ulbrich, I., Ziemba, L.D., Beckman, P.J., Sive, B.C., and Talbot, R.W. Submicron particles at Thompson Farm during ICARTT measured using aerosol mass spectrometry. J. Geophys. Res. 113, D08212, doi:10.1029/2007JD009192, 2008.

Draxler, R.R. and Rolph, G.D. HYSPLIT (Hybrid Single-Particle Lagrangian Integrated Trajectory) Model access via NOAA ARL READY Website (http://ready.arl.noaa.gov/HYSPLIT.php). NOAA Air Resources Laboratory, Silver Spring, MD, 2010.

Elliott, E.M., Kendall, C., Wankel, S.D., Burns, D.A., Boyer, E.W., Harlin, K., Bain, D.J., and Butler, T.J. Nitrogen isotopes as indicators of NO_x source contributions to atmospheric nitrate deposition across the Midwestern and northeastern United States. Environ. Sci. Technol. 41, 7661-7667, 2007.

Fisseha, R., Saurer, M., Jäaggi, M., Siegwolf, R.T.W., Dommen, J., Szidat, S., Samburova, V., Baltensperger, U. Determination of primary and secondary sources of organic acids and carbonaceous aerosols using stable carbon isotopes. Atmos. Environ. 43, 431-437, 2009.

Freyer, H.D. Seasonal variation of $^{15}N/^{14}N$ ratios in atmospheric nitrate species. Tellus 43B, 30-44, 1991.

Freyer, H.D., Kley, D., Volz-Thomas, A., and Kobel, K. On the interaction of isotopic exchange processes with photochemical reactions in atmospheric oxides of nitrogen. J. Geophys. Res. 98(D8), 14791-14796, 1993.

Garcia, A.Z., Coyotzin, C.M., Amaro, A.R., Veneroni, D.L., Martinez, L.C., and Iglesias, G.S. Distribution and sources of bioaccumulative air pollutants at Mezquital Valley, Mexico, as reflected by the atmospheric plant *Tillandsia recurvata* L. Atmos. Chem. Phys. 9, 6479-6494, 2009.

Graham, B., Mayol-Bracero, O.L, Guyon, P., Roberts, G.C., Decesari, S., Facchini, M.C., Artaxo, P., Maenhaut, W., Koll, P., and Andreae, M.O. Water-soluble organic compounds in biomass burning aerosols over Amazonia 1. Characterization by NMR and GC-MS. J. Geophys. Res. 107 (D20), 8047, doi:10.1029/2001JD000336, 2002.

Heaton, T.H.E. $^{15}N/^{14}N$ ratios of nitrate and ammonium in rain at Pretoria, South Africa. Atmos. Environ. 21, 843-852, 1987.

Heaton, T.H.E. $^{15}N/^{14}N$ ratios of NO_x from vehicle engines and coal-fired power stations. Tellus 42B, 304-307, 1990.

Ho, K.F., Lee, S.C., Cao, J.J., Li, Y.S., Chow, J.C., Watson, J.G., and Fung, K. Variability of organic and elemental carbon, water soluble organic carbon, and isotopes in Hong Kong. Atmos. Chem. Phys. 6, 4569-4576, 2006.

Hobbie, E. and Werner, R.A. Tansley review. Intramolecular, compound-specific and bulk carbon isotope patterns in C_3 and C_4 plants: a review and synthesis. New Phyt. 161, 371-385, 2004.

Huang, L., Brook, J.R., Zhang, W., Li, S.M., Graham, L., Ernst, D., Chivulescu, A., and Lu, G. Stable isotope measurements of carbon fractions (OC/EC) in airborne particulate: A new dimension for source characterization and apportionment. Atmos. Environ. 40, 2690-2705, 2006.

Irei, S., Huang, L., Collin, F., Zhang, W., Hastie, D., and Rudolph, J. Flow reactor studies of the stable carbon isotope composition of secondary particulate organic matter generated by OH-radical-induced reactions of toluene. Atmos. Environ. 40, 5858-5867, 2006.

Kawamura, K., Kobayashi, M., Tsubonuma, N., Mochida, M., Watanabe, T., and Lee, M. Organic and inorganic compositions of marine aerosols from East Asia: Seasonal variations of water-soluble dicarboxylic acids, major ions, total carbon and nitrogen, and stable C and N isotopic composition. Geochemical Investigations in Earth and Space Science: A Tribute to Isaac R. Kaplan. Geochem. Soc. 9, 243-265, 2004.

Li, D. and Wang, X. Nitrogen isotopic signature of soil-released nitric oxide (NO) after fertilizer application. Atmos. Environ. 42, 4747-4754, 2008.

López-Veneroni, D. The stable carbon isotope composition of $PM_{2.5}$ and PM_{10} in Mexico City Metropolitan Area air. Atmos. Environ. 43, 4491-4502, 2009.

Marley, N.A., Gaffney, J.S., Tackett, M., Sturchio, N.C., Heraty, L., Martinez, N., Hardy, K.D., Marchany-Rivera, A., Guilderson, T., MacMillan, A., and Steelman, K. The impact of biogenic carbon sources on aerosol absorption in Mexico City. Atmos. Chem. Phys. 9, 1537-1549, 2009.

Martinelli, L.A., Camargo, P.B., Lara, L.B.L.S., Victoria, R.L., and Artaxo, P. Stable carbon and nitrogen isotopic composition of bulk aerosol particles in a C_4 plant landscape of Southeast Brazil. Atmos. Environ. 36, 2427-2432, 2002.

Miyazaki, Y., Kawamura, K., and Sawano, M. Size distributions of organic nitrogen and carbon in remote marine aerosols: Evidence of marine biological origin based on

their isotopic ratios. Geophys. Res. Lett. 37, L06803, doi:10.1029/2010GL042483, 2010.

Moore, H. The isotopic composition of ammonia, nitrogen dioxide and nitrate in the atmosphere. Atmos. Environ. 11, 1239-1243, 1977.

Morin, S., Savarino, J., Frey, M.M., Domine, F., Jacobi, H.-W., Kaleschke, L., and Martins, J.M.F. Comprehensive isotopic composition of atmospheric nitrate in the Atlantic Ocean boundary layer from 65°S to 79°N. J. Geophy. Res. 114, D05303, doi: 10.1029/2008JD010696, 2009.

Nadelhoffer, K.J. and Fry, B. Controls on natural nitrogen-15 and carbon-13 abundances in forest soil organic matter. Soil Science Society of America Journal 52, 1633, 1988.

Poole, I. Braadbaart, F., Boon, J.J., and van Bergen, P.F. Stable carbon isotope changes during artificial charring of propagules. Org. Geochem. 33, 1675-1681, 2002.

Rudolph, J., Anderson, R.S., Czapiewski, K.V., Czuba, E., Ernst, D., Gillespie, T., Huang, L., Rigby, C., Thompson, A.E. The stable carbon isotope ratio of biogenic emissions of isoprene and the potential use of stable isotopic ratio measurements to study photochemical processing of isoprene in the atmosphere. J. Atmos. Chem. 44, 39-55, 2003.

Rudolph, J., Czuba, E., Norman, A.L., Huang, L., Ernst, D. Stable carbon isotope composition of nonmethane hydrocarbons in emissions from transportation related sources and atmospheric observations in an urban atmosphere. Atmos. Environ. 36, 1173-1181, 2002.

Saxena, P. and Hildemann, L.M. Water-soluble organics in atmospheric particles: a critical review of the literature and application of thermodynamics to identify candidate compounds. J. Atm. Chem. 24, 57-109, 1996.

Shakya, K.M., Ziemba, L.D., Griffin, R.J. Characteristics and sources of carbonaceous, ionic, and isotopic species of wintertime atmospheric aerosols in Kathmandu Valley, Nepal. Aerosol Air. Qual. Res. 10, 219-230, 2010.

Smith, B.N. and Epstein, S. Two categories of $^{13}C/^{12}C$ ratios for higher plants. Plant Physiol. 47, 380-384, 1971.

Snape, C.E., Sun, C., Fallick, A.E., Irons, R., and Haskell, J. Potential of stable nitrogen isotope ratio measurements to resolve fuel and thermal NO_x in coal combustion. Prep. Am. Chem. Soc. Div. Fuel Chem. 48,3-5, 2003.

Tanner, R.L. and Miguel, A.H. Carbonaceous aerosol sources in Rio de Janeiro. Aerosol Sci. Technol. 10,213-223, 1989.

Turekian, V.C., Macko, S., Ballentine, D., Swap, R.J., and Garstang, M. Causes of bulk carbon and nitrogen isotopic fractionations in the products of vegetation burns: laboratory studies. Chem. Geol. 152, 181-192, 1998.

Wang, G., Xie, M., Hu, S., Gao, S., Tachibana, E., and Kawamura, K. Dicarboxylic acids, metals and isotopic compositions of C and N in atmospheric aerosols from inland China: implications for dust and coal burning emission and secondary aerosol formation. Atmos. Chem. Phys. 10, 6087-6096, 2010.

Widory, D. Nitrogen isotopes: Tracers of origin and processes affecting PM_{10} in the atmosphere of Paris. Atmos. Environ. 41, 2382-2390, 2007.

Widory, D., Roy, S., Moullec, Y.L., Goupil, G., Cocherie, A., and Guerrot, C. The origin of atmospheric particles in Paris: a view through carbon and lead isotopes. Atmos. Environ. 38, 953-961, 2004.

Yeatman, S.G., Spokes, L.J., Dennis, P.F., and Jickells, T.D. Can the study of nitrogen isotopic composition in size-segregated aerosol nitrate and ammonium be used to investigate atmospheric processing mechanisms?, Atmos. Environ. 35, 1337-1345, 2001.

Yttri, K.E., Dye, C., and Kiss, G. Ambient aerosol concentrations of sugars and sugar-alcohols at four different sites in Norway. Atmos. Chem. Phys. 7, 4267-4279, 2007.

Zhang, Q., Anastasio, C., and Jimenez-Cruz, M. Water-soluble organic nitrogen in atmospheric fine particles ($PM_{2.5}$) from northern California. J. Geophys. Res. 107, D11, doi: 10.1029/2001JD000870, 2002.

Ziemba, L.D., Fischer, E., Griffin, R.J., and Talbot, R.W. Aerosol acidity in rural New England: Temporal trends and source region analysis. J. Geophys. Res. 112, D10S22, doi:10.1029/2006JD007605, 2007.

Table 4.1. Seasonal values of $\delta^{15}N$, $\delta^{13}C$, and C/N ratio in bulk aerosols collected at Thompson Farm.

		$\delta^{15}N$ (‰)			$\delta^{13}C$ (‰)			C/N ratio		
	n	Mean	Median	SD	Mean	Median	SD	*n*	Mean	SD
Winter	40	1.2	0.5	6.4	-26.2	-26.0	0.7	39	3.9	1.8
Spring	43	3.9	4.5	5.6	-26.3	-26.1	2.2	41	4.1	1.9
Summer	25	7.7	8.2	4.9	-25.9	-25.5	1.2	25	6.7	3.8
Fall	48	5.8	5.5	4.6	-25.8	-25.8	0.9	46	5.2	3.2
Annual	156	4.4	4.3	5.8	-26.0	-25.9	1.4	151	4.8	2.9

Table 4.2. Functional group composition (from H^+-NMR, Part 1) of aerosols with atypical carbon isotope values.

n	$\delta^{13}C$ (‰)	Functional groups (%)				
		FG1	FG2	FG3	FG4	FG5
1	-29.9	41.4	19.2	34.7	0.9	3.8
3	-24.1-24.9	35.3 ± 3.6	22.6 ± 5.8	24.3 ± 12.1	ND	17.8 ± 11.2

FG1: purely aliphatic groups (H-C); FG2: unsaturated aliphatics (H-C-C=); FG3: oxygenates (H-C-O); FG4: vinylic and acetalic groups; FG5: aromatic groups. ND = not detected. The functional groups were classified based on extreme isotope values from the sampling campaign; all the values were from summer to ensure the probability of similar source profiles.

Table 4.3. Seasonal mean values (standard deviations in parentheses) for trace gas concentrations and meteorological parameters at Thompson Farm.

	n	Winter	Spring	Summer	Fall
CO (ppbv)	147	237.76	178.57	163.36	158.26
		(80.14)	(19.33)	(30.06)	(38.93)
NO (ppbv)	143	1.35	0.22	0.14	0.41
		(2.70)	(0.22)	(0.13)	(0.66)
Temperature (°C)	156	-2.20	7.74	20.35	10.92
		(4.76)	(5.86)	(3.06)	(6.47)
RH (%)	156	69.93	63.85	79.27	75.15
		(16.16)	(17.99)	(11.32)	(13.53)
Precip.* (mm)	55	95.50	151.38	92.46	145.54

*Precipitation data represent the total precipitation during sampling days.

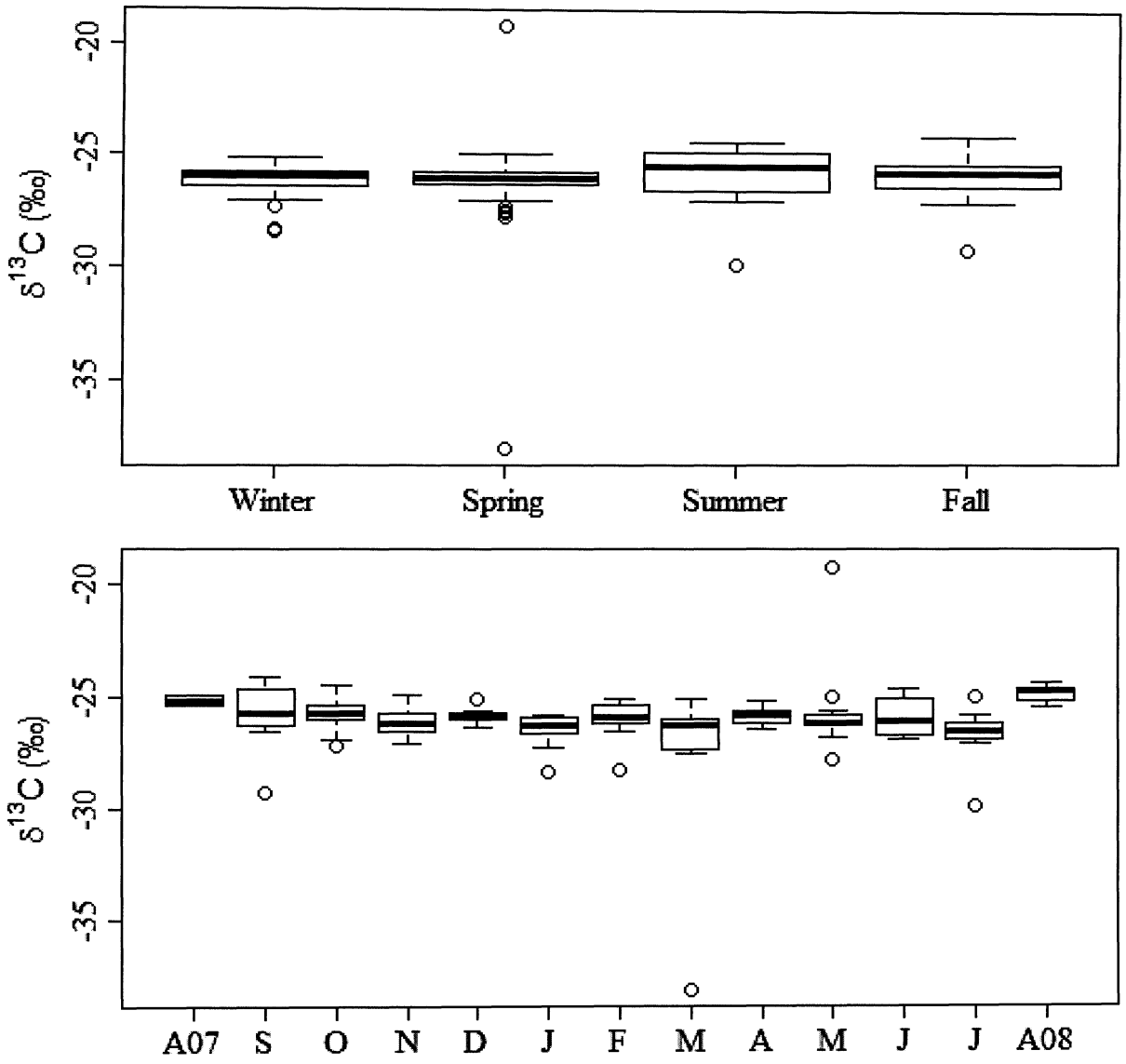

Figure 4.1. Seasonal and monthly $\delta^{13}C$ values at Thompson Farm. A07 to A08 on the x-axis represent the consecutive months from August 2007 to August 2008. The middle line in a box represents the median; ranges of the box represent the 25^{th} and 75^{th} quantiles. Two whiskers were drawn to include 99% of data points; the "o" signs outside the box represent outliers.

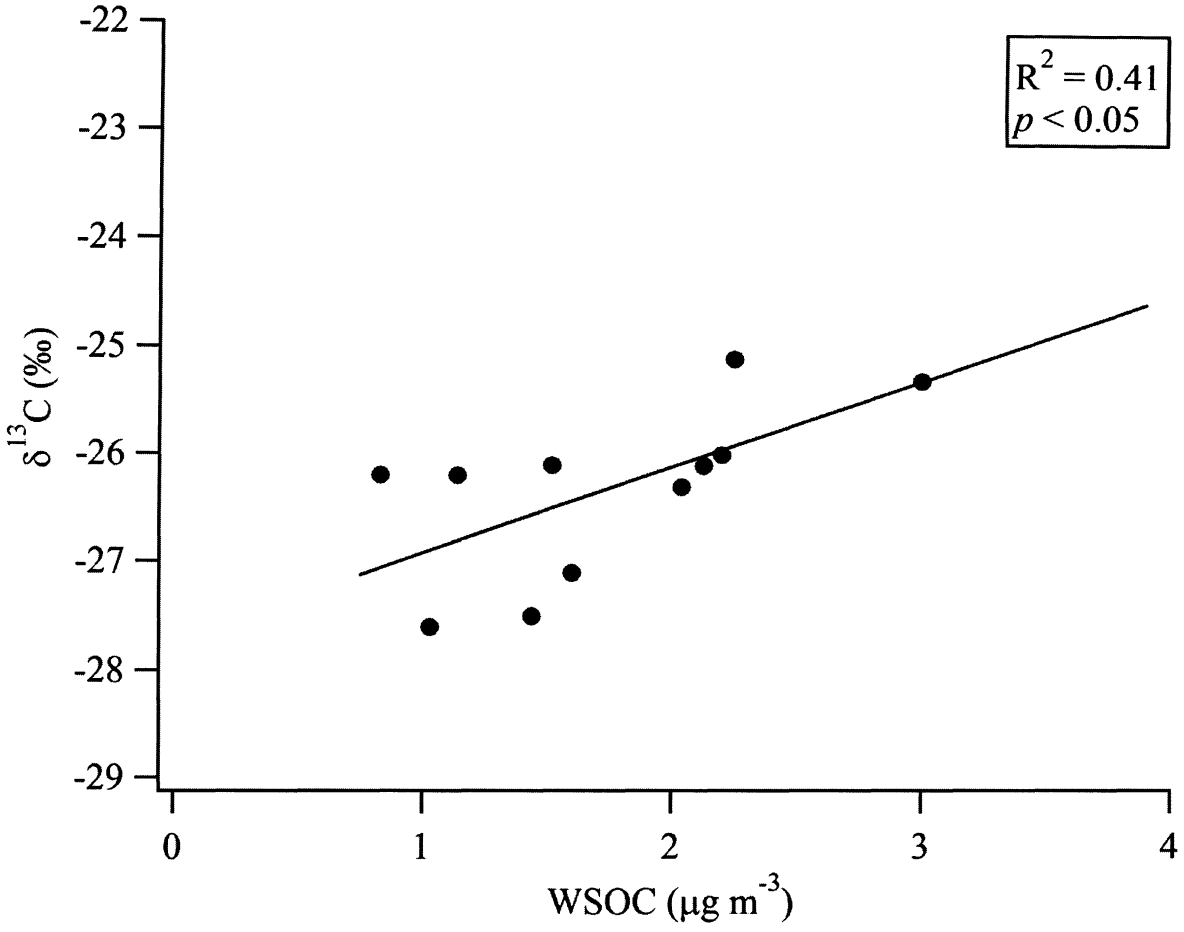

Figure 4.2. Correlation of $\delta^{13}C$ with WSOC at Thompson Farm during spring.

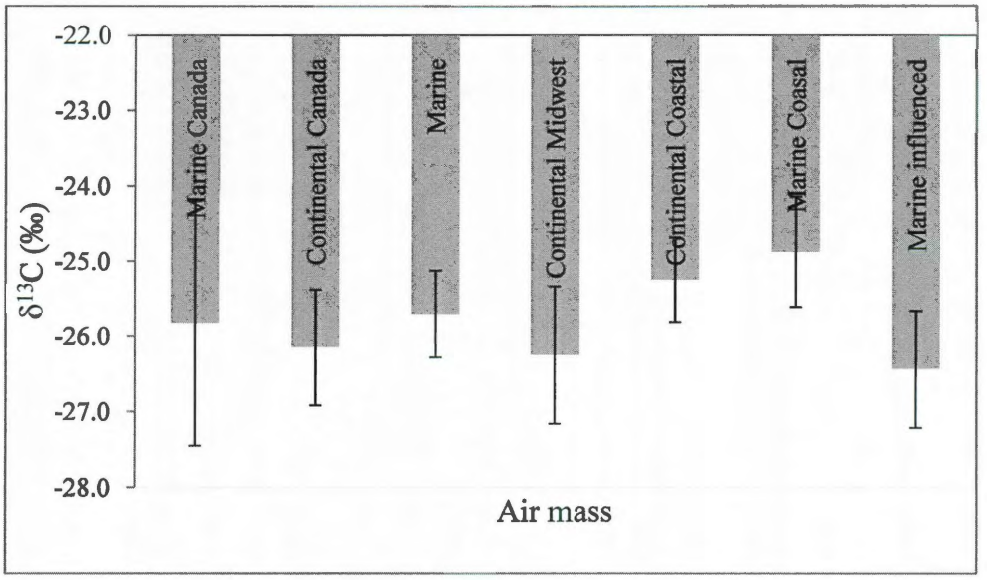

Figure 4.3. $\delta^{13}C$ values compared to seven air mass origins based on backward trajectory analyses.

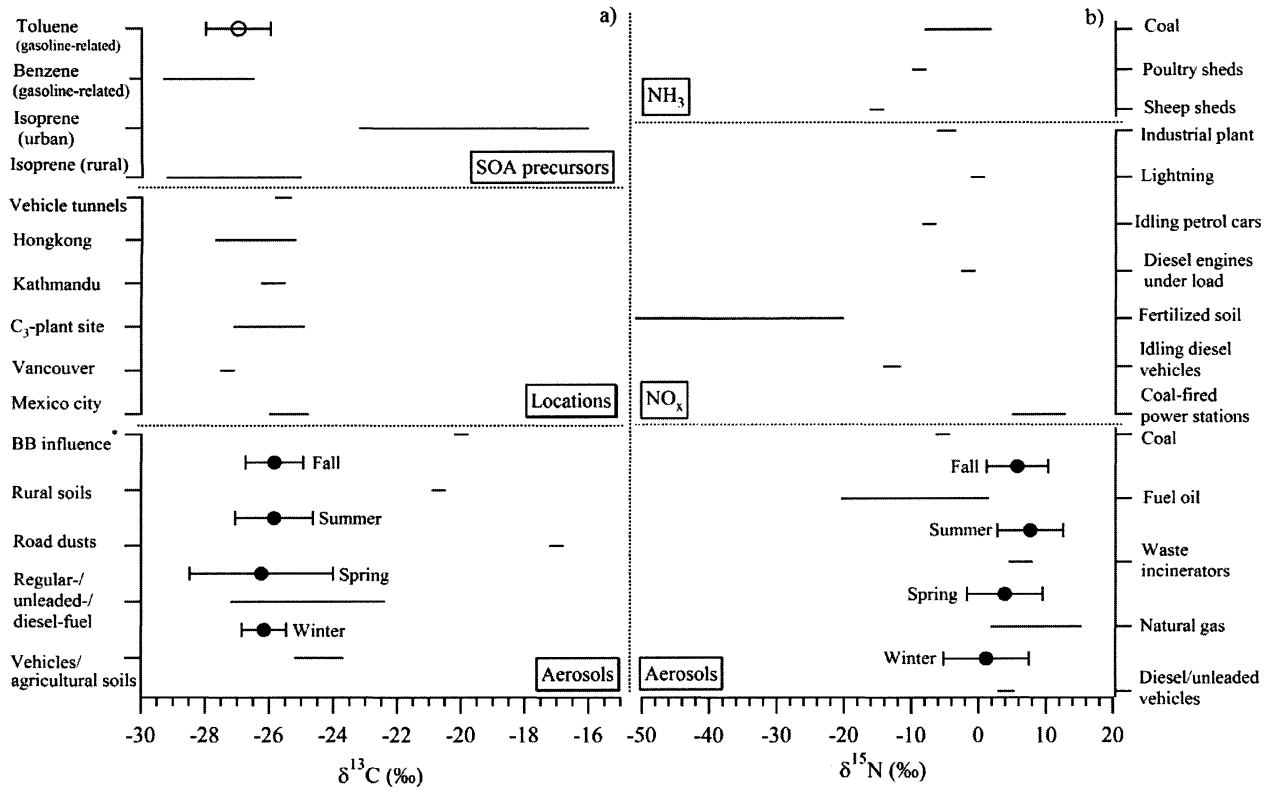

Figure 4.4. a) Comparison of seasonal $\delta^{13}C$ values in aerosols at Thompson Farm (filled circles with whiskers to show range of data) to the values in secondary organic aerosol precursors (first panel), in aerosols from various locations (second panel), and in aerosols emitted directly from the respective sources (third panel) (Cachier et al., 1985; Tanner and Miguel, 1989; Rudolph et al., 2002, 2003; Martinelli et al., 2002; Widory, et al., 2004; Ho et al., 2006; Huang et al., 2006; López-Veneroni, 2009; Marley et al., 2009; Shakya et al., 2010). *Background air influenced by biomass burning.

b) Seasonal $\delta^{15}N$ values in aerosols at Thompson Farm compared to isotope source signatures in precursor gases (NH_3, first panel; NO_x second panel) and in aerosols emitted directly from the respective sources (third panel) (Heaton, 1987, 1990; Snape et al., 2003; Widory, 2007; Li and Wang, 2008; Morin et al., 2009).

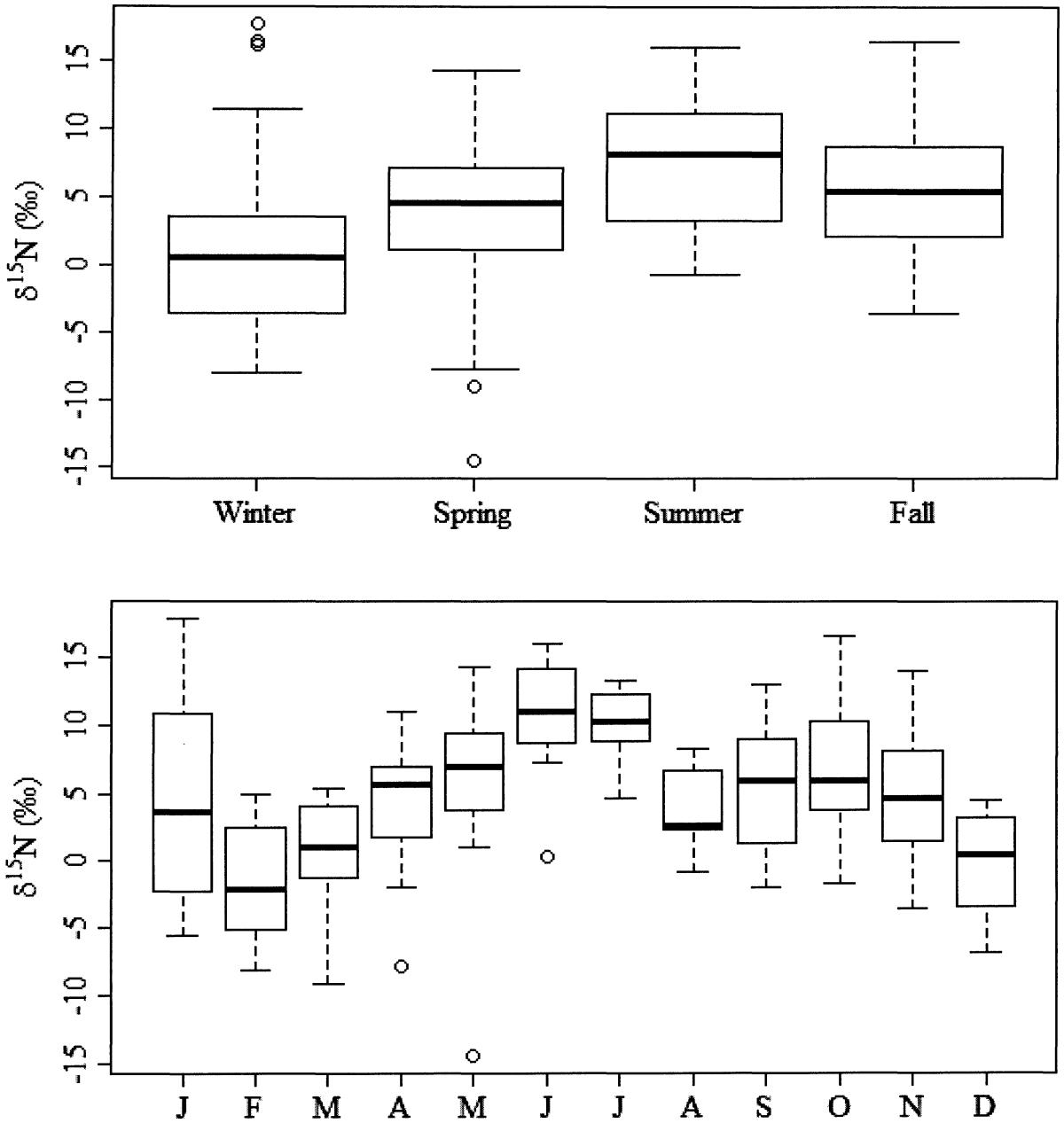

Figure 4.5. Seasonal and monthly $\delta^{15}N$ values at Thompson Farm. See Figure 1 for description.

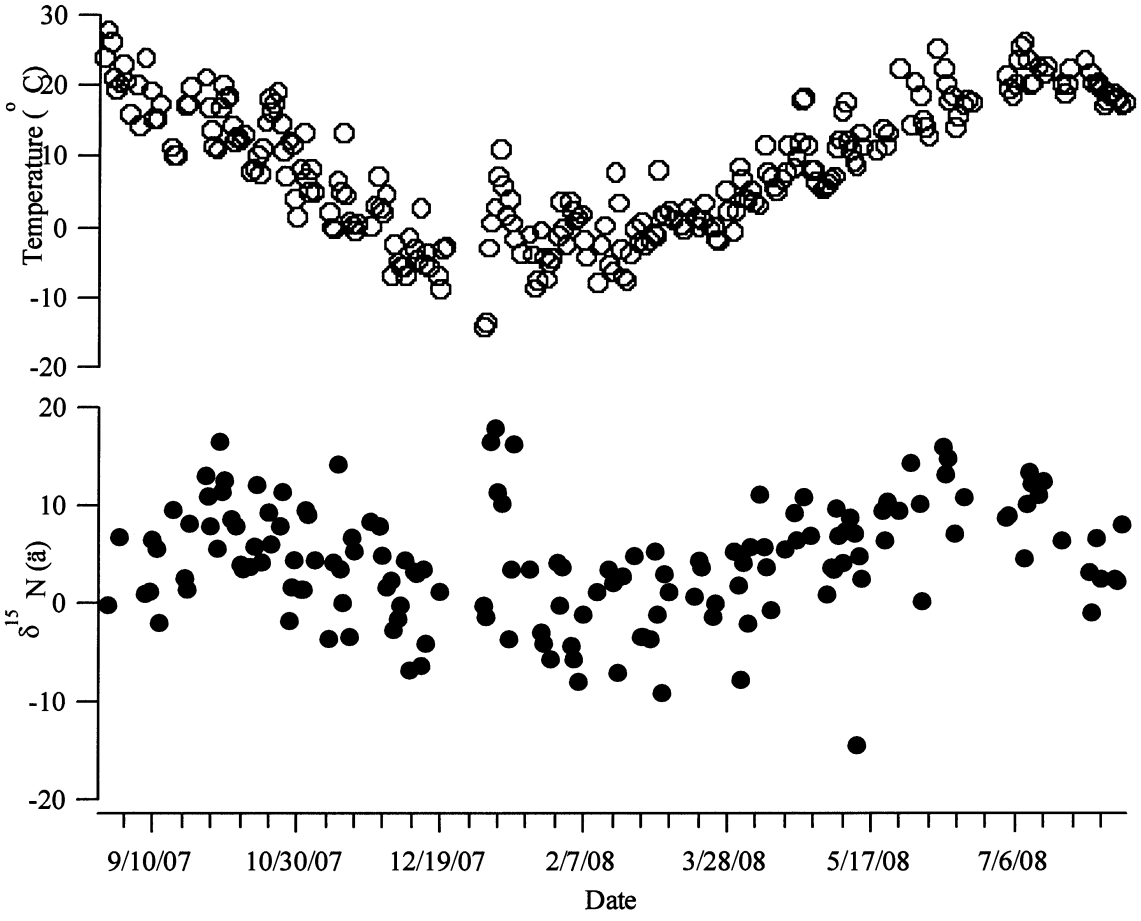

Figure 4.6. Time series of temperature and aerosol $\delta^{15}N$ at Thompson Farm.

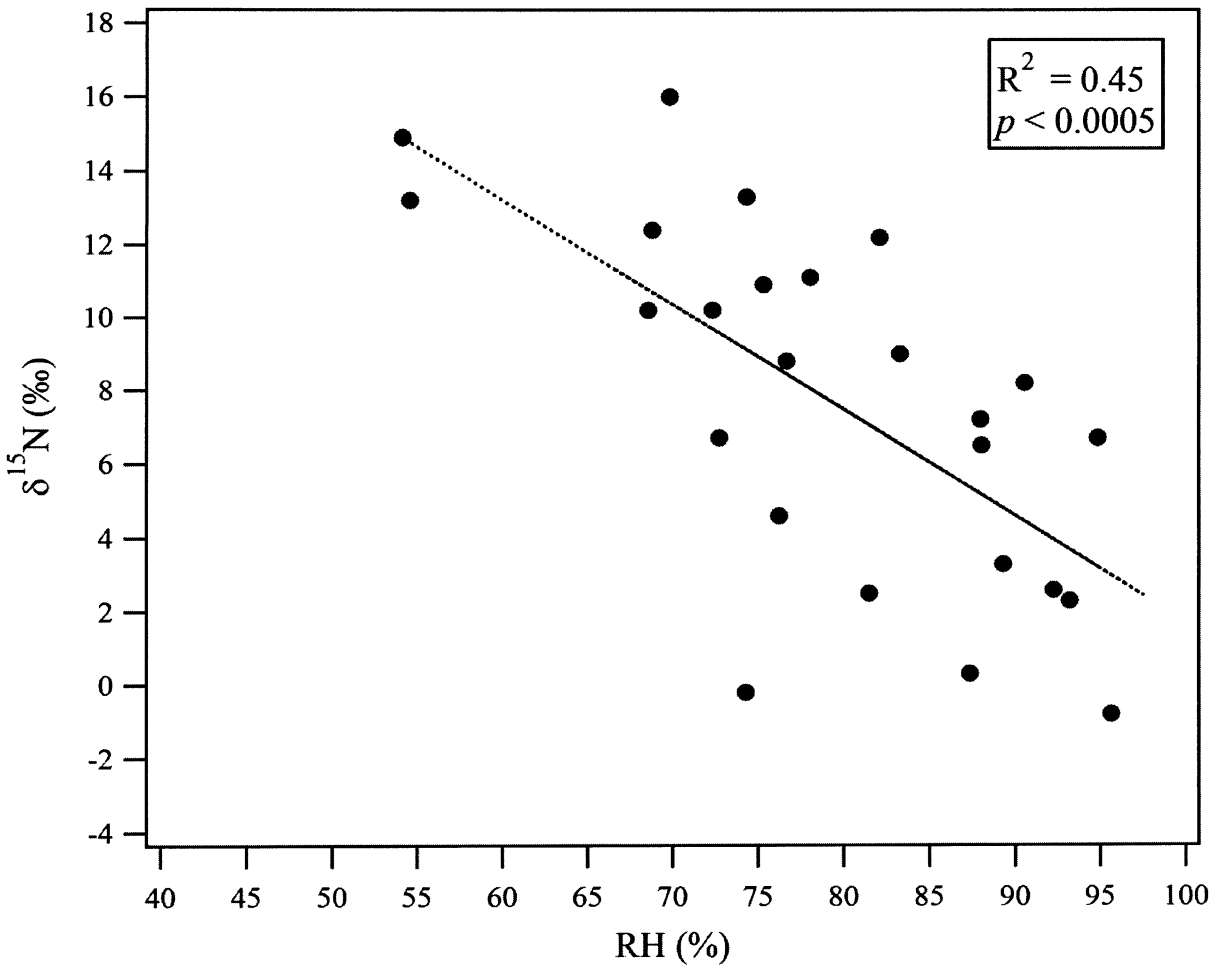

Figure 4.7. Correlation of RH with $\delta^{15}N$ during summer at Thompson Farm.

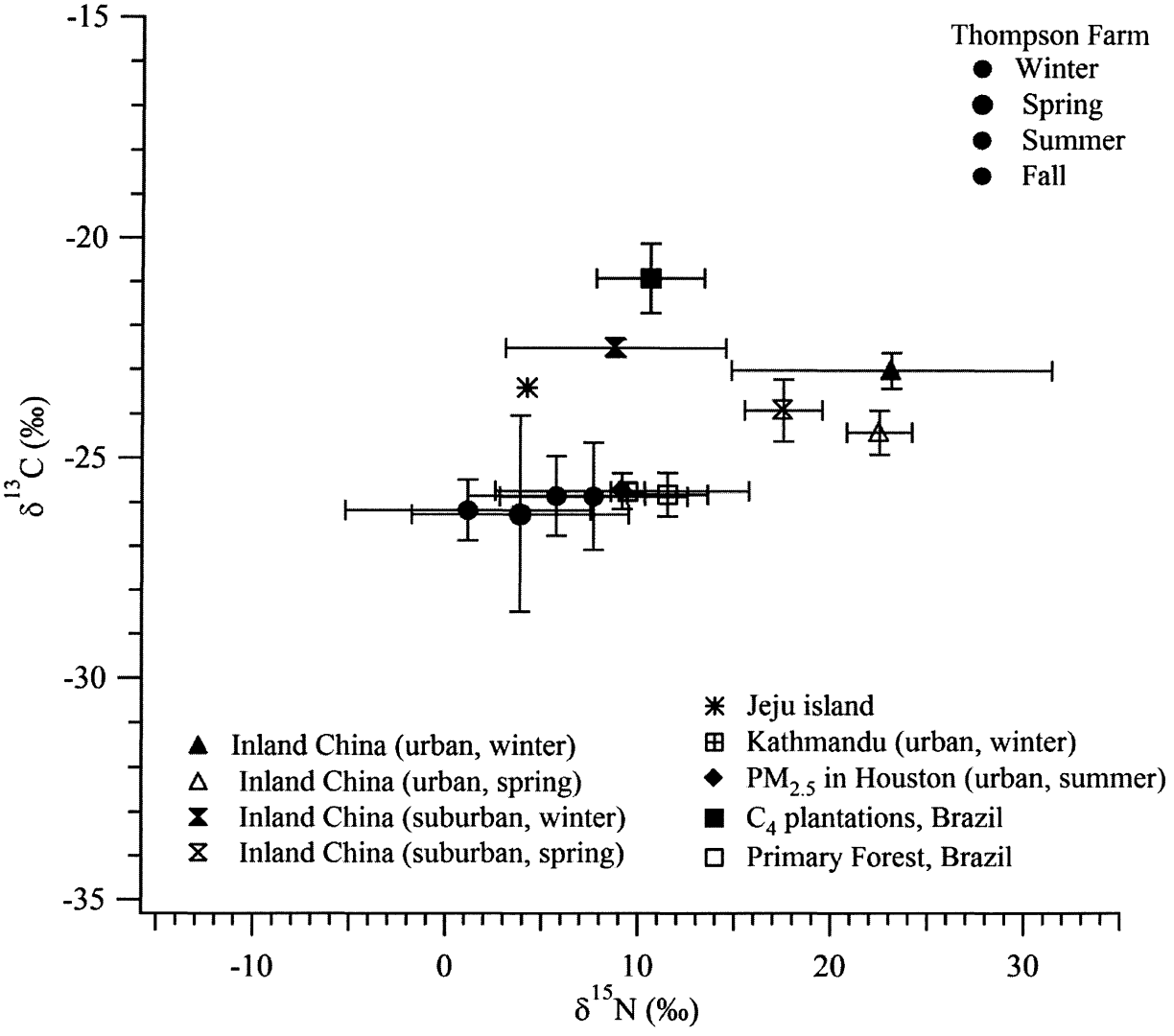

Figure 4.8. $\delta^{15}N$ versus $\delta^{13}C$ for the aerosols from this study are presented in circles in different colors by season. Other symbols represent stable carbon and nitrogen isotope composition from other cities: Jeju Island, East Asia, 2001-02 (Kawamura et al., 2004); Kathmandu, Nepal, winter 2007-08 (Shakya et al., 2010); C_4 plantations, Piracicaba, Brazil, 1999-2000 (Martinelli et al., 2002); urban and suburban site in Baoji City, China, winter 2008 (Wang et al., 2010). Only mean values are shown for Jeju Island (Range: -26.6 to -15.5 ($\delta^{13}C$) and -3.7 to 12.4 ($\delta^{15}N$)).

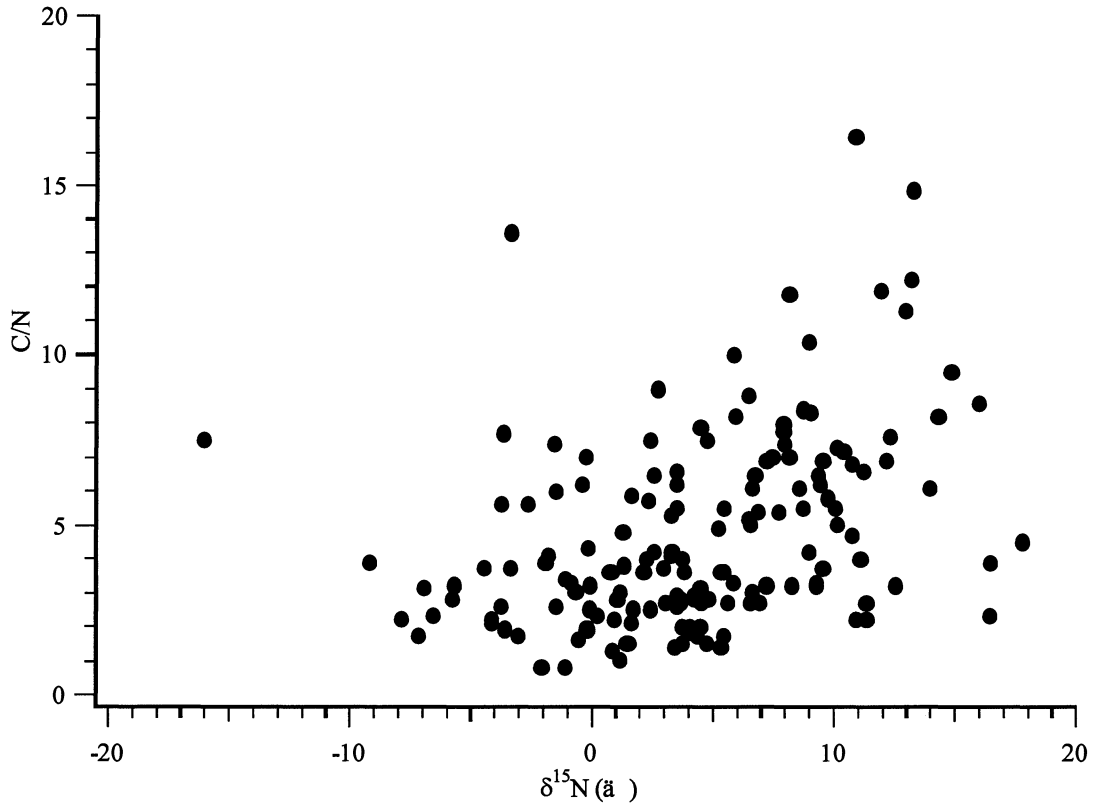

Figure 4.9. $\delta^{15}N$ versus C/N ratio in aerosols at Thompson Farm.

Chapter 5

Lignin-derived phenols in Houston aerosols: Implications for natural background sources

Abstract

Ambient aerosols (coarse and fine) collected in Houston during summer 2010 were analyzed by gas chromatography mass spectrometry (GC-MS) to characterize lignin-derived methoxyphenols in polymeric (from CuO oxidation) and monomeric (solvent-extractable free compounds; combustion-derived) forms in the organic aerosol fraction. The lignin oxidation products (LOPs) and solvent extractable lignin monomers can help identify the contribution of natural sources (lignin macropolymers) and biomass burning (lignin monomers) to ambient aerosols, respectively. The larger contribution of lignin-derived phenols (up to 142 ng m^{-3}) in coarse aerosols shows the importance of natural-borne aerosol particles in the coarse fraction, even in the urban atmosphere. The findings have an important implication in understanding primary biological aerosols, and this is the first time LOP macropolymers were used to characterize ambient aerosols. In both coarse and fine aerosols, *p*-hydroxyl phenols were the most dominant methoxyphenol group (>64% of twelve CuO oxidation products). The order of importance in the three remaining groups, was V>S>C in the coarse aerosols, and S>C>V in the fine aerosols. The LOP parameters suggest a predominant influence from woody tissue of angiosperms, with minor influence from soft tissues and gymnosperms, in addition to soil organic matter sources. The absence or small concentrations of free methoxyphenols (monomers) and levoglucosan point to the limited influence of PM

inputs from biomass burning during the sampling period. The trace levels of anhydrosugar concentrations (levoglucosan; 4.09 ± 2.82 ng m^{-3}; mannosan, 0.70 ± 0.39 ng m^{-3}; and galactosan, 0.54 ± 0.69 ng m^{-3}) most likely result from long-range transport. This observation is supported by the absence of co-occuring lignin monomers, which undergo photovhemical degradation during transport. The observed compositional differences between fine and coarse aerosols suggest that organic aerosols are comprised of a heterogeneous mixture of constituents from different origins and processes.

5.1 Introduction

Aerosols play an important role in atmospheric chemistry (e.g., affecting volatile organic compounds and ozone, heterogenous reactions), climate (direct and indirect effects), visibility, and human health. Important primary aerosol sources include plant materials (e.g., plant fragments, pollens,), biomass burning, road, soil and mineral dust, and sea salt (Pöschl, 2005). The natural background contribution to urban aerosol levels is not well studied, in particular because its determination is still hindered by analytical challenges (Pöschl, 2005). Natural biological debris is estimated to be emitted at a rate of 50 Tg yr^{-1} globally (Kiehl and Rodhe, 1995). However, the global flux might be significantly larger when accounting for primary biological aerosol particles (PBAP) that are compositionally not well defined (Jaenicke, 2005).

Lignin, the second-most abundant naturally occurring polymer (after cellulose), is composed of collective macromolecules that form the major structure of vascular plants, contributing about 28% and 20% of of softwood and hardwood biomass, respectively (Hatfield and Vermerris, 2001; Dimmel, 2010). Lignins are a tracer of natural plant

material sources (vascular plants) in aerosols because it is more preserved than other plant materials such as cellulose and hemicelluloses because of its slower biodegradation processes (Hedges and Mann, 1979; Louchouarn et al., 2010). Lignin is composed of three aromatic alcohols (*p*-coumaryl, coniferyl, and sinapyl alcohols) that give rise to phenolic aldehydes, ketones, and acids upon oxidation or pyrolysis (Hedges and Mann, 1979; Goñi and Hedges, 1992; Dimmel, 2010). In addition to the eight lignin-derived phenols mentioned above (vanillyls, syringyls, and cinnamyls), the *p*-hydroxyl phenol (P) (acid, aldehyde, and ketone) and 3,5-dihydroxybenzoic acid (3,5-Bd) also are released from the CuO oxidation of terrestrial organic matter, although these can have other sources as well (bacterial, phytoplankton, macroalgae; Goñi et al., 1995; 2000). The information on such lignin-derived methoxyphenols or lignin oxidation products (LOPs) in aerosols can thus be used not only to estimate the primary biogenic contribution to organic aerosols but also to identify the taxonomic class and the tissue type of source vascular plant because of the difference in distribution of these species in major plant classes and tissues (Hedges and Mann, 1979; Goñi and Hedges, 1992; Kuo et al., 2008b). However, the method has never been applied to study organics in atmospheric aerosols. This has probably been the result of analytical limitations (low sample size, sensitivity of instruments), rather than interest. Previous studies using lignin-derived phenols in aerosols are limited to solvent-extractible free phenols (without CuO oxidation) to characterize the aerosols derived from biomass burning (Hawthorne et al., 1988, 1989; Simoneit et al., 1993; Graham et al., 2002; Simoneit, 2002). Recently, however, Louchouarn et al. (2010) investigated the LOPs (macropolymers) in aerosol reference

materials (urban aerosols) providing the analytical capacity to address this issue and thus the motivation for the current work in ambient aerosols.

The LOPs provide insight into various biogenic organic aerosol characteristics such as fresh or altered (based on Ad/Al), gymnosperms or angiosperms (based on the presence or absence of S), or herbaceous or woody species (based on the presence or absence of C) (Hedges and Mann, 1979; Goñi and Hedges, 1992; Opsahl and Benner, 1995; Kuo et al., 2008b). Characterization of lignins (polymers and monomers) in ambient aerosols will increase our understanding of the contribution of natural background materials and biomass burning. The main objective of this paper is to characterize the organic aerosol composition in coarse and fine fractions using the lignin-derived phenols (or LOPs). Temporal variation, composition, and relative ratios of the LOPs as well as the application of LOPs as tracer for identification of natural plant materials or plant combustion sources in aerosols were investigated. The results on the twelve products (V, S, C, P, and 3,5-Bd) from CuO oxidation method (polymers) and the solvent extraction method (lignin monomers), and also the data on three anhydrosugars (levoglucosan, mannosan, and galactosan) from the solvent extraction method are presented in this paper.

5.2 Methodology

5.2.1 Sampling

Bulk aerosols were collected for every 24 hours on prebaked (550°C for 24 hours) 47-mm quartz fiber filters (QFF, Pallflex, Tissuquartz, Pall Life Sciences, NY) from 07/20 to 08/09/2010. A Versatile Air Pollutant Sampler (VAPS, URG, North Carolina)

was used for collecting the aerosol samples in coarse (diameter range of 2.5 – 10 μm) and fine (diameter <2.5 μm) fraction. A cyclone on the inlet removes any particles larger than 10 μm. Petri-dishes containing filter substrates were stored in a freezer (-20°C) until the time of analysis. The sampling was performed on the roof of the North Moody Tower (29° 43' 3.50" N, -95° 20' 28.50" W; 65 m above ground level) at the University of Houston. A total of 25 samples including six field blanks were collected, each for fine and coarse fraction. A sample could not be collected on 08/01 because of scheduled power outrage.

5.2.2 Lignin analysis from CuO oxidation

Two filters collected on consecutive days were lumped together for the lignin analysis to increase the sample mass. Due to the lack of sample from 08/01, the filter from 08/02 was processed alone. The aerosol substrate was analyzed for lignin content using an alkaline CuO oxidation method developed by Hedges and Ertel (1982) and Goñi and Hedges (1992) and modified by Louchouarn et al. (2010). Twelve oxidation by-products were analyzed: V (vanillin, acetovanillone, vanillic acid), S (syringaldehyde, acetosyringone, syringic acid), C (*p*-coumaric acid, ferulic acid), *p*-hydroxyl phenols (P) (*p*-hydroxybenzaldehyde, *p*-hyroxyacetophenone, *p*-hydroxybenzoic acid), and 3,5 dihydroxybenzoic acid (3,5 Bd).

The filters were put inside a stainless steel vessel (bomb) containing 330 mg of CuO, 150 mg of $Fe(NH_4)_2(SO_4)_2.6H_2O$, 5 mg of glucose, and a stainless steel ball bearing. Each reaction vessel was filled with 2N NaOH solution previously sparged with N_2 (45 minutes), and the headspace was flushed with N_2 for 40 minutes. Twelve vessels

were then heated in a gas chromatograph (Hewlett-Packard 5890) programmed with a 30 min temperature ramp (4 ^{o}C min^{-1}) to 150 ^{o}C, and then held at that temperature for another 2.5 hours. The solution was then spiked with a surrogate standard (*trans*-cinnamic acid), acidified with 6N HCl, and extracted with ethyl acetate (three times). After the removal of residual water using Na_2SO_4, the extracted solution was evaporated to dryness using a LabConco™ solvent concentrator. The dried sample was redissolved in pyridine and an aliquot (75 µL) was transferred to a 1.5 mL glass vial to which 75 µL of N,O-bis (trimethylsilyl)trifluoroacetamide (BSTFA) containing 1% trimethylchlorosilane (TMCS; Supelco, PA, USA) was added. The samples were then derivatized under normal atmosphere by heating at 75 °C for 1 h in a 20-wells block heater. After derivatization, each sample was transferred to a 250 µL glass autosampler vial insert.

Separation and quantification of trimethylsilyl (TMS) derivatives of CuO oxidation by-products were performed using gas chromatography–mass spectrometry (GC/MS) with a Varian triple quadrupole 480-300 system fitted with a fused silica column (J&W DB-5MS, 30 m x 0.25 mm i.d., 0.25 µm film thickness; Agilent Technologies). Each sample was injected, under splitless mode, into a deactivated glass liner inserted into the GC injection port and using He as the carrier gas (1.0 mL min^{-1}). The GC oven was programmed from 65 °C (with a 2 min initial delay) to 300 °C (held 10 min) using a 4 °C min^{-1} temperature ramp. The GC injector and GC/MS interface were maintained at 280 °C and 270 °C, respectively. The mass spectrometer was operated in the electron ionization mode (EI, 70 eV) using either full scan mode (FS) or selective ion monitoring (SIM). Compound identification was performed using GC retention times and

by comparing full mass spectra (FS) or target fragments (SIM) with those of commercially available standards. The instrument was operated in the mass range m/z 50–500 (FS) or to targeted mass fragments during specific chromatographic segments (SIM). In both detection modes, 1–3 target ions (including the base ion) were selected for quantification. Relative response factors from standard calibration compounds were used to quantify the LOPs in the samples. Standard reference materials (sediment: SRM 1949b; dust particles: SRM 1649b; filters containing atmospheric particulate matter: SRM 8585) were used for quality control purposes. All reported values are blank corrected. Vanillin and *p*-hydroxybenzoic acid were the only contaminants in the field blanks.

5.2.3 Lignin analysis from solvent extraction

Six one-day samples (five fine and one coarse aerosol sample) were analyzed for methoxyphenols and anhydrosugars (levoglucosan and its stereoisomers) using the solvent extraction method (without CuO oxidation). All the samples (except one) collected on coarse and fine size fraction by the VAPS were analyzed by using CuO oxidation method. Only five samples were collected randomly on QFF of the third channel (fine fraction) in the VAPS, which was otherwise used for collecting samples on Teflon filters for detailed elemental analysis. Details for this method are given in Kuo et al. (2008a) and Louchouarn et al. (2009) and are only described briefly here. The aerosol samples were extracted with dichloromethane and methanol (9:1, v/v) using pressurized fluid extraction with an accelerated solvent extractor (Dionex ASE 200) at a pressure of 1500 psi and 100°C. *Trans*-cinnamic acid (Sigma, MO, USA; Louchouarn et al., 2010)

and d_7-levoglucosan (NIST SRM 2267; Larsen et al., 2006; Louchouarn et al., 2009), were used as the surrogate standards for lignin and anhydrosugars solvent-extractable monomers, respectively. After drying, the pyridine-extracted sample was derivatized in a manner similar to that described for CuO oxidation, and analyzed with GC-MS in selective ion monitoring mode. All reported values are blank corrected.

5.2.4 Meteorology and trace gases

Meteorological parameters (temperature, relative humidity, and precipitation) and trace gases (carbon monoxide and ozone) mixing ratios were downloaded from the Texas Commission on Environmental Quality (TCEQ) website.

5.3 Results and discussion

5.3.1 Temporal variation of lignin macropolymers

The quantified biomarkers, derived mainly from lignin, were present primarily in coarse size fractions (~7 times greater than in fine fraction) (Table 5.1, and Figure 5.1 and 5.2) suggesting the predominant association of lignin with PBAP (Graham et al., 2003; Yttri et al., 2007). Though LOPs were present in higher concentrations in coarse aerosols, a large proportion of coarse aerosols was characterized by LOP concentrations below the detection limit. Mainly, cinnamyl phenols were the ones absent in coarse aerosols (Figure 5.2). In contrast, and despite lower overall concentrations, most of the fine aerosols demonstrated the consistent presence of LOPs (Figure 5.2).

Of the three main lignin components, the vanillyl and syringyl phenols were the most abundant in coarse aerosols, with a minor and occasional contribution from

cinnamyl phenols (Figure 5.2). The LOPs in the coarse fraction showed significant temporal variability compared to the fine fraction with syringyls exhibiting a decreasing pattern during the campaign. In fine aerosols, the LOPs were present in much smaller concentrations (mostly <1 ng m^{-3}) compared to that in coarse aerosols (5-30 ng m^{-3}). During the largest rainfall occurrence on 07/22 (27.94 mm), syringyl phenols could not be detected in the fine fraction, and none of the LOPs were detectable in coarse fraction.

From the CuO oxidation, several other aromatic compounds that do not solely derive from lignin were detected. These include *p*-hydroxyl phenols (*p*-hydroxybenzoic acid, *p*-hydroxybenzaldehyde, and *p*-hydroxyacetophenone) and 3,5-Bd. These species can also derive from proteins and tannins in plant materials (Hedges and Ertel, 1982; Goñi et al. 2000; Otto and Simpson, 2006). However, the small *p*-hydroxyacetophenone to total *p*-hydroxyl phenols (PON/P) ratio (0.1-0.3) argues against major non-lignin sources of p-hydroxyl phenols in these aerosols. Indeed, reported PON/P ratios for lignin extracted from fresh vascular plants (0.18-0.42; Hedges et al. 1982; Williams et al. 1998; Kuo, 2009), lake sediments (0.10-0.20; Teisserenc et al. 2010, Houel et al. 2006), and boreal soils (0.14-0.40; Houel et al. 2006) all fall in the same range as the one observed in the Houston aerosols supporting a predominant lignin source for these *p*-hydroxyl phenols. The *p*-hydroxyl phenols exhibited large variability in coarse aerosols but were much more uniformly distributed in fine aerosols during the campaign. In addition, the *p*-hydroxyl phenols were the main component of the CuO oxidation products accounting for 64.0 ± 21.7% and 68.4 ± 15.7% of the quantified twelve LOPs in coarse and fine aerosols, respectively (Figure 1). The *p*-hydroxybenzoic acid and *p*-hydroxybenzaldehyde were the most abundant *p*-hydroxyphenol with 41 ± 23% and 19 ± 10%, respectively, in

the coarse fraction and 27 ± 8% and 37 ± 10%, respectively, in the fine fraction. The parent polymer of *p*-hydroxyl phenols, *p*-coumaryl alcohol, is considered to be the tracer for the plant class gramineae (mainly grasses) (Simoneit, 2002). Hydroxybenzoic acids are also observed in the smoke from conifers (Simoneit, 2002). Syringyl phenol and V were positively correlated in fine aerosols (R^2=0.6, $p<0.05$). Carbon monoxide, an indicator of primary pollutant, was correlated only with fine P (R^2=0.59, $p<0.05$).

The 3,5 Bd was present only from 07/22 to 07/26 in the coarse aerosol and only during 07/30 to 08/05 in the fine aerosol (Table 5.1). The 3,5 Bd is an indicator for humidified soil organic matter (OM), and a tracer for soil OC in marine and terrestrial sediments (Prahl et al., 1994; Louchouarn et al., 1999; Houel et al., 2006; Dickens et al., 2007). The 3,5 Bd is also thought to be derived from biochemical sources such as tannins, flavonoids, and charcoal (Prahl et al., 1994; Dickens et al., 2007; Kuo et al., 2008b). The 3,5 Bd was not observed in CuO oxidation products from grass samples and was less abundant in Aspen leaves and Pine needles (Otto and Simpson, 2006).

5.3.2 Relative distribution of lignin macropolymers

Despite the differences in concentrations of LOPs in fine and coarse aerosols, the S/V and C/V ratios were similar in both size fractions (Figure 5.3), suggesting similar plant source inputs. The S/V ratios ranged from 0.6 to 2.0 in coarse particles and 0.8 to 1.6 in fine particles, indicating contribution from angiosperm tissues, as syringyls are absent in non-angiosperm tissues (Hedges and Mann, 1979; Hedges et al., 1988a and references there in). Fine S/V was positively correlated with coarse S/V (R^2=0.81, $p<0.05$). The C/V ratio ranged from 0.2 to 0.7 in coarse particles and 0.1 to 1.9 in fine

particles. The cinnamyl phenols were the least abundant LOPs and were mostly absent (7 of 9 days) in the coarse aerosol fraction, suggesting the source of plant material in aerosols to be most likely from woody tissues or degraded plant material (Hedges and Ertel, 1982; Goñi and Hedges, 1992). However, the presence of C in fine particles points to the limited influence of soft tissues such as tree leaves, conifer needles, grasses, or pollens in fine aerosols (Hedges et al., 1988a and references there in; Keil et al., 1998). The cinnamyl phenols observed during one sampling period (08/05), suggest that pollens are important contributors to the coarse fraction, as *p*-coumaric acid/ferulic acid ratio (Cad/Fad), an indicator of pollen tissue (Keil et al., 1998), was high during this date (3.1).

The P species dominated both the coarse and fine fractions, except on August 5-6, when the ratio of P to the sum of V and S (P/(V+S)) dropped to 0.3 in the coarse fraction (Figure 5.3). The P/(V+S) ratio also was highly variable, ranging from 0.3 to 12. Although the 3,5 Bd concentrations in aerosols were lower than V as indicated by 3,5 Bd/V ratios below unity in both coarse and fine aerosols (Figure 5.3), the average ratio ranged ~0.5. A 3,5 Bd/V ratio above 0.2-0.5 is often used as an indicator of degradation and humification in organic matter of soils (Prahl et al., 1994; Louchouarn et al., 1999; Houel et al., 2006; Dickens et al., 2007). Hence, the mean 3,5 Bd/V ratios of 0.9 and 0.6 in coarse and fine aerosols, respectively, suggest inputs from humified soil OM in the sampled aerosols (Houel et al., 2006; Otto and Simpson, 2006). Similarly, mean P/(V+S) ratios of 4.18 and 4.38 in coarse and fine aerosols, respectively, confirm the inputs of altered and/or degraded plant matter (Houel et al., 2006).

The ratio of acid to aldehyde in syringyl phenols ((Ad/Al)s) in coarse aerosols (0.50 ± 0.29) was more variable than in fine aerosols (0.59 ± 0.09). The ratio of acid to

aldehyde in vanillyl phenols ((Ad/Al)v) was larger than (Ad/Al)s and was also highly variable (Figure 5.4). The (Ad/Al)v ratio was larger in fine aerosols (4.47 ± 1.72) than in coarse aerosols (1.56 ± 0.51). The (Ad/Al)v ratio has been reported to be larger than (Ad/Al)s in previous measurements in natural environments (Hedges et al., 1988a and references there in). The (Ad/Al)v ratios differ among plant parts, with larger values in grass roots compared to grass blades (Otto and Simpson, 2006). The mean (Ad/Al)v and (Ad/Al)s in Houston aerosols were greater than the values (0.1-0.2) for fresh angiosperm and conifer wood and lie within the range (0.2-1.6) of non-woody tissues (leaves, needles, and grasses) and soils and sedimentary plant fragments (0.6-7.6) (Hedges and Mann, 1979; Opsahl and Benner, 1995; Otto and Simpson, 2006 and references there in). Acid to aldehyde ratios higher than 0.5 are considered to result from lignin degradation by fungal attack in case of soil samples (Hedges et al., 1988a) or photochemical degradation during atmospheric transport in the case of aerosols (Simoneit and Elias, 2001). Thus, the Ad/Al ratio further confirms the altered plant material sources in Houston aerosols, as suggested by P/(V+S) ratio previously. Photochemical alteration, oxidation, or cross-linking is also considered to be the cause of lignin degradation in soils and rivers (Opsahl and Benner, 1998; Otto and Simpson, 2006 and references there in).

Syringic acid concentrations were lower than those of vanillic acid (Figure 3). During biodegradation, syringyls seem to be preferentially degraded by fungi over vanillyl phenols (Hedges et al., 1988a), although this may be related to the structure of the lignin macropolymer rather than an intrinsic difference in monomer lability (Louchouarn, 1997). The ratio of syringilic acids to vanillic acids (Sd/Vd) exhibited little variability in both coarse and fine aerosols pointing to either a lack of degradation or

similar rates of degradation of these moieties in prior environments. Syringyl ketone (acetosyrigone) was absent in both size fractions of aerosol while vanillyl ketone (acetovanillone) was present only on 07/05.

5.3.3 Plant source signatures

To illustrate their contributions to aerosols sampled at Houston, the source signature domains for distinct plant materials were plotted using S/V ratio and C/V ratio (Figure 4) (Hedges and Mann, 1979; Alberts et al., 1991; Keil et al., 1998; Louchouarn et al., 2006). Only four samples fell close to a distinct plant source regions, three close to angiosperm soft tissues and one to gymnosperm soft tissues. The latter one was already recognized for its significant contribution from gymnosperm pollen inputs based on Cad/Fad ratio. These conclusions are in agreement with the inferences drawn from lignin phenol vegetation index (LPVI) values (Table S1). Tareq et al. (2004) proposed the LPVI values, calculated from S, C and V percentages, as an integrated index of vegetation source inputs to complex environmental mixtures (as opposed to the dual S/V *vs.* C/V property-property graphical representation). Whereas most samples show a LPVI in the woody angiosperm range (70-400; Tareq et al., 2004), a few samples are characterized by more typical gymnosperm signatures (10-30). In particular, the coarse sample from 08/05 is characterized by the lowest LPVI (12) and is the only sample which source signatures are different for coarse and fine aerosols. Because gymnosperm pollens tend to be relatively large (Knight et al., 2010), this difference in lignin source signatures across size fractions is again consistent with a predominance of gymnosperm pollen inputs to the coarse fraction during that sampling period.

Cinnamyl phenols were absent in most of the coarse aerosols. These coarse samples (without C) are most likely to be derived from angiosperm woody tissues based on large S/V ratios and small C/V ratios. Overall, the biogenic coarse aerosols seem to be dominated by angiosperm woody tissues with the occasional influence from both non-woody angiosperm and gymnosperm tissues.

5.3.4 Free methoxyphenols (lignin Monomers) and levoglucosan

Solvent-extractable lignin monomers, were often below the detection limit in fine aerosols during the study period(Table S2). Vanillyl phenols were present only on 08/02; whereas C and P were present during all days. The absence of the lignin free phenols suggests the absence of PM from biomass burning in fine aerosols because these methoxyphenols are released from lignin polymers during pyrolysis of wood (Hawthorne et al., 1988; Simoneit et al., 1993; Kuo et al., 2011). However, levoglucosan was present in small concentrations (<9 ng m^{-3}) in all these samples (Table S2). The anhydrosugar levoglucosan is a tracer for biomass burning (Simoneit et al., 1999; Simoneit and Elias, 2000), and its presence in low concentrations in the Houston aerosols suggests minor influence from plant combustion at relatively low temperatures (<350°C) (Kuo et al., 2008a and 2008b). These low levoglucosan and lignin phenol concentrations are in contrast with urban dust particulate matters (SRM, NIST 1649a-b, 2686, and 2687) analyzed previously, which contained high concentrations of both LOPs and levoglucosan, pointing to large contributions of low-temperature plant charcoal sources (Louchouarn et al., 2009; 2010). Similarly, PM_{10} (particles with diameter smaller than 10 μm) collected from Houston on 05/14/1998 during a haze episode with a major influence

from biomass burning, contained levoglucosan concentrations (0.2 to 0.4 μg m^{-3}) that were two orders of magnitude higher than the ones reported in the current study (Fraser and Lakshmanan, 2000). The urban location of the site (Moody Tower) and more importantly the period of sampling (summer with no home heating wood burning activities) may explain the limited inputs of combustion biomarkers from local biomass burning. Levoglucosan thus appears to be derived from long-range transport, consistent with the low and some times absent concentrations of lignin methoxyphenols. Methoxyphenols are considered to be relatively unstable compared to levoglucosan due to their higher sensitivity to photodegradation during long-distance transport (Simoneit and Elias, 2001; Simoneit, 2002; Hoffer et al., 2006; Jordan et al., 2006).

Levoglucosan was abundant in Houston aerosols compared to its two stereoisomers, galactosan and mannosan (Figure 5), consistent with previous work (Graham et al., 2002; Louchouarn et al., 2009). The concentrations of levoglucosan, mannosan, and galactosan in fine aerosols ranged 1.85-8.42, 0.37-1.24, and 0.13-1.58 ng/m^3, respectively (Table S2 and Figure 5). The largest concentrations of all anhydrosugars and free lignin phenols were observed on 08/02 suggesting a larger contribution from biomass combustion to the urban aerosol series. During this period, higher concentrations of levoglucosan and its stereoisomers were present in the fine rather than the coarse size fraction (Table S2), in agreement with previous studies from biomass burning sources (Simoneit, 2002).

In contrast to levoglucosan, a cellulose combustion byproduct, mannosan and galactosan are reportedly derived from the combustion of hemicellulose (Simoneit, 2002). The ratio of levoglucosan to mannosan (and galactosan) thus varies depending on

the type of biomass combusted (Louchouarn et al., 2009, and references therein). In the Houston aerosols, the L/M ratio remains below 20 in the fine fraction (7-18) and is below 5 in the only coarse sample analyzed (3; 08/02). These values suggest that wood combustion inputs, rather than herbaceous biomass or brown coal (L/M of 25-50 and >50, respectively; Louchouarn et al., 2009), are the predominant source of anhydrosugars in the atmospheric particles collected at the time. In addition, these ratios point to a mixture of hardwood/softwood input to the Houston fine aerosols, but a predominantly softwood source in the coarse aerosol. The mixed inputs from hardwood and softwood combustion to these aerosols is consistent with the similarly mixed lignin signatures. In particular, the clear angiosperm wood combustion signature in the fine aerosols of 08/02 to 08/08 (L/M: 7-18), corresponds to a clear angiosperm lignin signature (LPV: 80-100). On the other hand, the clear gymnosperm wood combustion signature in the coarse aerosol of 08/02 (L/M: 3), contrasts with the clear gymnosperm lignin signature in the sample from the same period (LPV: 92). This latter difference between fine and coarse aerosols supports the earlier suggestion that organic aerosols are comprised of a heterogeneous mixture of constituents from different origins and processes.

5.3.5 Atmospheric Significance

Despite the analytical challenge of extracting LOPs from aerosol samples, determining their presence and signatures can be of great value to trace the inputs from vascular plant OM and to estimate natural background aerosol concentrations from PBAP. Furthermore, relative ratios of lignin methoxyphenols can also help distinguish potential plant classes and their alteration. The analysis of lignin-derived

methoxyphenols by CuO oxidation reduces the gap in the understanding of organic aerosol composition and accounts for a portion of biogenic aerosol sources previously unquantified due to analytical limitations. In this study, the products (LOPs and anhydrosugar isomers) from three major macropolymers (lignin, cellulose, and hemi-cellulose), which account for ~90% of plant content were observed in most samples studied.

Characterization of lignin aerosols in the forms of vanillyl, syringyl, and cinnamyl phenols identified that biological particles in Houston aerosols are likely derived from woody tissues of flowering plants, with minor influence from soft tissues and some instances pollens. The material is likely to be altered (not freshly emitted). The LOPs in aerosols are also thought to contribute to humic-like substances in the water-insoluble organic fraction (Graber and Rudich, 2006). Particularly, the presence of *p*-hydroxyl phenols and 3,5 dihydroxybenzoic acid suggest the influence of suspended soil organic matter in Houston aerosols. The results also highlight the importance of primary biological materials in aerosols in the coarse size fraction. The data presented for lignin phenols in aerosols also illustrate that lignin phenols occur mainly as polymers (LOPs) rather than solvent-extractable monomers (free phenols) at an urban location such as Houston during summer. To our knowledge, this is the first report of quantification of LOPs in the ambient aerosols. Previous works on aerosols related to lignin phenols focused only on monomers (free phenols) collected at sites influenced by biomass burning. However, this paper clearly demonstrates the occurrence of lignin phenols as macropolymers in aerosols. Further studies need to address how long- and short-range

atmospheric transport of these vascular plant constituents may contribute to the carbon flux of terrigenous OM to aquatic systems.

5.4 References

Alberts, J.J., Price, M.T., and Lewis, S. Lignin oxidation product and carbohydrate composition of plant tissues from the South-eastern United States. Estuar. Coast. Shelf Sci. 33, 213-222, 1991.

Dickens, A.F., Gudeman, J.A., Gélinas, Y., Baldock, J.A., Tinner, W., Hu, F.S., and Hedges, J.I. Sources and distribution of CuO-derived benzene carboxylic acids in soils and sediments. Org. Chem. 38, 1256-1276, 2007.

Dimmel, D.R. Lignins and Lignans. Advances in Chemistry, Heitner, C., Dimmel, D.R., and Schmidt, J.A. (Eds.). CRC Press, Taylor and Francis Group, NY, 2010.

Dittmar, T. and Lara, R.J. Molecular evidence for lignin degradation in sulfate-reducing mangrove sediments (Amazonia, Brazil). Geochim. Cosmochim. Acta 65, 1417-1428, 2001.

Fabbri, D., Torri, C., Simoneit, B.R.T., Leszek, M., Rushdi, A.I., Fabianska, M.J. Levoglucosan and other cellulose and lignin markers in emissions from burning of Miocene lignites. Atmos. Environ. 43, 2286-2295, 2009.

Fraser, M.P. and Lakshmanan, K. Using levoglucosan as a molecular marker for the long-range transport of biomass combustion aerosols. Environ. Sci. Technol. 34, 4560-4564, 2000.

Goñi, M.A., and Hedges, J.I. Lignin dimers: Structures, distribution, and potential geochemical applications. Geochim. Cosmochim. Acta, 56, 4025-4043, 1992.

Goñi, M.A. and Hedges, J.I. Sources and reactivities of marine-derived organic matter in coastal sediments as determined by alkaline CuO oxidation. Geochim. Cosmochim. Acta 59, 2965-2981, 1995.

Goñi, M.A., Yunker, M.B., MacDonald, R.W. and Eglinton, T.I. Distribution and sources of organic biomarkers in arctic sediments from the Mackenzie River and Beaufort Shelf. Mar. Chem. 71, 23-51, 2000.

Graber, E.R. and Rudich, Y. Atmospheric HULIS: How humic-like are they? A comprehensive and critical review. Atmos. Chem. Phys. 6, 729-753, 2006.

Graham, B., Guyon, P., Taylor, P.E., Artaxo, P., Maenhaut, W., Glovsky, M.M., Flagan, R.C., and Andreae, M.O. Organic compounds present in the natural Amazonian aerosol: Characterization by gas chromatography-mass spectrometry. J. Geophys. Res. 108, doi: 10.1029/2003JD003990, 2003.

Graham, B., Mayol-Bracero, O.L, Guyon, P., Roberts, G.C., Decesari, S., Facchini, M.C., Artaxo, P., Maenhaut, W., Koll, P., and Andreae, M.O. Water-soluble organic compounds in biomass burning aerosols over Amazonia 1. Characterization by NMR and GC-MS. *J. Geophys. Res.* 107 (D20), 8047, doi:10.1029/2001JD000336, 2002.

Hatfield, R. and Vermerris, W. Lignin formation in plants. The dilemma of linkage specificity. Plant Physiol.126, 1351-1357, 2001.

Hawthorne, S.B., Krieger, M.S., Miller, D.J., and Mathiason, M.B. Collection and quantification of methoxylated phenol tracers for atmospheric pollution from residential wood stoves. Environ. Sci. Technol. 23, 470-475, 1989.

Hawthorne, S.B., Miller, D.J., Barkley, R.M., and Krieger, M.S. Identification of methoxylated phenols as candidate tracers for atmospheric wood smoke pollution. Environ. Sci. Technol. 22, 1191-1196, 1988.

Hedges, J.I. and Ertel, J.R. Characterization of lignin by gas capillary chromatography of cupric oxide oxidation products. Anal. Chem. 54, 174-178, 1982.

Hedges, J.I. and Mann, D.C. The characterization of plant tissues by their lignin oxidation products. Geochmi. Cosmochim. Acta 43, 1803-1807, 1979.

Hedges, J.I., Blanchette, R.A., Weliky, K., Devol, A.H. Effects of fungal degradation on the CuO oxidation products of lignin: a controlled laboratory study. Geochim.Cosmochim. Acta 52, 2717-2726, 1988a.

Hedges, J.I., Clark, W.A., and Cowie, G.L. Organic matter sources to the water column and surficial sediments of a marine bay. Limnol. Oceanogr. 33, 1116-1136, 1988b.

Hoffer, A., Gelenscér, A., Blazsó, M., Guyon, P., Artaxo, P., and Andreae, M.O. Diel and seasonal variations in the chemical composition of biomass burning aerosol. Atmos. Chem. Phys. 6, 3505-3515, 2006.

Houel, S., Louchouarn, P., Lucotte, M., Canuel, R., and Ghaleb, B. Translocation of soil organic matter following reservoir impoundment in boreal systems: Implications for in situ productivity. Limno. Oceanogr. 51, 1497-1513, 2006.

Jaenicke, R. Abundance of cellular material and proteins in the atmosphere. Science, 308, 73, 2005.

Jordan, T.B., Seen, A.J., Jacobson, G.E. Technical note. Levoglucosan as an atmospheric tracer for woodsmoke. Atmos. Environ. 40, 5316-5321, 2006.

Keil, R.G., Tsamakis, E., Giddings, J.C., and Hedges, J.I. Biochemical distributions (amino acids, neutral sugars, and lignin phenols) among size-classes of modern marine sediments from the Washington coast. Geochim. Cosmochim. Acta 8, 1347-1364, 1998.

Kiehl, J.T. and Rodhe, H. Modeling geographical and seasonal forcing due to aerosols, in Aerosol Forcing of Climate, R.J. Charlson and J. Heintzenberg, eds., Wiley, NY pp. 281-296, 1995.

Knight, C.A., Clancy, R.B., Götzenberger, L., Dann, L., and Beaulieu, J.M. On the relationship between pollen size and genome size. J. Botany, doi:10.1155/2010/612017, 2010

Kuo, L-J., Herbert, B.E., Louchouarn, P. Can levoglucosan be used to characterize and quantify char/charcoal black carbon in environmental media? Org. Geochem. 39, 1466-1478, 2008a.

Kuo, L-J., Louchouarn, P., Herbert, B.E. Fate of CuO-derived lignin oxidation products during plant combustion: application to the evaluation of char inputs to soil organic matter. Org. Geochem. 39, 1522-1536, 2008b.

Kuo, L-J. et al. Combustion condition-dependent anhydrosugars and solvent-extractable lignin phenols in chars: Implications for characterization of biomass combustion residues. Manuscript in preparation, 2011.

Larsen, R.K., Schantz, M.M., Wise, S.A. Determination of levoglucosan in particulate matter reference materials. Aero. Sci. Technol. 40, 781-787, 2006.

Louchouarn, P., Amon, R.M.W., Duan, S., Pondell, C., Seward, S.M., White, N. Analysis of lignin-derived phenols in standard reference materials and ocean dissolved

organic matter by gas chromatography/tandem mass spectrometry. Marine Chem. 118, 85-97, 2010.

Louchouarn, P., Kuo, L-J, Wade, T.L., Schantz, M. Determination of levoglucosan and its isomers in size fractions of aerosol standard reference materials. Atmos. Environ. 43, 5630-5636, 2009.

Louchouarn, P., Naehr, T., Silliman, J., Houel, S. Elemental, stable isotopic ($\delta^{13}C$), and molecular signatures of organic matter in late Pleistocene to Holocene sediments from the Peruvian margin (ODP Site 1229). In: Jørgensen, B.B., D'Hondt, S.L., Miller, D.J. (Eds.), Proceedings of the Ocean Drilling Program, Scientific Results 201, 1-21, 2006.

Louchouarn, P., Lucotte, M., and Farella, N. Historical and geographical variations of sources and transport of terrigenous organic matter within a large-scale coastal environment. Org. Geochem. 30, 675-699, 1999.

Opsahl, S. and Benner, R. Early diagenesis of vascular plant tissues: Lignin and cutin decomposition and biogeochemical implications. Geochim Cosmochim. Acta 59(23), 4889-4904, 1995.

Opsahl, S. and Benner, R. Photochemical reactivity of dissolved lignin in river and ocean waters. Limnol. Oceanogr 43, 1297-1304, 1998.

Otto, A. and Simpson, M.J. Evaluation of CuO oxidation parameters for determining the source and stage of lignin degradation in soil. Biogeochem. 80, 121-142, 2006.

Pöschl, U. Atmospheric aerosols: Composition, Transformation, Climate and Health Effects. Angew. Chem. Int. Ed. 44, 7520-7540, 2005.

Prahl, F.G., Ertel, J.R., Goni, M.A., Sparrow, M.A., and Eversmeyer, B. Terrestrial organic carbon contributions to sediments on the Washington margin. Geochim. Cosmochim. Acta 58, 3035-3048, 1994.

Reeves, A.D. and Preston, M.R. The composition of lignin in estuarine suspended particulates and the distribution of particulate lignin in estuaries as determined by capillary gas chromatography of cupric oxide oxidation products. Estuar. Coast. Shelf Sci. 29, 583-599, 1989.

Simoneit, B.R.T. Review. Biomass burning – a review of organic tracers for smoke from incomplete combustion. Appl. Geochem. 17, 129-162, 2002.

Simoneit, B.R.T. and Elias, V.O. Detecting organic tracers from biomass burning in the atmosphere. Mar. Poll. Bull. 42, 805-810, 2001.

Simoneit, B.R. T. and Elias, V.O. Organic tracers for biomass burning in atmospheric particulate matter over the ocean. Mar. Chem. 69, 301-312, 2000.

Simoneit, B.R.T., Rogge, W.F., Mazurek, M.A., Standley, L.J., Hildemann, L.M., and Cass, G.R. Lignin pyrolysis products, lignans, and resin acids as specific tracers of plant classes in emissions from biomass combustion. Environ. Sci. Technol. 27, 2533-2541, 1993.

Simoneit, B.R.T., Schauer, J.J., Nolte, C.G., Oros, D.R., Elias, V.O., Fraser, M.P., Rogge, W.F., and Cass, G.R. Levoglucosan, a tracer for cellulose in biomass burning and atmospheric particles. Atmos. Environ. 33, 173-182, 1999.

Simpson, C.D., Dills, R.L., Katz, B.S., Kalman, D.A. Determination of levoglucosan in atmospheric fine particulate matter. J. Air Waste Manag. Assoc. 54, 689-694, 2004.

Tareq, S.M., Tanaka, N., and Ohta, K. Biomarker signature in tropical wetland: lignin phenol vegetation index (LPVI) and its implications for reconstructing the paleoenvironment. Sci. Total Environ. 324, 91-103, 2004.

Yttri, K.E., Dye, C., and Kiss, G. Ambient aerosol concentrations of sugars and sugar-alcohols at four different sites in Norway. Atmos. Chem. Phys. 7, 4267-4279, 2007.

Table 5.1. Lignin-derived phenols, *p*-hydroxyl phenols, 3,5 dihydroxybenzoicacid to aldehyde ratio, and lignin phenol vegetation index in aerosols sampled at Houston during summer.

5.1a. Coarse aerosols

Date	S	C	V	P	3,5 Bd	(Ad/Al)v	(Ad/Al)s	LPVI
07/20	17.81	nd	nd	127.63	nd	nd	0.43	
07/22	nd	nd	nd	nd	nd	nd	nd	
07/24	10.10	nd	4.68	18.92	4.54	2.14	0.24	146[a]
07/26	4.44	3.09	4.33	24.50	3.95	nd	1.17	778[b]
07/28	5.51	nd	8.66	126.39	1.27	1.74	0.45	26[c]
07/30	2.58	nd	1.63	9.98	nd	nd	0.34	97[a]
08/03	3.43	nd	2.25	13.58	nd	nd	0.35	92[a]
08/05	4.48	5.54	28.43	10.66	nd	0.94	0.62	12[c]
08/07	4.86	nd	6.46	18.92	nd	1.42	0.37	33

5.1b.Fine aerosols

Date	S	C	V	P	3,5 Bd	(Ad/Al)v	(Ad/Al)s	LPVI
07/20	0.52	1.32	0.66	3.40	nd	nd	nd	1818[b]
07/22	nd	0.23	0.25	3.04	nd	nd	nd	47
07/24	0.93	nd	0.57	3.87	nd	nd	0.44	101[a]
07/26	0.84	0.17	0.68	3.72	nd	6.17	0.53	223[a]
07/28	0.30	nd	0.31	2.60	nd	nd	0.68	49
07/30	0.55	0.11	0.39	1.75	0.25	nd	0.66	296[a]
08/03	0.84	0.10	0.80	2.73	0.25	4.50	0.55	98[a]
08/05	1.05	0.20	1.31	2.59	0.81	2.73	0.65	79[a]
08/07	nd	nd	0.30	2.98	nd	nd	nd	

Syringyls (S), cinnamyls (C), vanillyls (V), p-hydroxy phenols (P), and 3,5 dihydroxybenzoic acid (3,5 Bd) are presented in ng m^{-3}.

LPVI = [{S(S+1)/(V+1)+1} × {C(C+1)/(V+1)+1}; interpretation for LPVI is given by three subscripts (a,b,c) based on the range of LPVI values reported for different plant classes in Table 3 of Tareq et al. (2004).

[a]Angiosperm woods; [b]non-woody angiosperms; [c]non-woody gymnosperms

nd = not detected

Table 5.2. Plant combustion-derived methoxyphenols and levoglucosan isomers in aerosols sampled at Houston during summer.

Fine aerosols									
Date	S	C	V	P	3,5 Bd	Levoglucosan	Mannosan	Galactosan	L/M
07/30	nd	0.14	nd	0.87	0.01	1.85	nd	nd	na
07/31	0.02	0.1	nd	0.85	0.01	1.81	nd	0.15	na
08/02	2.52	0.16	1.18	0.53	0.09	8.42	1.24	1.58	6.8
08/05	0.23	0.13	nd	1.52	0.02	6.69	0.37	0.29	18.1
08/08	nd	0.15	nd	1	nd	3.73	0.45	0.13	8.3
Coarse aerosols									
08/02	nd	0.72	9.3	6.06	nd	2.03	0.73	nd	2.8

nd = not detected; in case of V, it is mainly due to negative values after blank correction.
All above values are reported in ng m^{-3}.

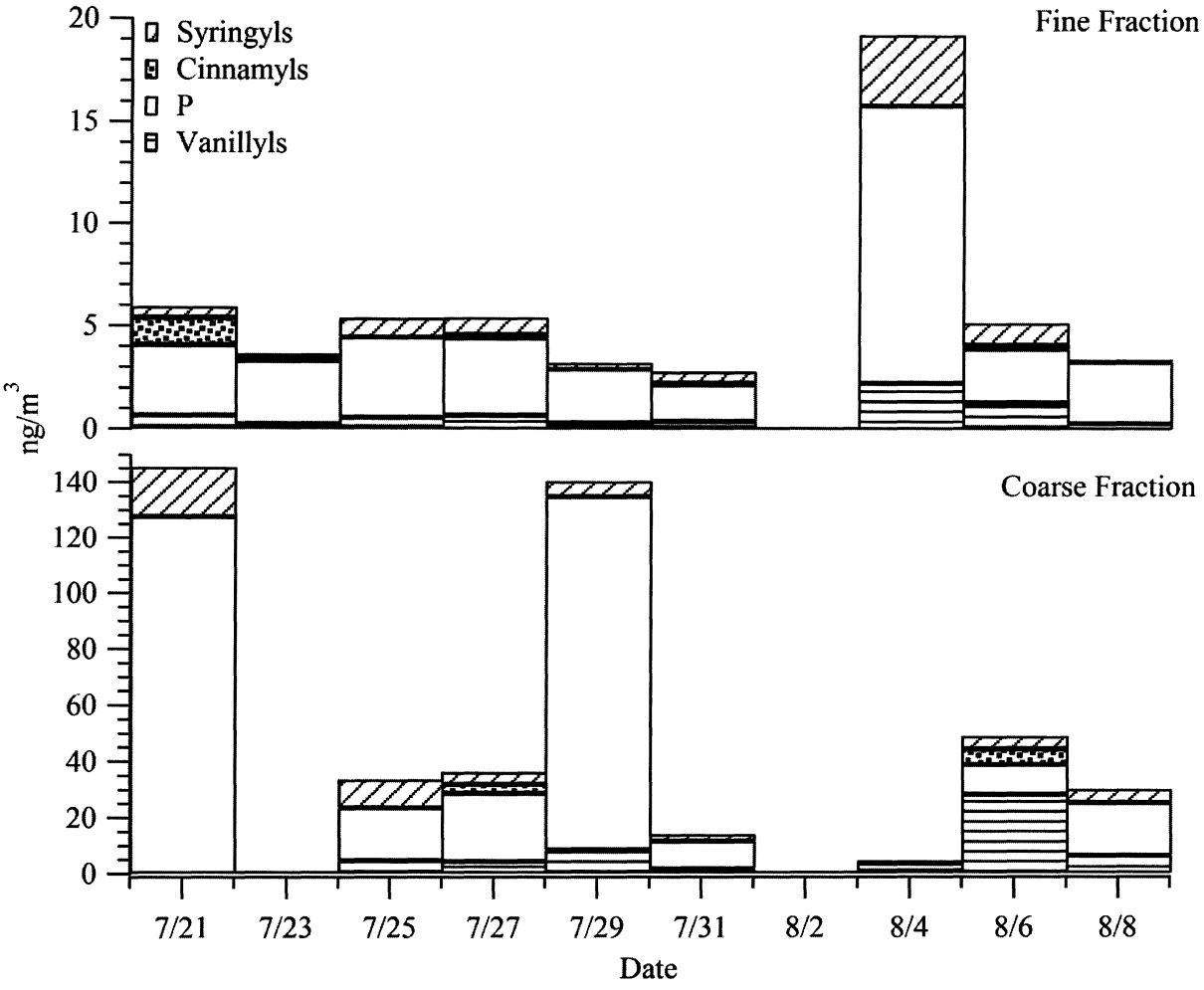

Figure 5.1. Time series of four main lignin oxidation products in coarse and fine fraction of aerosols collected in Houston during summer 2010.

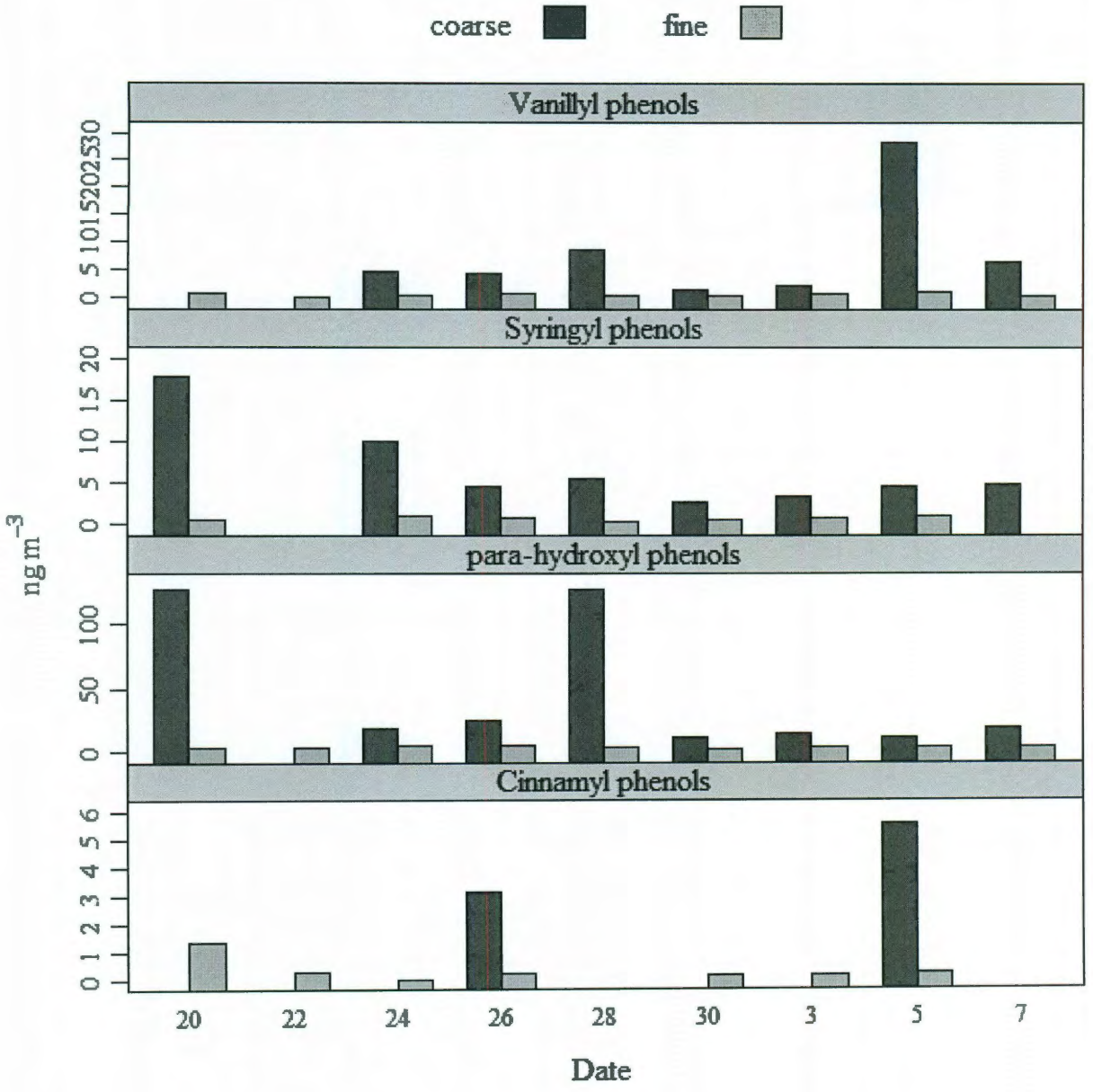

Figure 5.2. Time series of distribution of syringyls, cinnamyls, vanillyls, and *p*-hydroxyl phenols.

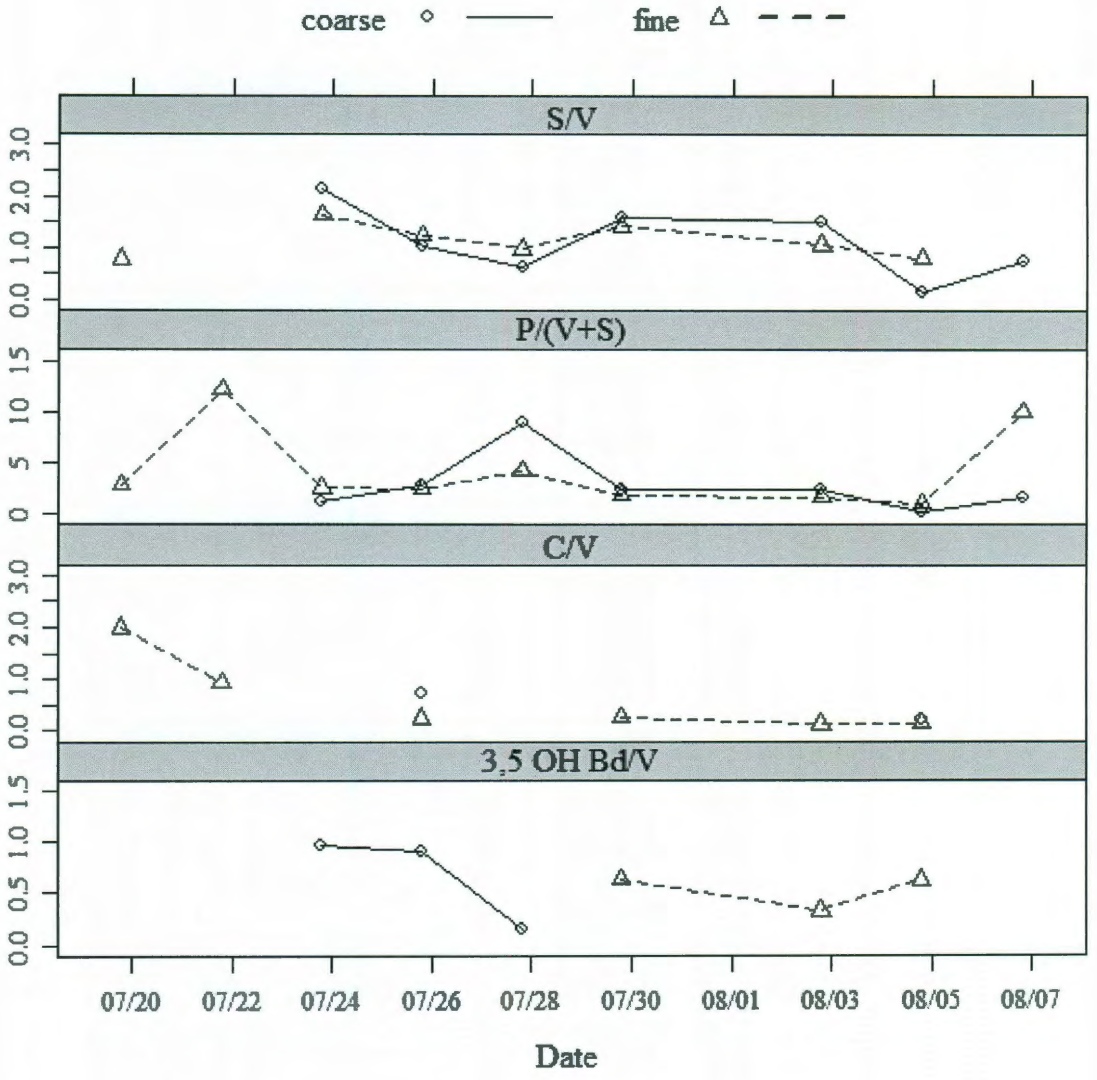

Figure 5.3. Relative distribution of lignin oxidation products.

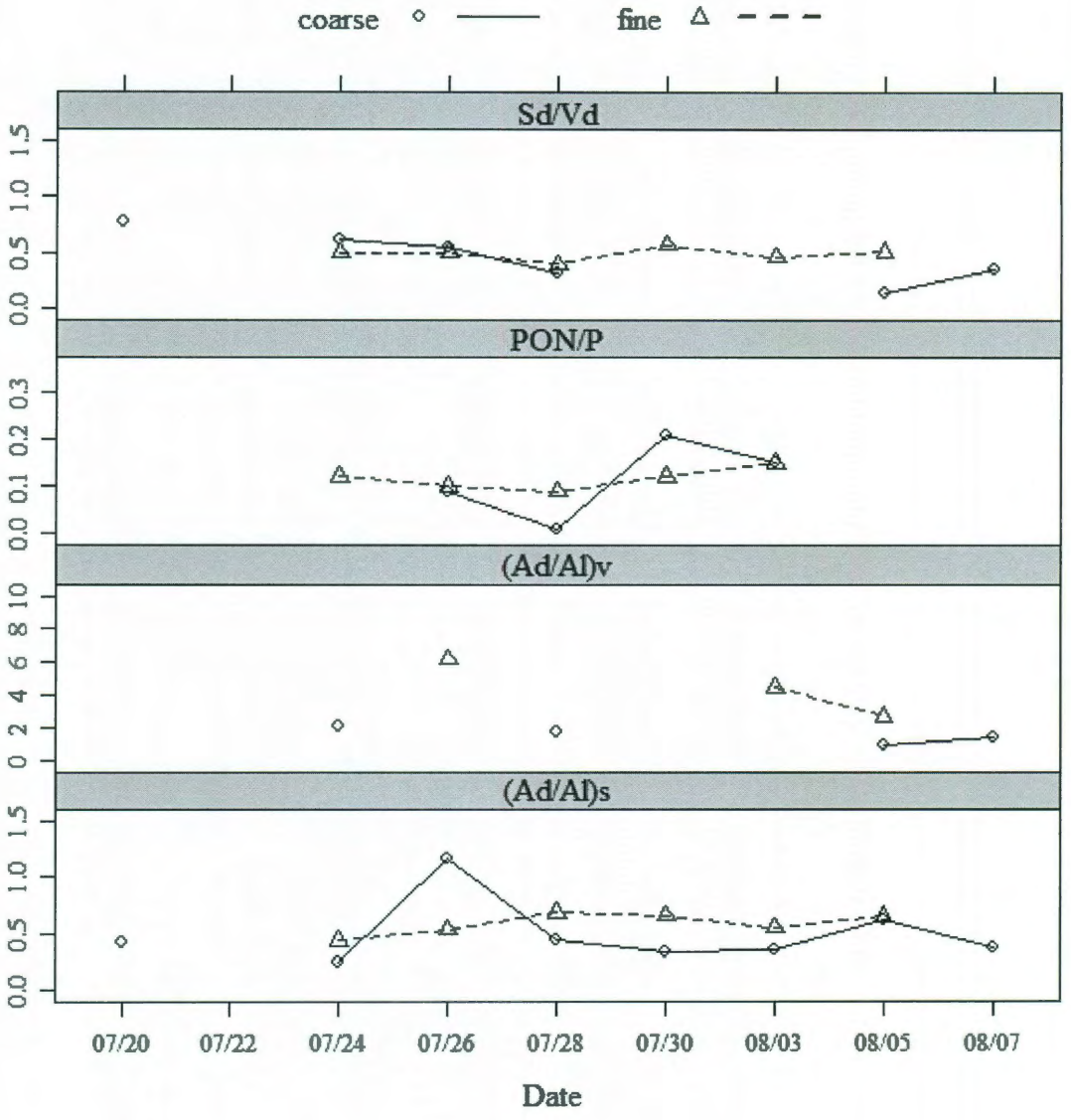

Figure 5.4. Acid to aldehyde ratios in vanillyls ((Ad/Al)v) and syringyls ((Ad/Al)s), syringic acid to vanillic acid (Sd/Vd) ratio, and *p*-hydroxyacetophenone to total *p*-hydroxyl phenols (PON/P) ratio in coarse and fine fraction of aerosols.

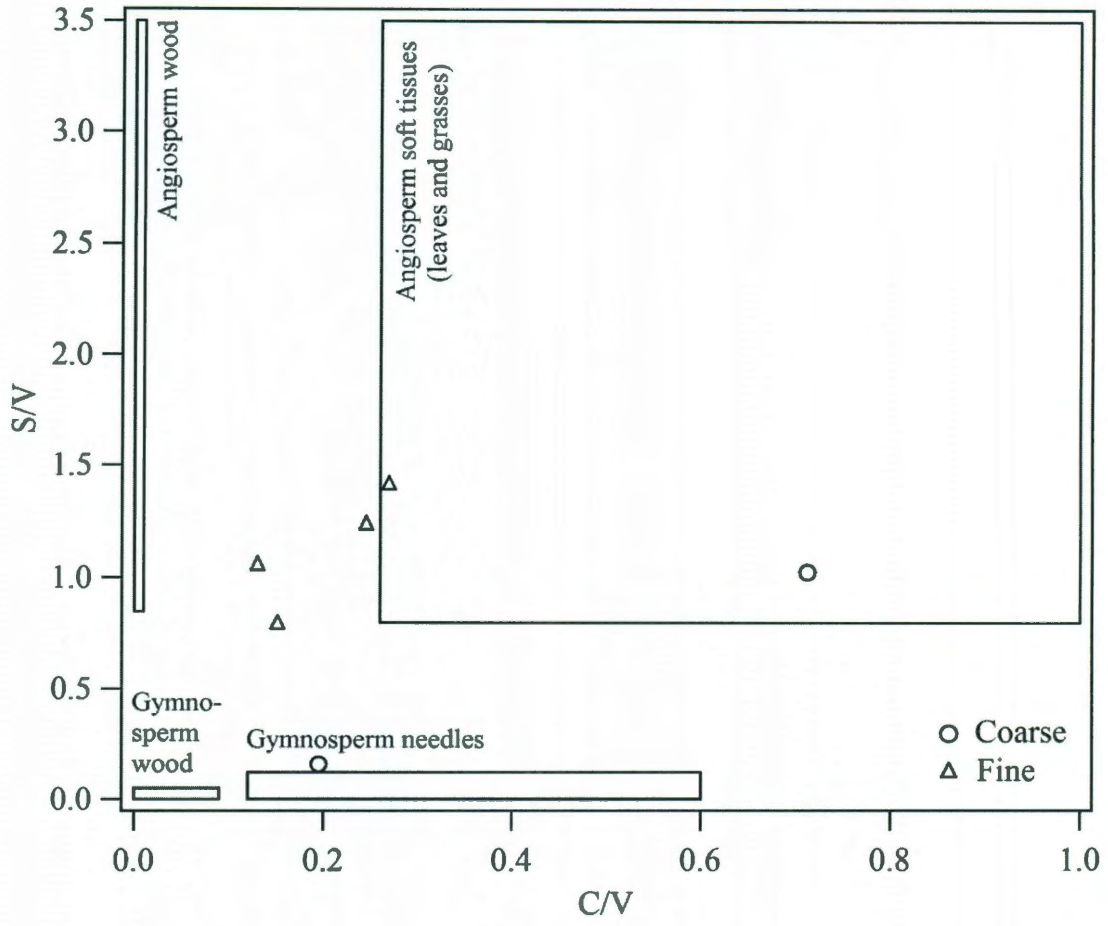

Figure 5.5. Distribution of syringyls and cinnamyls with respect to vanillyls. Boxes inside the graph represent the signatures from the respective plant materials (Hedges and Mann, 1979; Alberts et al., 1991; Louchouarn et al., 2006). One sample with C/V value of 2 is not included in this plot.

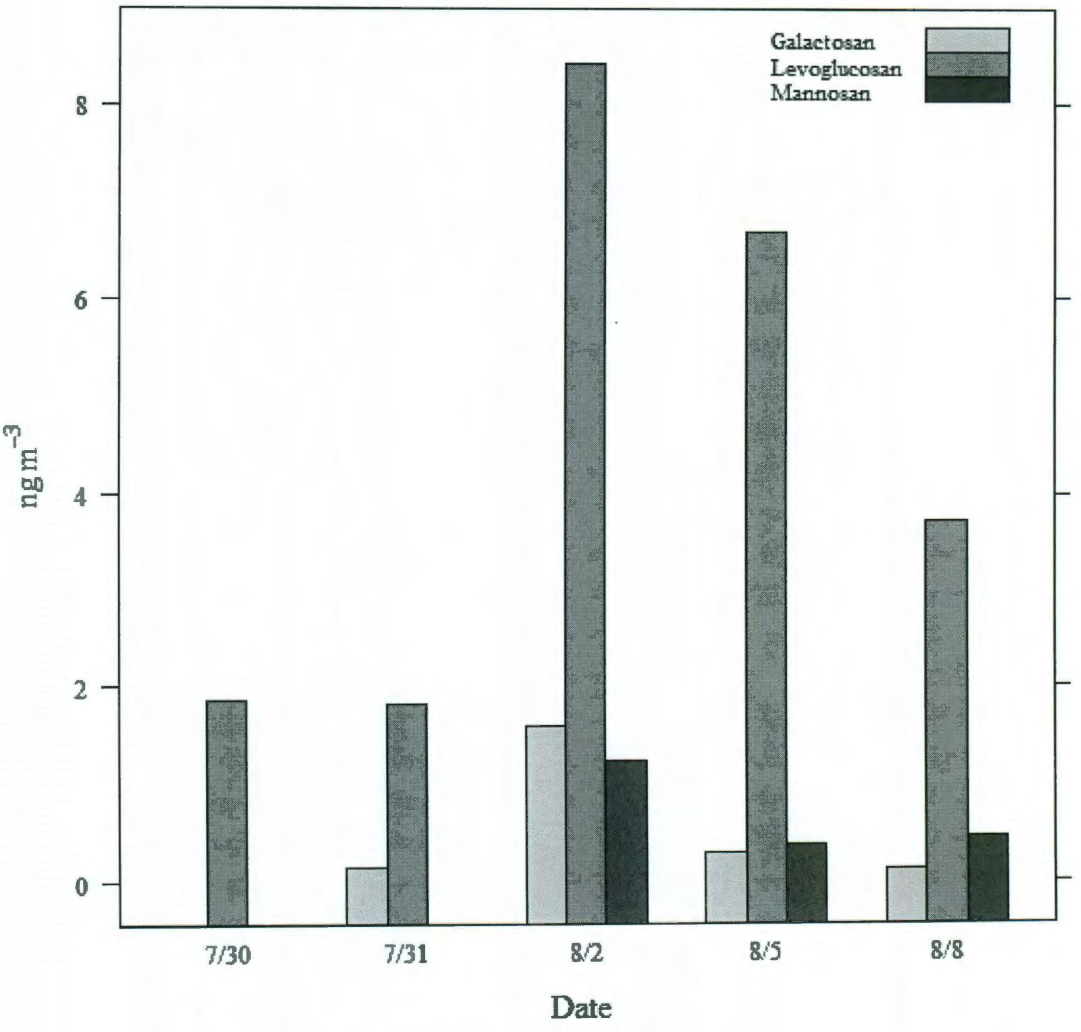

Figure 5.6. Concentration of levoglucosan isomers in Houston aerosols during summer 2010.

Chapter 6

Conclusions

6.1 Summary

An aerosol characterization study in Kathmandu using principal component analysis identified vehicular emissions as the main source of aerosols. Other potential sources include secondary gas-to-particle conversion, aqueous processing, and dust transport. Indicator of primary emissions, EC, was present on average at a concentration of 4.48 ± 1.17 μg C m^{-3}. POC contributed an average of 69% of OC (20.02 ± 6.59 μg C m^{-3}). Elemental carbon and OC were correlated (R^2 = 0.56, $p<0.0001$) indicating a common source, i.e., primary emissions. Aerosols at Kathmandu are most likely to be acidic as indicated by the neutralization ratio. Values for carbonaceous species and stable carbon and nitrogen isotopes in aerosol at Kathmandu were comparable to other Asian urban locations and urban and anthropologically influenced locations around the world.

Aerosols in a semi-rural location, in the Northeastern United States (Thompson Farm) exhibited a strong seasonal variation for carbonaceous species, aromatic groups of water-soluble aerosols, and stable nitrogen isotope ratios. Carbonaceous aerosol concentrations were the largest during winter and the smallest during summer. Correlations between OC and EC were strongest to weakest during winter, spring, and fall, respectively, with no correlation during summer. Results indicate secondary aerosols to be the main type of aerosols at Thompson Farm, with enhanced importance of primary aerosols during winter. Aliphatic (H-C), unsaturated aliphatic (H-C=C), oxygenated (H-C-O), and aromatic groups were the abundant chemical functional groups, constituting 30.6 ± 5.3%, 22.9 ± 6.1%, 25.4 ± 7.0%, and 20.7 ± 13.4%, respectively, of

the water-soluble carbon. Decreases in WSOC concentrations and contributions from unsaturated aliphatics and aromatic groups were observed with the increased precipitation. Increases in EC, POC, and oxygenates were observed at Thompson Farm when the air masses originated from the continental Midwest, indicating the influence from upwind industrial and urban sources.

Similar to that of total carbon aerosols (TC), the total nitrogen (TN) content in aerosols was the largest during winter compared to other seasons. The largest TN and the lowest $\delta^{15}N$ during winter suggest the strong influence of natural gas combustion during winter at Thompson Farm. Stable nitrogen isotope values also showed a correlation with meteorological parameters such as relative humidity and temperature suggesting the influence of meteorology-dependent nitrogen isotope fractionations. Stable carbon isotope values did not vary greatly, and the observed value (annual mean: -26.0 ± 1.4, 1σ) indicate the likely influence of anthropogenic source signatures and that any plant-related influence results from C_3 plants.

Detection of LOPs in aerosols collected during summer in Houston indicates the potential of using LOPs as tracers of primary biogenic aerosol sources. Though LOPs have been widely exploited in other fields such as geochemistry, limnology, and plant science, the results from the current study are the first to report the successful utilization of LOPs as tracers of vascular plants in ambient aerosols. Lignin-derived phenols were present mainly in the form of macropolymers (detected only after CuO oxidation) in aerosols collected during summer in Houston. Free phenol (lignin-derived monomers) and sugar isomer (levoglucosan, mannosan, and galactosan) concentrations in aerosols were very small, suggesting no influence from biomass burning. The observed free

phenols and sugar isomers are most likely to be from long-range transport. Vanillyl and syringyl phenols were the dominant LOPs and identified woody angiosperms as the plant source. The LOPs were present in much larger concentration in the coarse fraction compared to the fine fraction. Of all the detected phenols, concentrations of *p*-hydroxyphenols were the largest in both coarse and fine aerosols. The *p*-hydroxyphenols are reported to originate from plant components such as proteins and tannins in addition to lignin.

6.2 Recommendations for Future Research

Due to the large aerosol concentrations in Kathmandu, the aerosol composition and its sources need further study to determine how to best control and manage air pollution in the valley. Studies related with hazardous components such as heavy metals and PAHs in the fine size fraction of aerosols in Kathmandu are recommended to help assess the health-related risks from aerosols in the valley.

H^+-NMR spectroscopy is a powerful tool for characterizing organic aerosols. Detailed studies quantifying different functional groups using internal standards and analysis of different subsets after chromatographic separations (Decesari et al., 2000) can be performed. A comparison with other methods for WSOC characterization such as Fourier Transform Infrared (FTIR) Spectroscopy can be done to further quantify different functional groups and validate the measurements. Furthermore, positive matrix factorization (PMF) and other statistical technique and laboratory investigations of tracer compounds can be used along with H^+-NMR to identify and quantify the aerosol sources.

Source signature plots based on Decesari et al. (2007) need further investigation in different location and seasons.

Seasonal variation in stable nitrogen isotope of aerosols and gases and the association with meteorological parameters such as temperature and relative humidity need further study and confirmation to investigate the mechanism responsible for isotope fractionation. Furthermore, the determination of stable carbon and nitrogen isotope in different carbon and nitrogen species in aerosols as well as the precursor gases and primary emission sources can have applications in aerosol chemistry models and source apportionment studies.

More studies on lignin-derived phenols including the seasonal variations are needed to know the spatial and temporal variation in background natural aerosol concentration. Cutin-derived CuO oxidation products and lignin dimers in aerosols are one of the potential areas that have not been studied previously. Lignin-derived phenols can also be used to study the type of carbonaceous residues and the thermal alteration processes.

Although not included in this thesis, chamber studies of SOA formation from PAHs have been performed (Appendix A). The SOA modeling needs to incorporate SOA formation from PAHs, and PAH contributions to SOA formation from different sources at urban location need to be assessed. Furthermore, effects of acidity and seed aerosols on SOA formation from PAHs need to be investigated.

As with the PAH study, chamber studies on oxidation of gaseous elemental mercury are presented in Appendix B and C. Various environmental conditions, under conditions mimicking the real atmosphere, affecting atmospheric mercury chemistry need

to be investigated. The exact chemical mechanism influencing the oxidation of GEM by different parameters such as peroxy radicals, dark or light conditions, aerosol surface area, or others need to be investigated. Besides GEM oxidation by O_3, studies involving other oxidants, mainly bromine, need to be performed. After determining the mechanisms by which these parameters influence the system, the relevant expressions can be incorporated into mathematical model to verify the improvement in the model performance.

More studies on semi-volatile (SVOC) or intermediate volatility (IVOC) organic compounds in the ambient environment are needed to improve the understanding on SOA formation, especially in the light of its recent discovery in the ambient atmosphere in the gulf (de Gouw et al., 2011). Improvement on tracer analysis is needed for better characterization of aerosols and assigning the sources. Focus should be on using the multiple tracers and investigating the novel tracer compounds (Iinuma et al., 2010). A combination of analytical techniques (both online and offline) are needed for the comprehensive characterization of organic aerosols (Kroll and Seinfeld, 2008; Hallquist et al., 2009).

6.3 References

de Gouw, J.A. et al. Organic aerosol formation downwind from the deepwater horizon oil spill. Science, 331, 1295-1297, 2011.

Hallquist et al. 2009. The formation, properties, and impact of secondary organic aerosol: current and emerging issues. Atmos. Chem. Phys., 9: 5155-5236.

Iinuma, Y., Boge, O., Grafe, R., and Hermann, H. Methyl-Nitrocatechols: Atmospheric tracer compounds for biomass burning secondary organic aerosols. Environ. Sci. Technol., 44, 8453-8459, 2010.

Kroll, J.H. and Seinfeld, J.H. Chemistry of secondary organic aerosol: Formation and evolution of low-volatility organics in the atmosphere. Atmos. Environ. 42, 3593-3624, 2008.

CHAPTER A1

SECONDARY ORGANIC AEROSOL FROM PHOTOOXIDATION OF POLYCYCLIC AROMATIC HYDROCARBONS

Reference: Shakya, K.M. and Griffin, R.J. *Environ. Sci. Technol.* 44, 8134-8139, 2010.

Abstract

Secondary organic aerosol (SOA) formation from the photooxidation of five polycyclic aromatic hydrocarbons (PAHs, naphthalene, 1- and 2-methylnaphthalene, acenaphthylene, and acenaphthene) was investigated in a 9-m^3 chamber in the presence of nitrogen oxides and the absence of seed aerosols. Aerosol size distributions and PAH decay were monitored by a scanning mobility particle sizer and a gas chromatograph with a flame ionization detector. Over a wide range of conditions, the aerosol yields for the investigated PAHs were observed to be in the range of 2 to 22%. The observed evolution of aerosol and PAH decay indicate that light and oxidant sources influence the time required to form aerosol and the required threshold reacted concentration of the PAHs. The SOA yields also were related to this induction period and the hydroxyl radical concentrations, particularly for smaller aerosol loadings (<~6 μg m^{-3}). Estimation of SOA production from oxidation of PAHs emitted from mobile sources in Houston shows that PAHs could account for more than 10% of the SOA formed from emissions from mobile sources in this region.

A1.1 Introduction

Secondary organic aerosol (SOA) constitutes a significant fraction of the fine aerosol in the atmosphere (Zhang et al., 2007). However, there is large uncertainty in predicted SOA formation, with global modeling indicating a range of 12 to 70 Tg SOA yr^{-1} (Kanakidou et al., 2005). Reactive organic gases (ROGs) emitted from natural and anthropogenic sources are oxidized by hydroxyl (OH) and nitrate (NO_3) radicals, ozone (O_3), and/or halogen atoms. The subset of oxidation products that are non- and/or semi-volatile partitions into either a new or pre-existing aerosol phase in one SOA formation pathway (Hallquist et al., 2009). There still may exist a number of unidentified compounds that contribute to SOA formation in the atmosphere via this route (Goldstein and Galbally, 2007). Identifying these compounds, quantifying their SOA yields, and studying their effects on climate and health are critical. The main objective of this study is to quantify further the conversion of gas-phase polycyclic aromatic hydrocarbons (PAHs) with two aromatic rings into particle-phase products.

These PAHs are products of incomplete combustion, are ubiquitous in the environment, and are emitted from both natural and anthropogenic sources. The main anthropogenic emission sources are coal, oil, gas, wood, tobacco, and refuse combustion and domestic heating (Nikolaou, 1984; Ravindra et al., 2008). Naphthalene, 1- and 2-methylnaphthalene, acenaphthylene, and acenaphthene are often the dominant PAHs found in an urban environment (Arey et al., 1989; Reisen and Arey, 2005), and their gas-phase oxidation forms products, some toxic, that partition into the aerosol phase (Atikinson and Arey, 1994; Sauret-Szczepanski and Lane, 2004; Chan et al., 2009; Lee and Lane, 2009; Kautzman et al., 2010, Dekermenjian et al., 1999; Mihele et al., 2002). A

large fraction of photooxidation products from PAHs are reported to form SOA in chamber experiments (Sauret-Szczepanski and Lane, 2004; Chan et al., 2009). PAHs could contribute an important fraction of urban SOA based on using phthalic acid and 4-nitro-1-naphthol as naphthalene SOA tracers (Kautzman et al., 2010).

Conventionally, SOA formation has been described by a dimensionless fractional aerosol yield, Y (Pandis et al., 1992), defined as the ratio of the mass concentration of SOA formed (ΔM) to the mass concentration of ROG consumed (ΔROG):

$$Y = \frac{\Delta M}{\Delta ROG} \tag{1}$$

Using a semi-empirical partitioning model for semi-volatile products, SOA yield can be expressed as a function of the organic aerosol mass concentration (Odum et al., 1996):

$$Y = \Delta M_o \sum_i \frac{\alpha_i K_{om,i}}{1 + \Delta M_o K_{om,i}} \tag{2}$$

where α_i is the mass-based stoichiometric coefficient for product i, $K_{om,i}$ (m^3 μg^{-1}) is its equilibrium absorptive partitioning coefficient between the gas phase and an absorbing condensed organic medium based on Raoult's law (Pankow, 1994), and ΔM_o (μg m^{-3}) is the total organic aerosol mass concentration. Generally, two hypothetical products are used to parameterize yields. Combination of equations (1) and (2) yields a required threshold ΔROG (THC or threshold reacted hydrocarbon concentration) to initiate SOA formation within chambers (Song et al., 2005; Cai and Griffin, 2006):

$$THC = \left(\sum_i \alpha_i K_{om,i} \right)^{-1} \tag{3}$$

To further understand the volatility distribution of the products, a volatility basis set (VBS) approach can be used (Donahue et al., 2006, 2009; Stanier et al., 2008):

$$\xi = \frac{\Delta c_{OA}}{\Delta ROG} = \sum_j \frac{\alpha_j}{1 + (c_j^* / c_{OA})} \quad (4)$$

where ξ is the overall aerosol mass fraction, c_j^* is the effective saturation concentration of product j (analogous to the inverse of the partitioning coefficient), and c_{OA} is the organic aerosol mass concentration. The VBS approach typically uses nine bins with set c_j* that step by an order of magnitude to fit observed aerosol yields (ξ) and masses (c_{OA}) to determine α_j.

$K_{om,i}$ (m^3 μg^{-1}), the equilibrium absorptive partitioning coefficient for 1- and 2-nitronaphthalenes, and 1,2- and 1,4-naphthoquinone were predicted using the following expression (Pankow, 1994):

$$K_{om,i} = \frac{RT}{10^6 M_{om} \gamma_i p^0_{L,i}} \quad (5)$$

where R is the ideal gas constant (8.206×10^{-5} m^3 atm mol^{-1} K^{-1}), T is the temperature (K), M_{om} is the average molecular weight of the absorbing *om* phase (g mol^{-1}), γ_i is the activity coefficient of i in the *om* phase, and $p^0_{L,i}$ is the sub-cooled liquid vapor pressure of i at T (atm).

A1.2 Experimental

A 9-m^3 Teflon laboratory chamber (surface-to-volume ratio 2.97 m^{-1}) (Welch Fluorocarbon) was used for all experiments. A set of Sylvania (30W, G30T8; 254-nm ultraviolet (UV)) germicidal lamps (10 tubes) was used for the experiments in which hydrogen peroxide (H_2O_2) was used as the OH source; a set of Sylvania (40W, 350 BL; 365-nm UV) blacklights (20 tubes) was used for the experiments in which nitrous acid (HONO) was used as the OH source. Illumination of the appropriate set of lights

initiated the experiments by photolyzing H_2O_2 or HONO to generate OH. The chamber used is similar to that described previously (Cai and Griffin, 2006; Cai et al., 2008).

A gas chromatograph with a flame ionization detector (GC-FID; GC-17A, Shimadzu Corporation) and a DB-5 column (Agilent Technologies) was used for monitoring PAH mixing ratios throughout each experiment. Optimization of oven temperature and flow rates was performed for each compound. Nitric oxide (NO) and O_3 were monitored by a chemiluminescence analyzer (ML 9841A, Monitor Labs, Inc.) and a photometric O_3 analyzer (Model 400A, API, Inc.). Purified air was provided by a zero-air generator (Model 111, Thermo Environmental Instruments) followed by three packed-bed scrubbers (Purafil, activated charcoal, and Drierite) and a HEPA filter. The purified air also was passed through a flask surrounded by dry ice to strip water vapor.

A scanning mobility particle sizer (SMPS, Classifier 3080, DMA 3085, and CPC 3776; TSI, Inc.) was used to monitor the aerosol size distribution. Aerosols were monitored in 3-minute intervals in the size range of 4.5 to 159.6 nm. Aerosol densities of 1.5 and 1.3 g cm^{-3} were used for estimating mass of aerosol from naphthalene and 2-methylnaphthalene, respectively, and a density of 1.4 g cm^{-3} was used in experiments with 1-methylnaphthalene, acenaphthylene, and acenaphthene (Chan et al., 2009). Number concentrations and aerosol density are assumed to be accurate to within 5% for the purpose of relative error calculation. Aerosol data were corrected for wall losses using first-order kinetics (Bowman et al., 1997). However, no wall loss correction was applied for PAHs or their gas-phase oxidation products. The deposition rate of gaseous species to Teflon walls is usually limited by diffusion or surface reaction processes (McMurry and Grosjean, 1985). Wall losses are unavoidable (Carter et al., 2005), and the greatest

uncertainty in the experimental results is due to the wall loss of gas-phase PAH oxidation products.

The O_3 analyzer was calibrated with O_3 generated by a multi-gas calibrator (Series 100, Environics, Inc.). The NO monitor was calibrated with NO from a standard tank (10 or 100 ppm of NO in nitrogen, Airgas, Inc.) that was diluted through the multi-gas calibrator. Calibrations were performed before the set of chamber experiments for each PAH. Sizing checks for particle equipment were performed with 81- and 150-nm polystyrene latex spheres (PSLs, Thermo Scientific or Duke Scientific) generated by atomizing a solution of deionized water and PSLs after approximately every eighth chamber experiment. No significant shift in peak diameter (<2 nm) was observed over the course of these experiments. On this basis, an uncertainty of 2 nm in aerosol diameter is assumed for calculating relative errors.

For calibration of PAHs by GC-FID, at least four PAH concentrations were prepared. A known volume of PAH in methanol was injected into a small ~250-L Teflon bag filled with a known volume of zero air. The gases in the bag were allowed to mix and then the sample from the bag was transferred to the GC-FID through a loop attached to the inlet of GC-FID using a vacuum pump. The peak from methanol did not interfere with the peak of any PAHs when a DB-5 column (Agilent Technologies) was used. The ranges of PAH concentrations were varied depending on the calibration for the particular experiment so that the desired initial PAH concentration for the chamber experiment was within the calibration curve. The GC-FID response to the PAH was determined by the slope of the regression line forced through the origin in a scatterplot for each four or five point calibration.

Each PAH, hydrogen peroxide (50 wt. % in deionized water), and sulfuric acid (H_2SO_4, 99.99%) were purchased from Sigma-Aldrich. Sodium nitrite ($NaNO_2$) (2% w/v aqueous solution) was purchased from Fisher Scientific. Sulfuric acid and $NaNO_2$ are reagents in the generation of HONO.

Between experiments, the chamber was flushed for 30 to 36 hours with zero air, during which the lights were illuminated for at least 8 hours. For each experiment, the chosen volume of PAH (in methanol) was injected by syringe into a glass bulb connected to the chamber. The glass bulb was heated to facilitate evaporation of the PAH solution, and the zero air was passed through the bulb to introduce PAH to the chamber. Oxidation products of methanol do not produce SOA, and the lifetime against OH oxidation is weeks for methanol compared to hours for PAHs (Atkinson and Arey, 1994; Jiménez et al., 2003). Therefore, the unknown effects of methanol on SOA yields would be caused by any methanol influence on HO_2 and OH levels.

As the OH radical source, 20-30 ml of H_2O_2 solution was injected into the glass bulb followed by slight heating; zero air was passed through the bulb to introduce H_2O_2 to the chamber. In some experiments, OH was generated from the photolysis of HONO generated from the drop-wise addition of 0.3 ml of 2% $NaNO_2$ to 0.6 ml of 12% H_2SO_4 (Ng et al., 2007a, 2007 b). Purified air was passed through the flask containing these compounds into the chamber. Nitric oxide (gas) from standard tanks (10 or 100 ppm of NO in nitrogen; Airgas, Inc.) was also added.

All experiments were conducted at the laboratory temperature of 21-24°C and in dry conditions (RH<5%). No seed aerosols were injected. The experiments were conducted on the five PAHs described in Table A1.1. Concentrations of PAH ranging

from 4.46 to 41.67 ppb were used for this study; hydrocarbon to NO ratios at the beginning of the experiments varied between 0.41 and 10.99 ppbC ppb^{-1}. Experimental details are given in Table A1.2. It should be noted a range of experiment types and conditions were used purposefully with the aim of identifying a consistent way in which data from different experiments could be related. Blank experiments with irradiated zero air or irradiated zero air with a radical source were performed regularly between experiments to ensure that the chamber continued to be free from major contamination. In all cases, less than 0.1 $\mu g\ m^{-3}$ of aerosol was generated.

A1.3 Results and Discussion

An illustrative example of PAH decay and SOA formation is shown in Figure A1.1a. After OH starts to form, PAH starts to decay. However, aerosol did not start to form immediately upon initial consumption of ROG (Figure A1.1a). The required THC of the PAH needed to be consumed prior to SOA formation. Figure A1.1b shows the corresponding increase in the concentration of particles and growth of aerosol size. The largest aerosol concentration corresponded to the aerosol size range of 65 to 85 nanometers. Aerosol concentrations ranging from 14,000 to 109,000 cm^{-3} were observed in the experiments. The largest average aerosol number concentration of 56,870 ± 26,060 (1σ) was observed for naphthalene.

SOA yields. SOA yields ranged from 8 to 16% for naphthalene, 3 to 22% for 1-methylnaphthalene, 2 to 15% for 2-methylnaphthalene, 4 to 13% for acenaphthylene, and 3 to 11% for acenaphthene (Table A1.2, Figure A1.2). Most of the aerosol mass concentrations were smaller than 10 $\mu g\ m^{-3}$. Despite considerable scatter in data due to

varying experimental conditions (discussed subsequently), yield data are fit to the two-product model of equation (2) for comparative purposes and to determine a typical THC for each PAH. Values of THC for naphthalene, 1- and 2-methylnaphthalene, acenaphthylene, and acenaphthene are 3.57, 7.73, 7.58, 8.31, and 7.76 ppb, respectively. Naphthalene, with the smallest THC and the largest equilibrium partitioning coefficients, also had the largest SOA yield. Conversely, acenaphthylene had the largest THC, and 1- and 2-methylnaphthalene had the smallest partitioning coefficients.

The maximum SOA yield of 22% was observed for one of the experiments with 1-methylnaphthalene (09/06/07). On average, the SOA yields were the largest to the smallest in the following order: naphthalene (0.13 ± 0.02), 1-methylnaphthalene (0.08 ± 0.06), acenaphthylene (0.07 ± 0.04), 2-methylnaphthalene (0.06 ± 0.05), and acenaphthene (0.06 ± 0.03), respectively. The larger SOA yields for naphthalene (and therefore shorter induction periods and lower THC) can be attributed to larger concentrations of OH and larger initial ratios of the mixing ratios of hydrocarbons and NO (HC/NO) in naphthalene experiments compared with other PAHs. The smallest SOA yield (0.08) was obtained for naphthalene (07/06/07) when OH concentration was also the smallest (6.7×10^{6} molecules cm^{-3}) compared to all other naphthalene experiments, in which OH concentrations were on the order of $\sim10^{7}$ molecules cm^{-3}. The concentrations of OH played a role in variation in aerosol yields as indicated in the case of 1-methylnaphthalene with the strong correlation (R^2 = 0.90; $p<0.001$; slope = 4×10^{-8}) between OH concentrations and the aerosol yields. The gas-phase kinetics play a role in determining the concentrations of partitioning semi-volatile products and thus SOA formation (Ng et al., 2007b; Chan et al., 2007; Song et al., 2007; Warren et al., 2008).

An increase in SOA growth was not observed in any of the experiments after the PAHs were completely consumed (Figure A1.1a), indicating that SOA formation was related to first generation oxidation products or to products from very fast reactions of the first or subsequent generation products (Ng et al., 2006).

Based on the aerosol mass fraction estimated from equation (4) using the VBS approach, the SOA distributions for two naphthalene experiments are illustrated in Figure A1.3, showing the predominance of non-volatile ($C^* = 0.1\ \mu g\ m^{-3}$) products. An increase in this non-volatile product was found to shift the SOA mass to include products with increased volatilities, indicating its effect on enhancing the ability of oxidation products with increased volatility to partition into the aerosol phase (Donahue et al., 2009). A VBS analysis of PAHs other than naphthalene shows a wider distribution of condensed-phase SOA mass to products with higher volatilities compared to naphthalene, which supports the observed larger yield and smaller THC of naphthalene. The lack of functionality on the naphthalene rings may promote formation of less volatile products, potentially those of a ring-opening nature as for reactions of monoaromatics with chlorine atoms (Cai et al., 2008).

An increased HC/NO enhanced SOA formation in chamber experiments conducted for α-pinene ozonolysis (Presto et al., 2005b) and photooxidation of m-xylene (Song et al., 2005), toluene (Hurley et al., 2001), and naphthalene and methylnaphthalenes (Chan et al., 2009), especially when HC/NO was greater than 4.5 (Presto et al., 2005b). The HC/NO ratio affects reaction pathways and products, causing changes in aerosol yield (Song et al., 2005) and toxicity of the products (Sasaki et al., 1997). Because most of the experiments in this study had large NO_x concentrations, the

RO_2 + NO pathway likely dominated the RO_2 + HO_2 pathway, leading to the observed smaller aerosol yields in this study.

Presto et al. (2005a) also observed that UV light (350 nm) plays a significant role in determining aerosol yield, with a reduction of as much as 40% compared to dark experiments in aerosol yields during chamber ozonolysis experiments conducted for smaller initial mixing ratios (15-30 ppb) of α-pinene in the absence of seeds. Similarly, Warren et al. (2008) observed the reduction (by ~20%) in SOA mass concentration formed with black lights (~350 nm) compared to argon arc lamps (>400 nm) and attributed the results to differences in concentrations of OH and hydroperoxy and organic peroxy radicals. They also suggested that use of black lights decreased photolysis of secondary products, inhibiting some reactions leading to SOA formation.

Reisen and Arey (2002), based on product identifications, indicate that SOA formation from the oxidation of acenaphthene and acenaphthylene is insignificant (<1%). Grosjean (1992) estimated the aerosol yield of approximately 4 and 5% from reacted naphthalene and 2-methylnaphthalene, respectively, during a smog episode. The yield curves of naphthalene, 1-methylnaphthalene, and 2-methylnaphthalene observed in this study are compared with the yield curves from Chan et al. (2009) under high-NO_x conditions in Figure A1.4. Though SOA yield curves observed in this study are smaller than the ones observed by Chan et al. (2009), the largest SOA yields of 15 to 22% with 20 to 30% uncertainty in this study are within the range of 25-45% for high-NO_x conditions observed by Chan et al. (2009). Experiments by Chan et al. (2009) were conducted with seed aerosols and thus are not comparable directly to this study due to the "seed induction period" (Ng et al., 2007b).

Ozone. During all the chamber experiments for naphthalene and 1-methylnaphthalene, ozone concentrations were observed to be less than 20 ppb while for 2-methylnaphthalene, acenaphthylene, and acenaphthene, the concentrations increased to as much as 91 ppb in some experiments. Ozone slowly starts to form during the experiment and peaks at the end of the experiment. Peak ozone concentrations of 9 to 21 ppb were observed for the experiments conducted using the photolysis of H_2O_2 as the OH radical source. Peak ozone concentrations of 6 to 91 ppb were observed when the photolysis of HONO was used as the OH radical source.

Induction Period. Kroll et al. (2007) reported the reduction in SOA yields in the absence of seed aerosol. Loss of semivolatiles is larger when seed aerosols are absent, leading to the decrease in aerosol yield in the current observation. In addition, the chamber used in this study (9 m^3) was smaller than that used by Chan et al. (2009) (28 m^3), enhancing the probability of material depositing to the wall in the current study. All of these factors play an important role in quantifying SOA formation in chambers, and the differences between the experimental conditions caused the variation in SOA yields. The decrease in SOA yield also can be caused by the formation of volatile products from the reaction of first or second-generation products by photolysis or with OH, as exemplified by the fact that the peak of aerosol mass concentration did not always occur after the complete consumption of all the PAHs (Ng et al., 2007a).

The experiments were performed without seed aerosols. The period of time between the start of the experiment and the time at which aerosol had grown to a detectable size is termed the induction period (Table A1.2). On average, the induction period was ~18 minutes, with the shortest average induction period of ~15 minutes for naphthalene and the longest of ~21 minutes for 2-methylnaphthalene. The maximum aerosol concentration and yield decreased with increasing induction time (Figure A1.5), indicating that the time required to achieve saturation affects the total SOA mass formation.

Experiments conducted in the absence of seed aerosols have longer lag-times for aerosol growth, indicating the dependence of SOA yields on the timing of the onset of gas-particle partitioning (Kroll et al., 2007). Naphthalene, with the largest average aerosol yields observed in this study, also has the shortest average induction period (~15 min) and the smallest THC (3.57 ppb) implying the possible effect of induction period on SOA yields. Sauret-Szczepanski and Lane (2004) observed the significant partitioning of oxidation products from acenaphthene into the particulate phase only after 23 minutes of irradiation. The effects of seed aerosols are more pronounced with smaller aerosol loadings because smaller aerosol surface area enhances the loss to the chamber walls. With a smaller aerosol loading of 5 $\mu g\ m^{-3}$, Kroll et al. (2007) observed two-times larger aerosol yields in seeded experiments compared to non-seeded experiments. This also may explain the smaller aerosol yields in the present study because more than half of the experiments had aerosol loadings smaller than 5 $\mu g\ m^{-3}$. Pathak et al. (2007) also observed smaller SOA yields in the absence of seed aerosols and reported the largest sensitivity when both HC(α-pinene) and oxidant (O_3) concentrations were small.

Because SOA started to form in the current study only after the complete consumption of NO, similar to other work (Song et al., 2005; Ng et al., 2007b), the potential effect of NO_x on induction period is also plausible. The OH and light sources also may play an important role in initiating aerosol production, especially for experiments performed without seed aerosols.

Chemistry of PAH Products. Though the SOA yields have been quantified previously for naphthalene and 1- and 2-methylnaphthalene (Chan et al., 2009), product chemistry and kinetic parameters of these products have been studied for the five PAHs here (Atkinson and Arey, 1994; Sasaki et al., 1997; Reisen and Arey, 2002; Atkinson et al., 1987; Zielinska et al., 1989; Bunce et al., 1997; Wang et al., 2007). A few studies on aerosol products from oxidation of naphthalene, methylnaphthalenes, and acenaphthene also are available (Sauret-Szczepanski and Lane, 2004; Chan et al., 2009; Lee and Lane, 2009; Kautzman et al., 2010; Dekermenjian et al., 1999; Mihele et al., 2002).

The major identified aerosol products from the oxidation of naphthalene by OH were naphthols, nitronaphthalenes, 2-formylcinnamaldehyde, 2-formylcinnamic acid, diones, nitronaphthols, naphthoquinones, phthalic acid, and hydroxy benzoic acids (Lee and Lane, 2009; Kautzman et al., 2010, Mihele et al., 2002). Using the vapor pressures of 1- and 2-nitronaphthalenes (INCHEM, 2009) and 1,2- and 1,4-naphthoquinones (Lee and Lane, 2009; Jakober et al., 2007), $K_{om,i}$ values on the order of $\sim 10^{-5}$ for 1,2-naphthoquinone and $\sim 10^{-4}$ for 1- and 2-nitronaphthalene and 1,4-naphthoquinone were predicted, indicating that 1,4-naphthoquinone and nitronaphthalenes are more likely to be present in the aerosol phase, as reported by Lee and Lane (2009). For naphthalene in the present study, a $K_{om,1}$ on the order of unity and a $K_{om,2}$ on the order of $\sim 10^{-3}$ were

determined; these are orders of magnitude larger than the ones predicted using the vapor pressures, indicating that lower volatility products must constitute the bulk of the mass, a result supported by the VBS analysis.

Environmental Implications. This study affects estimates of the contribution of PAHs to SOA formation by providing the first knowledge on SOA yields from acenaphthylene and acenaphthene. This study also confirms that *Y* depends on not only organic aerosol mass and reacted hydrocarbon concentrations, but also on multiple factors such as oxidant concentrations, HC/NO ratio, UV light, chamber size, and seeds.

To estimate the importance of SOA from gas-phase oxidation of these PAHs, their contribution to SOA production from emissions from mobile sources in Houston was estimated. The number of daily miles driven by motor vehicles in Houston was obtained from the projections for 2009 (TTI, 2005). It is assumed that 8% of the miles result from vehicles with diesel engines and 92% from vehicles with gasoline-engines equipped with catalytic converters based on 24-hour vehicle miles traveled mix data in Houston (TTI, 2009). Because of this important assumption, much larger SOA production was estimated from gasoline engines compared to diesel engines. For the purposes of selecting an appropriate SOA yield, total organic aerosol mass loadings of 5 $\mu g\ m^{-3}$ in Houston were assumed (Buzcu et al., 2006). Only the reaction of PAHs with OH radical is considered for the estimation of SOA. Emission factors ($\mu g\ mile^{-1}$) for the respective PAHs were obtained from Schauer et al. (1999, 2002), and SOA production was calculated by (Chan et al., 2009):

$$\Delta M_0 = PAH_e\ (1-e^{-k[OH]t})\ Y \qquad (6)$$

where PAH_e is the emitted mass of the respective PAH in μg day^{-1}, k is the second-order rate constant for the reaction between PAH and OH, [OH] is the hydroxyl radical concentration (assumed to be $2x10^6$ molecules cm^{-3}), and t is time (1 day). This method ignores any nighttime chemistry and considers only the reaction with OH radicals using the rate constants from Table A1.1.

A range of 37 to 162 kg day^{-1} of SOA production from the PAHs was estimated (Table A1.3) based on the yields from this study and that of Chan et al. (2009). Based on fractional aerosol coefficients of VOCs, approximately 268 kg day^{-1} of SOA formation for mobile sources was estimated previously in the Houston-Galveston area without including PAHs (Dechapanya et al., 2004). The values found in the current work are a significant fraction of the previous total, indicating that PAH oxidation could be an important source of SOA in Houston.

A1.4 References

Atkinson, R., Arey, J., Zielinska, B., and Aschmann, S. Kinetics and products of the gas-phase reactions of OH radicals and N_2O_5 with naphthalene and biphenyl. Environ. Sci. Technol. 21, 1014-1022, 1987.

Arey, J., Atkinson, R., Zielinska, B., and McElroy, P.A. Diurnal concentrations of volatile polycylic aromatic hydrocarbons and nitroarenes during a photochemical air pollution episode in Glenora, California. Environ. Sci. Technol. 23, 321-327, 1989.

Atkinson, R. and Arey, J. 1994. Atmospheric chemistry of gas-phase polycyclic aromatic hydrocarbons: formation of atmospheric mutagens. Environ. Heal. Persp. 102 (Suppl 4), 117-126, 1994.

Bowman, F.M., Odum, J.R., Seinfeld, J.H., and Pandis, S.N. Mathematical model for gas-particle partitioning of secondary organic aerosols. Atmos. Environ. 31, 3921-3931, 1997.

Bunce, N.J., Liu, L., and Zhu, J. Reaction of naphthalene and its derivatives with hydroxyl radicals in the gas phase. Environ. Sci. Technol. 31, 2252-2259, 1997.

Buzcu, B.Z., Yue, Z.W., Fraser, M.P., Nopmongcol, U., and Allen, D.T. Secondary particle formation and evidence of heterogenous chemistry during a wood smoke episode in Texas. J. Geophys. Res. 111, D10S13, DOI:10.1029/2005JD006143, 2006.

Cai, X. and Griffin, R.J. Secondary aerosol formation from the oxidation of biogenic hydrcocarbons by chlorine atoms. J. Geophys. Res. 111, D14206; DOI:1029/2005JD006857, 2006.

Cai, X., Ziemba, L.D., and Griffin, R.J. Secondary aerosol formation from the oxidation of toluene by chlorine atoms. Atmos. Environ. 42, 7348-7359, 2008.

Carter, W.P.L., Cocker III, D.R., Fitz, D.R., Malkina, I.L., Bumiller, K., Sauer, C.G., Pisano, J.T., Bufalino, C., and Song, C. Atmos. Environ. 39, 7768-7788, 2005.

Chan, A.W.H., Kautzman, K.E., Chhabra, P.S., Surratt, J.D., Chan, M.N., Crounse, J.D., Kurten, A., Wennberg, P.O., Flagan, R.C., and Seinfeld, J.H. Secondary organic aerosol formation from photooxidation of naphthalene and alkylnaphthalenes:

implications for oxidation of intermediate volatility organic compounds (IVOCs). Atmos. Chem. Phys. 9, 3049-3060, 2009.

Chan, A.W.H., Kroll, J.H., Ng, N.L., and Seinfeld, J.H. Kinetic modeling of secondary organic aerosol formation: effects of particle- and gas-phase reactions of semivolatile products. Atmos. Chem. Phys. 7, 4135-4147, 2007.

Dechapanya, W., Russell, M., and Allen, D.T. Estimates of anthropogenic secondary organic aerosol formation in Houston, Texas. Aer. Sci. Technol. 38, 156-166, 2004.

Dekermenjian, M., Allen, D., Atkinson, R., and Arey, J. FTIR analysis of aerosol formed in the photooxidation of naphthalene. Aer. Sci. Technol. 30, 273-279, 1999.

Donahue, N.M., Robinson, A.L., and Pandis, S.N. Atmospheric organic particulate matter: from smoke to secondary organic aerosol. Atmos. Environ. 43, 94-106, 2009.

Donahue, N.M., Robinson, A.L., Stanier, C.O., and Pandis, S.N. Coupled partitioning, dilution, and chemical aging of semivolatile organics. Environ. Sci. Technol. 40, 2635-2643, 2006.

Goldstein, A.H. and Galbally, I.E. Known and unexplored organic constituents in the earth's atmosphere. Environ. Sci. Technol. 41, 1514-1521, 2007.

Grosjean, D. In situ organic aerosol formation during a smog episode-estimated production and chemical functionality. Atmos. Environ. 26A, 953-963, 1992.

Hallquist, M. et al. The formation, properties and impact of secondary organic aerosol: current and emerging issues. Atmos. Chem. Phys. 9, 5155-5235, 2009.

Hurley, M.D., Sokolov, O., Wallington, T.J., Takekawa, H., Karasawa, M., Klotz, B., Barnes, I., and Becker, K.H. Organic aerosol formation during the atmospheric degradation of toluene. Environ. Sci. Technol. 35, 1358-1366, 2001.

INCHEM. Selected nitro- and nitro-oxy-polycyclic aromatic hydrocarbons. Environmental Health Criteria 229. International Program on Chemical Safety, 2009.

Jakober, C.A., Riddle, S.G., Robert, M.A., Destaillats, H., Charles, M.J., Green, P.G., and Kleeman, M.J. Quinone emissions from gasoline and diesel motor vehicles. Environ. Sci. Technol. 41, 4548-4554, 2007.

Jiménez E., Gilles, M.K., and Ravishankara, A.R. Kinetics of the reactions of the hydroxyl radical with CH_3OH and C_2H_5OH between 235 and 360 K. J. Photochem. Phobiol. A 157, 237-245, 2003.

Kanakidou, M. et al. Organic aerosol and global climate modeling: a review. Atmos. Chem. Phys. 5, 1053-1123, 2005.

Kautzman, K.E., Surratt, J.D., Chan, M.N., Chan, A.W.H., Hersey, S.P., Chhabra, P.S., Dalleska, N.F., Wennberg, P.O., Flagan, R.C., and Seinfeld, J.H. Chemical composition of gas- and aerosol-phase products from the photooxidation of naphthalene. J. Phys. Chem. A. 114, 913-934, 2010.

Kroll, J.H., Chan, A.W.H., Nga, N.L., Flagan, R.C., and Seinfeld, J.H. Reactions of semivolatile organics and their effects on secondary organic aerosol formation. Environ. Sci. Technol. 41, 3545-3550, 2007.

Lee, J.Y. and Lane, D.A. Unique products from the reaction of naphthalene with the hydroxyl radical. Atmos. Environ. 43, 4886-4893, 2009.

McMurry, P.H. and Grosjean, D. Gas and aerosol wall losses in Teflon film smog chambers. Environ. Sci. Technol. 19, 1176-1182, 1985.

Mihele, C.M., Wiebe, H.A., and Lane, D.A. Particle formation and gas/particle partition measurements of the products of naphthalene-OH radical reaction in a smog chamber. Pol. Arom. Comp. 22, 729-736, 2002.

Ng, N.L., Chhabra, P.S., Chan, A.W.H., Surratt, J.D., Kroll, J.H., Kwan, A.J., McCabe, D.C., Wennberg, P.O., Sorooshian, A., Murphy, S.M., Dalleska, N.F., Flagan, R.C., and Seinfeld, J.H. Effect of NO_x level on secondary organic aerosol (SOA) formation from the photooxidation of terpenes. Atmos. Chem. Phys. 7, 5159-5174, 2007a.

Ng, N.L., Kroll, J.H., Chan, A.W.H., Chhabra, P.S., Flagan, R.C., and Seinfeld, J.H. Secondary organic aerosol formation from m-xylene, toluene, and benzene. Atmos. Chem. Phys. 7, 3909-3922, 2007b.

Ng, N.L., Kroll, J.H., Keywood, M.D., Bahreini, R., Varutbangkul, V., Flagan, R.C., and Seinfeld, J.H. Contributions of first- versus second-generation products to secondary organic aerosols formed in the oxidation of biogenic hydrocarbons. Environ. Sci. Technol. 40, 2283-2297, 2006.

Nikolaou, K., Masclet, P., and Mouvier, G. Sources and chemical reactivity of polynuclear aromatic hydrocarbons in the atmosphere – a critical review. Sci. Tot. Environ. 32, 103-132, 1984.

Odum, J.R., Hoffmann, T., Bowman, F., Collins, D., Flagan, R.C., and Seinfeld, J.H. Gas/particle partitioning and secondary organic aerosol yields. Environ. Sci. Technol. 30, 2580-2585, 1996.

Pandis, S.N., Harley, R.A., Cass, G.R., and Seinfeld, J.H. Secondary organic aerosol formation and transport. Atmos. Environ. 13, 2269-2282, 1992.

Pankow, J.F. An absorption model of gas/particle partitioning of organic compounds in the atmosphere. Atmos. Environ. 28, 185-188, 1994.

Pathak, R.K., Stanier, C.O., Donahue, N.M., and Pandis, S.N. Ozonolysis of α-pinene at atmospherically relevant concentrations: Temperature dependence of aerosol mass fractions (yields). J. Geophys. Res. 112, DO3201, DOI:10.1029/2006JD007436, 2007.

Presto, A.A., Huff Hartz, K.E., and Donahue, N.M. Secondary organic aerosol production from terpene ozonolysis. 1. Effect of UV radiation. Environ. Sci. Technol.39, 7036-7045, 2005a.

Presto, A.A., Huff Hartz, K.E., and Donahue, N.M. Secondary organic aerosol production from terpene ozonolysis. 2. Effect of NO concentration. Environ. Sci. Technol. 39, 7046-7054, 2005b.

Ravindra, K., Sokhi, R., and Grieken, R.V. Review. Atmospheric polycyclic aromatic hydrocarbons: Source attribution, emission factors and regulation. Atmos. Environ. 42, 2895-2921, 2008.

Reisen, F. and Arey, J. Reactions of hydroxyl radicals and ozone with acenaphthene and acenaphthylene. Environ. Sci. Technol. 36, 4302-4311, 2002.

Reisen, F. and Arey, J. Atmospheric reactions influence seasonal PAH and nitro-PAH concentrations in the Los Angeles basin. Environ. Sci. Technol. 39, 64-73, 2005.

Sasaki, J., Aschmann, S.M., Kwok, E.S.C., Atkinson, R., and Arey, J. Products of the gas-phase OH and NO_3 radical-initiated reactions of naphthalene. Environ. Sci. Technol. 31, 3173-3179, 1997.

Sauret-Szczepanski, N. and Lane, D.A. Smog chamber study of acenaphthene: gas/particle partition measurements of the products formed by reaction with the OH radical. Poly. Arom. Comp. 24, 161-172, 2004.

Schauer, J.J., Kleeman, M.J., Cass, G.R., and Simoneit, B.R.T. Measurements of emissions from air pollution sources. 2. C_1 through C_{30} organic compounds from medium duty diesel trucks. Environ. Sci. Technol. 33, 1578-1587, 1999.

Schauer, J.J., Kleeman, M.J., Cass, G.R., and Simoneit, B.R.T. Measurements of emissions from air pollution sources. 5. C_1-C_{32} organic compounds from gasoline-powered motor vehicles. Environ. Sci. Technol. 36, 1169-1180, 2002.

Song, C., Na, K., and Cocker, D. Impact of the hydrocarbon to NO_x ratio on secondary organic aerosol formation. Environ Sci. Technol. 39, 3143-3149, 2005.

Song, C., Na, K., Warren, B., Malloy, Q., and Cocker, D.R. Secondary organic aerosol formation from m-xylene in the absence of NO_x. Environ. Sci. Technol. 41, 7409-7416, 2007.

Stanier, C.O., Donahue, N.M., and Pandis, S.N. Parametrization of secondary organic aerosol mass fractions from smog chamber data. Atmos. Environ. 42, 2276-2299, 2008.

TTI. 2002, 2009, and 2012 emissions inventories for the Houston/Galveston eight-hour nonattainment counties. Texas Transportation Institute, The Texas A& M University System, College Station, Texas, 2005.

TTI. 2008 on-road mobile source statewide air toxics annual emissions inventories. Texas Transportation Institute, The Texas A& M University System, College Station, Texas, 2009.

Wang, L., Atkinson, R., and Arey, J. Dicarbonyl products of the OH radical-initiated reactions of naphthalene and the C_1-and C_2-alkylnaphthalenes. Environ. Sci. Technol. 41, 2803-2810, 2007.

Warren, B., Song, C., and Cocker, D.R. III. Light intensity and light source influence on secondary organic aerosol formation for the m-xylene/NO_x photooxidation system. Environ. Sci. Technol. 42, 5461-5466, 2008.

Zielinska, B., Arey, J., Atkinson, R., and McElroy, P.A. Formation of methylnitronaphthalenes from the gas-phase reactions of 1- and 2-methylnaphthalene with OH radicals and N_2O_5 and their occurrence in ambient air. Environ. Sci. Technol. 23, 723-729, 1989.

Zhang, Q. et al. Ubiquity and dominance of oxygenated species in organic aerosols in anthropogenically-influenced Northern Hemisphere midlatitudes. Geophys. Res. Lett. 34, L13801, doi:10.1029/2007GL029979, 2007.

Table A1.1. Description of the five PAH compounds used in this study (Atkinson and Arey, 1994).

Name of PAH	Structure	Mol. For.	Mol.wt. ($g\ mol^{-1}$)	Rate constants ($cm^3\ molec^{-1}\ s^{-1}$)		
				k_{OH}	k_{NO3}	k_{O3}
Naphthalene	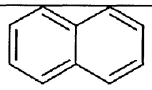	$C_{10}H_8$	128.17	$2.2*10^{-11}$	$3.6*10^{-28}$ [NO_2]	$<2*10^{-19}$
1-Methylnaphthalene	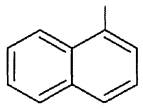	$C_{11}H_{10}$	142.20	$5.3*10^{-11}$	$7.7*10^{-28}$ [NO_2]	$<1.3*10^{-19}$
2-Methylnaphthalene	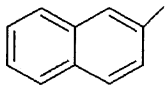	$C_{11}H_{10}$	142.20	$5.2*10^{-11}$	$1.08*10^{-27}$ [NO_2]	$<4*10^{-19}$
Acenaphthylene	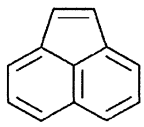	$C_{12}H_8$	152.19	$1.1*10^{-10}$	$5.5*10^{-12}$	$5.5*10^{-16}$
Acenaphthene	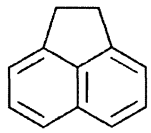	$C_{12}H_{10}$	154.21	$1.0*10^{-10}$	$4.6*10^{-13}$+ $1.7*10^{-27}$ [NO_2]	$<5*10^{-19}$

Table A1.2. Experimental information, initial conditions, and output data for SOA from PAHs in this study.

Date	Run[a,b]	ΔROG ($\mu g\ m^{-3}$)	ΔM ($\mu g\ m^{-3}$)	Y	HC/NO ($ppbC\ ppb^{-1}$)	Induction Time (min)	[OH][c] ($molecules\ cm^{-3}$)
06/26/07	1-NAP	64.95	8.07	0.12	4.77	d 1.03×10^{7}	
06/29/07	2-NAP	59.03	8.58	0.15	8.66	d 1.37×10^{7}	
07/02/07	3-NAP	35.07	5.59	0.16	6.08	16	2.74×10^{7}
07/04/07	4-NAP	88.59	10.15	0.11	3.76	13	1.23×10^{7}
07/06/07	5-NAP	103.79	8.74	0.08	5.08	18	6.70×10^{6}
07/09/07	6-NAP	40.31	4.78	0.12	10.99	13	3.35×10^{7}
07/11/07	7-NAP	28.41	3.74	0.13	7.74	15	3.14×10^{7}
07/13/07	8-NAP	59.23	8.84	0.15	5.65	d 1.25×10^{7}	
07/16/07	9-NAP	138.97	18.03	0.13	6.80	d 1.23×10^{7}	
08/20/07	1-MEN1	31.87	1.77	0.06	2.54	d 3.77×10^{6}	
08/22/07	2-MEN1	27.10	3.44	0.13	4.66	14	4.47×10^{6}
08/24/07	3-MEN1	86.08	3.52	0.04	5.04	27	2.21×10^{6}
08/26/07	4-MEN1	80.21	4.06	0.05	4.74	24	2.26×10^{6}
08/28/07	5-MEN1	94.92	2.61	0.03	3.90	26	3.30×10^{6}
08/30/07	6-MEN1	118.59	5.20	0.04	5.34	23	2.22×10^{6}
09/01/07	7-MEN1	131.51	6.07	0.05	3.32	22	2.12×10^{6}
09/04/07	8-MEN1	242.37	22.21	0.09	5.27	11	3.68×10^{6}
09/06/07	9-MEN1	59.73	13.05	0.22	2.35	10	6.71×10^{6}
09/10/07	1-MEN2	69.91	1.08	0.02	2.88	24	5.05×10^{6}
09/12/07	2-MEN2	110.86	8.35	0.08	NA	17	6.54×10^{6}
04/23/08	3-MEN2	30.89	4.55	0.15	0.57	15	3.48×10^{6}
04/25/08	4-MEN2	54.73	1.51	0.03	0.99	20	4.36×10^{6}
04/27/08	5-MEN2	59.44	3.54	0.06	0.70	24	3.40×10^{6}
04/29/08	6-MEN2	79.80	1.95	0.02	0.93	27	4.59×10^{6}
04/07/08	1-ACNY	77.93	4.08	0.05	1.55	19	2.89×10^{6}
04/09/08	2-ACNY	27.76	1.25	0.04	0.41	d 2.94×10^{6}	
04/11/08	3-ACNY	43.63	1.79	0.04	0.79	d 3.75×10^{6}	

Date	Run[a,b]	ΔROG ($\mu g\ m^{-3}$)	ΔM ($\mu g\ m^{-3}$)	Y	HC/NO (ppbC ppb^{-1})	Induction Time (min)	[OH][c] (molecules cm^{-3})
04/13/08	4-ACNY	93.31	8.06	0.09	0.83	17	2.04×10^{6}
04/15/08	5-ACNY	114.16	14.99	0.13	1.96	14	3.88×10^{6}
04/17/08	6-ACNY	129.91	6.22	0.05	2.43	d 5.18×10^{6}	
04/19/08	7-ACNY	169.06	8.91	0.05	2.88	16	2.95×10^{6}
04/21/08	8-ACNY	72.33	8.98	0.12	1.17	15	2.91×10^{6}
05/27/08	1-ACNE	95.74	7.06	0.07	1.77	13	2.11×10^{6}
05/29/08	2-ACNE	36.46	1.43	0.04	0.64	13	3.13×10^{6}
05/31/08	3-ACNE	67.99	4.05	0.06	1.23	15	2.86×10^{6}
06/02/08	4-ACNE	93.28	2.63	0.03	1.89	13	3.08×10^{6}
06/04/08	5-ACNE	65.15	7.40	0.11	1.22	14	3.82×10^{6}
06/06/08	6-ACNE	50.96	4.60	0.09	0.94	16	1.85×10^{6}
06/08/08	7-ACNE	55.38	3.23	0.06	1.33	18	e
06/10/08	8-ACNE	86.22	4.77	0.06	1.09	20	2.39×10^{6}
06/12/08	9-ACNE	110.75	4.25	0.04	1.31	20	2.01×10^{6}
06/16/08	10-ACNE	129.11	6.20	0.05	0.99	21	1.37×10^{6}

[a]NAP: naphthalene; MEN1: 1-methylnaphthalene; MEN2: 2-methylnaphthalene; ACNY: acenaphthylene; ACNE: acenaphthalene

[b]All experiments for naphthalene and 1-methylnaphthalene, and two experiments for 2-methylnaphthalne (1-MEN2 and 2-MEN2) were performed with H_2O_2 as OH source and germicidal lamps (254-nm) as the light source. Remaining experiments were performed with HONO as OH source and black lights (365-nm) as the light source. For all experiments with naphthalene, 1-methylnaphthalene, 2-methylnaphthalene, and acenaphthylene the SMPS described was used; for acenaphthene, a laboratory-assembled system with an in-house written Labview code was used.

[c]Average OH concentration in molecules cm^{-3} derived from GC-FID data and rate constants in Table S1.

[d]Small concentration of aerosol ($<0.1\mu g\ m^{-3}$) present in the background.

[e]GC-FID decay data unavailable.

Table A1.3. Estimated SOA production from PAHs contributed by diesel- or gasoline-powered vehicles in Houston, Texas. Emissions ($\mu g\ km^{-1}$) for the PAHs from Schauer (1999, 2002) were used to calculate the SOA production based on approximately 1.67×10^{8} kilometers driven on the road (TTI, 2005, 2009).

PAHs	Emissions, $\mu g\ km^{-1}$		This study			Chan et al.(2009)		
	Diesel	Gasoline	Yields	ΔM_0, kg day^{-1}		Yields	ΔM_0, kg day^{-1}	
				Diesel	Gasoline		Diesel	Gasoline
NAP	617	1000	0.11	0.89	16.51	0.18	21.90	35.50
1-MEN	378	500	0.07	0.35	5.38	0.18	13.84	18.30
2-MEN	611	1000	0.08	0.65	12.30	0.22	27.31	44.70
ACNY	19.3	37	0.06	0.02	0.34			
ACNE	70.1	6.55	0.07	0.07	0.07			
				1.97	**34.61**		**63.05**	**98.50**

NAP: naphthalene; MEN1: 1-methylnaphthalene; MEN2: 2-methylnaphthalene; ACNY: acenaphthylene; ACNE: acenaphthalene

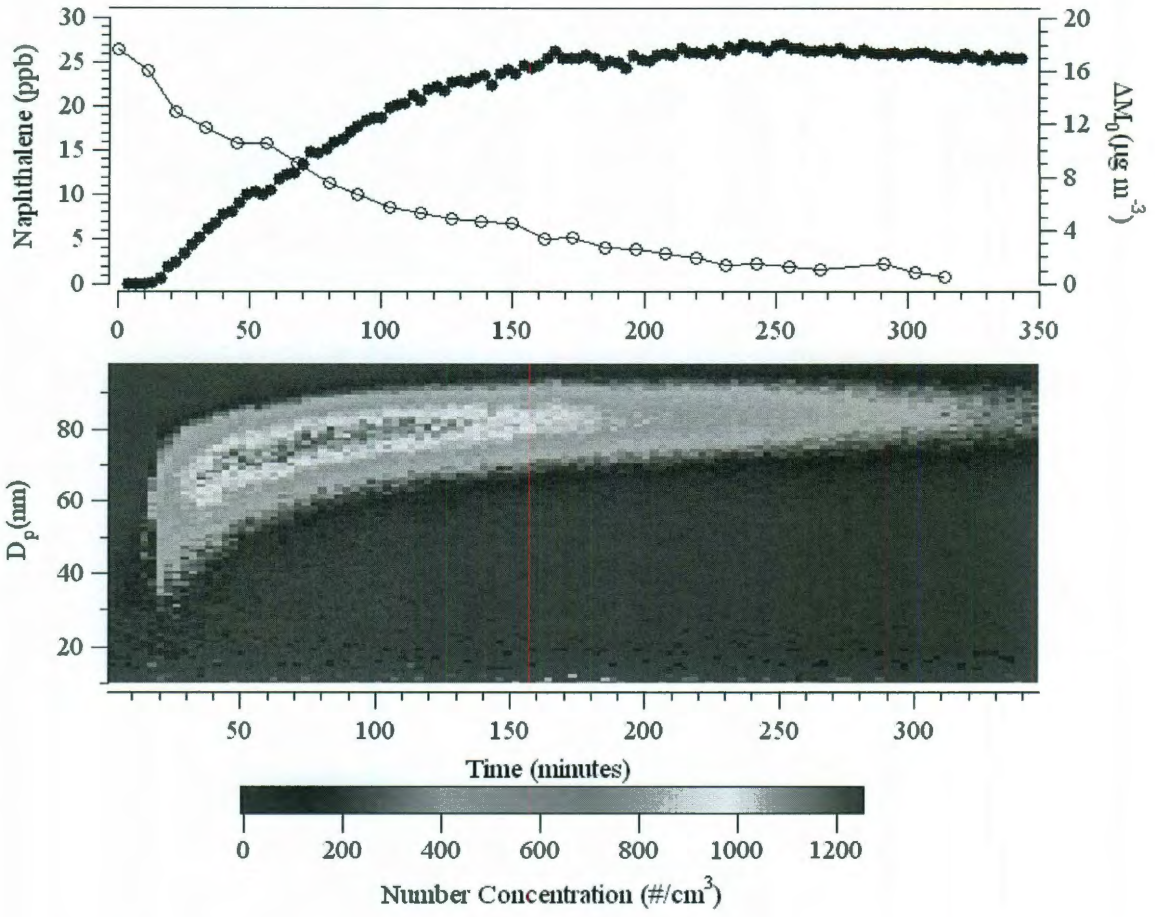

Figure A1.1. a.) (upper panel) Time evolution of SOA formation and naphthalene decay (07/16/07) in a typical experiment. The dark circles indicate the increase in SOA mass and the open circles indicate the depletion of naphthalene. SOA data are wall corrected; b.) (lower panel) An increase in particle concentration and shifting of particle diameter with respect to time in a chamber experiment with naphthalene (07/16/07).

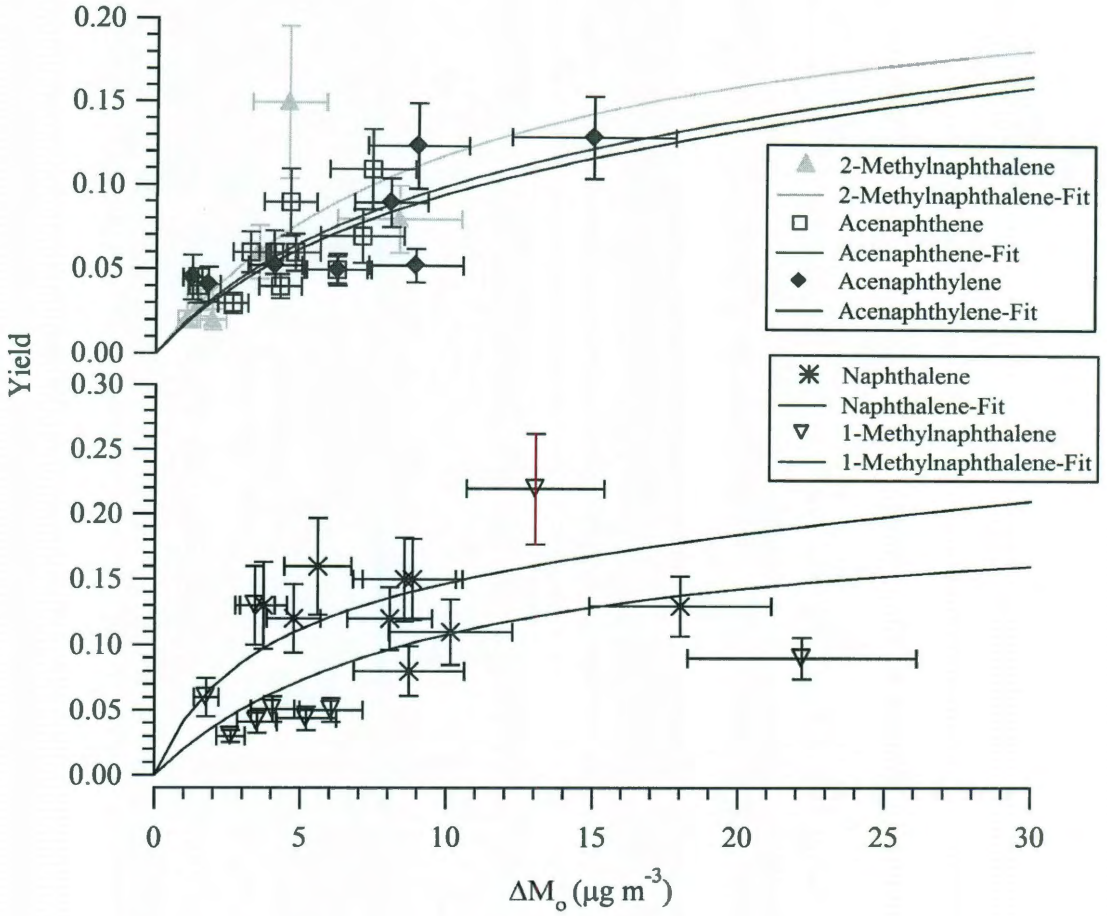

Figure A1.2. Aerosol yields for the five PAHs studied. Lines are the yield curves generated using equation (2) with the following values of α_1, α_2, $K_{om,1}$, and $K_{om,2}$ for naphthalene (0.167, 0.308, 0.852, 0.003), 1-methylnaphthalene (0.206, 0.107, 0.193, 0.001), 2-methylnaphthalene (0.247, 0.092, 0.193, 0.001), acenaphthylene (0.136, 0.128, 0.759, 0.003), and acenaphthene (0.145, 0.128, 0.758, 0.003).

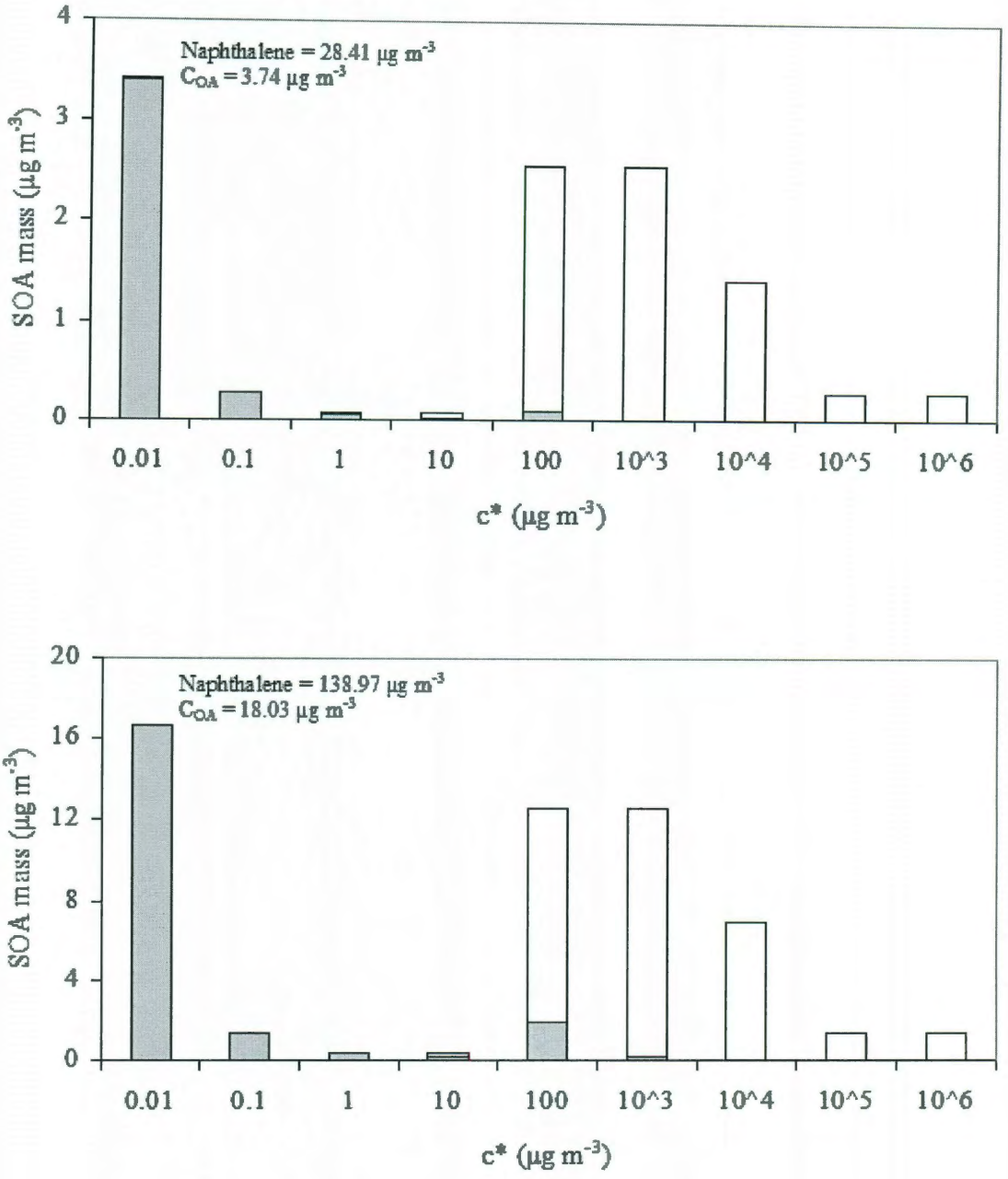

Figure A1.3. SOA mass distribution in different sets of bins based on the VBS of effective saturation concentration (c*). A shaded portion in the bar represents the condensed-phase and an unshaded portion represents the vapor phase. Larger naphthalene concentration with the larger SOA loadings shifts the partitioning to the right of the basis set.

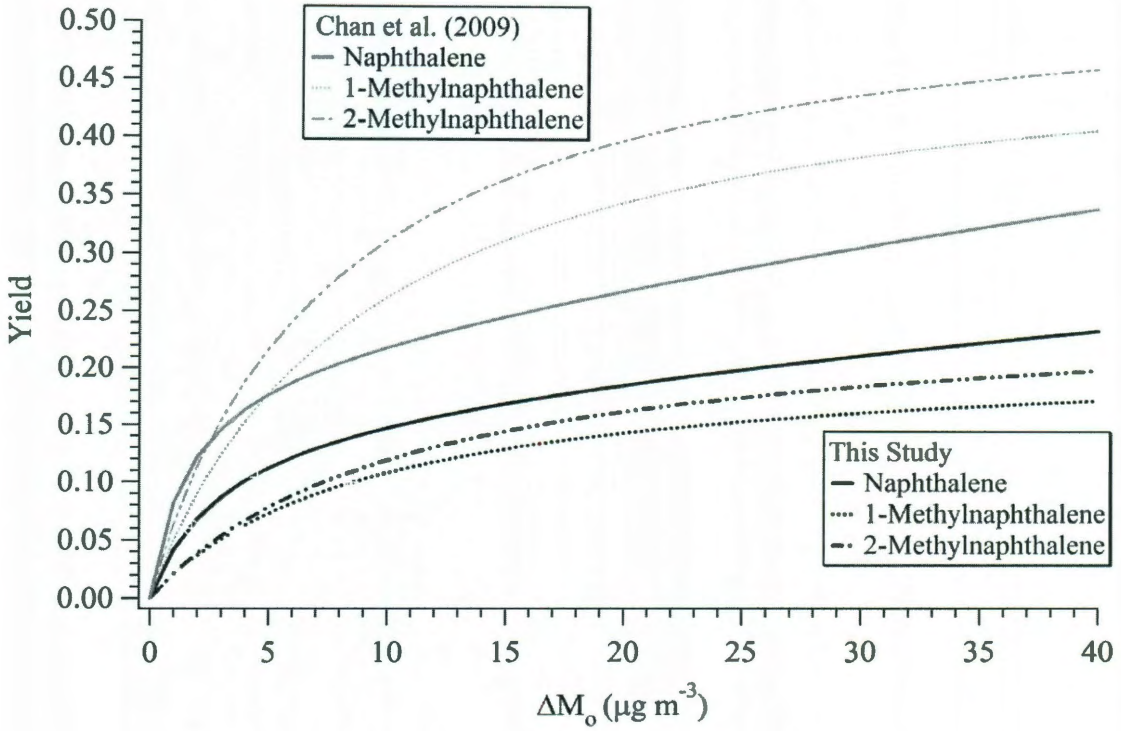

Figure A1.4. Comparison of observed SOA yield curves of naphthalene, 1-methylnaphthalene, and 2-methylnaphthalene from this study with those from Chan et al. (2009).

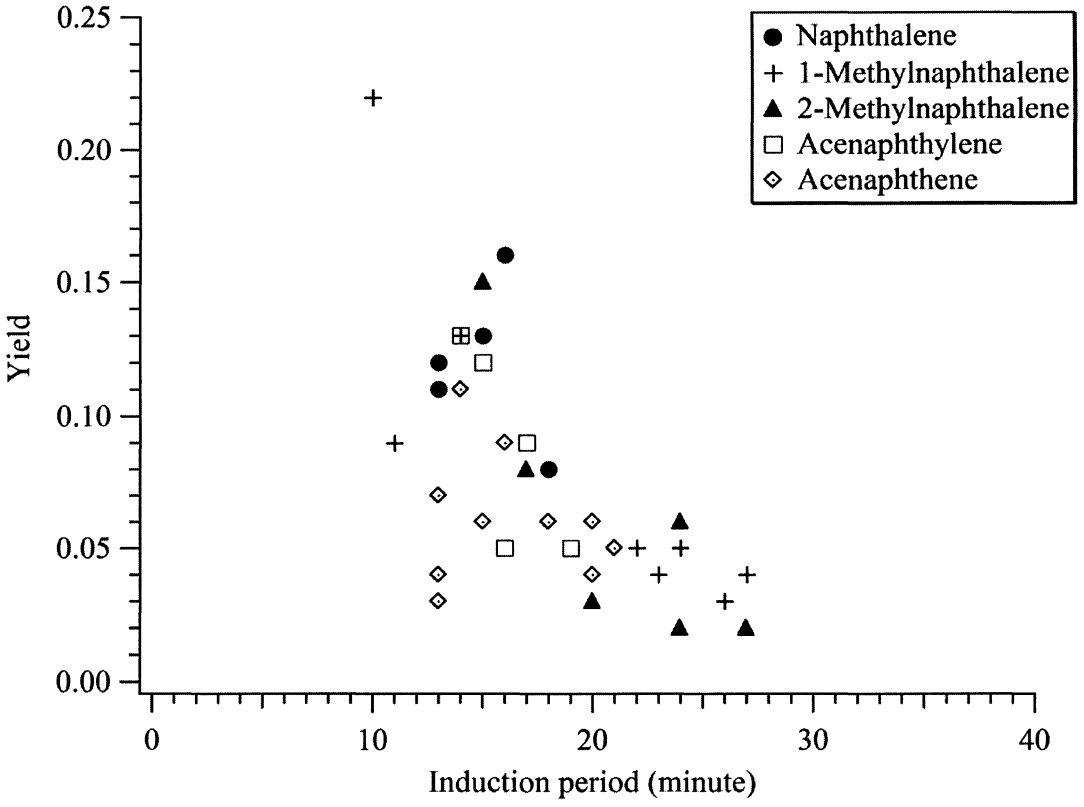

Figure A1.5. Observed SOA yields as a function of induction period for the five PAHs studied.

CHAPTER A2

Observation of Decreased Net Oxidation of Gaseous Elemental Mercury In the Presence of Secondary Organic Aerosol Formation in the Dark

Reference: Rutter, A.P., Shakya, K.M., Lehr, R., Schauer, J.J., and Griffin, R.J. Submitted to *Atmos. Environ.* 2011.

Abstract

The net oxidation of gaseous elemental mercury (GEM; $Hg^0_{(g)}$) was measured in a 9-m^3 Teflon chamber using a reaction mixture which modeled the chemistry that occurs when volatile organic compounds are oxidized in the troposphere by ozone and hydroxyl radicals to form secondary organic aerosol (SOA). Comparisons made between the net oxidation of GEM observed in the model reaction system and published gas-phase studies revealed a decrease in net oxidation during SOA formation with an overall final condition of net zero change. The reactants used in the model reaction system were propene, isoprene, α-pinene, and toluene, which were mixed with ozone in the dark to produce a matrix containing hydrogen oxide species, organic radicals, and SOA. The losses of GEM in the first 30 minutes after mixing compared well to losses seen in experiments using matricies of GEM-ozone and GEM-ozone-propene. However, after this point, GEM losses decreased considerably in the SOA case, constituting a shortfall between GEM measurements and numerically modeled oxidative losses predicted from ozone and secondary hydroxyl radicals. The shortfall was interpreted to be due the inhibition of the reaction or the reduction of oxidation products by species related to the SOA formation. Recent modeling studies of mercury atmospheric cycling have found that use of

laboratory-based GEM-ozone reaction rate coefficients caused overestimation of GEM oxidation, while theoretical studies cast doubt over the viability of the GEM-ozone oxidation reaction in the real atmosphere. The results presented here suggest that the reaction is viable in both the absence and the presence of pre-existing aerosol particles, but that a reduction or inhibition reaction does occur in the real atmosphere in the gas-phase and/or on the surfaces of dry aerosol particles. Further investigation of these mechanisms is needed to determine their prevalence and to determine if they are relevant for the halogen reaction pathways which are currently believed to dictate the global lifetime of GEM.

A2.1 Introduction

Gaseous elemental mercury (GEM, $Hg^0_{(g)}$) is the longest-lived atmospheric mercury species (Lin et al., 2006) typically constituting the majority of the total mercury mass in most locations. Oxidation of GEM to Hg(II) followed by dry and wet deposition are the main pathways by which mercury enters surface waters, leading to the bioaccumulation of methylmercury in freshwater and marine fish. Methylmercury in fish continues to be a public health concern due to its potential to impair prenatal and neonatal neurological development, and recent epidemiological studies suggest that fish methylmercury consumption in senior adults can increase the risk of fatal heart attacks and subclinical neurological symptoms (Guallar et al., 2002; Virtanen et al., 2005; Knobeloch et al., 2006; Axelrad et al., 2007; Rice et al., 2010). Over land direct dry deposition of GEM to vegetation is probably the more important removal pathway particularly where point source impacts of Hg(II) are low (Rutter et al., 2011). However,

most of the GEM deposited to leaves will not be transferred to surface water bodies, and therefore does not generate as much concern over human health.

Current understanding of GEM oxidation in the atmosphere centers around gas-phase oxidation reactions with halogens, ozone and hydroxyl radical (OH). Reaction rate coefficients for these reactions were measured experimentally using small (<5L) reaction vessels, with a more recent study using a 17-m^3 smog chamber (Hall, 1995; Sommar et al., 2001; Ariya et al., 2002; Ariya and Ryzhkov, 2003; Raofie and Ariya, 2003; Pal and Ariya, 2004a;b; Sumner et al., 2005; Ariya et al., 2008; Raofie et al., 2008; Snider et al., 2008). The exact reaction mechanisms of oxidation by these species remain poorly understood, although theoretical modeling studies have established that a gas-phase only reaction between GEM and ozone is only thermodynamically favorable via complex intermediate species and short chain oligomers of $(HgO)_n$. Furthermore, GEM oxidation has been shown theoretically and empirically to be enhanced by interactions with surfaces and reaction with water (Calvert and Lindberg, 2005; Tossell, 2006; Castro et al., 2009; Hall, 1995; Pal and Ariya, 2004b; Snider et al., 2008). In an earlier laboratory study conducted by Hall, 1995, attempts were made to correct the measure reaction rate for wall mediated reactions which led to a reaction rate of 0.3×10^{-19} cm^3 $molecule^{-1}$ s^{-1}, approximately 20 times slower than measurements made in the more recent studies cited above ($\sim 6 \times 10^{-19}$ cm^3 $molecule^{-1}$ s^{-1}). Therefore, it is currently thought that many of the recent laboratory-based measurements of GEM oxidation by ozone were enhanced by surface reactions on the reactors walls. Several model studies of the atmospheric mercury life cycle found that global GEM concentrations were underestimated when the rate coefficient published by Pal and Ariya, (2004b) was used (7.5×10^{-19} cm^3 $molecule^{-1}$ s^{-1}),

further supporting the idea that empirical measurements of the GEM-ozone reaction rate coefficients were too fast (Holmes et al., 2006; Seigneur et al., 2006; Holmes et al., 2010). The possibility of a missing reduction mechanism was proposed in the modeling studies to complement the possibility that the reactor studies may have produced coefficients which were enhanced by surface reactions. When these considerations were taken into account by Holmes et al., (2010), the bromine oxidation pathways in the free troposphere were found sufficient to explain global GEM concentrations, and the ozone reaction was deemed unimportant in most situations. However, a study performed in a 17-m^3 Teflon chamber by Sumner et al. (2005) gave a very similar rate coefficient to measurements of Pal and Ariya, (2004b) and Snider et al. (2008), calling into question the importance of enhancement on the reactor walls and suggesting that the oligomeric formation route may be the reason for the reactor-based observations. The corroboration between the results from the large and small reactor studies strengthens the case for a missing reduction or inhibition mechanism for atmospheric oxidized mercury, and reopens the possibility that the GEM-ozone reaction may be important in certain situations where the reduction mechanism may not be particularly active, or where the bromine pathway has little impact.

While considerable research efforts have been directed at more accurate measurements and deeper mechanistic understanding of these homogeneous oxidation reactions, great uncertainty remains regarding the atmospheric oxidation of GEM in complex heterogeneous aerosol systems characteristic of the real atmosphere. To our knowledge there are no laboratory studies of mercury oxidation which attempt to simulate any region of the atmosphere to a realistic level of complexity, and there may be

phenomena that will be discovered by performing such exploratory experiments. Now that oxidation reaction rate coefficients for GEM have been established in simplified reaction systems that include the presumed most important oxidants, there is a need to move toward investigations that better represent the atmosphere. Without such experiments, we cannot properly evaluate our understanding of GEM oxidation in the real atmosphere or hope to conclusively resolve the conflicting results produced by the laboratory and modeling studies cited above.

This study is an empirical comparison between the published reaction rate coefficients for GEM oxidation by ozone, and novel measurements of heterogeneous GEM oxidation using a proxy for tropospheric aerosol. The three reaction systems studied represent a progression of complexity from two component gas-phase reactions to a complex system involving the parallel formation of secondary organic aerosol (SOA). The reaction matrices studied were GEM with: i) ozone; ii) ozone and propene; and, iii) ozone, propene, isoprene, α-pinene, and toluene. Reaction systems i) and ii) have been previously studied (Pal and Ariya, 2004b; Sumner et al., 2005; Snider et al., 2008) and served as reference points for this study. The oxidation of GEM in the SOA reaction matrix was novel and provided the opportunity to observe the effects of reactive organic species (beyond those provided by the propene-ozone system) and the chemical composition of SOA surfaces.

A2.2 Methods

Reaction Chamber

The reaction chamber (Shakya and Griffin, 2010) was made of Teflon film and measured 9 m^3 in volume (Welch Flurocarbon, Dover, NH). Stainless steel bulkheads were inserted at both ends of the chamber. Reactants and fill air were injected at one end, while measurements of gaseous and aerosol species were made at the other end. Fill air was supplied from a zero air generator (Model 737; Aadco, Cleves, OH ; Model 111; Thermo Electron Instruments, Waltham, MA) which included three packed-bed scrubbers (Purafil, activated charcoal, and Drierite) and a HEPA filter. The purified air was further dried with a cold trap packed with dry ice. Between experiments, the chamber was flushed with zero air for 36 hours, and in the case of the SOA experiment, the chamber was irradiated for 6 hours before the reactants were injected. The chamber was shrouded in heavy black curtains when experiments were in progress to block ambient light. All of the experiments presented in this study were performed in the dark.

Injection of Reactants

GEM was injected into the chamber using a GC syringe (Hamilton Co, Reno, NV) from the headspace of a closed reservoir which contained a bead of mercury liquid (Oak Ridge National Laboratory, TN; Rutter et al., 2008a). Propene, isoprene, α-pinene, and toluene were injected into the chamber from a smaller Teflon bag called a dosing chamber. Isoprene and α-pinene were model compounds of biogenic VOCs, toluene was a model compound for anthropogenic VOCs, and propene was used to provide an organic reaction system that did not lead to SOA. Propene (SpecAir; 99.5%) was introduced into the dosing chamber from a compressed cylinder through a volumetric flow meter. Isoprene, α-pinene, and toluene vapor were injected into the dosing chamber with a GC syringe from the head space above pure liquids of the compounds (Sigma Aldrich, >99%

for isoprene and toluene; >98% for α-pinene). The gases in the dosing chamber were diluted to the appropriate concentration with zero air before an aliquot was taken from the dosing chamber and injected into the reaction chamber using a GC syringe. Reactant injections were performed into a stream of zero air when the chamber was very close to full. Ozone was generated by irradiance of zero air with ultraviolet (UV) light using a Jelight M400 (Irvine, CA) and was the last reactant added to the chamber. The bag was manually agitated gently to aid initial mixing, which was observed to finish between 50 and 60 minutes after injections in the experiments presented in Figures 1-2. Ozone, GEM, and toluene concentration time series were used to determine when mixing finished in each experiment.

Measurements

GEM concentrations were measured using a Tekran 2537A analyzer which is a cold vapor atomic fluorescence spectrometer (CVAFS), with a single stage gold amalgamation sample collection device. The instrument inlet was filtered with a soda lime-Tenax trap to prevent passivation of the gold traps by water vapor and semi-volatile organic compounds (Rutter and Schauer, 2007; Rutter et al., 2008a). A 47-mm Teflon membrane placed after the soda lime-Tenax trap was used to remove particles. Propene, isoprene, α-pinene, and toluene were measured using a gas chromatograph with a flame ionization detector (GC-17A; Shimadzu, Columbia, MD) fitted with a DB-5 column (Agilent Technologies). The GC was calibrated using standards injected into a small Teflon bag which was connected the GC inlet. Ozone was measured with UV photometry (model number 49C; ThermoElectron Instruments). Relative humidity and temperature were monitored using a portable probe and meter connected directly to one of the

bulkheads in the chamber wall. Relative humidities and temperatures were measured at the start of the experiments and ranged between 20-23% and 21-23°C. Particle measurements were made with a Scanning Mobility Particle Sizer (SMPS; 3936; TSI St Paul, Minnesota) fitted with a TSI 3081 differential mobility analyzer.

Experimental Matrix

The experimental matrix began with a study of the published GEM plus ozone reaction system (Hall, 1995; Pal and Ariya, 2004b; Sumner et al., 2005; Snider et al., 2008) which until recently was thought to be the most important oxidation pathway for GEM in the atmosphere (Holmes et al., 2006; Seigneur et al., 2006; Bullock et al., 2008; Selin et al., 2008). This served as a reference point for the new reaction system explored in this study in which SOA precursors were added. The initial reactant concentrations shown in Table A2.1 were chosen to reflect atmospheric concentrations while still providing a strong enough signal to detect oxidative GEM losses above wall losses (Figure A2.1) and allowing measurements of the VOC reactants using GC-FID. GEM concentrations ranged between 11 and 95 ng m^{-3}, and ozone mixing ratios were nominally set to 250ppb, with a mixing ratio of 500ppb in one of the GEM plus ozone experiments to vary the reactant ratio as much as possible in this experiment. Alpha-pinene, isoprene, and toluene concentrations were 18 ppb, 42 ppb and 62 ppb respectively.

In contrast with the GEM and ozone concentrations used here, previous studies have used initial GEM concentrations (1 μg m^{-3} to 16 mg m^{-3}) and ozone mixing ratios (10ppm to 1500ppm) which were considerably larger than ambient concentrations (Hall,

1995; Pal and Ariya, 2004b; Snider et al., 2008). However, Sumner et al., 2005) used concentrations similar to those used in this study and more representative of ambient conditions: initial GEM concentrations between 48 and 130 ng m^{-3} and ozone concentrations between 75 ppb and 14 ppm. Typical ambient GEM concentrations can range between 1.5 ng m^{-3} in unimpacted rural settings to a few hundred ng m^{-3} in plumes from industrial point sources (Manolopoulos et al., 2006; Rutter et al., 2008b; Rutter et al., 2009); ozone concentrations are typically range a few tens of ppb in continental airmasses, and can reach a few hundred ppb in air masses heavily impacted by human activity. Published alpha-pinene and isoprene concentrations are typically 0.02-2 ppbV and 0.1-4 ppbV, respectively (Guenther, 1997; Jia et al., 2008; Apel et al., 2010; Cai et al., 2010; Leuchner and Rappenglück, 2010). Toluene concentrations reported in the literature are typically less than 0.4-1 ppbV in urban areas, and benzene and m-, p- and o-xylenes which are very similar in structure to toluene and also lead to SOA, have been measured over comparable concentration ranges (Jia et al., 2008; Mukerjee et al., 2009; Apel et al., 2010; Cai et al., 2010; Leuchner and Rappenglück, 2010; von Schneidemesser et al., 2010).

A comparison between literature ranges and the initial reactant concentrations presented in Table A2.1 reveals that GEM, ozone, alpha-pinene, isoprene, and toluene were higher than typical atmospheric concentrations by one to two orders of magnitude. However, the ratios between the values in experiments were similar to those typically observed. This means that relative changes in the concentration of GEM due to reactions with ozone and reactive species evolved during SOA formation would be applicable to atmospheric scenarios.

Wall Losses

Experiments to measure wall losses were conducted using injections of GEM only, at low (10-20 ng m^{-3}) and high concentrations (100 ng m^{-3}). These experiments revealed wall losses to be zero order with respect to mercury (first order with respect to wall surface area), with measured rates of -56±63 molecules cm^{-3} s^{-1}, and -95±74 molecules cm^{-3} s^{-1} for the low and high concentration experiments, respectively.

Numerical Modeling

Time-dependent concentration changes in GEM, ozone, propene, isoprene, α-pinene, toluene, and a variety of reaction products were modeled numerically. Oxidation pathways for GEM were modeled using calculations of ozone and secondary OH concentrations. The model used reaction rate coefficients reported in the literature for all experiments (Pal and Ariya, 2004a;b; Sumner et al., 2005; Snider et al., 2008), with the exception that our GEM-ozone rate coefficient was used to model the GEM losses in the ozone-propene and ozone-SOA experiments. A detailed gas-phase chemistry model (Caltech Atmospheric Chemistry Mechanism, CACM; Griffin et al., 2002; Chen and Griffin, 2005) was used and optimized to simulate VOC chemistry. The starting concentrations from the respective chamber experiments were used to initialize the model simulations. The concentrations calculated after the first 50 to 60 minutes were adjusted for the dilution observed due to mixing over this time frame. These dilution corrected concentrations were then used to re-initialize the model at 60 minutes, and the model was then allowed to simluate the remainder of the experiment.

A2.3 Results

Net oxidation of GEM was observed when ozone (Figure A2.2a) and ozone with propene (Figure A2.2b) were introduced into the chamber. The decrease in GEM concentration was statistically significant (at 3σ) compared to the wall losses presented in Figure A2.1. Numerical model predictions of GEM losses caused by ozone, secondary OH, and wall losses reproduced the experimentally observed behavior reasonably well in the first hour. The numerical model used in Figure A2.2a employed reaction rate coefficients from three different published studies. While Pal and Ariya, (2004b) and Snider et al., (2008) used halocarbon-wax-coated reaction vessels with volumes $\leq$5L, Sumner et al., (2005) used 17-m^3 environmental chambers made of Teflon film. The favorable comparison between reaction rate coefficients measured in each of the published studies and by this study suggests that measures taken by all authors to account for and minimize walls effects were successful. Reaction rate coefficients determined in this study from analytical second order model fits of our data (Figure A2.3) were $(5.9\pm0.2)\times10^{-19}cm^3$ $molec^{-1}$ s^{-1} for the high GEM concentration experiment (r^2 = 0.99) and $(6.5\pm0.5)\times10^{-19}cm^3$ $molec^{-1}$ s^{-1} for a low concentration experiment (r^2 = 0.97; Initial GEM concentration = 10.7 ng m^{-3}; Figure A2.4). These rate coefficients compare well to recently published values of $(6.2\pm1.1)\times10^{-19}$ cm^3 $molec^{-1}$ s^{-1} (Snider et al., 2008) and $(6.4\pm2.3)\times10^{-19}$ cm^3 $molec^{-1}$ s^{-1} (Sumner et al., 2005).

The numerical model used to calculate the GEM time series in the GEM-ozone-propene case (Figure A2.2b) used the reaction rates measured in this study, alongside the published OH reaction rate coefficient. OH concentrations were provided by the numerical model of the propene-ozone reaction system. There was some suggestion that

the losses of GEM in this case were slightly less than would be expected if the propene were not present (compare with Figure A2.2a). However, only 0.7 hours of data were available for this experiment, preventing the confirmation of this shortfall as statistically significant.

Aerosol particles were observed in both the GEM-ozone case (306 ± 122 p cm^{-3} between 2 nm and 150 nm for first case in Table A2.1; 309 ± 28 for all sizes in second case; 0.04 ± 0.01 p cm^{-3} in a GEM only wall loss experiment) and the GEM-ozone-propene case (Figure A2.5). The observation of particle formation corroborated observations made by Snider et al., (2008) of $HgO_{(s)}$ particle chains collected on TEM grids placed on reactor walls. Taken together, these observations are consistent with the formation of mercury oxidation products (oligomeric or otherwise) in the bulk of the reactor rather than on the reactor walls. Although the GEM-ozone reaction may have been mediated by the aerosol particle surfaces associated with mercury oxidation products in the chamber (Ariya and Peterson, 2005), such mediation may also occur in the atmosphere on the particle surfaces already present, meaning this reaction pathway is likely to be relevant in the environment.

The oxidation of GEM in a reaction mixture more representative of the continental troposphere was performed by adding isoprene, α-pinene, and toluene (Table A2.1; Figure A2.6) to the GEM-ozone-propene case. Oxidative losses were observed in the first 0.5 hours as predicted by the numerical model, which included the ozone and OH pathways, meaning that the GEM and ozone reaction is viable in the presence of pre-existing aerosol particles. During this initial period the reaction progressed at a rate consistent with that observed in the absence of pre-existing aerosol particles. After 0.5

hours a divergence from the model was observed, indicating the onset of a reduction pathway or an inhibition of the reaction mechanism. This divergence was only seen when the SOA reaction system was introduced, suggesting that either some gas-phase or heterogeneous process only associated with the SOA system was responsible for the decreased net oxidation. The SOA particle mass and surface area concentrations did not substantially diminish during the time period where the decreased net oxidation began to occur (Figures 2b and 2c), indicating that some aspect of the particle surface composition or the gas-phase chemistry, rather than the particle surface area, was responsible for the decreased net oxidation. This would be consistent with measurements made by Sax et al., (2005) who observed the particle composition of SOA formed form alpha-pinene continuing to evolve towards higher oxidation states for up to 20 hours after particle formation had finished.

Previous publications performed in reaction vessels of 5 liters or smaller observed variations in the reaction rate coefficients due to wall mediated reactions (Hall, 1995; Pal and Ariya, 2004b). Such reactions were not expected to have a significant impact on our data due to very large volume to surface area ratio of our reaction vessel (3:1) and the closer proximity of particle surface areas to most of the GEM oxidation reactions occurring in the chamber air, as compared to the much larger distances to the chamber walls. This is also supported by the good agreement between the published GEM-ozone reaction rate coefficients (Pal and Ariya, 2004b; Sumner et al., 2005; Snider et al., 2008) and the rates of the initial losses of GEM observed at this condition. It might be possible though that the net decrease in oxidation observed as the experiment progressed was due to reduction of the oxidized mercury attached to the surfaces of SOA particles after they

had been deposited to the walls. Losses of SOA particles to the walls were observed after 0.4 hours (Figures 2b and 2c), but the rate at which this occurred was not sufficient for the net decrease in oxidation of GEM to be explained by an artifact. The proximity of the aerosol particle surfaces in the chamber to the GEM oxidation reactions suggests that if any surface was likely to have an impact on the reaction it would be that associated with the SOA and not the chamber walls.

Several studies in aqueous media have observed reduction of oxidized mercury with carboxylic acids and humic organic matter in both light and dark conditions (Matthiessen, 1998; Si and Ariya, 2008; Zheng and Hintelmann, 2009), while Pehkonen and Lin, (1998) linked aqueous photo-reduction to the photolysis of oxalate which produced the HO_2 radical. These findings provide a starting point for understanding the behavior observed in this study, although caution should always be exercised in translating aqueous phase chemistry to undeliquesced aerosols because the chemical matrices are so different. Secondary organic aerosol is thought to become increasing more enriched in carboxylic acid groups as it is oxidized and aged in the atmosphere (Jimenez et al., 2009; Sax et al., 2005) and the gas phase of the reaction system studied in these experiments is known to include reactive species such as hydrogen oxides and organic radicals (Griffin et al., 2002; Jenkin et al., 2003; Saunders et al., 2003; Chen and Griffin, 2005). Therefore, it is reasonable to expect that these species may be involved in the decreased GEM losses observed in this study.

A2.4 Conclusions

The results of this study suggest that the oxidation of GEM by ozone is a viable reaction in the atmosphere, but may be countered by a reduction or inhibition mechanism, the presence of which was proposed by the authors of recent atmospheric model studies (Seigneur et al., 2006; Holmes et al., 2010). The prevalence of such a mechanism in the atmosphere will need to be further investigated because although a net zero loss of GEM was achieved as the SOA system matured, normal GEM-ozone oxidation during the initial phases of SOA formation indicated that this reaction may occur under some atmospheric conditions. Also, this study only included experiments which were conducted in the dark. Work is currently ongoing on a wider data set which includes UV irradiance and variations in OH concentration.

Our study results strengthen the claim that bromine is the most important global oxidation pathway for mercury (Holmes et al., 2006; Holmes et al., 2009; Holmes et al., 2010), although it may not be appropriate to assume a decreased GEM-ozone rate coefficient in all circumstances, particularly when performing regional or airshed scale modeling of GEM oxidation on short time scales. Furthermore, the question of whether a reduction mechanism may apply to the halogen oxidation pathways is raised by a study conducted by Lyman et al., 2010 in which oxidized mercury loaded and collected on KCl coated denuders was lost as GEM under high ozone conditions. Lyman et al., observed this phenomenon in field collections of reactive gaseous mercury as well as $HgCl_2$ and $HgBr_2$ standards which were loaded onto the denuders. Additionally, Engle et al., (2005) found ozone caused releases of GEM, as well as RGM from soils with elevated $HgCl_2$ contents. Further research is needed to understand the mechanisms behind the decreased

net oxidations observed in this study and whether they occur in atmospheric aerosols for Hg(II) compounds besides those generated by reaction with ozone and OH.

A2.5 References

Apel, E.C., Emmons, L.K., Karl, T., Flocke, F., Hills, A.J., Madronich, S., Lee-Taylor, J., Fried, A., Weibring, P., Walega, J., Richter, D., Tie, X., Mauldin, L., Campos, T., Weinheimer, A., Knapp, D., Sive, B., Kleinman, L., Springston, S., Zaveri, R., Ortega, J., Voss, P., Blake, D., Baker, A., Warneke, C., Welsh-Bon, D., de Gouw, J., Zheng, J., Zhang, R., Rudolph, J., Junkermann, W. and Riemer, D.D. Chemical evolution of volatile organic compounds in the outflow of the Mexico City Metropolitan area. Atmos. Chem. Phys. 10, 2353-2375, 2010.

Ariya, P. and Peterson, K. Chemical Transformation of Gaseous Elemental Hg in the Atmosphere. In: N. Pirrone and K.R. Mahaffey, Editors, Dynamics of Mercury Pollution on Regional and Global Scales:, Springer US, 261-294, 2005.

Ariya, P.A., Khalizov, A. and Gidas, A. Reactions of gaseous mercury with atomic and molecular halogens: Kinetics, product studies, and atmospheric implications, J. Phys. Chem. A 106, 7310-7320, 2002.

Ariya, P.A. and Ryzhkov, A. Atmospheric transoformation of elemental mercury upon reactions with halogens. J Phys IV 107, 57-59, 2003.

Ariya, P.A., Skov, H., Grage, M.M.L. and Goodsite, M.E. Gaseous elemental mercury in the ambient atmosphere: Review of the application of theoretical calculations and experimental studies for determination of reaction coefficients and mechanisms

with halogens and other reactants. Advances in Quantum Chemistry, Vol 55: Applications of Theoretical Methods to Atmospheric Science 55, 43-55, 2008.

Axelrad, D.A., Bellinger, D.C., Ryan, L.M. and Woodruff, T.J., Dose-response relationship of prenatal mercury exposure and IQ: An integrative analysis of epidemiologic data, Environ. Health Perspect. 115, 609-615, 2007.

Bullock, O.R., Atkinson, D., Braverman, T., Civerolo, K., Dastoor, A., Davignon, D., Ku, J.Y., Lohman, K., Myers, T.C., Park, R.J., Seigneur, C., Selin, N.E., Sistla, G. and Vijayaraghavan, K. The North American Mercury Model Intercomparison Study (NAMMIS): Study description and model-to-model comparisons, *J. Geophy. Res.* 113, 17, 2008.

Cai, C.J., Geng, F.H., Tie, X.X., Yu, Q.O., Peng, L. and Zhou, G.Q. Characteristics of Ambient Volatile Organic Compounds (VOCs) Measured in Shanghai, China. Sensors 10, 7843-7862, 2010.

Calvert, J.G. and Lindberg, S.E. Mechanisms of mercury removal by O3 and OH in the atmosphere. Atmos. Environ. 39, 3355-3367, 2005.

Castro, L., Dommergue, A., Ferrari, C. and Maron, L. A DFT study of the reactions of O3 with Hg degrees or Br. Atmos. Environ. 43, 5708-5711, 2009.

Chen, J.J. and Griffin, R.J. Modeling secondary organic aerosol formation from oxidation of alpha-pinene, beta-pinene, and d-limonene. Atmos. Environ. 39, 7731-7744, 2005.

Engle, M.A., Gustin, M.S., Lindberg, S.E., Gertler, A.W. and Ariya, P.A. The influence of ozone on atmospheric emissions of gaseous elemental mercury and reactive gaseous mercury from substrates. Atmos. Environ. 39, 7506-7517, 2005.

Griffin, R.J., Dabdub, D. and Seinfeld, J.H. Secondary organic aerosol - 1. Atmospheric chemical mechanism for production of molecular constituents. *J. Geophy. Res.* 107, 2002.

Guallar, E., Sanz-Gallardo, M.I., van't Veer, P., Bode, P., Aro, A., Gomez-Aracena, J., Kark, J.D., Riemersma, R.A., Martin-Moreno, J.M. and Kok, F.J. Mercury, fish oils, and the risk of myocardial infarction. N. Engl. J. Med. 347, 1747-1754, 2002.

Guenther, A. Seasonal and spatial variations in natural volatile organic compound emissions. Ecol. Appl. **7**, 34-45, 1997.

Hall, B. The Gas-Phase Oxidation Elemental Mercury by Ozone. Water Air Soil Poll. 80, 301-315, 1995.

Holmes, C.D., Jacob, D.J., Corbitt, E.S., Mao, J., Yang, X., Talbot, R. and Slemr, F. Global atmospheric model for mercury including oxidation by bromine atoms. Atmos. Chem. Phys. 10, 12037-12057, 2010.

Holmes, C.D., Jacob, D.J., Mason, R.P. and Jaffe, D.A. Sources and deposition of reactive gaseous mercury in the marine atmosphere. Atmos. Environ. 43, 2278-2285, 2009.

Holmes, C.D., Jacob, D.J. and Yang, X. Global lifetime of elemental mercury against oxidation by atomic bromine in the free troposphere. Geophys. Res. Lett. 33, 5, 2006.

Jenkin, M.E., Saunders, S.M., Wagner, V. and Pilling, M.J. Protocol for the development of the Master Chemical Mechanism, MCM v3 (Part B): tropospheric degradation of aromatic volatile organic compounds. Atmos. Chem. Phys. 3, 181-193, 2003.

Jia, C., Batterman, S. and Godwin, C. VOCs in industrial, urban and suburban neighborhoods, Part 1: Indoor and outdoor concentrations, variation, and risk drivers. Atmos. Environ. 42, 2083-2100, 2008.

Jimenez, J.L., Canagaratna, M.R., Donahue, N.M., Prevot, A.S.H., Zhang, Q., Kroll, J.H., DeCarlo, P.F., Allan, J.D., Coe, H., Ng, N.L., Aiken, A.C., Docherty, K.S., Ulbrich, I.M., Grieshop, A.P., Robinson, A.L., Duplissy, J., Smith, J.D., Wilson, K.R., Lanz, V.A., Hueglin, C., Sun, Y.L., Tian, J., Laaksonen, A., Raatikainen, T., Rautiainen, J., Vaattovaara, P., Ehn, M., Kulmala, M., Tomlinson, J.M., Collins, D.R., Cubison, M.J., Dunlea, E.J., Huffman, J.A., Onasch, T.B., Alfarra, M.R., Williams, P.I., Bower, K., Kondo, Y., Schneider, J., Drewnick, F., Borrmann, S., Weimer, S., Demerjian, K., Salcedo, D., Cottrell, L., Griffin, R., Takami, A., Miyoshi, T., Hatakeyama, S., Shimono, A., Sun, J.Y., Zhang, Y.M., Dzepina, K., Kimmel, J.R., Sueper, D., Jayne, J.T., Herndon, S.C., Trimborn, A.M., Williams, L.R., Wood, E.C., Middlebrook, A.M., Kolb, C.E., Baltensperger, U. and Worsnop, D.R.. Evolution of Organic Aerosols in the Atmosphere. Science 326, 1525-1529, 2009.

Knobeloch, L., Steenport, D., Schrank, C. and Anderson, H.. Methylmercury exposure in Wisconsin: A case study series. Environ. Res. 101, 113-122, 2006.

Leuchner, M. and Rappenglück, B. VOC source-receptor relationships in Houston during TexAQS-II. Atmos. Environ. 44, 4056-4067, 2010.

Lyman, S.N., Jaffe, D.A. and Gustin, M.S. Release of mercury halides from KCl denuders in the presence of ozone. Atmos. Chem. Phys. 10, 8197-8204, 2010.

Manolopoulos, H., Snyder, D.C., Schauer, J.J., Turner, J.R., Olson, M.L. and Krabbenhoft, D.P. Sources of Speciated Atmospheric Mercury at a Residential Neighbourhood Impacted by Industrial Sources. In preparation for submission to Environ. Sci. and Technol. 2006.

Matthiessen, A.. Reduction of divalent mercury by humic substances - kinetic and quantitative aspects. Sci. Total Environ. 213, 177-183, 1998.

Mukerjee, S., Smith, L.A., Johnson, M.M., Neas, L.M. and Stallings, C.A. Spatial analysis and land use regression of VOCs and NO2 from school-based urban air monitoring in Detroit/Dearborn, USA. Sci. Total Environ. 407, 4642-4651, 2009.

Pal, B. and Ariya, P.A. Gas-phase HO center dot-Initiated reactions of elemental mercury: Kinetics, product studies, and atmospheric implications. Environ. Sci. Technol. 38, 5555-5566, 2004a.

Pal, B. and Ariya, P.A. Studies of ozone initiated reactions of gaseous mercury: kinetics, product studies, and atmospheric implications. Phys. Chem. Chem. Phys. 6, 572-579, 2004b.

Pehkonen, S.O. and Lin, C.J. Aqueous photochemistry of mercury with organic acids. J. Air Waste Manag. Assoc. 48, 144-150, 1998.

Raofie, F. and Ariya, P.A. Kinetics and products study of the reaction of BrO radicals with gaseous mercury. J Phys IV 107, 1119-1121, 2003.

Raofie, F., Snider, G. and Ariya, P.A. Reaction of gaseous mercury with molecular iodine, atomic iodine, and iodine oxide radicals - Kinetics, product studies, and atmospheric implications. Can. J. Chem.-Rev. Canad. De Chim. 86, 811-820, 2008.

Rice, G.E., Hammitt, J.K. and Evans, J.S. A Probabilistic Characterization of the Health Benefits of Reducing Methyl Mercury Intake in the United States. Environ. Sci. Technol. 44, 5216-5224, 2010.

Rutter, A.P., Hanford, K.L., Zwers, J.T., Perillo-Nicholas, A.L., Schauer, J.J., Worley, C.A., Olson, M.L. and DeWild, J.F. Evaluation of an off-line method for the analysis of atmospheric reactive gaseous mercury and particulate mercury. J. Air Waste Manag. Assoc. 58, 377-383, 2008a.

Rutter, A.P. and Schauer, J.J. The impact of aerosol composition on the particle to gas partitioning of reactive mercury. Environ. Sci. Technol. 41, 3934-3939, 2007.

Rutter, A.P., Schauer, J.J., Lough, G.C., Snyder, D.C., Kolb, C.J., Von Klooster, S., Rudolf, T., Manolopoulos, H. and Olson, M.L. A comparison of speciated atmospheric mercury at an urban center and an upwind rural location. J Environ Monitor 10, 102-108, 2008b.

Rutter, A.P., Schauer, J.J., Shafer, M.M., Creswell, J., Olson, M.R., Clary, A., Robinson, M., Parman, A.M. and Katzman, T.L.. Climate Sensitivity of Gaseous Elemental Mercury Dry Deposition to Plants: Impacts of Temperature. Light Intensity, and Plant Species, Environ. Sci. Technol. 45, 569-575, 2011.

Rutter, A.P., Snyder, D.C., Stone, E.A., Schauer, J.J., Gonzalez-Abraham, R., Molina, L.T., Márquez, C., Cárdenas, B. and de Foy, B. In situ measurements of speciated atmospheric mercury and the identification of source regions in the Mexico City Metropolitan Area. Atmos. Chem. Phys. 9, 207-220, 2009.

Saunders, S.M., Jenkin, M.E., Derwent, R.G. and Pilling, M.J. Protocol for the development of the Master Chemical Mechanism, MCM v3 (Part A): tropospheric

degradation of non-aromatic volatile organic compounds. Atmos. Chem. Phys. 3, 161-180, 2003.

Sax, M., Zenobi, R., Baltensperger, U. and Kalberer, M. Time resolved infrared spectroscopic analysis of aerosol formed by photo-oxidation of 1,3,5-trimethylbenzene and alpha-pinene. Aer. Sci. Technol. 39, 822-830, 2005.

Seigneur, C., Vijayaraghavan, K. and Lohman, K. Atmospheric mercury chemistry: Sensitivity of global model simulations to chemical reactions. J. Geophy. Res. 111, 2006.

Selin, N.E., Jacob, D.J., Yantosca, R.M., Strode, S., Jaegle, L. and Sunderland, E.M. Global 3-D land-ocean-atmosphere model for mercury: Present-day versus preindustrial cycles and anthropogenic enrichment factors for deposition. Global Biogeochem. Cycles 22, 13, 2008.

Shakya, K.M. and Griffin, R.J. Secondary organic aerosol from photooxidation of polycyclic aromatic hydrocarbons. Environ. Sci. Technol., 44, 8134-8139, 2010.

Si, L. and Ariya, P.A.. Reduction of oxidized mercury species by dicarboxylic acids (C-2-C-4): Kinetic and product studies. Environ. Sci. Technol. 42, 5150-5155, 2008.

Snider, G., Raofie, F. and Ariya, P.A. Effects of relative humidity and CO(g) on the O-3-initiated oxidation reaction of Hg-0(g): kinetic & product studies. Phys. Chem. Chem. Phys. 10, 5616-5623, 2008.

Sommar, J., Gardfeldt, K., Stromberg, D. and Feng, X.B. A kinetic study of the gas-phase reaction between the hydroxyl radical and atomic mercury. Atmos. Environ. 35, 3049-3054, 2001.

Sumner, A.L., Spicer, C.W., Satola, J., Mangaraj, R., Cowen, K.A., Landis, M.S., Stevens, R.K. and Atkeson, T.D. Environmental Chamber Studies of Mercury Reactions in the Atmosphere. In: N.M. Pirrone, K.R.; Editor, Dynamics of Mercury Pollution on Regional and Global Scales: Atmospheric Processes and Human Exposures Around the World. Springer US, 193-212, 2005.

Tossell, J.A. Calculation of the energetics for the oligomerization of gas phase HgO and HgS and for the solvolysis of crystalline HgO and HgS. J. Phys. Chem. A 110, 2571-2578, 2006.

Virtanen, J.K., Voutilainen, S., Rissanen, T.H., Mursu, J., Tuomainen, T.P., Korhonen, M.J., Valkonen, V.P., Seppanen, K., Laukkanen, J.A. and Salonen, J.T. Mercury, fish oils, and risk of acute coronary events and cardiovascular disease, coronary heart disease, and all-cause mortality in men in eastern Finland. Arterioscler. Thromb. Vasc. Biol. 25, 228-233, 2005.

von Schneidemesser, E., Monks, P.S. and Plass-Duelmer, C. Global comparison of VOC and CO observations in urban areas. Atmos. Environ. 44, 5053-5064, 2010.

Zheng, W. and Hintelmann, H. Mercury isotope fractionation during photoreduction in natural water is controlled by its Hg/DOC ratio. Geochim. Cosmochim. Acta 73, 6704-6715, 2009.

Table A2.1. Initial reactant concentrations (after initial mixing concluded). All reactions were performed in the dark. OH concentrations were modeled; all others were measured.

Description	$[Hg^0]_0$	$[O_3]_0$	$[OH]_0$	$[C_3H_8]_0$	$[\alpha\text{-pinene}]_0$	$[isoprene]_0$	$[toluene]_0$
$Hg^0(g)$ with…	ng m^{-3}	ppb	molec cm^{-3}	ppb	ppb	ppb	ppb
O_3	76	265	0	NA*	NA	NA	NA
	11	495	0	NA	NA	NA	NA
O_3-propene	90	242	4×10^6	25	NA	NA	NA
O_3-propene-SOA	95	266	1×10^6	91	18	42	62

*NA- not added

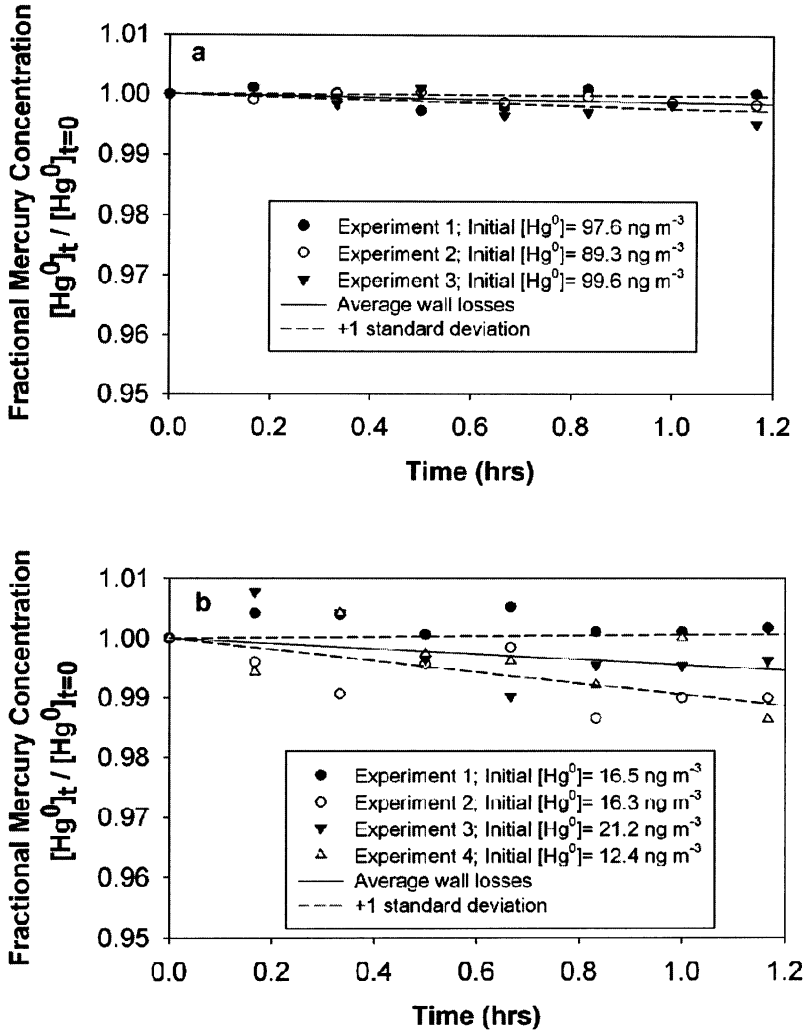

Figure A2.1. Measurements of $Hg^0_{(g)}$ wall losses for high (a) and low (b) concentration experiments.

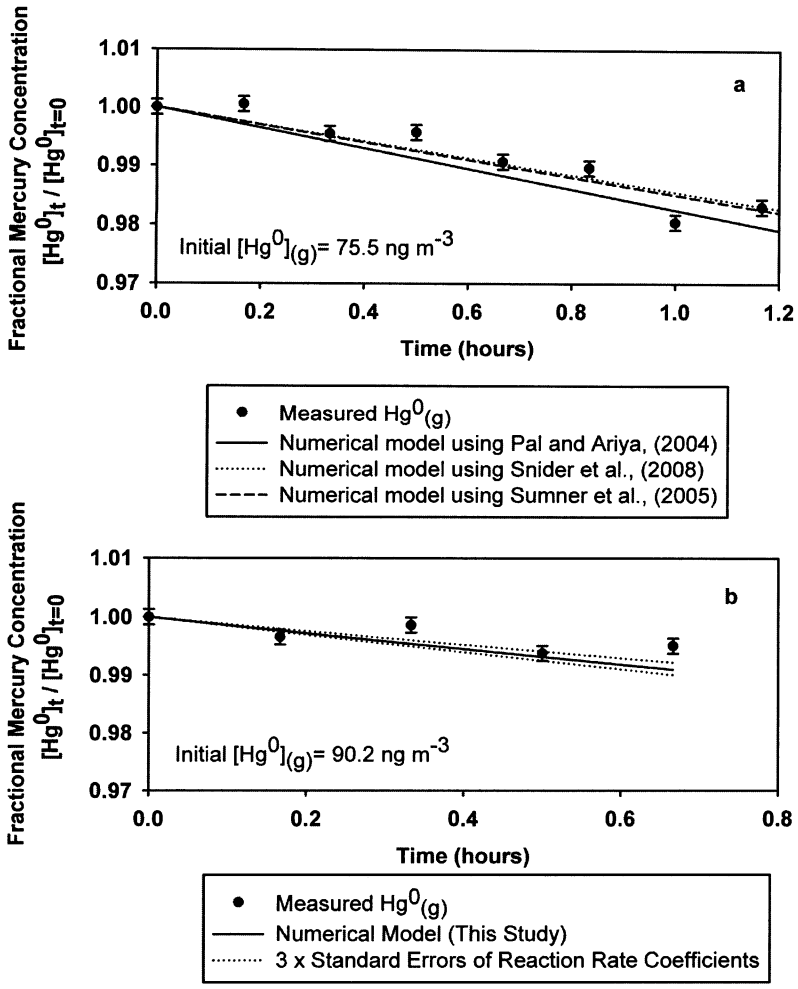

Figure A2.2. Oxidative losses of GEM with ozone (a) and ozone with propene (b). Numerical model predictions are shown for the ozone case (a) using previously published rate coefficients. The propene and ozone case (b) is also compared to a numerical model which used the ozone rate coefficients measured in this study, published OH rate coefficients, and numerically modeled ozone and OH concentrations. Uncertainties in the model predictions are represented using the published rate coefficients uncertainties multiplied by three. Uncertainties in GEM measurements were estimated from averages of the residuals from fits of the wall loss data presented in the supplemental materials.

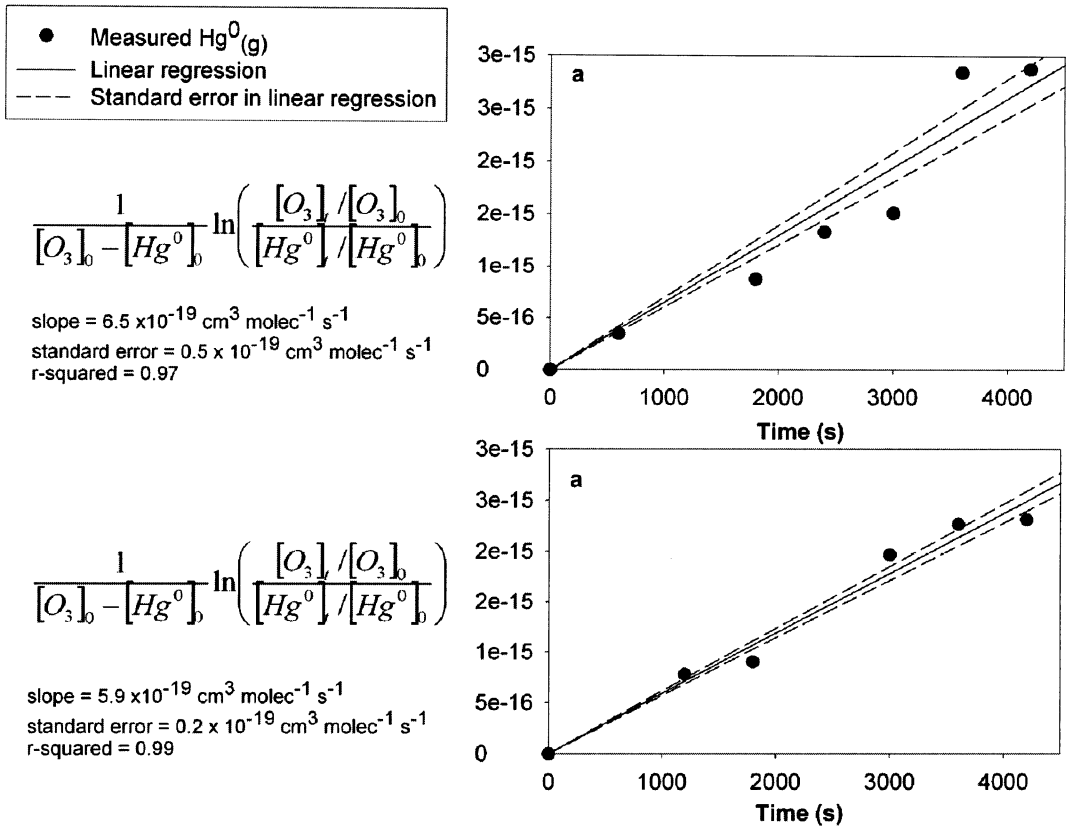

Figure A2.3. Second order model fits of the $Hg^0_{(g)}$ measurements made in the $Hg^0_{(g)}$ + ozone experiments.

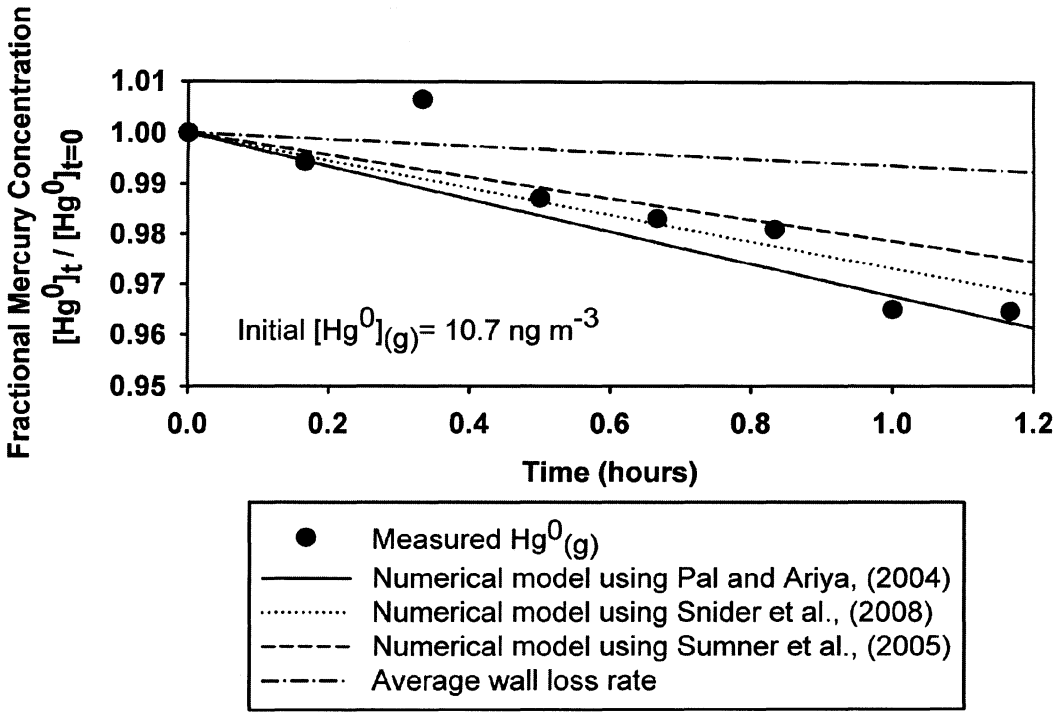

Figure A2.4. Oxidative losses of $Hg^0_{(g)}$ with ozone at low mercury concentrations. Numerical model fits are shown using previously published rate coefficients.

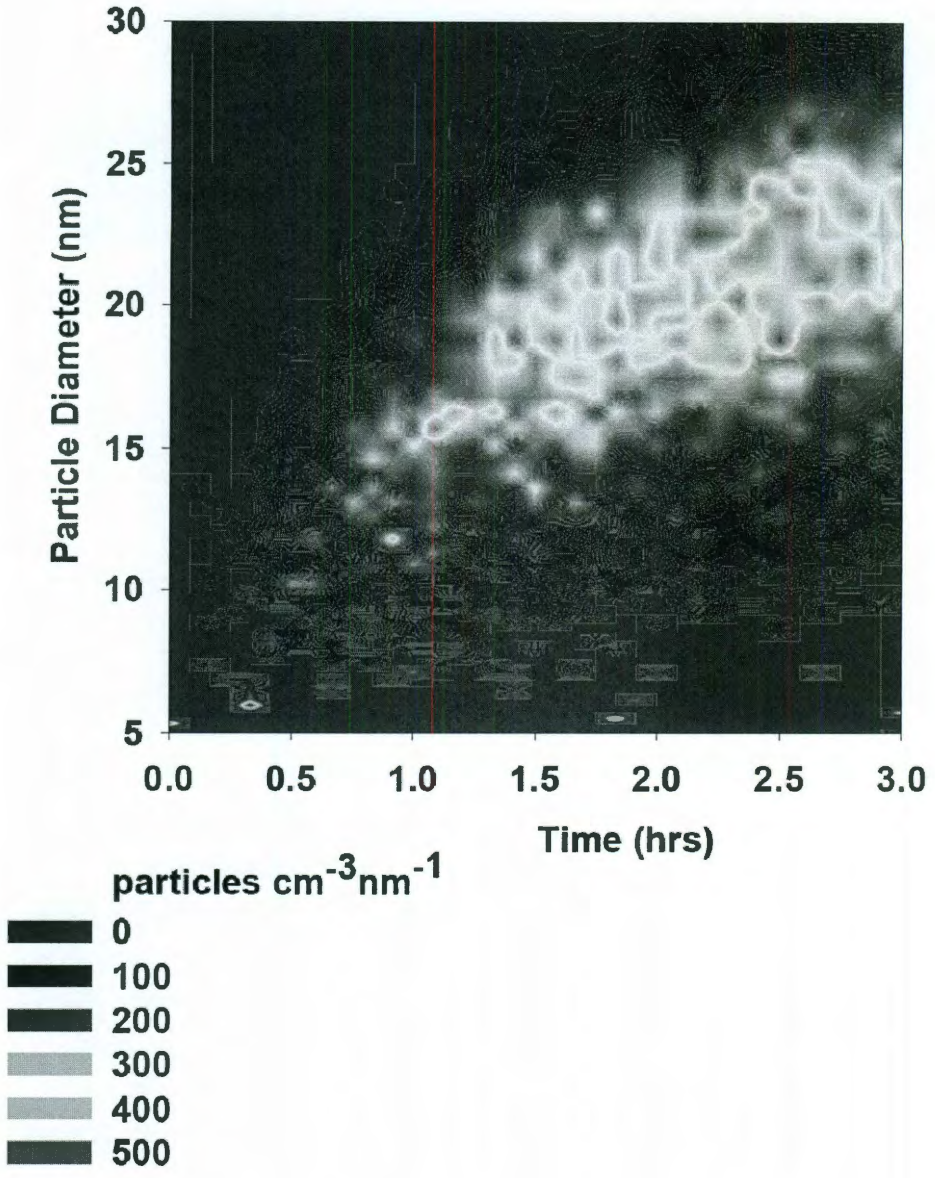

Figure A2.5. Size resolved measurements of particle concentration with a TSI SMPS in the $Hg^0_{(g)}$ + ozone + propene experiment, revealing nucleation and then particle growth by gas to particle conversion.

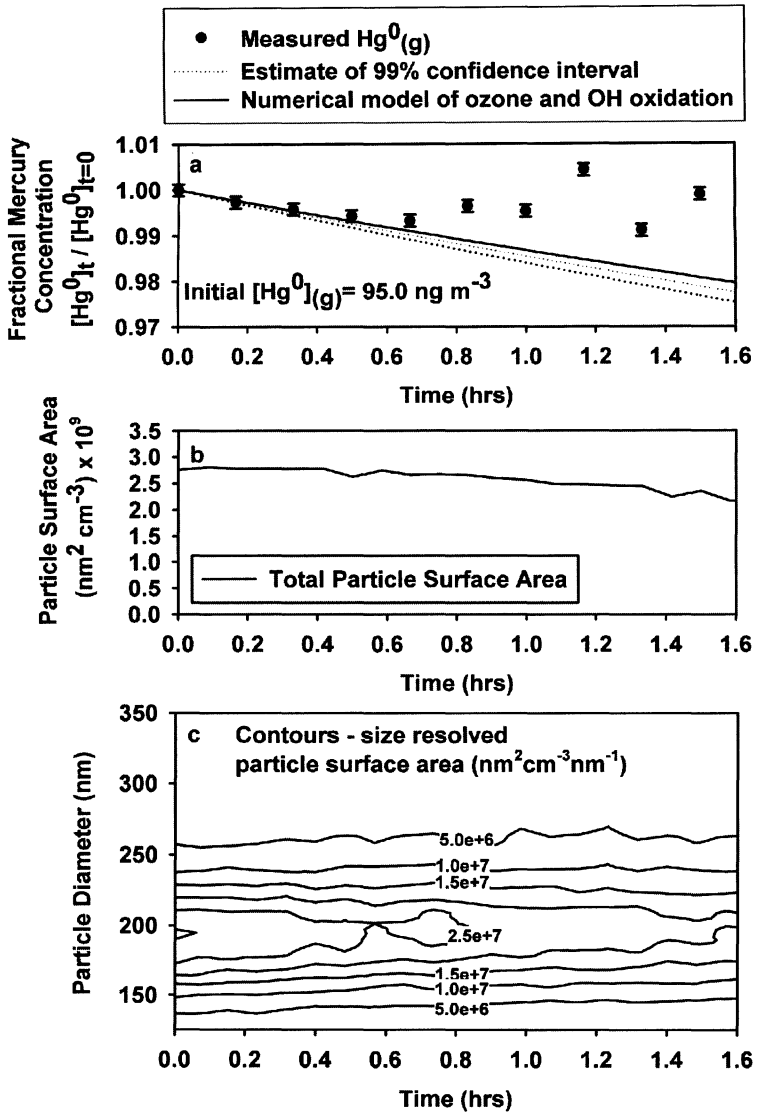

Figure A2.6. Oxidation of GEM by ozone and OH in a SOA forming reaction system consisting of propene, α-pinene, isoprene, and toluene, initiated with ozone (a); size resolved surface area from a TSI SMPS (b and c). The measurements of GEM were compared to a numerical model which included losses by ozone and OH oxidation. Uncertainties in GEM measurements were estimated from averages of the residuals from fits of the wall loss data presented in the supplemental materials.

CHAPTER A3

The Effect of UV light and Hydroxyl Radicals on the Oxidation of Gaseous Elemental Mercury During the Formation of Secondary Organic Aerosol

Reference: Rutter, A.P., Shakya, K.M., Schauer, J.J., Griffin, R.J, and Lehr, R. Manuscript in preparation.

Abstract

The oxidation of gaseous elemental mercury (GEM) was performed using a simulated continental aerosol formed from ozonolysis of alpha-pinene, isoprene, and toluene. The effects of UV irradiance and OH concentration on the oxidative losses of GEM were measured by comparing dark and irradiated experiments, and the addition of 2-butanol to scavenge OH radicals in select experiments. During the first 50 minutes oxidative losses of GEM followed trends predicted by simplified model which included ozone and hydroxyl radical oxidation reactions. However, after this point oxidative losses deviated from model predictions in all but the irradiated case, to arrive at a condition of zero net conversion. Numerical modeling of the VOC oxidation products found good correlations between deficits in GEM oxidative loss (the difference between measured and expected GEM concentrations) and carboxylic acids, acyl peroxy radicals (C<6), and phenolic peroxy radicals. Although these correlations do not demonstrate causal relationships, they do reflect published results from studies of aqueous systems. Furthermore, the inhibition or reduction mechanisms responsible for the decreased amounts of GEM loss, were apparently sensitive to light and OH concentrations,

suggesting this process to be complex, and that different pathways may be active under the variety of conditions studied here.

A3.1 Introduction

The oxidation of gaseous elemental mercury (GEM) in the atmosphere remains a poorly understood component of the mercury environmental cycle, depsite being an important factor in its atmospheric residence time. Until now oxidation rates have been measured in simplified laboratory experiments, which have provided valuable knowledge of the central reactions (Pal and Ariya, 2004a & 2004b; Sumner et al., 2005). The atmosphere is much more complicated than can be represented with such experiments, and studies must now begin to explore mercury oxidation in scenarios which reflect this complexity. Such experiments should investigate the effects of irradiance, oxidant ratios, aerosol surfaces of various compositions, and reactive gases beyond the known oxidants.

Relatively little is known about the reaction mechanisms which are important to the gas and particle phase chemistry of mercury in the real atmosphere. Laboratory and numerical modeling studies suggest that the hydroxyl radical is not central to mercury oxidation (Pal and Ariya, 2004a & 2004b; Calvert and Lindberg, 2005; Sumner et al., 2005;). Little is known about the effect of irradiance. In contrast, ultra violet light and the hydroxyl radical are central to atmospheric chemistry in general, and as a result may exert secondary, non-intuitive effects on the known mercury oxidation pathways. Continental aerosol (where aerosol refers to both the gas phase and interstitial particles) are composed of a complex mixture of organic and inorganic compounds, both of which encompass the gas and particle phases. The oxidation of gas phase organics leads to OH,

HO_2, and peroxy radicals (RO_x) which are highly reactive (Seinfeld and Pandis, 2006). A modeling study indentified the reaciton of HgOH with HO_x and RO_x as feasible (Calvert and Lindberg, 2005), and studies of aqueous chemistry between $Hg^0_{(aq)}$ and dissolved organic matter (DOM) identified $HO_{2(aq)}$ formed from irradiation of oxalate as capable of reducing of Hg(II). However, the aqueous mechanism would not occur in the gas phase due to the production of charged species (Pehkonen and Lin, 1998). The particle phase organics are an equally complex mixture of compounds which become steadily more oxidized with aging (Jimenez et al., 2009). During this aging process, the concentrations of alcohol, aldehyde, and carboxylic acid functional groups in the particles increase. This is significant, because dark and light studies in aqueous systems have discovered that DOM bearing oxygenated functional groups, such as carboxylic acids, are capable of reducing oxidized mercury by Ligand to Metal Charge Transfer (in the light only), and the production of radicals (Matthiessen, 1998; Si and Ariya, 2008; Zheng and Hintelmann, 2009). To our knowledge such chemistry has not been studied in an aerosol system.

It is reasonable to expect that the interaction of oxidized mercury with such aerosol systems, in either dark or light conditions would lead to previously unknown reaction chemistry which may affect the results of atmospheric model studies. Dry deposition of mercury to aquatic systems is strongly dependent upon GEM oxidation to Hg(II) species in locations unimpacted by point sources. Even modest biases in model representations of this process may be important to predictions of methyl mercury accumulation in fish.

This study explored how GEM oxidation varies with irradiance and hydroxyl radical concentrations in simulated continental aerosols. The aerosols were formed from volatile organic compounds which are known precursors of secondary organic aerosol (SOA): isoprene and alpha-pinene were used to model biogenic SOA; toluene was selected to model anthropogenic SOA. Oxidations were initiated with ozone. In some experiments secondary OH was allowed to evolved uninhibited, otherwise 2-butanol was used as an OH-scavenger.

A3.2 Method

Environmental Chamber

A 9000 liter Teflon environmental chamber was used as a batch reactor to perform heterogeneous oxidations of GEM (Shakya and Griffin, 2010; Welch Flurocarbon, Dover, NH). Reactants were introduced into the chamber with fill and flush air which came from a zero air generator (Model 737; Aadco, Cleves, OH ; Model 111; Thermo Electron Instruments, Waltham, MA). Eighteen ultraviolet fluorescent tubes were suspended above the chamber (Sylvania 350BL; Carter et al., 2005) which provided 2070 W m^{-2} of UV. The chamber was enclosed by heavy black curtains to block out ambient light during every experiment.

Reactants

GEM enriched in stable isotope 198 (89.5% purity; Oak Ridge National Laboratory, TN) was injected into the chamber with a gas chromatography syringe (Hamilton Co, Reno, NV) directly from the head space above a sample reservoir which contained a liquid bead. The syringe was conditioned prior to injection (Dumarey et al.,

1985). Propene, isoprene, alpha-pinene, and toluene were first mixed in a 1000 liter Teflon dosing bag. Then an amount of this mixture was transferred to the main chamber by GC syringe. Propene was delivered to the dosing bag from a compressed cylinder (SpecAir; 99.5%). Isoprene, alpha pinene, and toluene were obtained as pure liquids (Sigma Aldrich, >99% for isoprene and toluene; >98% for alpha-pinene, 2-butanol) and kept in half full GC autosampler vials with Teflon septa. Aliquots of the head spaces of these vials were transferred to the dosing bag using a GC syringe. Zero air was used to inflate the dosing chamber to appropriate volume before the mixture was injected into the 9000 liter chamber. Ozone was made using by irradiating zero air with ultraviolet light (Model number M400; Jelight, Irvine, CA). Seed aerosols of ammonium sulfate (Alfa Aesar; 99.999%) were generated using a collision style atomizer (model number 3076; TSI St Paul, MN) with 0.01 M solutions in milliQ water (18.2MΩ). The aerosols were passed through an electrostatic classifier (model number 3080; TSI) with a long differential mobility analyzer (model number 3081; TSI) set to select particles of 100 nm. Seed concentrations in the 9000L chamber were between 200 and 1000 particles cm^{-3} before reactants were introduced and were rapidly dwarfed by SOA formation when ozone was added to the chamber.

Initial mixing times were between 2400-3000 seconds. The cessation of mixing was identified by using ozone and toluene concentration time series in each experiment. Ozone displayed a monotonic decrease in concentration once mixing had finished, and toluene reacted slowly enough that decreases in concentration due to mixing and oxidative losses were easily distinguishable. The numerical model described later was used to confirm the mixing times derived from observations. Two models were run; one

from the time ozone addition finished until mixing had stopped, and a second which then continued from the cessation of mixing. Comparisons were made between measured reactant concentrations and the model outputs at the end of mixing. Observed discrepancies appeared very rapidly and were considerable by 3000s in most cases. By contrast, the second model agreed well with measurements from the cessation of mixing until the system deviated from the expected chemistry, which if observed, began after 3000s.

Measurements

GEM concentrations were measured using cold vapor atomic fluorescence spectrometer (CVAFS; model number 2537A; Tekran Instruments Corp., Toronto, Canada) with gold traps to preconcentrate the GEM before analysis. The gold traps were protected from passivation by water vapor and semi-volatile organic compounds using soda lime and tenax after which was a 47mm Teflon membrane to remove particles (Rutter and Schauer, 2007; Rutter et al., 2008). RM concentrations were measured using thermal desorption analyses of PHg and RGM collected on uncoated and coated quartz fiber filters, respectively. Only the KCl coated filters were used inorder to collect PHg and RGM on the same substrate. Two filters were placed in series to assess breakthrough. KCl coated substrates have been shown in the published literature to perform well when compared with KCl coated denuders (Rutter et al., 2008). Passive and dynamic blanks were collected and measured. Passive blanks were collected by loading and immediately unloading the filter holders. The filter holders were connected to the chamber but no air was pulled through them. The dynamic blank was collected from the chamber when it was full of zero air and 15 ng m^{-3} of GEM. Filter loadings of total mercury for the passive

and dynamic blanks RM collected by the filter substrates was thermally reduced, desorbed and collected using gold coated beads in quartz tubes. The gold bead traps were then desorbed into a cold vapor fluorescence spectrometer (CVAFS; model number 2500; Tekran Instruments, Toronto, Canada) (Rutter et al., 2008). RM measurements were made within two days of the experiment. Volatile organic carbon reactants were measured using a gas chromatograph (model number GC-17A; Shimadzu, Columbia, MD), with a DB-5 column (Agilent Technologies), and flame ionization detection. The GC was calibrated using standard injections into the 1000L dosing chamber. Ozone was measured using a differential UV photometer (model number 49C; ThermoElectron Instruments) which was calibrated at the start of the campaign (model number S-100; Environics, Toland, CT). Total and size resolved measurements of aerosol number concentrations, surface areas and masses were made using a Scanning Mobility Particle Sizer (SMPS; model number 3936; TSI) fitted with a long differential mobility analyzer (model number 3081; TSI). Relative humidity and temperature portable device connected directly to the chamber wall. Relative humidities and temperatures ranged between 20-23% and 21-23°C, respectively.

Experimental Matrix

Initial reactant concentrations were chosen to reflect atmospheric concentrations while still providing a strong enough signal for detection by each instrument, and ensuring that GEM concentration decreases due to oxidation could be robustly measured above wall losses (Table A3.1; Figure A3.1). Experiments to measure GEM wall losses

were conducted in dark and light conditions giving zero order reaction rates with respect to mercury at a rate of -95±74 ng m^{-3} s^{-1}.

Numerical Modeling

Time dependent concentration changes in GEM, ozone, propene, isoprene, alpha-pinene, and toluene were modeled Oxidation pathways for GEM were modeled using a numerical model which calculated ozone and secondary OH concentrations as a function of time. The model used reaction rate coefficients reported in the literature for all experiments, except for the ozone reaction rate which was determined from GEM-ozone rate measurements made with this chamber, which will be reported elsewhere (Pal and Ariya, 2004a & 2004b; Snider et al., 2008). The rate coefficient measured for the GEM-ozone system was $(6.2\pm0.4)\times10^{-19}$ cm^3 $molec^{-1}$ s^{-1} where the uncertainty was the standard deviation of individual experiments. This rate coefficient agreed very well with recent measurements $(6.2\pm1.1)\times10^{-19}$ cm^3 $molec^{-1}$ s^{-1}; Snider et al., 2008; and $(6.4\pm2.3)\times10^{-19}$ cm^3 $molec^{-1}$ s^{-1}; Sumner et al., 2005). VOC chemistry was reproduced using a detailed gas-phase chemistry model (Caltech Atmospheric Chemistry Mechanism, CACM; Griffin et al., 2002) which was updated and optimized (Chen and Griffin, 2005). Model simulations presented in this study were initialized with species concentrations after initial mixing had been adjusted for.

A3.3 Results and Discussion

The effects of UV irradiance on GEM oxidation were measured by exposing GEM to simulated continental SOA under dark and light conditions (Figure A3.2a&b). In parallel experiments, the effects of OH concentration on GEM losses were measured by

scavenging OH with 2-butanol. In all cases oxidative losses of GEM in the 30 mins after mixing followed model predictions, which accounted for oxidation by ozone and hydroxyl radicals. After this initial period the GEM losses in all but one case deviated away from the model predictions, arriving at a decreased, or zero net loss condition. This behaviour is very similar to that observed in aqueous media with $Hg^0(aq)$ and DOM by Zheng and Hintelmann (2009), who were unable to fit the observed behaviour to simple first and second order reaction models. The mechanisms responsible for this may have been either inhibition of further reaction by destabilization of an intermediate, or by reduction of oxidation products. The GEM lost to oxidation before the onset of decreased loss was not recovered afterwards, which implicated either inhibition of an intermediate, reduction reactions which arrived at an equilibrium with oxidation reactions, or the reduction of nascent oxidation products. In this last instance short oligomers may be available for reduction before they further accret with other oligomers, or are adsorbed to SOA particles thereby becoming unavailable. A comparison of the dark (Figure A3.2a) and light (Figure A3.2b) cases showed that the mechanism causing the net zero condition to occur after 0.5 hours in the dark was not active in the light. This implied either a light sensitivity of the inhibiting or reducing mechanism active in the dark, or that this mechanism was itself removed by photochemistry not occuring in the dark case.

When OH was scavenged, the loss behaviours of GEM appeared to partially reverse after the initial period of agreement with the model. Under the dark, scavenged case, the condition of decreased loss was not reached until 1.5 hours, whereas under the light, this condition was reached after only 50 minutes. A replicate of the dark scavenged condition, performed without ammonium sulfate seed exhibited decreased loss at 70

minutes (Figure A3.3). These experimental and numerical modeling results support previous claims that OH is not important in direct oxidation of GEM (Calvert and Lindberg, 2005). Despite this, it was clear that after the initial period of good agreement with the model, OH did have a significant, and complex, indirect effect on GEM oxidative losses which may have been due to its importance in VOC and SOA oxidation chemistry.

In order to gain insight into the mechanisms behind the decreased losses of GEM, a numerical model of VOC oxidation products was used. Two possibilities are raised by both the aqueous phase and aerosol literature, although not all aqueous chemistry is applicable to the atmosphere: Ligand to Metal Charge Transfer through bonding to carboxyl groups (light only); and reaction of the oxidation products with radicals (Calvert and Lindberg, 2005; Si and Ariya, 2008; Zheng and Hintelmann, 2009). The difference between the measured and expected losses of GEM were compared against all of the modeled parameters and several components were found to correlate well with the deficits showing similar relationships between conditions (Figure A3.4a-d; Figures A3.5-A3.8): Total Carboxylic Acids and carbon monoxide (Figure A3.4a); HO_x Reservoir Species (Figure A3.4b); Acyl Peroxy Radicals (backbones smaller than 6 carbons; Figure A3.4c); and, Phenolic Peroxy Radicals from toluene oxidation (Figure A3.4d). Several other components were also found to correlate well with deficits of GEM loss and demonstrated very similar relationships between experiments (methyl vinyl ketone, methacrolein), or were of different intercepts or regression slopes: i.e. methylglyoxal, many of the organic peroxy radicals, oxalic acid. Although these correlations do not demonstrate causal relationships, they do reflect published results from studies of

aqueous systems and indicate that some aspects of the VOC oxidation chemistry are important to the oxdation of GEM. Furthermore, the inhibition or reduction mechanisms responsible for the decreased amounts of GEM loss, were apparently sensitive to light and OH concentrations, suggesting this process to be complex, and that different pathways may be active under the variety of conditions studied here.

As mentioned above, the appearance of a reducing agent in the reaction system might be expected to cause complete reduction of all the mercury oxidized during the experiment. This would only be the case the oxidized mercury were in a speciation conducive to reduction, or which was available to the carboxylic acid. Oxidized mercury formed early in the experiment may have been incorporated into the SOA particles and covered by successive deposition of semi-volatile VOC oxidation products. The HO_x Reservoir Species are unidentified compounds which consume OH and HO_2 when formed, and regenerate these species when they are decomposed by OH or UV light. Organic peroxy radicals, such as the Acyl and Phenolic Peroxy Radicals, and possibly some of the HO_x Reservoir Species, have been identified by modeling studies as capable of reacting with oxidation products of Hg and OH (HgOH; Calvert and Lindberg, 2005), and may also be therefore capable of reacting with Hg-ozone intermediates and oxidation products. Organic peroxy radicals also lead to the formation of carboxylic acids in this system. As a result, it cannot be determined which of these species is responsible, or if all are involved.

The concentrations of RM measured using the KCl-impregnated filters were significantly lower than were predicted using the real time Tekran 2537A measurements (Table A3.2), but provided qualitative evidence that the decreases in GEM concentration

where due to conversion to a stable oxidation product. The filter based measurements were made over the entire 6 hours that air was sampled from the chamber. The predictions of RM concentrations made from the real time data were also determined using measurements made over this same time period. Wall losses of particles and gases were expected to begin within the first hour and a half; the onset of SOA wall losses was found to vary between experiments (Figure A3.9). Changes in particle mass concentrations after the end of initial mixing were between -9% and +5% at 1.5 hours, and between -17% and -29% of SOA mass at 2 hours, and between -33 and -42% at 6 hours. The total fraction of SOA mass lost could not explain the deficits in the RM in every experiment: deficits of between 40% and 90% were found between the filter-based measurements and the predictions. This suggested that both RGM and PHg were present in the measured RM, and that both species were being lost to the walls. As the chamber was collapsable, and nearly empty at the end of the experiments, wall losses were expected to escalate after the bag was 1/3 emptied at 2 hours. A similar discrepancy (60-70% deficit) between expected and measure filtrable RM was measured by Sumner et al. (2005) using a $17m^3$ Teflon environmental chamber. Line losses for SOA particles, and therefore PHg, between the chamber and the filter were calculated to be less than 0.1%. Breakthrough of RM from the front to rear KCl coated filter was observed to be 8% in the SOA Dark case and not statistically different than zero in the OH scavenger cases (Dark 3%; Light 2%).

The observation of GEM oxidation inhibition or the action of a reduction pathway is potentially significant to our understanding of mercury deposition and atmopsheric residence times. These experiments demonstrated an onset of decreased oxidation which

appeared to be related in some way to carboxylic acids or peroxy radicals formed during VOC oxidation. The relationship may be a direct interaction, or may be indicative of some yet unidentified process which occurs during VOC oxidation. As the mechanisms causing decreased loss were sensitive to both UV light and OH concentrations the effect of the mechanism on oxidized mercury concentrations in the atmosphere are potentially complex. Despite these questions regarding the mechanism, it is still informative to use these results to estimate the magnitude of the effect on atmospheric concentrations of reactive mercury formation. To do this relationships between select, representative VOC oxidation products and deficits of GEM oxidative losses were determined (Figure A3.1 and Figure A3.5-A3.7; Table A3.3 and A3.9). The deficits between expected and measured GEM losses were assumed to constitute a reactive mercury deficit. For the unamended dark case, such estimates of a reactive mercury deficit were approximately 1 ng m^{-3} for every 6 ppb of carboxylic acid, 12 ppb of carbon monoxide, 3-5 ppb of HO_x reservoir species, 0.06 ppb of acyl peroxy radicals, and 0.07 ppb of Phenolic Peroxy Radicals (Table A3.3). An important consideration was that the absolute concentrations of mercury, VOCs and SOA in the chamber were higher than seen the atmosphere (GEM 100 times; VOCs ~10 times; SOA ~10 times). However, the experimental reactant ratios (GEM = 90-110 ng m^{-3} : Isoprene = 35-80 ppb : alpha-pinene = 10-50 ppb) could be corrected (GEM = 1.5 ng m^{-3} : Isoprene 1-10 ppb; Wiedinmyer et al., 2001; Rizzo et al, 2010; Schwartz et al., 2010: alpha-pinene = 0.01-1 ppb; Yu et al., 1999; Hakola et al., 2009) to provide atmopsherically relevant estimates of the observed effect. The ratio of GEM to VOCs isoprene and alpha-pinene were approximately 3-80 times greater and 10-500 times greater than in the atmosphere, respectively. Therefore, the RM deficit

calculated using these relationships was divided by factors of 10 and 100 to provide reasonable bounds to the estimates. Ambient measurements of carboxylic acids in $PM_{2.5}$ (Wang and Shooter, 2004; Hsieh et al., 2008; Timonen et al., 2008; Kourtchev et al., 2009) as a very simple representation of all of the chemistry identified in this study as potential candidates for the cause of the RM deficit. Reactive mercury deficits of approximately 1-100 pg m^{-3} in rural and urban atmospheres (factor of 10 case; 0.1-10 pg m^{-3} for 100 factor case) were calculated compared to predictions from a simple ozone and hydroxyl radical oxidation model. The upper limit of these ranges corresponded to elevated pollution events in urban areas, while predictions under less polluted conditions were in the lower 20% of these ranges. These deficits are similar to atmospheric concentrations of reactive mercury measured in the continental atmosphere (Rutter et al., 2008), and may therefore be of importance to predictions of dry deposition of reactive mercury in modeling studies.

A3.4 References

Calvert, J. G. and Lindberg, S. E. Mechanisms of mercury removal by O3 and OH in the atmosphere. Atmos. Environ. 39, (18), 3355-3367, 2005.

Carter, W. P. L., Cocker, D. R., Fitz, D. R., Malkina, I. L., Bumiller, K., Sauer, C. G., Pisano, J. T.; Bufalino, C.; Song, C. A new environmental chamber for evaluation of gas-phase chemical mechanisms and secondary aerosol formation. Atmos. Environ. 39, (40), 7768-7788, 2005.

Chen, J. J., and Griffin, R. J. Modeling secondary organic aerosol formation from oxidation of alpha-pinene, beta-pinene, and d-limonene. Atmos. Environ. 39, (40), 7731-7744, 2005.

Dumarey, R., Temmerman, E., Dams, R., and Hoste, J. The Accuracy of the Vapor-Injection Calibration Method for the Determination of Mercury by Amalgamation Cold-Vapour Atomic-Absorption Spectrometry. Analytica Chimica Acta 170, (APR), 337-340, 1985.

Griffin, R. J., Dabdub, D., and Seinfeld, J. H. Secondary organic aerosol - 1. Atmospheric chemical mechanism for production of molecular constituents. J. Geophy. Res. 107, (D17), 2002.

Hakola, H., Hellen, H., Tarvainen, V., Back, J., Patokoski, J., and Rinne, J. Annual variations of atmospheric VOC concentrations in a boreal forest. Bor. Environ. Res. 14, (4), 722-730, 2009.

Hsieh, L. Y., Chen, C. L., Wan, M. W., Tsai, C. H., and Tsai, Y. I. Speciation and temporal characterization of dicarboxylic acids in PM2.5 during a PM episode and a period of non-episodic pollution. Atmos. Environ. 42, (28), 6836-6850, 2008.

Jimenez, J. L., Canagaratna, M. R., Donahue, N. M., Prevot, A. S. H., Zhang, Q., Kroll, J. H., DeCarlo, P. F., Allan, J. D., Coe, H., Ng, N. L., Aiken, A. C., Docherty, K. S., Ulbrich, I. M., Grieshop, A. P., Robinson, A. L., Duplissy, J., Smith, J. D., Wilson, K. R., Lanz, V. A., Hueglin, C., Sun, Y. L., Tian, J., Laaksonen, A., Raatikainen, T., Rautiainen, J., Vaattovaara, P., Ehn, M., Kulmala, M., Tomlinson, J. M., Collins, D. R., Cubison, M. J., Dunlea, E. J., Huffman, J. A.,

Onasch, T. B., Alfarra, M. R., Williams, P. I., Bower, K., Kondo, Y., Schneider, J., Drewnick, F., Borrmann, S., Weimer, S., Demerjian, K., Salcedo, D., Cottrell, L., Griffin, R., Takami, A., Miyoshi, T., Hatakeyama, S., Shimono, A., Sun, J. Y., Zhang, Y. M., Dzepina, K., Kimmel, J. R., Sueper, D., Jayne, J. T., Herndon, S. C., Trimborn, A. M., Williams, L. R., Wood, E. C., Middlebrook, A. M., Kolb, C. E., Baltensperger, U., and Worsnop, D. R. Evolution of Organic Aerosols in the Atmosphere. Science 326, (5959), 1525-1529, 2009.

Kourtchev, I., Copolovici, L., Claeys, M., and Maenhaut, W.. Characterization of Atmospheric Aerosols at a Forested Site in Central Europe. Environ. Sci. Technol. 43, (13), 4665-4671, 2009.

Matthiessen, A. Reduction of divalent mercury by humic substances - kinetic and quantitative aspects. Sci. Total Environ. 213, (1-3), 177-183, 1998.

Pal, B. and Ariya, P. A. Gas-phase HO center dot-Initiated reactions of elemental mercury: Kinetics, product studies, and atmospheric implications. Environ. Sci. Technol. 38, (21), 5555-5566, 2004a.

Pal, B. and Ariya, P. A. Studies of ozone initiated reactions of gaseous mercury: kinetics, product studies, and atmospheric implications. Phys. Chem. Chem. Phys. 6, (3), 572-579, 2004b.

Pehkonen, S. O. and Lin, C. J. Aqueous photochemistry of mercury with organic acids. J.Air Waste Manag. Assoc. 48, (2), 144-150, 1998.

Rizzo, L. V., Artaxo, P., Karl, T., Guenther, A. B., and Greenberg, J. Aerosol properties, in-canopy gradients, turbulent fluxes and VOC concentrations at a pristine forest site in Amazonia. Atmos. Environ. 44, (4), 503-511, 2010.

Rutter, A. P., Hanford, K. L., Zwers, J. T., Perillo-Nicholas, A. L., Schauer, J. J., Worley, C. A., Olson, M. L., and DeWild, J. F. Evaluation of an off-line method for the analysis of atmospheric reactive gaseous mercury and particulate mercury. J. Air Waste Manag. Assoc. 58, 377-383, 2008.

Rutter, A. P. and Schauer, J. J. The impact of aerosol composition on the particle to gas partitioning of reactive mercury. Environ. Sci. Technol. 41, (11), 3934-3939, 2007.

Rutter, A. P., Schauer, J. J., Lough, G. C., Snyder, D. C., Kolb, C. J., Von Klooster, S., Rudolf, T., Manolopoulos, H., and Olson, M. L. A comparison of speciated atmospheric mercury at an urban center and an upwind rural location. J. Environ. Monitor. 10, (1), 102-108, 2008.

Schwartz, R. E., Russell, L. M., Sjostedt, S. J., Vlasenko, A., Slowik, J. G., Abbatt, J. P. D., Macdonald, A. M., Li, S. M., Liggio, J., Toom-Sauntry, D., and Leaitch, W. R. Biogenic oxidized organic functional groups in aerosol particles from a mountain forest site and their similarities to laboratory chamber products. Atmos. Chem. Phys. 10, (11), 5075-5088, 2010.

Seinfeld, J. H. and Pandis, S. N., Atmospheric Chemistry and Physics:from Air Pollution to Climate Change. 2nd ed. Wiley-Interscience: New York, NY, 2006.

Shakya, K.M. and Griffin, R.J. Secondary organic aerosol from photooxidation of polycyclic aromatic hydrocarbons. Environ. Sci. Technol., 44, 8134-8139, 2010.

Si, L. and Ariya, P. A. Reduction of oxidized mercury species by dicarboxylic acids (C-2-C-4): Kinetic and product studies. Environ. Sci. Technol. 42, (14), 5150-5155, 2008.

Snider, G., Raofie, F., and Ariya, P. A. Effects of relative humidity and CO(g) on the O-3-initiated oxidation reaction of Hg-0(g): kinetic & product studies. Phys. Chem. Chem. Phys. 10, (36), 5616-5623, 2008.

Sumner, A. L., Spicer, C. W., Satola, J., Mangaraj, R., Cowen, K. A., Landis, M. S., Stevens, R. K., and Atkeson, T. D. Environmental Chamber Studies of Mercury Reactions in the Atmosphere. In Dynamics of Mercury Pollution on Regional and Global Scales: Atmospheric Processes and Human Exposures Around the World. Pirrone, N. M., K.R.; , Ed. Springer US, 193-212, 2005.

Timonen, H. J., Saarikoski, S. K., Aurela, M. A., Saarnio, K. M., and Hillamo, R. E. J. Water-soluble organic carbon in urban aerosol: concentrations, size distributions and contribution to particulate matter. Bor. Environ. Res. 13, (4), 335-346, 2008.

Wang, H. B., and Shooter, D. Low molecular weight dicarboxylic acids in PM10 a city with intensive solid fuel burning. Chemosphere 56, (8), 725-733, 2004.

Wiedinmyer, C., Friedfeld, S., Baugh, W., Greenberg, J., Guenther, A., Fraser, M., and Allen, D. Measurement and analysis of atmospheric concentrations of isoprene and its reaction products in central Texas. Atmos. Environ. 35, (6), 1001-1013, 2001.

Yu, J. Z., Griffin, R. J., Cocker, D. R., Flagan, R. C., Seinfeld, J. H., and Blanchard, P. Observation of gaseous and particulate products of monoterpene oxidation in forest atmospheres. Geophys. Res. Lett. 26, (8), 1145-1148, 1999.

Zheng, W., and Hintelmann, H. Mercury isotope fractionation during photoreduction in natural water is controlled by its Hg/DOC ratio. Geochim. Cosmochim. Acta 73, (22), 6704-6715, 2009.

Table A3.1. Initial reactant concentrations (after initial mixing concluded) and light conditions of the experiments presented in this study.

Description $Hg^0(g)$ with…	$[Hg]_0$ ng m^{-3}	$[O_3]_0$ ppb	$[propene]_0$ ppb	[2-butanol]$_0$ ppb	[α-pinene]$_0$ ppb	$[isoprene]_0$ ppb	$[toluene]_0$ ppb	Irradiance
O_3-propene-SOA precursors	95	266	91	NA	18	42	62	Dark
	109	272	82	NA	16	50	69	UV
O_3-propene-SOA precursors-OH scavenger	87	255	121	2653	14	40	77	Dark
	92	219	91	1356	4	63	69	UV

Table A3.2. Measurements of reactive mercury concentrations. The filter-based measurements used KCl impregnated filter collections with cold vapor atomic fluorescence spectroscopy after thermal desorption. The real time measurement was performed by assessing the difference between observed GEM concentrations and those expected if GEM was only being removed from the chamber by losses to the walls. The ratio between filter-based and real time measurements, and the SOA mass lost to the walls provide insight into the loss mechanisms for RM and the performance of the RM measurement method. The fraction of RM which was collected on the rear filter is shown as a fraction of the filter-based measurement column, which is a sum of both the front and rear filter measurements.

Experimental Conditions	Filter-Based Measurement pg m^{-3} ± unc	Real Time Measurement pg m^{-3} ± unc	Ratio Filter : Real Time	SOA mass lost to walls fraction	Filter Breakthrough fraction
SOA Dark	323 ± 34	550	0.6	0.4	0.08
SOA Light	ND	2360	ND	0.42	ND
SOA Dark, OH Scavenger	151 + 19	1350	0.1	0.38	NSD/
SOA Light, OH Scavenger	176 ± 21	550	0.3	0.33	NSDZ

ND- No data available

NSS- Not statistically different than zero

Table A3.3. Regression parameters for the relationships between the deficit between measured and modeled GEM, and various species in the SOA model. The units of the slopes are ppb of species in the left column per ng m^{-3} of difference in GEM between the model and measurements. This could also be expressed ppb per pg m^{-3} of deficit between expected and measured reactive mercury formation. The uncertainty in the slope is the standard error (sde) from the regression package in MS Excel.

	SOA DARK			SOA LIGHT		
	slope	sde	r^2	slope	sde	r^2
Lumped Carboxylic Acids	6	1	**0.79**	4	3	0.10
Carbon Monoxide	12	2	**0.79**	8	7	0.10
HO_x Reservoir Species 1	5	1	**0.74**	2	3	0.05
HO_x Reservoir Species 2	3	0	**0.79**	2	2	0.09
Acyl Peroxy Radicals (C<6)	0.06	0.05	0.13	0.48	0.44	0.10
Phenolic Peroxy Radicals	0.07	0.01	**0.72**	0.02	0.03	0.05
Total Peroxy Radicals	-0.9	0.4	0.33	0.2	0.5	0.01

	SOA DARK w/ OH SC			SOA LIGHT w/ OH SC		
	slope	sde	r^2	slope	sde	r^2
Lumped Carboxylic Acids	5	1	0.51	9	1	**0.87**
Carbon Monoxide	9	3	0.50	17	2	**0.87**
HO_x Reservoir Species 1	4	1	0.39	7	1	**0.84**
HO_x Reservoir Species 2	3	1	0.50	6	1	**0.86**
Acyl Peroxy Radicals (C<6)	0.03	0.04	0.04	0.25	0.03	**0.83**
Phenolic Peroxy Radicals	0.05	0.02	0.39	0.12	0.02	**0.84**
Total Peroxy Radicals	-1.4	0.4	0.51	-2.3	0.3	**0.87**

Table A3.4. Pearson correlation coefficients for the relationships between the deficit between measured and modeled GEM, and various species in the SOA model

	Pearson Correlation Coefficients			
Species	**SOA Dark**	**SOA w/OH Sc Dark**	**SOA Light**	**SOA w/OH Sc Light**
Lumped Carboxylic Acids	0.88	0.77	0.42	0.93
Carbon Monoxide	0.88	0.77	0.41	0.93
HO_x Reservoir Species 1	0.88	0.72	0.35	0.93
HO_x Reservoir Species 2	0.89	0.77	0.40	0.93
Acyl Peroxy Radicals (C<6)	-0.71	-0.77	0.16	-0.93
Phenolic Peroxy Radicals	0.88	0.72	0.35	0.93
Hydroperoxy Radical	-0.83	-0.65	-0.27	-0.91
Ozone	-0.89	-0.76	-0.39	-0.93
Hydroxyl Radical	-0.87	-0.66	-0.33	-0.92

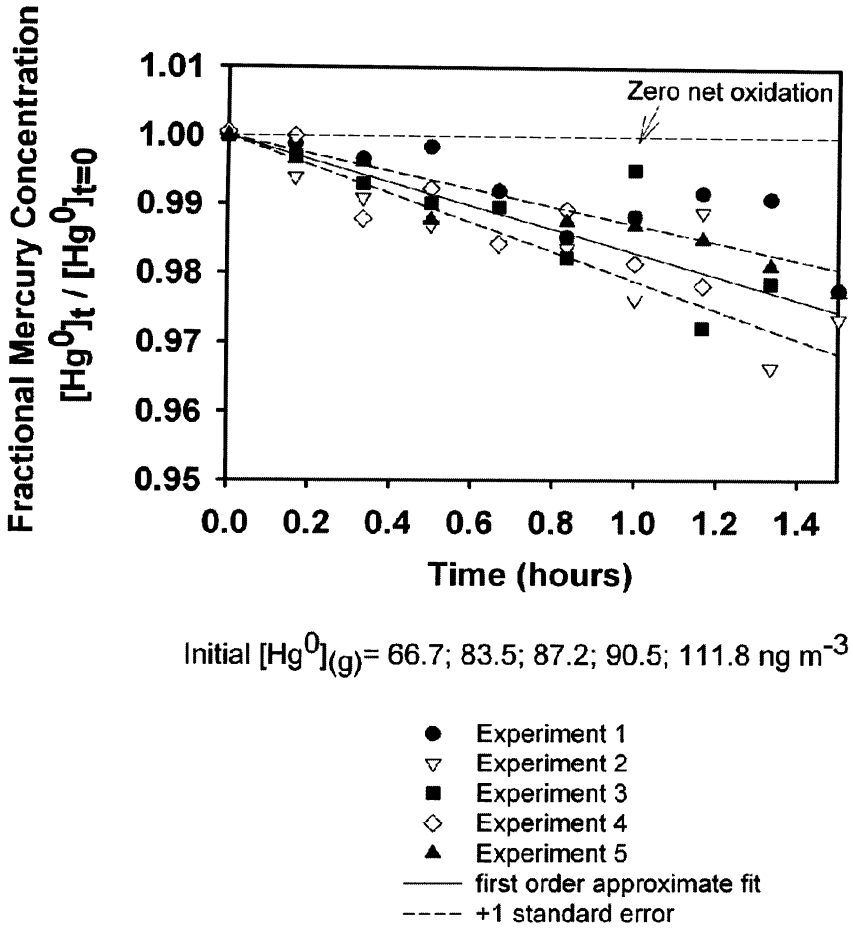

Figure A3.1. Replicate measurements of $Hg^0_{(g)}$ oxidative loss in the dark with OH scavenger case during the first hour and a half, with a first order fit and 1 standard error uncertainties to provide a measure of the precision of the experimental set up.

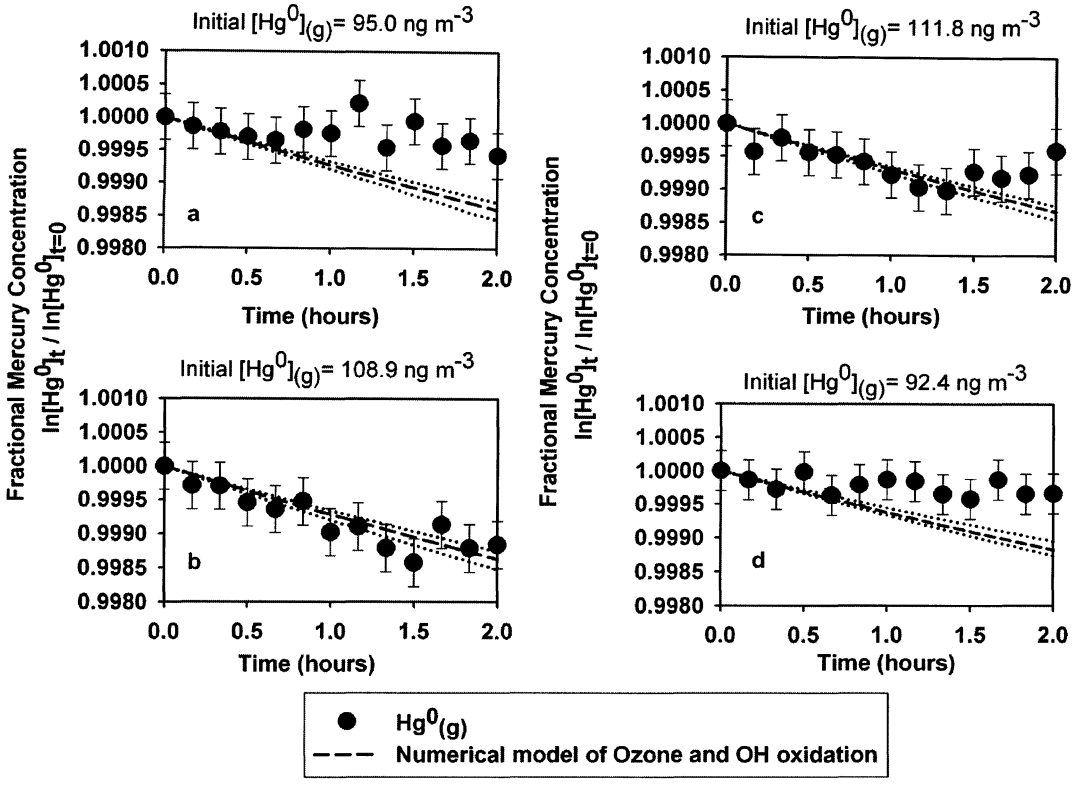

Figure A3.2. Measurements of $Hg^0_{(g)}$ in the four secondary organic aerosol systems each generated by ozone initiation of α-pinene, isoprene, and toluene: (a) dark; (b) UV light; (c) dark with 2-butanol OH scavenger; and, (d) UV light with 2-butanol OH scavenger. The measurements are compared with a numerical model which included ozone and OH oxidation.

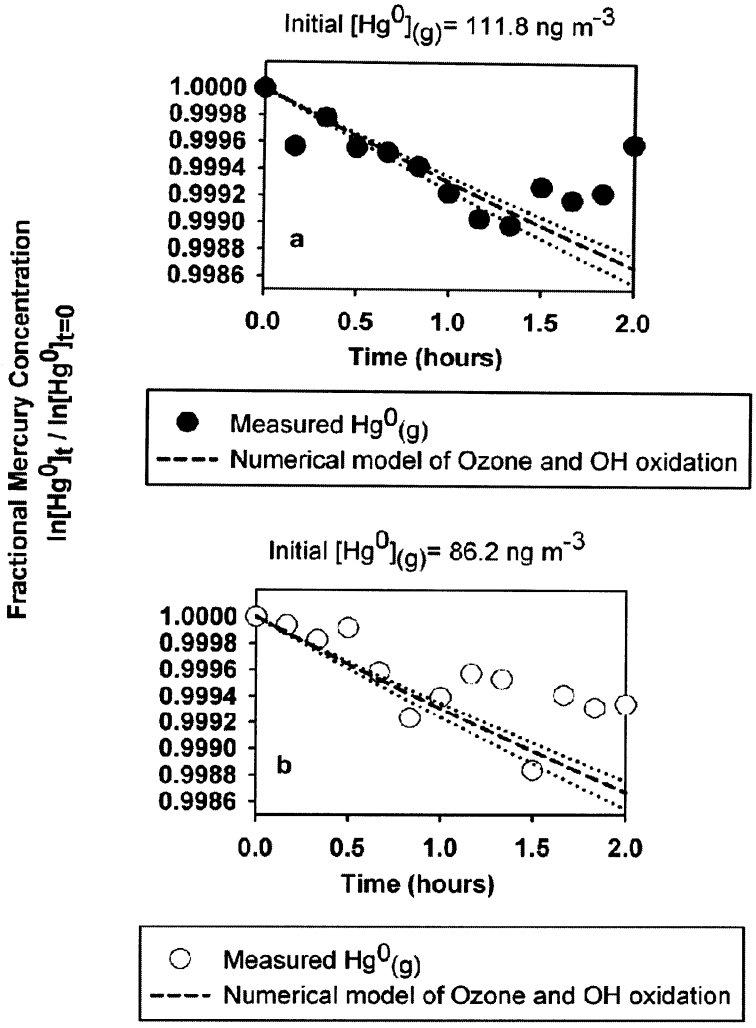

Figure A3.3. Replicate measurements of $Hg^0_{(g)}$ oxidative loss in the dark with OH scavenger case for an experiment with ammonium sulfate seed (a) and an experiment without seed (b).

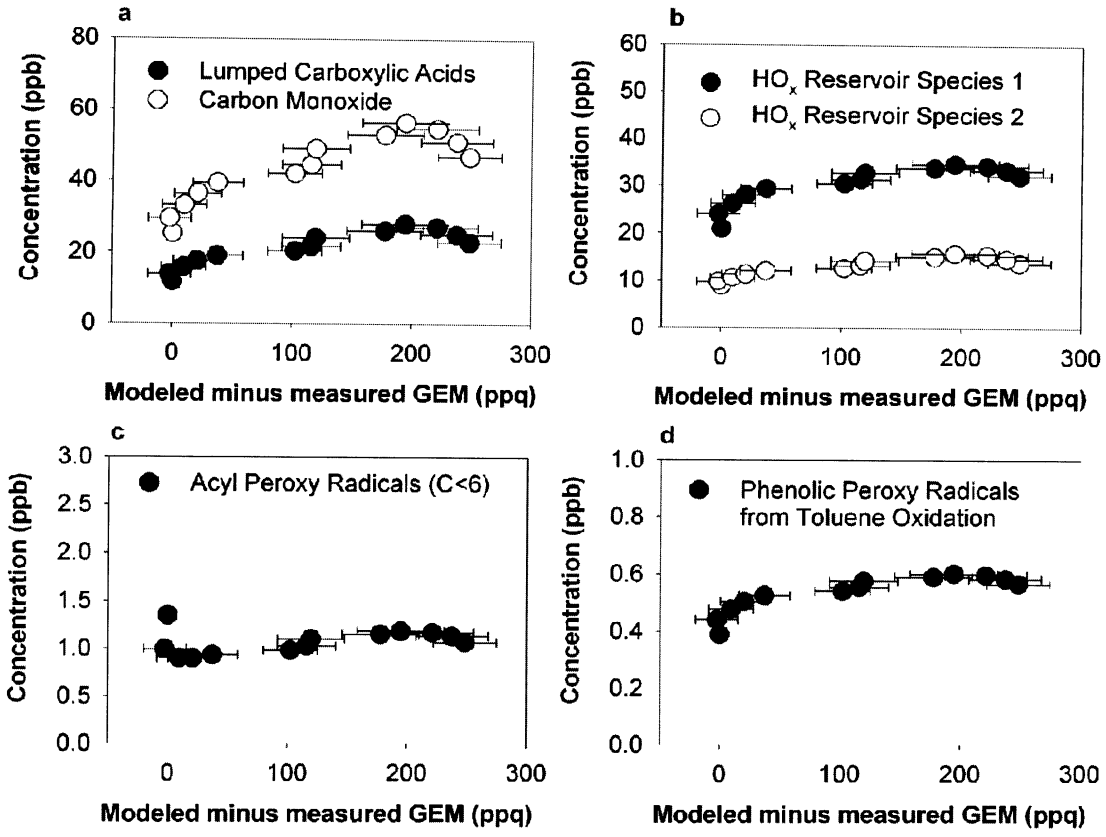

Figure A3.4. Correlations between SOA numerical model parameters and the difference between expected and measured losses of $Hg^0_{(g)}$, for the dark case. The SOA numerical model parameters shown are: (a) Lumped Carboxylic Acids; (b) HO_x reservoir species 1 and 2; (c) Acyl Peroxy Radicals (C<6); and, (d) Phenolic Peroxy Radicals from Toluene Oxidation. HO_x reservoir species are unidentified organic compounds which give rise to OH and HO2 when decomposed by light or oxidative species.

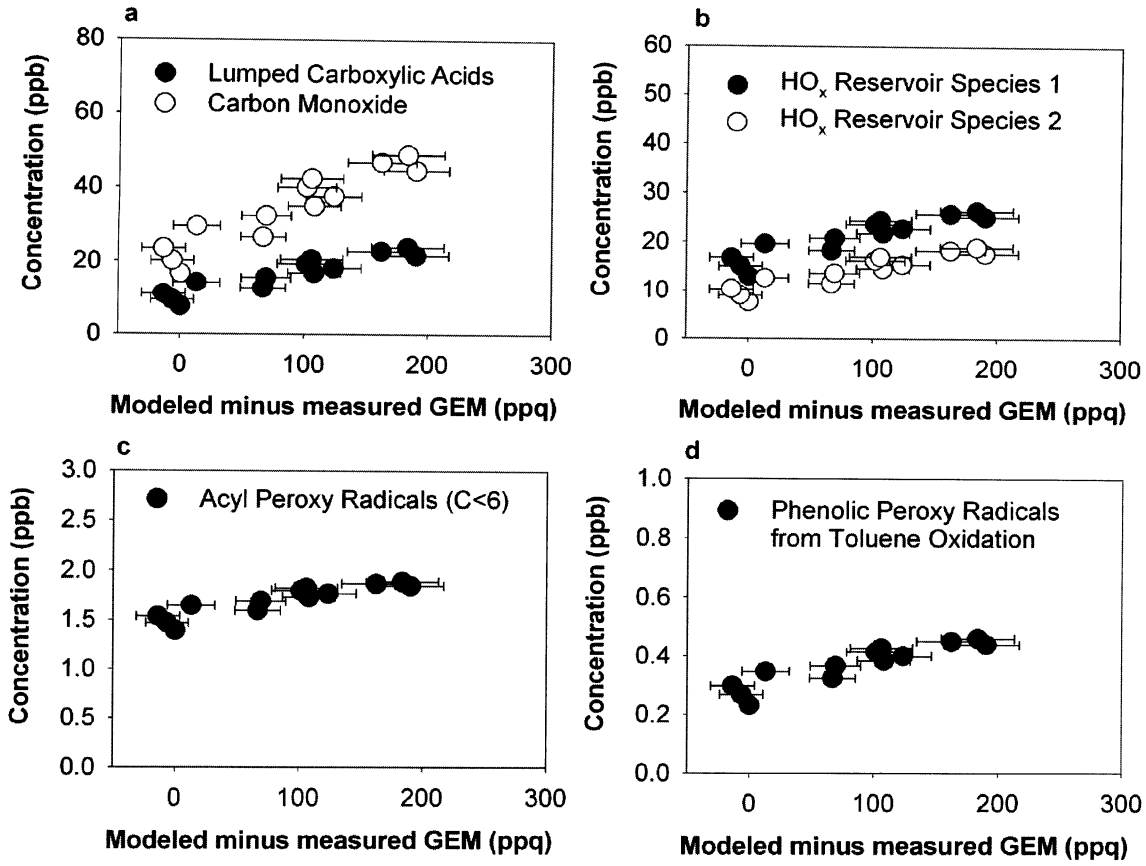

Figure A3.5. Correlations between SOA numerical model parameters and the difference between expected and measured losses of $Hg^0_{(g)}$, for the irradiated case with OH scavenger added. The SOA numerical model parameters shown are: (a) Lumped Carboxylic Acids; (b) HO_x reservoir species 1 and 2; (c) Acyl Peroxy Radicals (C<6); and, (d) Phenolic Peroxy Radicals from Toluene Oxidation. HO_x reservoir species are unidentified organic compounds which give rise to OH and HO2 when decomposed by light or oxidative species.

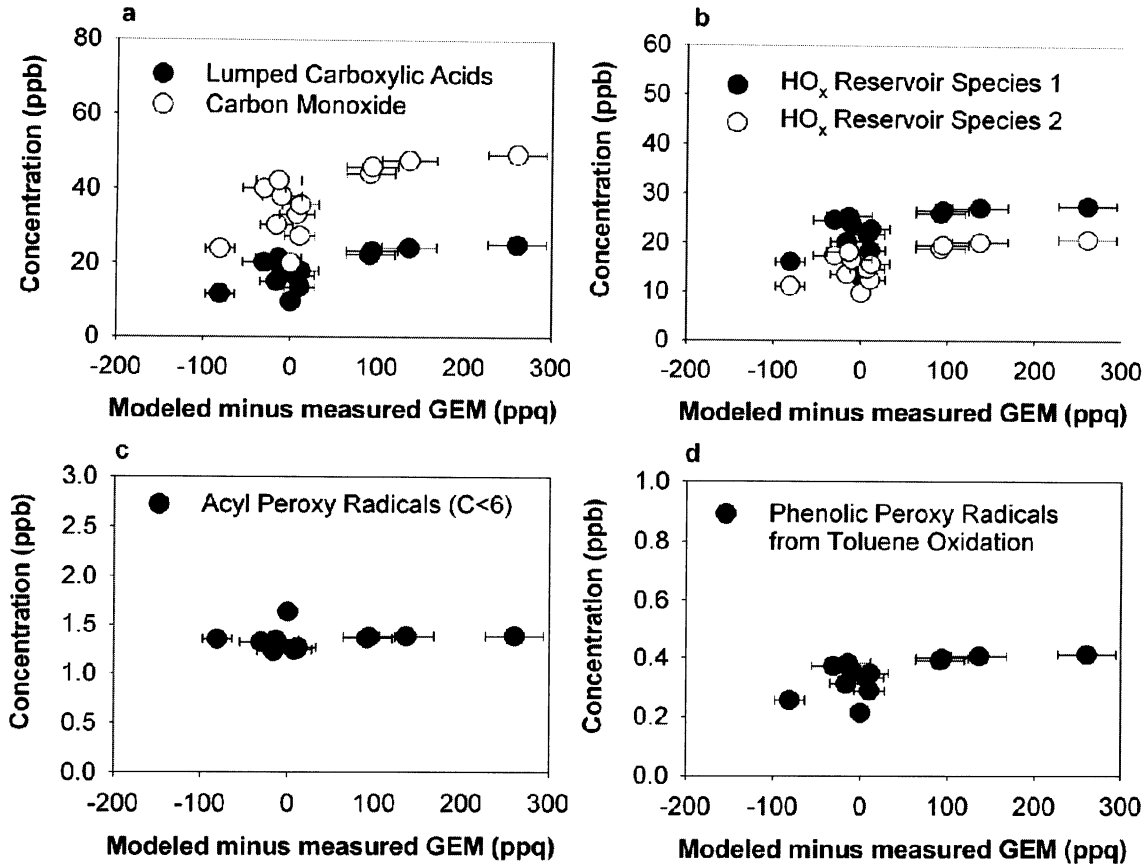

Figure A3.6. Correlations between SOA numerical model parameters and the difference between expected and measured losses of $Hg^0_{(g)}$, for the dark case with OH scavenger added. The SOA numerical model parameters shown are: (a) Lumped Carboxylic Acids; (b) HO_x reservoir species 1 and 2; (c) Acyl Peroxy Radicals (C<6); and, (d) Phenolic Peroxy Radicals from Toluene Oxidation. HO_x reservoir species are unidentified organic compounds which give rise to OH and HO2 when decomposed by light or oxidative species.

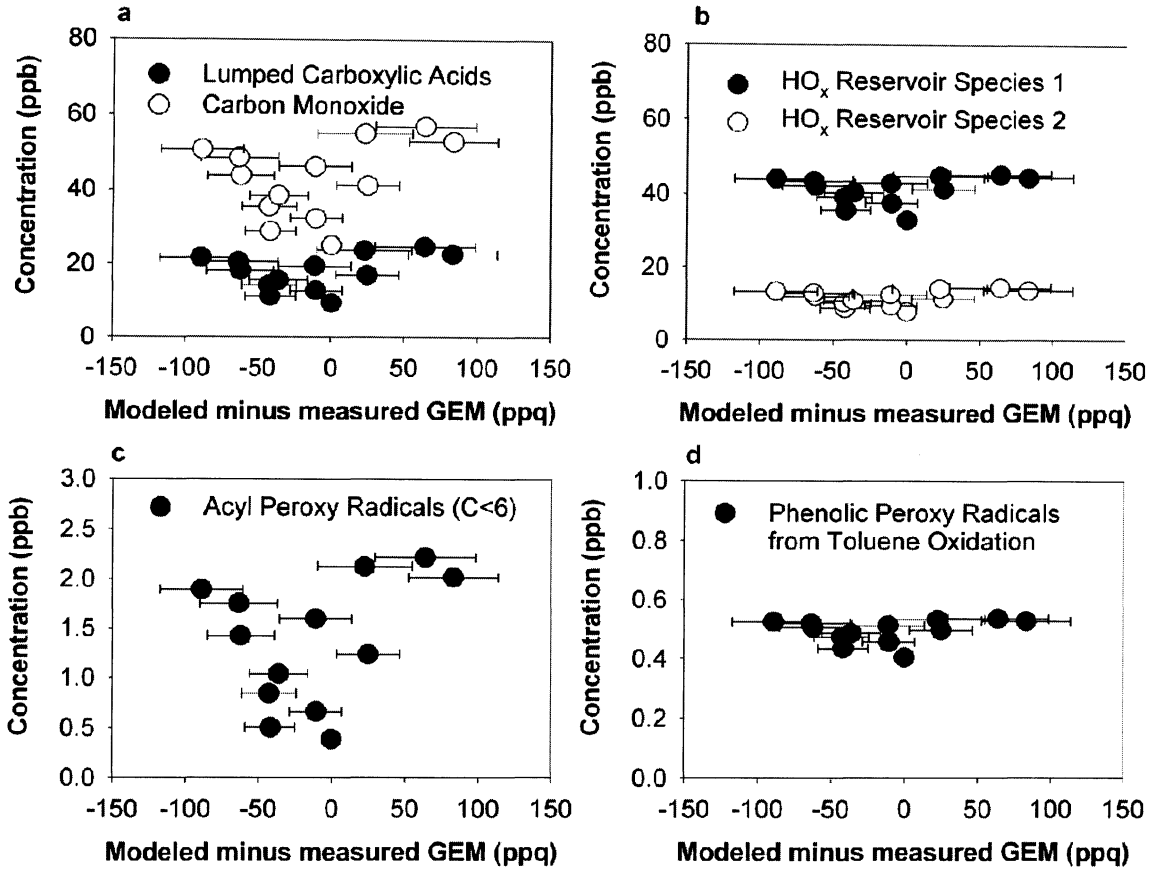

Figure A3.7. Correlations between SOA numerical model parameters and the difference between expected and measured losses of $Hg^0_{(g)}$, for the irradiated case. The SOA numerical model parameters shown are: (a) Lumped Carboxylic Acids; (b) HO_x reservoir species 1 and 2; (c) Acyl Peroxy Radicals (C<6); and, (d) Phenolic Peroxy Radicals from Toluene Oxidation. HO_x reservoir species are unidentified organic compounds which give rise to OH and HO2 when decomposed by light or oxidative species.

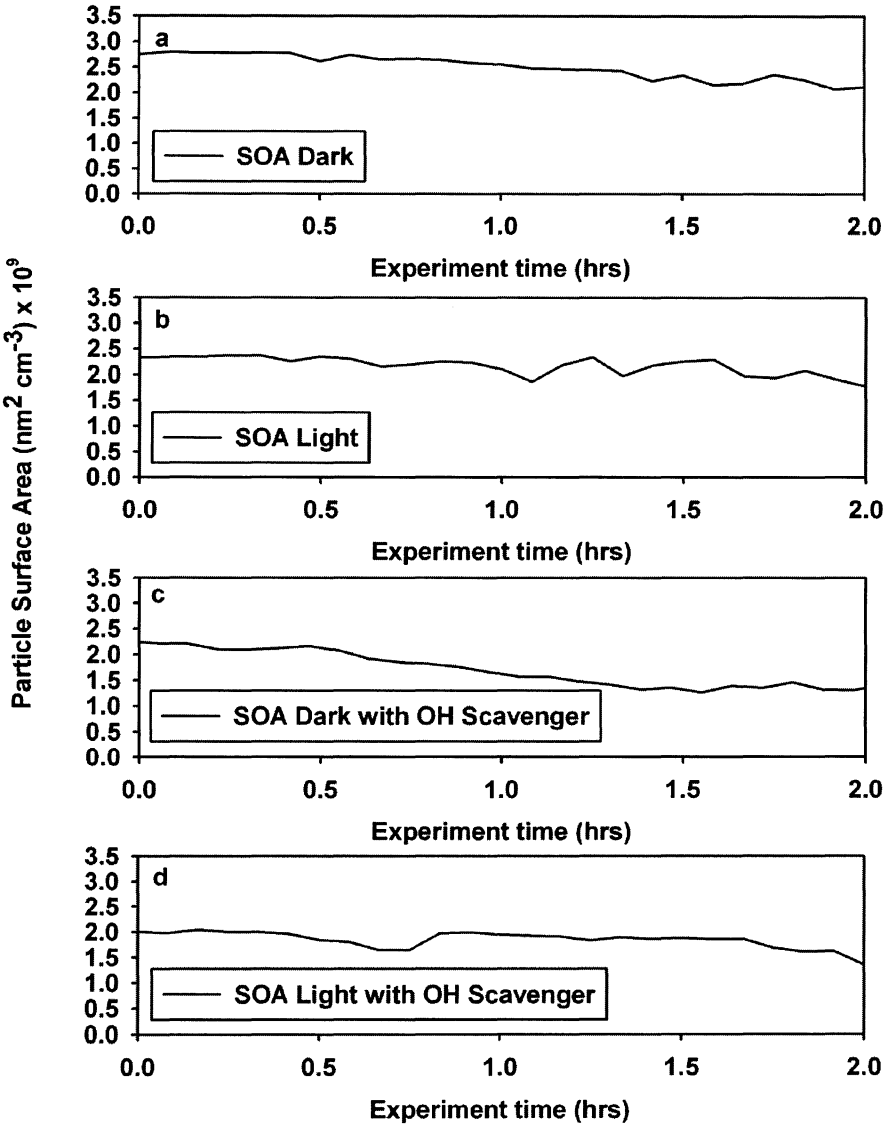

Figure A3.8. Time series of total particle surface area measurements made with a TSI SMPS.

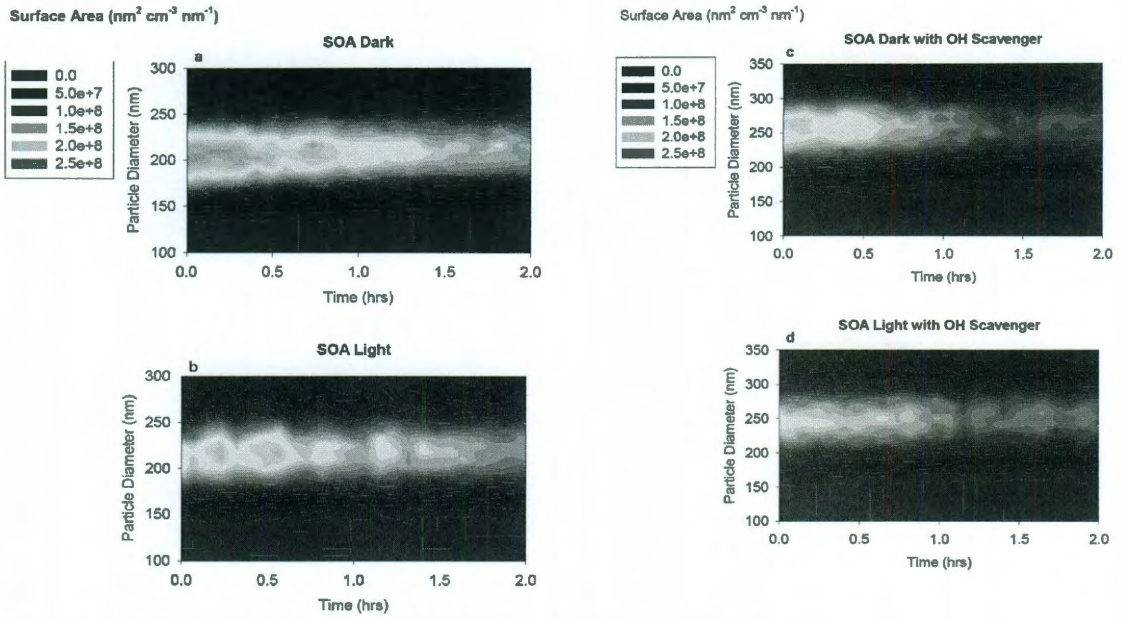

Figure A3.9. Size resolved measurements of particle surface area